Removal of pesticides using bacteria and hydrogel-silver nanocomposite

A thesis submitted in fulfilment of the
requirements for the award of the degree of

DOCTOR OF PHILOSOPHY

IN

BIOTECHNOLOGY

Submitted By

RAVNEET KAUR

(Reg No. 901400008)

Under the supervision of

Dr. DINESH GOYAL

Professor

THAPAR INSTITUTE
OF ENGINEERING & TECHNOLOGY
(Deemed to be University)

Department of Biotechnology
Patiala – 147004
INDIA

December, 2020

CERTIFICATE

Certified that the thesis **"Removal of pesticides using bacteria and hydrogel-silver nanocomposite"** which is submitted by Ms. Ravneet Kaur, in fulfilment of the requirement for the award of the degree of Doctor of Philosophy in the Department of Biotechnology, Thapar Institute of Engineering & Technology (Deemed to be University), Patiala, Punjab, India is a record of the candidate's own independent and original research work carried out by her under my supervision and guidance. The matter embodied in this thesis has not been submitted in part or full to any other University or Institute for the award of any degree.

Place: Patiala
Date: December 21, 2020

Supervisor
(Dr. Dinesh Goyal)
Professor,
Department of Biotechnology,
Thapar Institute of Engineering & Technology
(Deemed to be University)
Patiala - 147004
Punjab, India

DECLARATION

I hereby declare that the work which is being presented in this thesis **"Removal of pesticides using bacteria and hydrogel-silver nanocomposite"** submitted by me for the award of the degree of Doctor of Philosophy in the Department of Biotechnology, Thapar Institute of Engineering & Technology, Patiala is true and original record of my own independent and original research work carried out under the supervision of Dr. Dinesh Goyal, Professor, Department of Biotechnology, Thapar Institute of Engineering & Technology (Deemed to be University), Patiala, Punjab. The matter embodied in this thesis has not been submitted in part or full to any other University or Institute for the award of any degree in India or Abroad.

Ravneet Kaur

Place: Patiala
Date: December 21, 2020

(Ravneet Kaur)

ACKNOWLEDGEMENT

The time has eventually arrived when my journey of Ph.D has reached the other end of the stupendous road of research. Being the most remarkable stretch traversed so far, not just gave me the academic knowledge, rather taught me different aspects of life by helping me to grow in stature, building some invaluable self-confidence, as well as vision and determination to achieve substantially big in life. In all these years, many people have helped me in shaping up what I am today. It was hardly possible for me to thrive my doctoral work without the precious support of these personalities.

First and foremost, I would like to praise and thank God, the *Almighty*, for showering his countless blessings and granting me good health, knowledge, strength, and patience to work through all these years, so that today I can stand proud with my head held high.

I would like to express my sincere gratitude and respect to my supervisor ***Dr. Dinesh Goyal*** for his keen interest and valuable guidance, strong motivation and constant encouragement throughout my journey in TIET, Patiala. His continuous support, great patience, immense knowledge, constructive criticism and myriad useful suggestions helped me a lot making my Ph.D easier and comfortable. His contribution and faith in me, helped me to smoothly sail through this journey. I greatly appreciate the freedom he gave me to pursue my independent work and find my own path during this research endeavour.

I am highly grateful to the authorities of ***Thapar Institute of Engineering & Technology, Patiala***, for providing infrastructure and helping me towards the smooth and timely completion of my research work. I would like to thank Science & Technology Entrepreneur's Park **(*STEP*)**, TIET for providing me necessary equipments and facilities to carry out work. This research was made much easier by Department of Science and Technology- Science and Engineering Research Board **(*DST-SERB), Government of India*** for proving me financial support to accomplish my work.

My special word of thanks should also go to members of my doctoral committee, ***Dr. N. Das***, ***Dr. Shekhar Agnihotri, Dr. Manoj Baranwal***, DBT, TIET and ***Dr. B. N. Chudasama***, School of Physics and Material Science, for their invaluable suggestions, constant support and encouragement during the course of my study.

This magnificent period would have been incomplete and tasteless without company of my TIET colleagues. I owe a word of thanks to my labmates ***Prerna, Jyotika, Purnima, Nirmalya***

Halder for their generous help and support in infinite number of ways every time and anytime. I appreciate my juniors ***Simarpreet, Ishtpreet***, ***Harmeet*** and friends ***Samriti Thakur, Ravneet Sidhu, Loveleen, Gurpreet, Vagish*** for their continuous support and encouragement.

Most of the work would have been incomplete without the sincere support of Lab assistants. So, I owe a word of thanks to ***Mr. Ram Newal (Babban ji)*** and all the ***non-teaching staff*** for helping and their ungrudging assistance.

I am very thankful to ***Mr. Inder Sain*** (Asst. Registrar), ***Mr. Vijay*** (Accountant) and ***Mrs. Manjula Kamra*** for their timely help and cooperation.

It is a blessing to have good friends around. I am indeed fortunate for having stress-busters whom we call "friends"- ***Dr. Sanchari Sircar, Dr. Anurag Dobhal, Dr. Ankush Masand, Kamal, Parambir***. Thank you for your support, motivation and words of encouragement. Words cannot express how indebted I am to ***Nupur Grover***, my bestie from last 13 years, who has been a source of love and energy ever since. Words fail to express my deepest gratitude to my sisters ***Ajmeet, Harneet, Gurman, Sarvansh*** for their all-time emotional support, constant care and love. Thank you everybody for being part of this journey and my life.

I find it difficult to pen down my deepest sense of indebtedness towards my beloved parents ***Dr***. ***Kashmir Singh*** and **Mrs.** ***Kulmeet Kaur*** who soulfully provided me their constant support and right impetus to undertake the challenge of this proportion like all other spheres of life, for what I cannot measure but treasure. I remember their constant support when I encountered difficulties during my research. Their encouragement never made me feel alone and only supported me to act high. They believed in me before I believed in myself. I highly appreciate unsolicited cooperation and cheery assistance of my loving brother SDE ***Khushwant Singh*****.** When I felt low and my enthusiasm waned, it was my family who helped me getting out of it, a deed that can never be paid back in feelings or words. To them, I owe my wonderful today and dream filled future. I consider myself luckiest in the world for the everlasting love and support of my ***maternal grandmother, my aunts*** and entire family standing behind me.

Last but not the least, I wish to acknowledge all those, whose names have not been figured here, but who helped me in any form during the period of my research work.

Date: December 21, 2020
Place: Patiala **(Ravneet Kaur)**

Dedicated to my

parents

&

loving brother



ABSTRACT

To combat crop loss due to pest infestation, pesticide application has become integral part of agriculture. Despite of benefits like improved crop yield and pest removal, frequent use and lack of timely degradation of pesticides has led to their persistence in the environment, worsening the soil quality, contaminating ground water, entering the food chain and affecting all living systems. The current study was aimed at screening of bacterial isolates capable of degrading butachlor and monocrotophos and synthesis of silver immobilized chitosan-PVA hydrogel nanocomposite (Ch/PVA-Ag) for their remediation under *in-vitro* conditions.

Degradation of monocrotophos and butachlor was carried out using 15 bacterial isolates, where maximum monocrotophos degradation was carried out by *Bacillus licheniformis* BPRIST030 (NA14), whereas, isolate A16 identified as *B. altitudinis* A16 by 16S rRNA sequencing showed maximum butachlor degradation. Monocrotophos spiked in Bushnell Hass broth was solely used as nutrient source by NA14, with increase in viable cell count from 0.8×10^6 to 54×10^{12} cfu ml^{-1} in 120 h. Monocrotophos degradation took longer in comparison to butachlor degradation by bacteria, as about 70% monocrotophos was degraded in 5 days. GC-MS analysis showed generation of five major metabolites including, dimethyl phosphate, phosphoric acid, malonic acid, dihydrazide, *N*-3-dimethylbut-2-enamide and N-methyl acetoacetamide. Based on the produced metabolites, a metabolic pathway was proposed.

Butachlor was utilised as a sole source of carbon by *B. altitudinis* A16 degrading 90% of 50 mg L^{-1} butachlor in 5 days at a rate constant and half-life ($t_{1/2}$) of 0.02 h^{-1} and 34.65 h, respectively, following the first-order reaction kinetics. Five metabolites (*N*-(butoxymethyl)-*N*-(2-chloroethyl)-2,6-diethylaniline, (*N*-(butoxymethyl)-2-chloro-*N*-(2-ethylphenyl) acetamide, *N*-(butoxymethyl)-2,6-diethyl-*N*-propylaniline, 2-chloro-*N*-(2,6-diethylphenyl) acetamide and 2,6-diethylaniline) were produced during the breakdown of butachlor by *B. altitudinis* A16 as identified by GC-MS analysis, which are further mineralized to carbon dioxide and water. A metabolic pathway was proposed and compared with other bacteria.

Silver nanoparticle (AgNP) incorporated chitosan-PVA (Ch/PVA) hydrogel nanocomposite was fabricated by repeated freeze-thaw treatment using glutaraldehyde as crosslinker for removal of herbicide butachlor from aqueous solution. Ch/PVA hydrogel acted as a nanoreactor in providing a matrix for *in-situ* immobilization of AgNPs and was characterized by FTIR, SEM-EDS, TEM, ICP-AES, XRD, XPS, TDA-DSC and BET analysis. Incorporation of AgNPs led to increase in thermal stability and surface area and possessed crystalline

structure with a size of about 5-20 nm. Effect of adsorption parameters such as pH, butachlor concentration, sorbent dosage, temperature and contact time on removal of butachlor was investigated. Comparative adsorption capacity of Ch/PVA hydrogel showed a maximum adsorption of 86.55%, while Ch/PVA-Ag showed an increased adsorption of about 96.87%. Linear and non-linear forms of Langmuir and Freundlich models with different error functions (R^2, R^2_{adj}, RSME, χ^2 and RSS) confirmed monolayer adsorption of butachlor, favouring linear Langmuir model.

Ch/PVA-Ag nanocomposite employed for adsorption-coupled-photocatalytic removal of butachlor proved to be a promising photocatalyst, degrading 85% of 10 mg L^{-1} butachlor in the presence of UV-light following first order kinetic model with a half-life of 114.54 min. Activity of nanocomposite hydrogel was due to synergism effect taking place between biopolymer nanocomposite hydrogel part acting as adsorbent and AgNPs as photocatalyst. Based on eight major metabolites ((1-(2-butoxy-7-ethyl-3-methylindolin-1-yl)propan-1-one, 1-(2-butoxy-7-ethyl-3-methylindolin-1-yl)ethenone, 3-(2,6-diethylphenyl)-1,3-oxazonan-4-one, 3-(2,6-diethylphenyl)-1,3-oxazonane, (((2,6-diethylphenyl)amino)methoxy)methanol, 2,6-diethyl-N-(hydroperoxymethyl)cyclohexa-2,4-dienamine, (E)-2,4,5-trihydroxypent-2-enoic acid and (Z)-penta-2,4-dienoic acid) obtained from LC-ESI-Q-TOF-MS analysis, a plausible degradation pathway was proposed. Reusability of nanocomposite and break-down of butachlor with no release of Ag ions in the solution makes it highly suitable for photocatalytic degradation of pesticides.

TABLE OF CONTENT

	Page No
Acknowledgement	**iii-v**
Abstract	**vi-vii**
Table of content	**viii-x**
List of Figures	**xi-xiii**
List of Tables	**xiv**
List of Abbreviations	**xv-xix**
List of Symbols	**xx**
Chapter I- Introduction	**1-2**
Chapter II- Review of Literature	**4-54**
2.1 Organophosphate insecticides	**4-24**
2.1.1 Monocrotophos	5
2.1.2 Distribution and fate of monocrotophos in environment	8
2.1.3 Toxicity of monocrotophos	9
2.1.4 Degradation of monocrotophos	11
2.1.5. Biodegradation of monocrotophos	12
Bacterial degradation of monocrotophos	12
Fungal degradation of monocrotophos	22
Algal degradation of monocrotophos	23
Factors affecting biodegradation of monocrotophos	23
2.2 Chloroacetanilide herbicides	**25-37**
2.2.1 Butachlor	25
2.2.2 Distribution and fate of butachlor	25
2.2.3 Toxicity and effects of butachlor	27
Microbial toxicity	27
Aquatic toxicity	28
Toxicity to mammals, frogs and earthworms	28
Phytotoxicity	29
Effect on soil microbial systems and enzymatic activity	29
2.2.4 Biodegradation of butachlor	31
Bacterial degradation of butachlor	31
Fungal degradation of butachlor	33
Algal degradation of butachlor	34
Products and metabolites of butachlor degradation	34
2.3 Nanotechnology in remediation	**38-54**
2.3.1 Nano-based approaches for pesticide degradation	40
2.3.1.1 Metal nanoparticles	40
Iron nanoparticles	40
Gold nanoparticles	45
Silver nanoparticles	45
2.3.1.2 Bimetallic nanoparticles	46
2.3.1.3 Metal oxide nanoparticles	47
Titanium oxide nanoparticles	47
Zinc oxide nanoparticles	47
Silica nanoparticles	48
Iron oxide nanoparticles	48
2.3.1.4 Nanotubes	49

Carbon nanotubes (CNTs) 49
Halloysite nanotubes (HNTs) 49
2.3.1.5 Nanocomposites 50
2.3.2. Chitosan based nanocomposites in nanoremediation 50
2.3.3 Hydrogel as an immobilizing matrix for nanoparticle synthesis 51
2.3.3.1 Fabrication of chitosan-based hydrogel 52
2.3.3.2 Silver nanoparticle-polymer hydrogel nanocomposite 52
2.3.3.3 Characterization of synthesized silver nanoparticles and chitosan-based hydrogel 52
2.4 Conclusion **54**
Objectives 54
Chapter III- Materials and methods **55-64**
3.1 Materials required **55-56**
3.1.1 Chemicals and glassware 55
General (analytical) chemicals 55
Bacteriological media 55
Bacterial strains 55
Glassware and plasticware 56
3.1.2 Sterilization techniques 56
3.2 Screening of bacterial isolates for degradation of pesticides **56-60**
3.2.1 Isolation of monocrotophos degrading bacteria 57
3.2.2 Biodegradation of monocrotophos by *Bacillus licheniformis* BPRIST030 and identification of metabolites 57
3.2.3 Isolation of butachlor degrading bacteria 58
3.2.4 Identification of bacterial isolate by 16S rRNA analysis 58
3.2.5 Biodegradation of butachlor by *Bacillus altitudinis* A16 59
3.2.6 Degradation Kinetics 59
3.2.7 Chemical analysis and identification of intermediates 60
3.3 Fabrication and characterization of hydrogel-nanoparticulate system for degradation of pesticide **60-62**
3.3.1 Preparation of crosslinked Chitosan/PVA hydrogel 60
3.3.2 Preparation of Ch/PVA-Ag Nanocomposite Hydrogels 61
3.3.3 Swelling studies of the crosslinked Ch/PVA hydrogel discs 61
3.3.4 Characterization and analysis of hydrogel composites 61
Surface morphology and size 61
Fourier transform infrared (FTIR) 62
X-ray diffraction (XRD) 62
X-ray photoelectron spectroscopy (XPS) 62
Thermal analysis and BET analysis 62
3.4 Removal of butachlor from synthetic water using hydrogel-nanoparticulate system **62-64**
3.4.1 Adsorption 62
3.4.2 Photocatalytic degradation 63
Chapter IV- Results & Discussion **65-116**
4.1 Screening of bacterial isolates for degradation of monocrotophos **65-74**
4.1.1 Biodegradation of monocrotophos by *Bacillus licheniformis* BPRIST030 and identification of the metabolites 67
4.1.2 Elucidation of metabolic pathway of monocrotophos degradation by *Bacillus licheniformis* BPRIST030 69
4.2 Screening of bacterial isolates for degradation of butachlor **75-76**

4.2.1 Degradation of butachlor by bacterial isolate A16 76
4.2.2 Butachlor degradation kinetics 80
4.2.3 Identification of metabolites and degradation pathway 81
4.3 Fabrication and characterization of hydrogel-nanoparticulate system for degradation of pesticide **86-95**
4.3.1 Fabrication of Ch/PVA hydrogel-nanoparticulate system 86
4.3.2 Swelling studies 87
4.3.3 Characterization and analysis of hydrogel composites 89
Structural and morphological properties 89
FTIR 91
XRD 92
XPS 92
Thermal behaviour and BET surface area analysis 93
4.4 Removal of butachlor from synthetic water using hydrogel-nanoparticulate system **96-116**
4.4.1 Removal of butachlor **96-98**
4.4.1.1 Effect of pH 98
4.4.1.2 Effect of sorbent dosage 100
4.4.1.3 Effect of initial concentration of butachlor 101
4.4.1.4 Effect of temperature 102
4.4.1.5 Effect of contact time 102
4.4.1.6 Adsorption isotherms 103
Langmuir isotherm 103
Freundlich isotherm 105
4.4.2 Photocatalytic degradation and kinetic studies **108-116**
4.4.2.1 Degradation pathway 110
4.4.2.2 Reusability 116
Summary **117-118**
Future scope of the work **119**
Salient Findings **120**
References **121-150**
List of publications **151**
Appendices **152-156**

LIST OF FIGURES

Figure	Description	Page no.
2.1	General structure of organophosphorous compounds	5
2.2	Proposed pathway of microbial degradation of monocrotophos	20
2.3	Chemical structure of butachlor	25
2.4	Proposed metabolic pathway of butachlor degradation by *Paracoccus* sp. FLY-8	35
2.5	Proposed degradation pathway of butachlor by *Catellibacterium caeni* sp. nov DCA-1^T	36
2.6	Proposed butachlor degradation pathway by syntrophic pair J7	36
2.7	Proposed metabolic pathway of butachlor by *Ammoniphilus* sp. JF	37
2.8	Classification of nanomaterials	38
2.9	Chemical structure of chitosan	51
2.10	Schematic representation of different characterization techniques	53
4.1	Tolerance of 500 mg L^{-1} monocrotophos by different bacterial isolates judged by zone of inhibition at 37 °C	65
4.2	Tolerance of bacterial isolates against of 500 mg L^{-1} monocrotophos as judged by Zone of inhibition on petri plates at 37 °C	66
4.3	Colony morphology of *Bacillus licheniformis* BPRIST030 (NA14)	67
4.4	Growth of *Bacillus licheniformis* BPRIST030 in 50 mg L^{-1} MCP supplemented BH media	68
4.5	GC-MS analysis of residual monocrotophos	69
4.6	Mass spectra analysis for peaks	70-72
4.7	Proposed possible metabolic pathways of monocrotophos degradation by *Bacillus licheniformis* BPRIST030	73
4.8	Tolerance of 64 mg L-1 butachlor by different bacterial isolates judged by zone of inhibition at 37 °C	75
4.9	Colony morphology of bacterial isolate *Bacillus altitudinis* A16	77
4.10	Neighbour- joining tree depicting the phylogenetic relationship between *Bacillus altitudinis* A16 with other related bacterial species based on 16S rRNA gene sequences	78

4.11	Change in absorption spectra of time course degradation of butachlor by *Bacillus altitudinis* A16	79
4.12	Growth of *Bacillus altitudinis* A16 in presence of 50 mg L^{-1} of butachlor in Bushnell Haas broth at different time intervals	79
4.13	Kinetic model fitting for rate of degradation of butachlor by strain A16	81
4.14	GC-MS analysis of residual butachlor	82
4.15	A mass spectra analysis for peaks	83
4.16	Proposed possible metabolic pathways of butachlor degradation by *Bacillus altitudinis* A16	85
4.17	Scheme for fabrication of Ch/PVA-Ag nanocomposite with *in situ* synthesis of AgNPs	86
4.18	a) Ch/PVA hydrogel, b) Ch/PVA hydrogel discs, c) Ch/PVA-Ag hydrogel and d) Ch/PVA-Ag hydrogel discs	87
4.19	SEM images of (a) chitosan, (b) PVA, (c) pure Ch/PVA hydrogel, (d) AgNP loaded Ch/PVA-Ag hydrogel, FE- SEM images of (e) pure Ch/PVA hydrogel and (f) AgNP loaded Ch/PVA-Ag hydrogel, (g) EDX spectra confirming presence of silver within the hydrogel, h) TEM image of synthesized AgNPs within the Ch/PVA-Ag hydrogel and (i-k) elemental mapping of Ch/PVA-Ag hydrogel	90
4.20	FTIR spectra of Ch/PVA hydrogel with and without AgNP loading	91
4.21	XRD a) chitosan b) PVA c) Ch/PVA hydrogel d) Ch/PVA-Ag hydrogel	92
4.22	XPS analysis	93
4.23	TGA and DTG curves for a) Ch/PVA and b) Ch/PVA-Ag hydrogel	94
4.24	BET analysis a) Nitrogen adsorption-desorption plots b) pore size distribution (BJH curve)	94
4.25	FTIR analysis of (a) Ch/PVA hydrogel and (b) Ch/PVA-Ag hydrogel, before and after adsorption of butachlor	96
4.26	Possible interaction between butachlor and the hydrogels	97-98
4.27	Effect of pH on butachlor removal	99
4.28	PZC plot for the hydrogels	99
4.29	Effect of sorbent dosage on butachlor removal	100

4.30	Effect of initial concentration on butachlor removal	101
4.31	Effect of temperature on butachlor removal	102
4.32	Effect of contact time on butachlor removal	103
4.33	Adsorption isotherms	105
4.34	(a) Adsorption coupled photocatalysis of butachlor, (b) UV-Vis spectra showing butachlor degradation	108
4.35	Degradation kinetics	109
4.36	LC-MS mass spectra of eight major metabolites	111-113
4.37	UV- induced degradation of butachlor by Ch/PVA-Ag hydrogel	115
4.38	Reusability of the Ch/PVA-Ag hydrogel	116

LIST OF TABLES

Table	Description	Page no.
2.1	Characteristics of monocrotophos	7
2.2	Degradation of monocrotophos by different bacteria, fungi and algae	14-19
2.3	Enzymatic degradation of monocrotophos	21
2.4	Physico-chemical properties of butachlor	26
2.5	Degradation of butachlor by bacteria	32
2.6	Different nanomaterials for detection of pesticides in different matrix	41
2.7	Different nanomaterials for removal of pesticides	42-43
2.8	Different nanomaterials for degradation of pesticides	44
3.1	Bacterial isolates used in the study	56
4.1	*In vitro* zone of inhibition activity of bacteria in the presence of 500 mg L^{-1} monocrotophos	66
4.2	Butachlor degradation (50 mg L^{-1}) by different bacteria	76
4.3	Kinetic models of butachlor degradation by *Bacillus altitudinis* A16	80
4.4	Swelling ratio of Ch/PVA hydrogel with different amount of chitosan, PVA and glutaraldehyde	88
4.5	Adsorption isotherm parameters for butachlor adsorption by Ch/PVA and Ch/PVA-Ag hydrogel	107
4.6	Kinetic models of photocatalytic degradation of butachlor by silver immobilized Ch/PVA-Ag hydrogel	110
4.7	Structures of butachlor intermediates detected by LC-ESI-Q-TOF-MS	115

LIST OF ABBREVATIONS

AChE	Acetylcholinesterase
$AgNO_3$	Silver nitrate
BCF	Bioconcentration factor
BET	Brunauer-Emmett-Teller
BH	Bushnell Haas
BJH	Barrett-Joyner-Halenda
BLAST	Basic Local Alignment Search Tool
BMTF-IL	1-butyl-3-methylimidazolium tetrafluoroboarte
BNP	Bimetallic nanoparticle
bp	Base pair
CB	Conduction band
cc g^{-1}	cubic centimeters per gram
CDEPA	2-chloro-*N*-(2,6-diethylphenyl) acetamide
C_e	Equilibrium concentration
cfu	Colony forming units
Ch/PVA	Chitosan- Polyvinyl alcohol
CIBRC	Central Insecticides Board and Registration Committee
CLT	chlorpyrifos-methyl
cm	centimeters
CNT	Carbon nanotube
CO_2	Carbon dioxide
CTAB	Cetyltrimethyl ammonium bromide
DDT	Dichlorodiphenyl trichloroethane
DLS	Dynamic light scattering
DNA	Deoxyribonucleic acid
dNTP	Deoxynucleoside triphosphate
DRS	Diffuse Reflectance Spectroscopy
DSC	Differential scanning calorimetry
DW	Dry weight
EDS/EDX	Energy Dispersive X-Ray Spectroscopy
EPA	Environment Protection Agency

ESI	Electrospray ionization
et al	And others
etc	And other things
FCC	Face centered cubic
FNT	Fenitrothion
FTIR	Fourier transform infrared spectroscopy
g	Gram
g cm^{-1}	Gram per centimetre
g kg^{-1}	Gram per kilogram
g L^{-1}	Gram per liter
g mol^{-1}	Gram per mole
GC-MS	Gas chromatography–mass spectrometry
GNP	Gold nanoparticle
h	Hour
H_2O	Water
H_2SO_4	Sulfuric acid
HCl	Hydrochloric acid
HNT	Halloysite nanotube
HPLC	High performance liquid chromatography
IC_{50}	Half maximal inhibitory concentration
ICDD	The International Centre for Diffraction Data
ICP-AES	Inductively coupled plasma atomic emission spectroscopy
k	Rate constant
kDa	kilodalton
kg	Kilogram
kg. a.i. ha^{-1}	kilograms of active ingredient per hectare
kg. ha^{-1}	Kilogram per hectare
KH_2PO_4	Potassium dihydrogen phosphate
L h^{-1}	Liter per hour
LC-ESI-Q-TOF-MS	Liquid Chromatography -electrospray ionization quadrupole time-of-flight mass spectrometry
LD_{50}	Median lethal dose
MCP	Monocrotophos

MEGA X	Molecular Evolutionary Genetics Analysis X
mg g^{-1}	milligram per gram
mg kg^{-1}	milligram per kilogram
mg L^{-1}	milligram per litre
MHA	Mueller hinton Agar
min	Minute
mL	Milliliter
mL ha^{-1}	Milliliter per hactare
mm	Millimeter
mM	Millimolar
MRL	Maximum residue limit
mRNA	Messenger RNA
MTCC	Microbial Type Culture Collection and Gene Bank
MWCNTs	Multi walled carbon nanotubes
N	Normal
NA	Nutrient Agar
$NaBH_4$	Sodium borohydride
NaOH	Sodium hydroxide
NB	Nutrient broth
NCBI	National centre for biotechnology information
ng	Nanogram
ng g^{-1}	Nanogram per gram
ng mL^{-1}	Nanogram per milliter
NIST	National Institute of Standards and Technology
nm	Nanometer
NM	nanomaterial
NP	Nanoparticle
OD	Optical Density
OP	Organophosphorus
Pa	Pascal
PCR	Polymerase chain reaction
pI	Isoelectric point
ppm	Parts per million

PTE	Phosphotriesterase
PZC	Point of zero charge
q_e	Sorption capacity
R^2	Regression coefficient
R^2_{adj}	Adjusted R-squared
RAPD	Random amplified polymorphic DNA
RB	Rhodamine B
RBC	Red blood cell
rGO	Reduced graphene oxide
RMSE	Root-mean square error
rpm	Revolution per minute
rRNA	Ribosomal ribonucleic acid
RSS	Residual sum of squares
RT	Retention time
s	Second
SEM	Scanning electron microscopy
SiO_2 NP	Silica nanoparticle
SWCNTs	Single walled carbon nanotubes
$t_{1/2}$	Half-life
TCh	thiocholine
TEM	Transmission electron microscopy
TGA	Thermo gravimetric analysis
TiO_2	Titanium dioxide
TPF	triphenyl formazan
US	United States
UV	Ultra violet
VB	Valence band
viz.	As follows
WBC	White blood cell
WW	Wet weight
XPS	X-ray photoelectron spectroscopy
XRD	X-ray diffraction
ZnO	Zinc oxide

ZOH	Zone of inhibition
ZV-FeNP	Zero- valent iron nanoparticles
α-Fe_2O_3	Hematite
β-Fe_2O_3	Maghemite
γ-Fe_2O_3	Magnetite
μg	Microgram
$\mu g\ g^{-1}$	Microgram per gram
$\mu g\ kg^{-1}$	Microgram per kilogram
$\mu g\ L^{-1}$	Microgram per liter
$\mu g\ mL^{-1}$	Microgram per milliliter
μL	Microliter
μm	Micrometer
χ^2	Reduced Chi-square

LIST OF SYMBOLS

%	Percentage
μ	Micron
Da	Dalton
L	Litre
M	Molar
K	Kelvin
v/v	Volume by volume
w/v	Weight by volume
β	Beta
°C	Degree Celsius
θ	Angle
C	Carbon
H	Hydrogen
N	Nitrogen
O	Oxygen
P	Phosphorus
Hg	Mercury
α	Alpha
γ	Gamma
Pd	Palladium
Fe	Iron
Ni	Nickel
Pt	Platinum
Zn	Zinc
Ag	Silver
Au	Gold
λ	Lambda
Cu	copper
π	pi

Chapter I- Introduction

Industrialization and intensive agricultural activities have led to tremendous increase in global environmental pollution, where pesticides hold a very important position (Abigail et al., 2015). Pesticides are agrochemicals that eliminate, repel or prevent the growth and multiplication of pests such as insects, rodents, nematodes, bacterial and fungal pathogens and weeds, which causes harm to crop plants and agricultural produce. Statistical data shows an annual crop loss of more than Rs 6,000 crores in India, where weeds, insects, birds and rodents are responsible for 33%, 20% and 10% crop loss, respectively (Rani and Dhania, 2014). To overcome these losses, ≈ 0.6 kg ha^{-1} of pesticides are used in India (Roy et al., 2014) for crop protection, of which only 0.1% of the overall pesticide used acts on its target, whereas rest remains in the soil. This worsens the soil quality and contaminates ground water and persists in the environment and enters the food chain affecting all living systems (Sharma et al., 2020). Their fate is governed by different factors, that determine their persistence, mobility and potential for volatilization, leaching, run-off or plant uptake. These factors include properties of pesticide such as soil adsorption, water solubility and half-life and physicochemical properties of a soil such as texture, pH, depth, slope and permeability. Interaction of all these factors along with environmental conditions determines the fate and behaviour of a pesticide (Gavrilescu 2005; Pam 2015). As per Environment Protection Agency (EPA) report published in 1990, more than 50% of the water pollution occurs due to leaching, improper disposal in water systems and agricultural run-off (Agrawal et al., 2010; Dwivedi et al., 2014), posing threat to non- target organisms, including humans; causing skin disorders, cardiopulmonary, neurological problems, alterations in reproductive systems along with miscarriages, and these accumulated pesticide residues may be carcinogenic ultimately leading to death (Singh et al., 2016; Kaur and Goyal, 2019).

Different methods such as advanced oxidation processes, solid phase extraction, ion-exchange, adsorption, photocatalytic methods and bioremediation have been employed for the removal of pesticides (Dwivedi et al., 2014). Bioremediation involving diverse microbial systems plays a vital role in breakdown of synthetic organic compounds or xenobiotics present in the environment by utilizing them as carbon and energy source (Delgado et al., 2014). Microbial enzymes break down complex toxic pesticides into simpler and less toxic compounds (Kalyani et al., 2009; Verma et al., 2014), making biodegradation as one of the best, eco-friendly, less

hazardous and economically viable option for clean-up of harmful organo-chemicals. Several bacterial species such as *Bacillus*, *Flavobacterium*, *Azotobacter*, *Pseudomonas*, *Arthrobacter* etc. have effectively been utilized for degradation of different classes of pesticides, where degradation varies depending upon nature of target compound and the soil microbial diversity (Chaudhry et al., 2013; Verma et al., 2014; Patil et al., 2018; Phale et al., 2020).

Nanotechnology is an emerging field which has proven its effectiveness in several areas such as, pharmaceuticals, tissue engineering, agriculture and regenerative medicines (Hasnain et al., 2013), where because of small dimensions and large surface area to volume ratio, nanomaterials exhibit unique physical and chemical properties (Dehaghi et al., 2014). Due to several disadvantages (poor efficiency, high operational cost, generation of secondary waste and use of harsh chemicals) associated with several remediation techniques such as advanced oxidation processes, solid phase extraction, ion exchange etc., it is necessary to implement an effective method for pesticide removal which is highly efficient and environment friendly. Attention has been focused on use of nanomaterials or nanocomposites for adsorption or degradation of pesticides using several bio sorbents and/or their composites owing to their high efficiency, biocompatible nature and cost effectiveness (Dwivedi et al., 2014; Haq et al., 2019; Jiang et al., 2021). Biosorbents and their nano-composites such as mangosteen and rambutan peel (Ahmad and Alrozi, 2010; 2011), pistachio shell (Dolas et al., 2011), chitosan-gold nanoparticles (Dwivedi et al., 2014), chitosan zinc oxide nanoparticle composite (Dehaghi et al., 2014) and cantaloupe seed shell powder (Haq et al., 2019) have been utilized for the elimination of pollutants from the environment. Various other bio-materials such as bio-waste, chickpea, cotton stalk, olive stones and biomass have also been reported for pesticide removal (Ayranci and Hoda, 2005; Zhu et al., 2005).

Chitosan in the hydrogel or beads form have gathered significant attention (Dwivedi et al., 2014; Dehaghi et al., 2014). Chitosan (β-1,4-linked polysaccharide) is a cationic polymer produced in bulk from chitin (crustaceans shells) as a by-product (Agnihotri et al., 2012; Gholamali et al., 2020) and has extraordinary properties such as gel forming capability, low toxicity, biodegradability, biocompatibility, eco-friendliness and high adsorption capacity (Agnihotri et al., 2012; Habiba et al., 2019), which is attributed to amino and hydroxyl groups present on the glucosamine unit (Dwivedi et al., 2014). To enhance the adsorption properties and complete elimination of the contaminants, nanoparticles are incorporated within the crosslinked and swollen networks to form nanocomposite hydrogels (Habiba et al., 2019; Gholamali et al., 2020).

Monocrotophos, an organophosphate insecticide, is a nonspecific, systemic foliar insecticide used to protect crops from insects such as leaf hoppers, ticks, mites and aphids (Singh and Walker, 2006). It accounts for a total sale of roughly 3% of all the insecticides (Jia et al., 2006; Barathidasan and Reetha, 2013). European Union and the U.S. have withdrawn the product for use, in India despite its ban, it is still being used on large variety of crops and vegetables owing to its high efficiency in controlling pests, low cost and lack of alternative replacements (Kaur and Goyal, 2019). It has a half-life of 17-96 days depending upon pH and temperature (Mackay et al., 2006) and is readily soluble in water with 100% solubility but due to its hydrophilic character it is weakly adsorbed by soil particles, causing groundwater contamination because of leaching (Kaur and Goyal, 2019). It is classified as class (I) highly toxic compound by EPA (Sidhu et al., 2015), with median lethal dose (LD_{50}) of 18-20 mg kg^{-1} for mammals (Singh and Walker, 2006) and 0.9-6.5 mg kg^{-1} for birds (Goldstein et al., 1999).

Another harmful pesticide, butachlor is a chloroacetamide pre-emergence herbicide, with an annual utilization rate of about 4.5×10^7 kg in Asia, where India accounts for approximately 6.75×10^6 kg of its annual usage (Kaur and Goyal, 2020). It has a half-life of 1.6 to 29 days, however, under certain conditions such as high alkalinity, lack of bio-degraders, low temperature and moisture, butachlor persists in soil and remains biologically active for a longer time period (Kaur et al., 2017a). It has been detected in soil, surface and underground water with residual concentrations ranging from 29.5 - 74 µg kg^{-1} in soil (Yang et al., 2010) and 0.1 - 1.4 µg L^{-1} in surface water (Mamun et al., 2009), respectively, and persists in the environment causing toxic effect on living systems. It is suspected to be carcinogenic in nature, known to induce malignant transformation *in vitro* by stimulating cell proliferation, mitochondrial dysfunction, chromosomal breakage, oxidative DNA damage and disrupting endocrine system. Several reports suggest butachlor to be a neurotoxin and growth retardant in earthworms (Kaur and Goyal, 2020).

The rationale of current research work was screening of bacterial isolates capable of effectively utilizing butachlor and monocrotophos as nutrient/energy source and synthesis of chitosan hydrogel nanocomposites for their remediation. Degradation of monocrotophos by different bacterial isolates was studied and reviewed. Bioremediation of butachlor by a Gram-positive bacterial isolate from coal tar contaminated soil was studied and metabolites of degradation were identified and a plausible degradation pathway is proposed.

Chapter II- Review of Literature

Pesticide application has become integral part of agriculture for improving crop yield by removing or killing pests that causes harm to crop plants. Pesticides may be specific or non-specific, synthetic or non-synthetic and are classified in a number of ways based on usage, mode of action, toxicity, chemical structure and formulations. Based on chemical property and mode of action, pesticides may act as fungicides (kills parasitic fungi and spores), rodenticides (kills rodents), herbicides (kills unwanted herbs/plants) and insecticides (kills or repels insects). The frequent, intense use and lack of timely degradation of these pesticides has led to their persistence in the environment causing adverse effects on non-target organisms (Sood et al., 2011; Verma et al., 2014). Certain pesticides have been detected in groundwater, surface water, soil, ambient air, coastal fog, aquatic animals, umbilical cord blood, human blood and breast milk, and several foods (Sharma et al., 2015). Once a pesticide enters the environment, it keeps transforming from one form to another, based on the environmental conditions and its chemical nature. Chloroacetanilide herbicides, organophosphorus and organochlorine pesticides are the largely used pesticides in present day agriculture. Removal of organophosphorus insecticide monocrotophos and chloroacetanilide herbicide butachlor has been extensively studied in the present work.

2.1 Organophosphate insecticides

Organophosphorus compounds have been extensively used in agriculture worldwide for more than 40 years due to their high effectiveness (Karpouzas and Singh, 2006; Abraham and Silambarasan, 2015), broad-spectrum action against various pests and biodegradability. They account for approximately 30-34% of total world insecticide market (Singh and Walker, 2006; Iyer et al., 2013) and are used in agriculture to combat crop pests, in domestic to control mosquitoes and other insects and in veterinary to control mites and flies of cattle. Although organophosphates are biodegradable, their environmental exposure causes acute and chronic toxicity to mammals and other non-target organisms (Gill et al., 2018). Organophosphate (OP) poisoning in humans may cause diarrhoea, vomiting, general weakness, nausea, tremors, salivation, and respiratory failure in severe cases, causing death of the person (Kanekar et al., 2004; Deng et al., 2015). Yearly data of several developing countries indicates that OPs are responsible for approximately 3 million poisonings with 2,00,000 human deaths (Ragnarsdottir 2000; Karpouzas and Singh, 2006).

OP pesticides were first introduced in the form of tetraethyl pyrophosphate during the World War II in Germany, as a by-product of nerve gas development (Kanekar et al., 2004). They are thiols or esters of phosphinic, phosphonic, phosphoric or phosphoramidic acid. Chemically organophosphates have aryl or alkyl group (R_1 and R_2), which are either directly bonded to the phosphorus atom (forming phosphinates), or through sulphur or an oxygen atom (forming phosphothioates or phosphates) (Fig. 2.1). At least one of the groups is $–NH_2$ in phosphoramidates, which may be mono- or bi-substituted. Phosphorus shares double bond with either sulphur or oxygen. Finally, X group, which is a ‘‘leaving group’’ (as it is released upon hydrolysis of organophosphates), may be a halogen, aromatic, aliphatic or heterocyclic group (Sogorb and Vilanova, 2002).

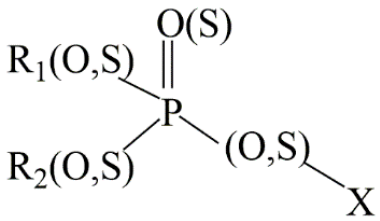


Fig. 2.1: General structure of organophosphorous compounds

2.1.1 Monocrotophos

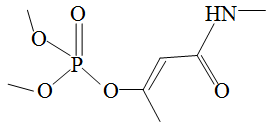
Monocrotophos, a dimethyl oxon compound sold under trade names Azodrin, Apadrin, Pillardrin, Plantdrin, Crisodrin, Nuvacron, Monocron, and Bilobran is a commonly used organophosphorus insecticide and acaricide (Mackay et al., 2006; Jose et al., 2015). It is a nonspecific, systemic foliar insecticide used to protect crops from insects such as leaf hoppers, mites, aphids and ticks (Singh and Walker, 2006). It was first produced in 1965 by Ciba AG and Shell Development Co. and is registered in about 60 countries including Spain, France, Italy, Austria, and Greece. It accounts for a total sale of roughly 3% of all the insecticides (Jia et al., 2006; Barathidasan and Reetha, 2013). Statistical data indicates Asia being the top user of insecticide monocrotophos, where countries like India (43%), South America (26%), China (15%), and Southeast Asia (9%) account for 90% usage (Kumar et al., 2014). In India, monocrotophos is registered for 14 crops by Central Insecticides Board and Registration Committee (CIBRC) (Bhushan et al., 2013) and the states of Punjab and Andhra Pradesh are the chief consumers of monocrotophos (Kumar et al., 2014). However, European Union and the U.S. have withdrawn the product for use, in India despite its ban, it is still being used on

large variety of crops and vegetables owing to its high efficiency in controlling pests, low cost and lack of alternative replacements. (Kodandaram et al., 2013; Sidhu et al., 2015).

Monocrotophos refers to a cis-isomer with its nomenclature based on its crotonamide structure. The technical grade monocrotophos contains 75-80 % of the cis-isomer and 9% of the trans-isomer along with a range of compounds including *N*-methyl acetoacetamide (2%) and dimethyl phosphate (5%) (Beynon et al., 1973). Trimethyl phosphate and mono-chloro-monomethyl acetoacetamide are also used for manufacturing monocrotophos (Bhadbhade et al., 2002b).

Monocrotophos (dimethyl (E)-1-methyl-2-(2-methylcarbamoyl) vinyl phosphate) is colourless in its pure form and its technical grade exists as reddish- brown solid/ liquid state (Mackay et al., 2006) (Table 2.1). It is classified as class (I) highly toxic compound by the EPA (Sidhu et al., 2015). Monocrotophos is readily soluble in water with 100% solubility (Subhas and Singh, 2003; Mackay et al., 2006), causing groundwater contamination due to leaching. It has a half-life of 17-96 days depending upon pH and temperature (Mackay et al., 2006). When stored in polyethylene and glass containers, technical grade monocrotophos is stable and has half-life of 2500 days at 38 ºC (JMPR 1972). The formulation of monocrotophos registered in India is 36% SL (Kodandaram et al., 2013) with application rates 0.25-1.5 kg ha^{-1} for cotton (Beynon et al., 1973).

Table 2.1. Characteristics of monocrotophos

S. No.	Properties	Values
1	Common name	Monocrotophos
2	IUPAC name	dimethyl (E)-1-methyl-2-(2-methylcarbamoyl)vinyl phosphate
3	CAS Registry No.	6923-22-4
4	Molecular weight	223.164 g mol^{-1}
5	Structural formula	
6	Molecular formula	$C_7H_{14}NO_5P$
7	Colour	Colorless (Pure) Reddish-brown solid and liquid (Technical grade)
8	Odour	Mild ester like
9	Density at 20 °C (g cm^{-3})	1.22
10	Boiling Point (°C)	125
11	Melting Point (°C)	Pure: 54-55; Technical: 25-30
12	Henry's Law Constant at 25°C ($Pa \cdot m^3$ mol^{-1})	2.08×10^{-6}
13	Vapour pressure at 25°C (Pa)	9.33×10^{-3}
14	Hexane/Water Partition Coefficient	<0.1
15	Octanol/Water Partition Coefficient (log K_{OW})	-1.97 to - 0.2
16	Solubility (20 ºC)	
	Water	1 kg kg^{-1}
	Acetone	700 g kg^{-1}
	Dichloromethane	800 g kg^{-1}
	Methanol	1 kg kg^{-1}
	Octan-1-ol	250 g kg^{-1}
	Toluene	60 g kg^{-1}
17	Stability	Stable on storage in polyethylene and glass containers. Half-life at 20°C at different pH: pH 5- 96 days pH 7- 66 days pH 9- 17 days Half-life in soil- 30 days
18	Acute oral LD_{50}:	
	male rats	17-18 mg kg^{-1}
	female rats	20 mg kg^{-1}

Source: Kaur and Goyal, 2019

2.1.2 Distribution and fate of monocrotophos in environment

With regular field application of pesticides, they persist in soil and sediments and even percolate to the ground/surface water and enters the food chain directly or indirectly. Their fate is governed by different factors, which determines their persistence, mobility, and potential for volatilization, leaching, run-off or plant uptake (Gavrilescu 2005; Pam 2015). These factors include properties of pesticide such as soil adsorption, water solubility, and half-life and physico-chemical properties of soil such as texture, pH, depth, slope and permeability. Interaction of all these factors along with environmental conditions, determine the fate and behaviour of a pesticide (Gavrilescu 2005; Megharaj et al, 2011; Yang et al., 2018).

Monocrotophos is a fast-acting and extremely toxic cholinesterase inhibiting organophosphorus insecticide (Bhadbhade et al., 2002c; Sidhu et al., 2015). Being readily water soluble and highly mobile in soil, it quickly contaminates groundwater and penetrates into plant tissues, hence making its removal impossible (Tomlin 1994; Balamurugan et al., 2010; Barathidasan and Reetha, 2013). In a study conducted by Imran et al. (2016), less than 0.02 mg L^{-1} monocrotophos residues were found in all 106 samples of different paddy varieties. Among 50 samples analyzed, monocrotophos was detected in 2 samples each of eggplant and tomatoes at mean concentrations of 0.060 ± 0.022 mg kg^{-1} and 0.063 mg kg^{-1}, respectively (Darko and Akoto, 2008). Residues of monocrotophos were found in different fruits such as apple, grapes, mango and melon (Hussain et al., 2002; Asi 2003; Khan 2005), vegetables (Asi 2003; Parveen et al., 2005; Khan 2005) and green tea (Huang et al., 2019). In another study, 0.6748- 1.3648 mg kg^{-1} of monocrotophos residues (above maximum residue limit 0.2 mg kg^{-1}) were detected in market samples of grapes (Reddy et al., 2000). In the United States of America and Europe, organophosphates are one of the causes reported for intoxication of wild birds due to ingestion of grains treated with insecticides. A study conducted on total of 182 dead birds from 2010-2013 revealed the presence of 0.6- 7557 mg kg^{-1} of monocrotophos in 57 dead birds (Kim et al., 2016).

Being readily soluble in water, it easily gains entry to water sources or industrial effluents during manufacturing process, which has led to several incidents of monocrotophos contamination. Waste effluent of monocrotophos manufacturing factory near Pune, India contained 0-125 mg L^{-1} monocrotophos (Bhadbhade et al., 2002c). In other studies, 4 µg L^{-1} and 0.165 µg L^{-1} of monocrotophos residues were detected in rain water (Kumari et al., 2007) and tap water in China (Kang et al., 2000). Tariq et al. (2004) reported the presence of upto 8.3

µg L^{-1} monocrotophos in shallow well water samples collected from four cotton-growing districts in Pakistan. Several cases of presence of monocrotophos above the maximum residue limits (MRL) have been reported (Sawaya et al., 1999; Kumari et al., 2004). Monocrotophos residues were found at a mean concentration of 0.063 ± 0.022 mg kg^{-1} in tomatoes (Darko and Akoto, 2008). In a study conducted by Arora (2009), 0.4 mg kg^{-1} monocrotophos was reported in okra samples. The residues were also detected at a mean concentration level of 1.63 ng g^{-1} in human breast milk (Sharma et al., 2014). Monocrotophos residues at an average concentration of 0.79 ng mL^{-1} in human blood (Sharma et al., 2015) poses high risk. Owing to the toxicity and its persistent nature, it is necessary to eliminate monocrotophos from the environment. Current review summarizes and presents assessment of various studies and reports on monocrotophos, its fate in the environment, quantification of its toxicity and degradation.

2.1.3 Toxicity of monocrotophos

Monocrotophos dose that kills half of the test organisms, i.e. half maximal inhibitory concentration (IC_{50}) for male and female rats is 17-18 mg kg^{-1} and 20 mg kg^{-1}, respectively. The IC_{50} value for dermal exposure for male rats, female rats and rabbits is 126 mg kg^{-1}, 112 mg kg^{-1}, and 354 mg kg^{-1}, respectively (Chakravarthi et al., 2009). In India, monocrotophos has been used as intentional self-harm chemical for committing suicides (Rao et al., 2005a).

Monocrotophos poisoning in human beings causes small pupils, blurred vision, vomiting, muscular weakness, confusion, profuse perspiration, and even death because of respiratory failure (Yaduvanshi et al., 2010). Most of the monocrotophos's toxicity and mutagenicity studies in humans have been conducted using cultured blood lymphocytes. Tripathi et al. (2017) studied the neurotoxic effects of monocrotophos on cultured neural and glial cells, where monocrotophos exposure triggered the apoptotic cell death. Comet assay conducted using cultured human blood lymphocytes revealed that monocrotophos exposure led to DNA damage due to increase in comet tail length indicating monocrotophos capable of altering the genetic material (Jamil et al., 2004; Das et al., 2006; Chakravarthi et al., 2009). Banu et al. (2001) reported similar results in mice model. Monocrotophos induced oxidative DNA damage along with lipid peroxidation in rat tissues (Yaduvanshi et al., 2010). Zahran et al. (2005) reported induction of structural and numerical chromosomal mutations in both germ and somatic cells of male liver and embryos of pregnant mice on monocrotophos exposure, confirming its mutagenic action. It exerts neurobehavioral effects in rodents by affecting their

noncholinergic functions that involve serotonergic and dopaminergic systems associated with increased oxidative stress (Mandhane et al., 1995; Sankhwar et al., 2016). Monocrotophos treatment caused an increase in WBC count along with mutagenicity in birds and male rats (Siddiqui et al., 1991; Siddiqui et al., 1993) and induced bone marrow depression along with splenic hyperplasia, which caused significant decrease in haemoglobin count, total RBC and platelet count, erythrocyte sedimentation rate and haematocrit value in mice (Gupta et al., 1982).

Earlier studies revealed exposure of monocrotophos induced transient hyperglycemia in rats in acute conditions (Joshi and Rajini, 2012; Velmurugan et al., 2013; Nagaraju et al., 2015). It also led to an increase in the weight of key white adipose pads, pancreatic islet diameter, and activity of enzymes involved in gluconeogenesis; thereby causing hyperglycemia, hyperinsulinemia, and dyslipidaemia (Nagaraju et al., 2015). Findings of the same group indicated the probability of beta-cell compensation responses under monocrotophos exposure (Nagaraju and Rajini, 2016). Velmurugan et al. (2013) studied the cardiotoxicology of prolonged monocrotophos intake. Wister rats administered orally with $1/50^{th}$ of lethal dosage of monocrotophos exhibited mild cardiac oxidative stress leading to cardiotoxicity, which was evidenced by the accumulation of lipid peroxidation, protein carbonyls, and glutathione production.

Monocrotophos has histopathological effect on kidney, liver, and muscles of both fish and rats, which were studied on the tissues of kidney, gills and intestines of fish *Cirrhinus mrigala* by light microscopy (Velmurugan et al., 2007). Cytotoxic effects of monocrotophos on different aquatic organisms have also been widely studied (Agrahari et al., 2007; Anbumani and Mohankumar, 2015; Binukumari et al., 2016; Mundhe et al., 2016; Zhang et al., 2017).

Monocrotophos is a potential endocrine-disrupting chemical with significant estrogenic properties, which significantly induces both secretion and vitellogenin mRNA expression in male Goldfish (Tian et al., 2009a). Estrogenic effects of monocrotophos are exerted *via* affecting the reproductive axis at multiple spots leading to increased 17β-estradiol plasma levels and decreased concentrations of plasma testosterone (Tian et al., 2010). This caused severe reproductive abnormalities in fish *Poecilia reticulata* (Tian et al., 2012). It is genotoxic to *Meretrix* ovum and induces retardation of somatic growth of the mussel (Revankar and Shyama, 2009).

Monocrotophos has proved to be extremely toxic to birds. Monocrotophos contamination was held responsible for mass deaths of raptors, owls, Swainson's hawks (*Buteo swainsoni*), Sarus cranes (*Grus antigon*) and peafowls reported in different regions of the world (Mendelssohn and Paz, 1977; Goldstein et al., 1999; Pain et al., 2004; Narang et al., 2016). Prolonged exposure of monocrotophos is also toxic to termites (Rao et al., 2005b), earthworms (Rao and Kavitha, 2004; Govindarajan 2014) and roundworms (Salim and Rajini, 2017).

2.1.4 Degradation of monocrotophos

Monocrotophos reaches the aquatic system and soil directly or indirectly, upon its application to the target crops, where it undergoes degradation by various chemical, photochemical and microbiological processes. Degradation is also influenced by various processes as volatilization, adsorption/desorption, leaching, runoff, plant and aquatic life uptake.

To investigate degradation behaviour of monocrotophos in soil, various experiments were conducted on different types of soil under anaerobic and aerobic conditions. On application of 1.5 kg a.i. ha^{-1} of 5% granular monocrotophos formulation to clay soil (Agnihotri et al., 1981), it rapidly disappeared from 0-15 cm soil layer, estimating a half-life of 10.3 days. Small traces were also detected in 15-30 cm layer due to its vertical movement but 45 days after the treatment, no detectable residues were found. Gundi and Reddy (2006) studied degradation of 10 and 100 µg g^{-1} monocrotophos in two Indian agricultural soils (black vertisol and red alfinsol) at 60% water-holding capacity, under aerobic conditions. The degradation in both the soil samples was rapid and accounted for 96–98% of the total application with half-lives 9.2 and 11.4 days, respectively, following first-order kinetics. Metabolism studies of ^{14}C-radiolabeled monocrotophos showed its rapid decomposition into *N*-methylacetoacetamide, O-desmethylmonocrotophos, 3-hydroxy-*N*-methylbutyramide, *N*-(hydroxymethyl) monocrotophos, mono methyl, and dimethyl phosphates and $^{14}CO_2$ (Dutton et al., 1974; Lee et al., 1990).

Monocrotophos degradation is greatly affected by presence and absence of soil microbial biomass. Decrease in degradation rate was observed in soils that were either air-dried (Schuler and Held, 1964) or sterilized (Lee et al., 1980), indicating absence or reduction of microbial biomass decreases rate of monocrotophos degradation in soil. Anaerobic conditions also decreased the rate of degradation with a half-life time of approximately 8 days compared with

a 4 days half-life under aerobic conditions in the same soil (Hernandez et al., 1986; Lee et al., 1990).

2.1.5. Biodegradation of monocrotophos

Microbial diversity plays a significant role in degradation of synthetic contaminants present in the environment by utilizing them as carbon and energy source (Balagurusamy 2005; Rodrigues et al., 2009). Monocrotophos is characterized by an amide bond and P-O-C linkage. It has been reported to be utilized as sole source of carbon or phosphorus in soil or aqueous medium (Singh and Walker, 2006; Abraham and Silambarasan, 2015). Monocrotophos degradation using the different soil microflora has been widely studied in several enrichment cultures (Table 2.2).

Bacterial degradation of monocrotophos

Several bacterial species showing capability to utilize monocrotophos as nutrient source and degrading it in liquid medium or soil have been isolated and characterized. Monocrotophos metabolization by different bacteria has been reported through catabolic mechanisms, where monocrotophos provides carbon or phosphorus source to the degrading micro-organisms (Singh and Walker, 2006). It acts as carbon source for *Pseudomonas* sp., *Arthrobacter* sp., *Arthrobacter atrocyaneus*, *Bacillus megaterium* (Bhadbhade et al., 2002b) and as phosphorus source for *Clavibacter michiganense* SBL11 and *Pseudomonas aeruginosa* F10B (Subhas and Singh, 2003).

In several studies, microbes have been employed for the degradation of monocrotophos (Table 2.2). Due to presence of novel catabolic enzymes, bacteria can survive in diverse ecological niches. *Rhodococcus phenolicus* strain MCP1 along with *Rhodococcus ruber* strain MCP-2, isolated from groundnut soils were able to utilize monocrotophos as a carbon source by hydrolysis leading to the formation of *N*-methylacetoacetamide, indicating the decomposition of parent compound (Srinivasulu et al., 2017). Different *Bacillus* sp. including *Bacillus licheniformis*, *Bacillus subtilis* (Acharya et al., 2015; Sidhu et al., 2015; Buvaneswari et al., 2017), *Bacillus coagulans*, *Bacillus brevis* (Bhadbhade et al., 2002a), *Bacillus megaterium* MCM B-423 (Bhadbhade et al., 2002b) and *Lactobacillus bulgaricus* (Zhao and Wang, 2012) have been widely studied to metabolize monocrotophos present in soil. Degradation of monocrotophos by various *Pseudomonas* strains viz. *Pseudomonas stutzeri* (Barathidasan and Reetha, 2013; Buvaneswari et al., 2017), *Pseudomonas moraviensis* JAS18 (Abraham et al.,

2014), *Pseudomonas synxantha* (Sidhu et al., 2015), *Pseudomonas aeruginosa* (Subhas and Singh, 2003; Balamurugan et al., 2010) and *Pseudomonas mendocina* (Bhadbhade et al., 2002a) has been widely reported.

Serratia marsescens JAS16 isolated from prolonged exposure of soil to monocrotophos was able to use it as carbon source and degraded 1000 mg L^{-1} of the insecticide in aqueous medium at a degradation rate constant of 136 per day with a half-life of 3.7 days. Degradation rate constant in soil inoculated with bacteria was 105 per day with a half-life of 4.8 days. The bacteria could tolerate 1200 mg L^{-1} of the insecticide. Phytotoxicity of degraded metabolites to seeds of *Vigna unguiculata*, *Vigna radiata* and *Macrotyloma uniflorum* and its genotoxicity to *Allium cepa* bulbs were found to be low (Abraham and Silambarasan, 2015). Another bacterial isolate, YW6 characterized as *Starkeya novella* could utilize monocrotophos for its growth as the sole carbon and nitrogen source. Within 36 h, it degraded 0.2 mM monocrotophos with no lag period. The initial rate of monocrotophos degradation was slowed down by addition of carbon source, whereas the presence of a more favorable nitrogen source enhanced the degradation of monocrotophos (Sun et al., 2016). In another research, *Paracoccus* sp. M1 was able to mineralize 300 mg L^{-1} of monocrotophos along with other organophosphorus insecticides and amide herbicides under different culture conditions. The key enzyme responsible for the initial break down of monocrotophos was a constitutively expressed cytosolic protein (Jia et al., 2006).

Subhas and Singh (2003) studied two bacterial isolates *Pseudomonas aeruginosa* F10B and *Clavibacter michiganense* subsp. *insidiosum* SBL 11 capable of degrading 98.9% and 86.9% technical monocrotophos respectively, under laboratory conditions and 79% and 80% of pure monocrotophos within 24 h at 37°C, where 500 ppm was the optimal monocrotophos concentration required for their normal growth by the production of enzyme phosphotriesterase (PTE). Purified PTE isolated from *Clavibacter michiganense* subsp. *insidiosum* SBL11 was found to be a monomeric enzyme (molecular mass- 43.5 kDa; pI-7.5), while PTE from *Pseudomonas aeruginosa* F10B was a heterodimeric enzyme (molecular mass - 43 and 41 kDa; pI-7.9 and 7.35). The enzyme isolated from strain F10B was more thermostable (half-life 7.3 h) than that from SBL11 (half-life 6.4 h at 50 °C), while both the enzymes showed the same temperature optimum of 37 °C (Das and Singh, 2006). Similar research was conducted by a research group, where they isolated 17 bacterial isolates (16 different *Bacillus* sp. and *Arthrobacter atrocyaneus*) (Bhadbhade et al., 2002b). Among them, *Bacillus megaterium* and

Table 2.2. Degradation of monocrotophos by different bacteria, fungi and algae

S.No	Microorganism/s	Sources	Findings	References
	Bacteria			
1.	*Bacillus sonorensis* (KY287930), *Pseudomonas stutzeri* (KY287931) and *Bacillus licheniformis* (KY287928)	Isolated from different MCP contaminated agricultural soil in Sivagangai district, Tamilnadu, India	Bacteria individually degraded MCP to non-toxic metabolites, whereas in consortia complete degradation occurred	Buvaneswari et al., 2018
2.	*Sphingobium* sp. YW16	Paddy soil, China	Bacteria utilized degraded metabolite dimethyl phosphate as carbon source but could not utilize *N*-methylacetoacetamide	Sun et al., 2018
3.	*Rhodococcus phenolicus* strain MCP1, *Rhodococcus ruber* strain MCP-2	Isolated from the Groundnut (*Arachis hypogaea L*.) soils by enrichment culture technique	*R. phenolicus* strain MCP1 and *R. ruber* strain MCP-2 degraded 30% and 45% MCP after 4 days leaving *N*-methylacetoacetamide as the degraded product; About 21% loss of MCP was observed in uninoculated medium after 4^{th} day	Srinivasulu et al., 2017
4.	*Bacillus subtilis* (BAGN005), *Pseudomonas stutzeri* (BVGN010), *Bacillus licheniformis* (BKGN007)	Isolated from different MCP contaminated agricultural soil in Sivagangai district, Tamilnadu, India	3-hydroxy-*N*-methyl butyramide, methyl phosphate and dimethyl phosphate observed as intermediate compounds	Buvaneswari et al., 2017
5.	*Bacillus subtilis* (KPA-1)	Isolated from different vegetable and cotton fields of Gujarat, India	Under aerobic conditions, MCP was degraded to an extent of 94.2%. RT-qPCR indicates presence of an enzyme organophosphate hydrolase (*opd*A)	Acharya et al., 2015
6.	*Serratia marsescens* strain JAS16	Isolated from soil sample of a sugarcane field, Vellore district, Tamil Nadu, India	50% degradation of 1000 mg L^{-1} MCP 3.7 days, whereas 4.8 days in soil; Bacteria was able to tolerate 1200 mg L^{-1} MCP	Abraham and Silambarasan, 2015

(*Continued on next page*)

Table 2.2. (*Continued*)

7.	*Starkeya novella* YW6	Isolated from soil samples of a paddy field located in Hunan province, China	0.2 mM MCP was completely degraded within 36 h into different metabolites: *N*-methylacetoacetamide, dimethyl phosphate, *N*-methyl-4-oxopentanamide, 5-(methylamino)-5-oxo-pentanoic acid, methylamine and glutaric acid	Sun et al., 2016
8.	*Pseudomonas synxantha*, *Bacillus subtilis* and *Salmonella enterica*	Soil samples from Punjab's Malwa region	*Pseudomonas synxantha* showed maximum MCP degradation i.e 67.8% (in 17 days) whereas, 70.9% MCP still persisted after 120 days in control	Sidhu et al., 2015
9.	Bacterial consortium containing *Alcaligenes* sp. JAS1, *Ochrobactrum* sp. JAS2, *Sphingobacterium* sp. JAS3 (chlorpyrifos degrading), *Enterobacter ludwigii* JAS17, *Pseudomonas moraviensis* JAS18 and *Serratia marcescens* JAS16 (monocrotophos degrading), *Klebsiella pneumoniae* JAS8, *Enterobacter cloacae* JAS7, *Halophilic bacteria* JAS4, *Enterobacter asburiae* strain JAS5 (endosulfan degrading).	Isolated from different pesticide (chlorpyrifos, monocrotophos and endosulfan) contaminated soil	MCP degraded at a rate constant of 261.6 per day and 50% degradation in 1.91 days	Abraham et al., 2014
10.	*Pseudomonas stutzeri*	Obtained from MTCC, Chandigarh	96% degradation of 500mg L^{-1} in 6 days at 30°C with ammonia, phosphates and carbon dioxide as degraded products	Barathidasan and Reetha, 2013
11.	*Lactobacillus bulgaricus*, *L. plantarum* and *L. paracasei*	Obtained from the Centre of Lactic Acid Bacteria, Northeast Agricultural University, China	*L. bulgaricus* showed maximum degradation of MCP (0.5 mg kg^{-1}) in 24 h at 42°C with half life time of 31.5 h, followed by *L. plantarum* (34.8 h)	Zhao and Wang, 2012
12.	*Pseudomonas aeruginosa*	MTCC, Chandigarh	Regain of protein, carotenoid and chlorophyll content due to MCP degradation	Balamurugan et al., 2010
13.	*Burkholderia sp*. strain KR100	Rice paddy field, Korea	96.4% degradation of 300µg mL^{-1} MCP	Kim and Ahn, 2009

Table 2.2. (*Continued*)

14.	*Paracoccus* sp. (M-1)	Sludge sample from the chemical factory's wastewater treatment system	79.92% MCP (300 mg L^{-1}) degraded rapidly in 6 h at 30°C, pH 7.5; 500 mg L^{-1} MCP was toxic for bacterial growth	Jia et al., 2006
15.	*Pseudomonas aeruginosa* F10B, *Clavibacter michiganense* subsp. *insidiosum* SBL 11	Soil samples from cotton fields of Ludhiana, Punjab, India	98.9% and 86.9% degradation of technical MCP, whereas 79% and 80% degradation of pure MCP by *P. aeruginosa* F10B and *C. michiganense* subsp. *Insidiosum* SBL 11, respectively, within 24 h at 37°C, followed by increase in generation time of bacteria. Optimal concentration of MCP was 500 ppm	Subhas and Singh, 2003
16.	*Pseudomonas mendocina, P. stutzeri, Bacillus licheniformis, Bacillus coagulans, Bacillus brevis* and three different *Arthrobacter* sp.	MCP treated Black cotton field soil from Satara, Maharashtra, India,	*Pseudomonas mendocina* showed maximum degradation (73%) of MCP (500 mg L^{-1}) at pH 7, 150rpm at 28 ± 2 °C in 8 days	Bhadbhade et al., 2002a
17.	*Arthrobacter atrocyaneus* MCM B-425, *Bacillus megaterium* MCM B-423	MCP contaminated vegetable farm soil in Manjri and cotton field soil in Jalna, Maharashtra, India	93% and 83% MCP (1000 mg L^{-1}) degradation within 8 days, at 30 °C by *A. atrocyaneus* MCM B-425 and *B. megaterium* MCM B-423, respectively. Phosphates, ammonia and carbon dioxide were the degraded products with methylamine and acetic or valeric acid as intermediate products	Bhadbhade et al., 2002b
18.	*Arthrobacter atrocyaneus*, *Bacillus megaterium*, and *Pseudomonas mendocina*	MCP contaminated soil	Maximum MCP degradation (65-77%) at pH 8, temperature 35°C by *B. megaterium* and *P. mendocina* and at temperature 30°C by *A. atrocyaneus*	Bhadbhade et al., 2002c
19.	*Azospirillum lipoferum* and 4 *Bacillus* sp.	Black soil from a groundnut field	After 14 days, 40% MCP lost in uninoculated culture, whereas 62.86% MCP degraded by *A.lipoferum* and 79.16% by *Bacillus* sp.	Rangaswamy and Venkateswarlu, 1992
20.	*Bacillus* sp.	Field soil near Forest Research Institute from Dehradun	*Bacillus* sp. was able to degrade MCP (0.5%)	Samal and Kotiyal, 2013

Table 2.2. (*Continued*)

	Fungi			
21.	*Aspergillus sojae strain* JPDA1	MCP contaminated paddy field soil, Vellore district, Tamil Nadu, India	500 mg L^{-1} MCP degraded in 72 h in minimal media. In soil amended with nutrients, 500mg L^{-1} MCP degraded in 144 h compared to soil devoid of nutrients in 168 h	Abraham et al., 2016
22.	*A. niger, A. flavus, A. fumigatus, P. lanosum* and *T. viride*	MCP contaminated soil of Vallam and Rajagri, Thanjavur district	*A. niger* and *T. viride* showed maximum MCP (12 ppm) degradation	Thirugnanam and Senthilkumar, 2016
23.	*Aspergillus niger* JQ660373	-----	After 15 days, residual MCP concentration found was 64.94 ± 0.42 μg mL^{-1} with rate constant of 0.002 per day (first order kinetics) and half-life of 12.64 days	Jain and Garg, 2015
24.	*Aspergillus fumigatus*	-----	*A. fumigatus* could tolerate only 1% MCP; No growth at higher concentration (2% and 3%). Presence of 1% Tween 80 increased growth rate	Pandey et al., 2014
25.	*Aspergillus niger* JQ660373, *Penicillium aculeatum* JQ660374, *Aspergillus flavus, Macrophomina* sp. and *Fusarium pallidoroseum*	Agricultural soil containing chickpea, pearl millet and mung beans near Banasthali campus, Rajasthan, India.	78% MCP (0.5% stock) degradation in 168 h with significant increase in phosphatase activity. Order of MCP degradation: *A. niger* JQ660373 > *P. aculeatum* JQ660374 > *A. flavus* > *F. pallidoroseum* > *Macrophomina* sp.	Jain et al., 2015
26.	*Aspergillus flavus, Macrophomina* sp. and *Fusarium pallidoroseum*	Agricultural soil near Banasthali campus, Rajasthan, India	Degradation constant and half-life for MCP degaradtion (150 mg L^{-1}) by *A. flavus, Macrophomina* sp. and *F. pallidoroseum*: 0.007, 0.005 and 0.002 per day and 4.21, 6.32 and 12.64 days Overall order: *A. flavus* > *Macrophomina sp.*> *F. pallidoroseum*	Jain et al., 2014
27.	*Aspergillus* sp.	Snake guard crop *Trichosanthes cucumerina L.*) field	Complete degradation of 0.5% MCP in 8 days into non-toxic, volatile fatty acids- palmitic acid, behenic acid, stearic acid etc	Anitha and Das, 2011
28.	*Trichoderma viridae*	MTCC Chandigarh	Moderate rate of MCP degradation. Decrease in protein, carotenoid and chlorophyll content. No significant effect on root length	Balamurugan et al., 2010

Table 2.2. (*Continued*)

29.	Seven isolates: *Cunninghamella echinulata* (M1), *Fusarium oxysporum* (M5), *Emericella nivea* (M9), *Aspergillus niger* (E11), *Aspergillus oryzae* (E12), *Emericella nivea* (E16) and *Aspergillus oryzae* ARIFCC 1054 (M4)	MCP contaminated soil	*Aspergillus oryzae* ARIFCC 1054 (M4) exhibited highest tolerance of MCP (900mg L^{-1}) and possessed phosphatase activity; 70% degradation of MCP in 50 h, undetectable (< 1mg L^{-1}) at 168 h	Bhalerao and Puranik, 2009
	Algae			
30.	*Chlorogloea fritschii* ARM 342, *Nostoc* sp. BDU-2, *Nostoc muscorum* ARM 221, *Anabaena azollae* AX61A, *Aulosira fertilissima* ARM 68, *Anabaena* sp. ARM 340, *Tolypothrix tenuis* ARM 76, *Calothrix brevissima* ARM 451, *Haplosiphon* sp. ARM 98 and *Mastigocladus* sp. ARM 351	National Facility for Blue Green Algal Collections, IARI, New Delhi and R. W. Fischer, Virginia Commonwealth University, Virginia, USA	*Aulosira fertilissima* ARM 68 and *Nostoc muscorum* ARM 221 could tolerate MCP upto100 ppm and used it as phosphorus source. MCP induced acid phosphatase activity	Subramanian et al., 1994
31.	Soil microflora and different algal species: *Anabaena variabilis, Lyngbya gracilis, Nostoc punctiforme* and *Phormidium foveolarum*	Rice field	Algae could grow even at 1 and 2 kg ha^{-1} of MCP. Under flooded conditions no toxicity observed. MCP decreased to trace amounts in 20 days	Megharaj et al., 1988
32.	Two green algae: *Scenedesmus bijugatus* and *Chlorella vulgaris* Three BGA: *Phormidium tenue, Nostoc linckia* (Roth) B & F and - *Svnechococcus elongatus* Nageli	Soil	60.4 % MCP recovered in uninoculated samples, whereas in inoculated samples it decreased to 16.7% to insignificant levels in 30 days	Megharaj et al., 1987

Table 2.2. (*Continued*)

33.	*Chlorella vulgaris, Gloeocystis gigas, Chlorococcum humicola, N. punctiforme, Scenedesmus bijugatus, Phormidium sp., Nostoc linckia* and *Synechococcus elongatus.*	Cotton field	MCP (0.5 to 2 kg ha^{-1}) triggered germination of resting algal species. 5 kg ha^{-1} increased algal population by sixfold	Megharaj et al., 1986a
34.	Green alga- *Scenedesmus bijugatus* Three blue-green algae- *Nostoc linckia*, *Synechococcus elongatus* and *Phormidium tenue*	Black soil of a cotton field	5-10 µg mL^{-1} MCP enhanced cell number and chlorophyll *a* content of all algae. *S. elongatus* could grow at 100 µg mL^{-1} MCP; toxic above 20, 50 and 100 µg mL^{-1} to *S. bijugatus, Phormidium tenue* and *Nostoc linckia*, respectively	Megharaj et al., 1986b

MCP - Monocrotophos

Arthrobacter atrocyaneus were selected for further studies on monocrotophos degradation and its metabolic pathway. Within 8 days, the isolates degraded monocrotophos to an extent of 93% and 83% respectively, from synthetic media spiked with 1000 mg L^{-1} monocrotophos. Enzymes are the key factors responsible for bioremediation of pesticides including monocrotophos (Verma et al., 2012) (Table 2.3).

Phosphatases (mono and dimethyl) and esterases are the enzymes involved in biodegradation of monocrotophos into ammonia, carbon dioxide, and phosphates through formation of intermediate compounds as valeric acid or acetic acid, methylamine and other metabolites (Bhadbhade et al., 2002b). The first step of monocrotophos degradation involves hydrolysis, producing *N*-methyl acetoacetamide along with dimethyl phosphate (Beynon et al., 1973). In the next step, degradation of *N*-methyl acetoacetamide produces valeric acid in *Arthrobacter atrocyaneus* and acetic acid in *Bacillus megaterium* (Bhadbhade et al., 2002b) (Fig. 2.2). Acetic acid is the key intermediate of the metabolic pathways in different microbes.

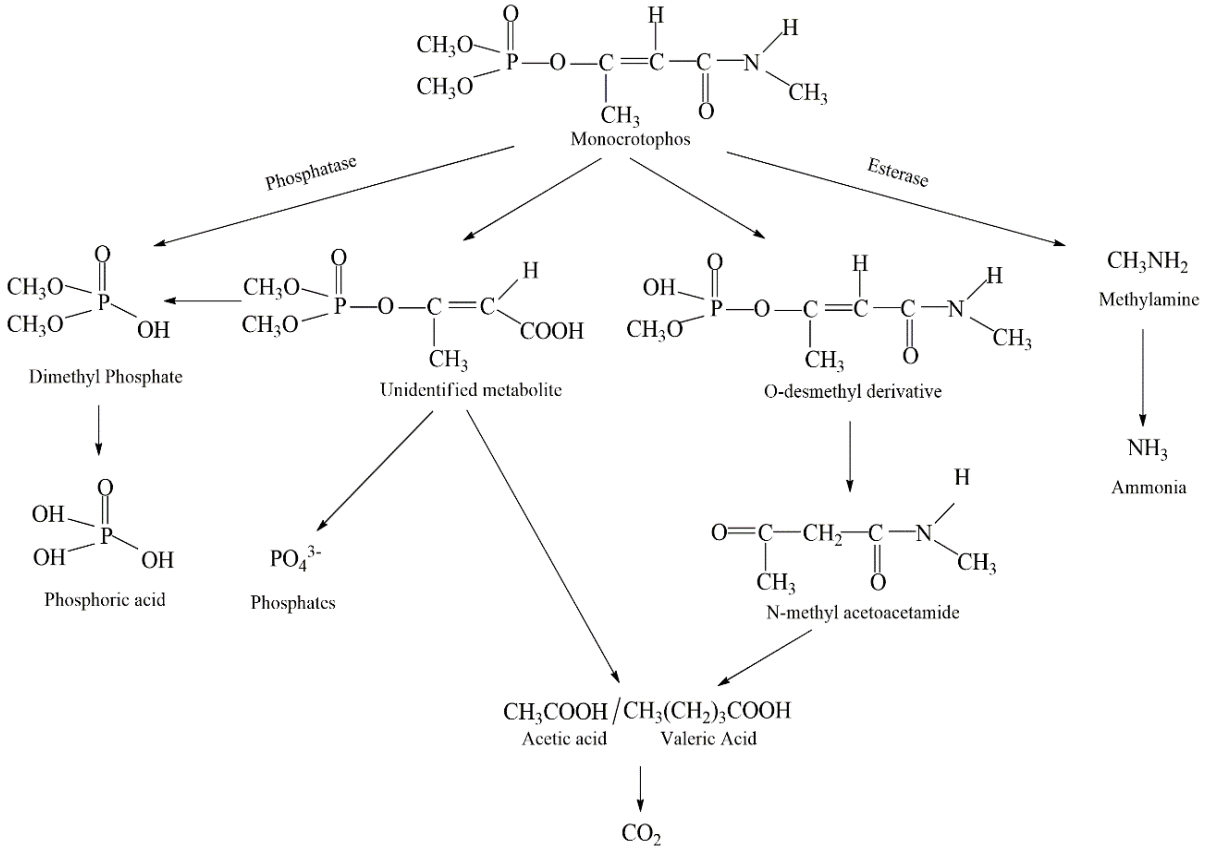


Fig. 2.2: Proposed pathway of microbial degradation of monocrotophos. (Kaur and Goyal, 2019)

Table 2.3. Enzymatic degradation of monocrotophos

S. No	Enzyme/s used	Source	Findings	References
1.	Laccase	*Pseudomonas* sp. S2	Alkali- stable extracellular enzymes; degraded 80.56 ± 0.6% MCP, without addition of any mediator	Chauhan and Jha, 2017
2.	Hydrolases	*Aspergillus niger* JQ660373	After 15 days, residual MCP was 16.95 ± 0.55 µg mL^{-1} with rate constant of 0.136 per day (first order kinetics) and half-life of 5.14 days	Jain and Garg, 2015
3.	Hydrolases	*Aspergillus niger J*Q660373	MCP half-life time with enzymatic method was 0.79 days	Jain and Garg, 2014
4.	Hydrolases (OPH33 and OPH67)	*Penicillium aculeatum* ITCC 7980.10 (M3) and *Fusarium pallidoroseum* ITCC 7785.10 (M4)	M3 OPH67 hydrolase was more efficient in bioremediation of MCP.	Jain et al., 2013a
5.	Acid phosphatases (P33 and P67)	*Aspergillus niger* ITCC 7782.10	Both the acid phosphatases can be used in MCP bioremediation	Jain et al., 2013b
6.	Hydrolases	*Aspergillus niger* (M1), *Aspergillus flavus* (M2), *Penicillium aculeatum* (M3), *Fusarium pallidoroseum* (M4), and *Macrophomina* sp. (M5)	90% MCP degraded by 150 µg mL^{-1} of enzyme in 120 h, with rate constants 0.0368, 0.0138, 0.048, 0.016 and 0.0138 per day and half-life of 0.79, 2.11, 0.6, 1.8 and 2.11 days for M1, M2, M3, M4 and M5, respectively. Overall order of degradation: *P. aculeatum* > *A. niger* > *F. pallidoroseum* > *A. flavus* = *Macrophomina* sp.	Jain and Garg, 2013
7.	Phosphotriesterase	*Pseudomonas aeruginosa* F10B and *Clavibacter michiganense* subsp. *insidiosum* SBL11	MCP degrading phosphotriesterase was capable of degrading other organophosphate insecticides like paraoxon. Also degraded tris – *p*-nitrophenyl phosphate	Das and Singh, 2006; Subhas and Singh, 2003
8.	Genetically engineered enzyme	Carboxylesterase B1 gene transferred to *E. coli*	13.4% MCP degraded in 2 h at 37ºC	Qiao et al., 2003

MCP - Monocrotophos

Fungal degradation of monocrotophos

Fungi are important part of the environment due to their significant role in biogeochemical cycles and their capacity to degrade xenobiotics including pesticides. Results of different published studies showed that fungi are capable of causing minor changes in the chemical structure of the applied pesticide resulting in formation of bio-transformed products which are further taken up and degraded by other potential soil microbes (Maqbool et al., 2016). Benefits of better tolerance, oxidizing ability, and mycelial niche are offered by fungi and they do not require prior exposure to any specific pollutant and are cost-effective bioremedial agent (Jain et al., 2014).

Among twenty-five isolated strains, isolate M-4 i.e. *Aspergillus oryzae* ARIFCC 1054 degraded 500 mg L^{-1} of monocrotophos, where monocrotophos concentration reached undetectable levels (< 1 mg L^{-1}) in 168 h (Bhalerao and Puranik, 2009) (Table 2.2). Complete enzymatic mineralization of monocrotophos by *Aspergillus* sp. in 8 days was reported by Anitha and Das (2011). Monocrotophos was broken down into non-toxic volatile fatty acids (stearic acid, palmitic acid, behenic acid) and other unknown metabolites. In another study, *Aspergillus fumigatus* was able to degrade 1% monocrotophos, whereas it was unable to grow at higher concentration (2% and 3%). However, presence of 1% Tween 80 enhanced monocrotophos degradation and increased fungal growth (Pandey et al., 2014). Also, *Aspergillus niger* and *Trichoderma viride* isolated from monocrotophos contaminated soil showed monocrotophos (12 mg L^{-1}) degradation (Thirugnanam and Senthilkumar, 2016). *Aspergillus sojae* strain JPDA1 isolated from sugarcane fields could degrade 500 mg L^{-1} of monocrotophos in 72 h in minimal media. Two types of trials were carried out in this study, where soil was spiked with 500 mg L^{-1} of monocrotophos. In first trail, soil was amended with nutrients, whereas in second trail soil was devoid of nutrients. In the former trail, the strain degraded the insecticide in 144 h, whereas in latter, it took 168 h for degradation (Abraham et al., 2016).

Jain and Garg (2015) studied biomineralization of monocrotophos by *Aspergillus niger* JQ660373. After an incubation of 15 days, the resulting residual concentration was 64.94 ± 0.42 µg mL^{-1}, following first order kinetics with the rate constant of 0.002 per day and half-life of 12.64 days. Rate of monocrotophos degradation by fungus was compared with degradation by enzymatic method. Various enzymes *viz*. hydrolases and acid phosphatases isolated and purified from the various fungal isolates like *Penicillium aculeatum, Aspergillus flavus*,

Fusarium pallidoroseum, Macrophomina sp., *Penicillium aculeatum* ITCC 7980.10, *Fusarium pallidoroseum* ITCC 7785.10, *Aspergillus niger* ITCC 7782.10 and *Aspergillus niger* JQ660373 (Jain and Garg, 2013; Jain et al., 2013a; Jain et al., 2013b; Jain and Garg, 2015) showed different capacity to degrade monocrotophos.

Algal degradation of monocrotophos

Different algal species have been studied for biodegradation of monocrotophos (Table 2.2). Among various algal isolates, *Nostoc muscorum* ARM 221 and *Aulosira fertilissima* ARM 68 used monocrotophos as phosphorus source and could tolerate it upto100 ppm. Monocrotophos induced acid phosphatase activity (Subramanian et al., 1994) and 0.5 to 2 kg $ha^{-1}$of the compound triggered germination of different resting algal species (*Chlorococcum humicola, Chlorella vulgaris, Nostoc linckia, Gloeocystis gigas, N. punctiforme, Scenedesmus bijugatus, Phormidium sp.* and *Synechococcus elongatus*). On using 5 kg ha^{-1} of monocrotophos, it increased algal population by sixfold (Megharaj et al., 1986a). Lower concentration of monocrotophos (5-10 µg mL^{-1}) enhanced cell number along with chlorophyll *a* content of all algae. Blue green algae *S. elongatus* could grow at 100 µg mL^{-1}, whereas other algal isolates *S. bijugatus, Phormidium tenue,* and *Nostoc linckia* could not tolerate even 20 µg mL^{-1} monocrotophos (Megharaj et al., 1986b). After 30 days of incubation with different algal isolates (*Scenedesmus bijugatus, Chlorella vulgaris, Phormidium tenue, Nostoc linckia* (Roth) B & F and - *Svnechococcus elongatus* Nageli) monocrotophos level decreased to 16.7% confirming their efficiency to degrade the insecticide (Megharaj et al., 1987). Other algal isolates viz. *Anabaena variabilis, Lyngbya gracilis, Nostoc punctiforme,* and *Phormidium foveolarum* utilized 1 and 2 kg ha^{-1} of monocrotophos and no toxicity was observed (Megharaj et al., 1988).

Factors affecting biodegradation of monocrotophos

The degradation ability of microbes is influenced by several factors. The operating parameters like pesticide concentration, temperature, pH, moisture content, available nutrients have been extensively studied for effective biodegradation of monocrotophos. The available literature shows that degradation efficiency of microbes decreases with higher initial concentration of pesticide. Samal and Kotiyal (2013) assessed the growth of *Bacillus* sp. in Bushnell Haas media spiked with different monocrotophos concentration (0.5%, 1%, 1.5%). Bacteria showed best growth in media spiked with 0.5% monocrotophos. *Paracoccus* sp. (M-1) could easily degrade

300 mg L^{-1} of monocrotophos, whereas 500 mg L^{-1} monocrotophos was toxic for its growth (Jia et al., 2006). *Bacillus megaterium*, *Arthrobacter atrocyaneus* and *Pseudomonas mendocina* were able to tolerate 2500 mg L^{-1} monocrotophos and use it as carbon source (Bhadbhade et al., 2002c).

Most of the research conducted shows the optimum temperature for monocrotophos degradation by bacteria ranges from 30-37 °C (Abraham et al., 2014; Abraham and Silambarasan, 2015; Acharya et al., 2015). Optimum degradation temperature for fungus ranges from 25-30 °C (Balamurugan et al., 2010; Jain et al., 2014; Abraham et al., 2016), whereas for algae it is 27-30 °C (Megharaj et al., 1986a; Megharaj et al., 1987; Subramanian et al., 1994). Different microbes degrade monocrotophos in the pH ranging from 5.5-8.5; however, the conclusions are divergent. *Bacillus megaterium*, *Arthrobacter atrocyaneus* and *Pseudomonas mendocina* showed maximum degradation of monocrotophos (100-500 mg L^{-1}) at varying temperature 30-35 °C, pH 7.0-8.0 and inoculum density 10^8 cells/mL under aerated conditions (Bhadbhade et al., 2002c).

The decomposition of pesticides by micro-organisms is greatly affected by the availability of both macro and micro nutrients (C, N, O, H, P, etc.) in the soil (Yadav et al., 2016). KaviKarunya and Reetha (2012) reported maximum growth of *Pseudomonas fluorescens*, *Bacillus subtilis*, and *Klebsiella* sp. at pH 6 and 35 °C. Bacteria showed maximum growth in the presence of dextrose as carbon source and malt extract as nitrogen source, whereas lesser growth in case of mannose (carbon source) and beef extract (nitrogen source). *Starkeya novella* effectively decomposed 0.2 mM monocrotophos in 36 h with no lag phase. Supplementing media with more carbon source slowed down the initial rate of monocrotophos degradation, whereas monocrotophos transformation was enhanced by addition of more favourable nitrogen source, which was ammonium chloride (Sun et al., 2016). Monocrotophos degradation in soil was enhanced by light (UV/sunlight), moisture content (more in flooded soil) and the type of water (more in tap water than the distilled water) (Dureja 1989). Proper aeration and shaking conditions are better for monocrotophos removal than the static conditions (Bhadbhade et al., 2002c).

2.2 Chloroacetanilide herbicides

Chloroacetanilide family of herbicides, comprising of alachlor, acetochlor, metachlor, propachlor and butachlor are among the highly effective agro-chemicals in the world with a utilization rate of about 14 million pounds in the European Union member states (Eurostat 2007). Their mode of action involves inhibiting the biosynthesis of fatty acids, alcohols, lipids, proteins, flavonoids and isoprenoids (Abigail et al., 2015). Due to their low adsorption constant in soil and high solubility in water, chloroacetanilides are easily leaked to the sub-surface and shallow groundwater *via* agricultural run-off and leaching, posing threat to living organisms (Bai et al., 2013). These herbicides along with their degraded metabolites are persistent in the environment and are often detected in surface and ground water samples (Abigail et al., 2015). They have also been classified by the United States EPA as group 2B carcinogen (PAN UK 2001) and are suspected as endocrine disruptors. Chloroacetanilide herbicides and their degraded metabolites are considered mutagens and can cause sister chromatid exchange in human lymphocytes (Bai et al., 2013). Butachlor is maximally applied in agriculture in Asian countries.

2.2.1 Butachlor

Butachlor (*N*-(butoxymethyl)-2-chloro-*N*-(2,6-diethylphenyl) acetamide), commonly known as machete, is a non-ionic chloroacetamide compound extensively used as a pre-emergence or early post-emergence herbicide for controlling unwanted annual grass, certain broadleaved weeds and underwater macrophytes found in freshwater and fish water bodies (Wang et al., 2013a; Abigail et al., 2015). Fig. 2.3 shows the chemical structure of butachlor with a molecular formula $C_{17}H_{26}NO_2Cl$.

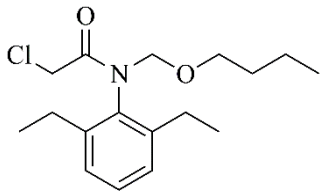


Fig. 2.3: Chemical structure of butachlor

It is a selective and systemic herbicide which acts by inhibiting the enzymes responsible for geranylgeranyl pyrophosphate cyclization and elongation of the long-chain fatty acids (Abigail et al., 2015). Butachlor absorption in plants takes place by translocation, primarily by the emerging shoots and secondarily by roots, where vegetative parts get higher concentration than

reproductive parts. It gets dissipated by microbial degradation, photo-decomposition and volatilization, and hence has a half-life of 1.6 days to 29 days in soil (Kaur et al., 2017a; PubChem 2019). However, under certain conditions such as high alkalinity, absence of biodegraders, low temperature and low moisture, butachlor persists in the soil and remains biologically active for a longer period of time (Kaur et al., 2017a).

Butachlor was first produced by Monsanto (USA) in 1968 by the reaction between chloroacetyl chloride with formaldehyde and azomethine of 2,6-diethylaniline, followed by n-butanol treatment. It was later introduced in Japan in 1973 to get rid of weeds in transplanted rice and is classified under K3 class of herbicides. Butachlor exists both in particulate and vapor phase when released into the air at a vapor phase of 2.90×10^{-6} mm Hg at 25 °C. It gets decomposed at temperatures equal to or greater than 165 °C and is stable to UV light (Table 2.4). Heating of butachlor leads to its disintegration and emission of toxic fumes of nitrous oxides and hydrogen chloride (Abigail et al., 2015).

Table 2.4: Physico-chemical properties of butachlor

S No.	Properties	Values
1.	Chemical name	*N*-(butoxymethyl)-2-chloro-*N*-2,6-diethyl acetanilide
2.	Molecular formula	$C_{17}H_{26}NO_2Cl$
3.	CAS No.	23184-66-9
4.	Physical state	Clear amber liquid at room temperature
5.	Odour	Faint, sweet odour
6.	Melting point (°C)	0.5 - 1.5
7.	Boiling point (°C)	156
8.	Molecular weight	311.9
9.	Water solubility (20°C)	20 mg L^{-1}
10.	Density (at 25°C)	1.070 g mL^{-1}
11.	Decomposing point (°C)	165
12.	Vapor pressure (at 25°C)	1.8×10^{-6} mm Hg
13.	Viscosity (at 25°C)	37 °Cp
14.	Adsorption coefficient (K_{oc})	700
15.	Water partition coefficient (K_{ow})	4.5

Source: Abigail et al., 2015

2.2.2 Distribution and fate of butachlor

Butachlor has become a very popular herbicide across Asia with a utilization rate of about 4.5 × 10^7 kg per year (Gao et al., 2015; Singh and Nandabalan, 2018) at a recommended field dosage of 3000 mL ha^{-1} (Alla et al., 2008). India accounts for approximately 6.75 × 10^6 kg of annual usage of butachlor (Verma et al., 2014). It enters the environment either from its production industry through waste streams or through various horticultural, agricultural practices or forestry, where rainfall and poor water management leads to butachlor run off from fields to waterbodies and surrounding areas (Ok et al., 2012). It has been detected in soil, surface and underground water with residual concentrations ranging from 29.5 - 74 µg kg^{-1} in soil (Yang et al., 2010) and 0.1 - 1.4 µg L^{-1} in surface water (Mamun et al., 2009), respectively. In air, butachlor can be photochemically degraded by the free radical reaction mechanism but is expected not to undergo direct photolysis as it doesn't absorb UV light greater than 290 nm. Whereas, in particulate phase, it is eliminated from the environment by dry and wet deposition mechanisms (Meylan and Howard, 1993; Abigail et al., 2015). High value of soil adsorption coefficient (K_{OC}) (Table 2.4), depicts butachlor's adsorption to the soil and confirms no mobility inside the soil system (Swann et al., 1983). Butachlor adsorption mainly takes place on carbonyl, phenolic and alcoholic groups of humic acids present in soil (Xu et al., 2005). Being lipophilic in nature, butachlor get accumulated un the aquatic organisms which is confirmed by the high bioaccumulation/bioconcentration factor (BCF) value of 1500 (Franke et al., 1994).

2.2.3 Toxicity and effects of butachlor

Persistence of butachlor in the environment due to its indiscriminate application has led to several health and environmental complications (Dwivedi et al., 2010). It is suspected to be carcinogenic in nature, known to induce malignant transformation *in vitro* by stimulating cell proliferation, mitochondrial dysfunction, chromosomal breakage, oxidative DNA damage and disrupting endocrine system (Dwivedi et al., 2012; Chang et al., 2013).

Microbial toxicity

Butachlor is known to inhibit growth of cyanobacteria such as *Anabaena* and *Nostoc* by negatively affecting photosynthesis, N_2- fixation, RNA, lipid and protein biosynthesis (Zargar and Dhar, 1990; Vandana and Rai, 2002; Chen et al., 2007; Agrawal et al., 2014; Das et al., 2015). Butachlor imparts toxicity and mutagenicity in cyanobacterium algae *Nostoc muscorum*

(Vaishampayana 1985). High concentrations of butachlor can significantly affect growth rate, synthesis of pigments, and photosynthesis system (II) activities in *Nostoc* sp., triggering dramatic intracellular antioxidant response in the cells (He et al., 2013).

Aquatic toxicity

Being lipophilic in nature, it is resistant to degradation in the environment and tend to bioaccumulate in aquatic organisms, causing several toxic effects (Li et al., 2016). Toxicological studies on different aquatic organisms have shown butachlor to be a suspected carcinogen (Tu et al., 2013; Ou et al., 2000) and resulted in morphological abnormalities, inhibited embryo hatching and caused significant mortality in zebrafish *Danio rerio* (Tu et al., 2013). It has a potential to cause cytotoxicity and oxidative toxicity in fish by depressing glutathione detoxification system in kidney and also affects reproduction and sex steroid endocrine systems in zebrafish (Farombi et al., 2008; Chang et al., 2013; Zhu et al., 2014). Genotoxic and cytotoxic effects of butachlor were studied in catfish *Clarias batrachus*, where degree of DNA damage caused was proportional to the butachlor concentration (Ateeq et al., 2005). In another work, a significant protein loss in *C. batrachus* was observed at both lethal and sub-lethal butachlor concentrations, either because of increased proteolysis (Muley et al., 2007) or by utilization of ketoacids for glucose synthesis in glucogenesis pathway (Rajput et al., 2012).

Toxicity to mammals, frogs and earthworms

Dwivedi et al. (2012) reported butachlor clastogenicity and genotoxicity in exposed human peripheral blood mononuclear cells which was indicated by cell cycle alterations and necrosis due to chromosomal and mitochondrial membrane damage. Several reports suggest butachlor to be genotoxic to frogs (Liu et al., 2011), a growth retardant in earthworm (Muthukaruppan et al., 2005) and potential tumor promoter with carcinogenic activity in mouse liver cells (Ou et al., 2000). It is considered as an indirect mutagen for rats and hamsters (Hsu et al., 2005). Liu et al. (2011) observed the harmful effects of butachlor on development and metamorphosis of alpine cricket frog tadpole (*Fejervarya limnocharis*), a pond breeding amphibian, along with DNA damage at dose less than 4.8 mg L^{-1}.

Phytotoxicity

Butachlor is known to affect seed germination, gibberellic acid and pigment synthesis, lipid metabolism, cell permeability, cell division, RNA and lipid biosynthesis in plants. When applied at a concentration of 100 µM, butachlor affected photosynthesis along with inhibition of lipid, protein and RNA synthesis in foliage of *Phaseolus vulgaris* L. (red kidney beans), whereas at 50 µM inhibited protein and RNA synthesis of rice *Oryza sativa* L. and root and shoot segments of barnyardgrass (*Echinochloa crusgalli* L.), respectively (Chang et al., 1985). Wang et al. (2013a) studied concentration dependent effect of butachlor on growth, physiology and biochemistry of Italian rye grass, where 5 mg L^{-1} led to 50% reduction in fresh biomass of the plant, majorly affecting root of the plant, followed by the shoot. This may be the result of oxidative stress induced by hydrogen peroxide rather than the superoxides. In a study conducted by Kumar and Jagannath (2015), butachlor showed negative effect on mitotic division in somatic cells of wheat variety HD-2189 (*Triticum aestivum* L).

Effect on soil microbial systems and enzymatic activity

Soil contains several microorganisms (fungi, bacteria and algae), which play significant part in soil fertility and other functions such as nutrient storage and release, soil structure and stability, biodegradation and immobilization of pollutants. As per guidelines for the approval of pesticides, it is an obligatory requirement to study the effect of pesticides on soil microbial systems, microbial enumeration and enzyme activities in order to maintain soil biodiversity and fertility. Soil enzyme activity is involved in metabolism of soil organic matter and may predict certain biological transformations vital for soil fertility. Dehydrogenases, referred as respiratory chain enzymes are one of the essential soil enzymes which oxidize organic substrate by removal of two hydrogen atoms. So, dehydrogenase activity is a measure of cell viability in soil and is used for indicating biological redox systems. Another soil enzyme urease play a major role in hydrolysis of urea to ammonia and CO_2, and soil phosphatases catalyse the breakdown of organic phosphorus present in soil (Saha et al., 2012).

The effect of butachlor on soil activity (microbial population, enzymatic population, microbial community structure and diversity, microbial respiration, nitrification and nitrogen fixation) has been studied by several researchers. Butachlor showed stimulatory as well as inhibitory effect on different microbes and enzyme activities, depending on concentration and conditions applied. Min et al. (2002) reported concentration dependent stimulatory effect of butachlor on

soil dehydrogenase activity and peroxidase activity. Nitrification and nitrogen fixation were both reduced after few days of butachlor application, whereas soil respiration was suppressed for about 20 days depending on initial butachlor concentration that was spiked in the soil. In another study, a gradual enhancement in dehydrogenase activity (501 µg TPF g^{-1} h^{-1} to 523 µg TPF g^{-1} h^{-1}) was also observed in butachlor spiked soil over a period of 42 days (Saha et al., 2012). Effect of different butachlor application rates (1.5, 15 and 150 kg a.i. ha^{-1}) on different soil enzymes (alkaline phosphatase, dehydrogenase, urease, protease and amidase) was studied under flooded and non- flooded conditions in silt loam soil at pH 7.5. Dehydrogenase activity was stimulated under flooded conditions and inhibited under non- flooded conditions. Under most of the butachlor concentrations, phosphatase activity was stimulated both under non-flooded and flooded conditions. Urease activity showed inconsistent response due to butachlor treatment under flooded conditions, but was reduced under un-flooded conditions. Protease activity was stimulated in flooded conditions and initially stimulated in non-flooded conditions, followed by reduction towards end of experiment. Amidase activity showed fluctuating results (Rasool et al., 2014).

Wang et al. (2007) studied the combined effect of butachlor along with cadmium on urease and phosphatase enzyme activity along with microbial diversity. High concentrations of butachlor (50 mg kg^{-1} of soil) significantly reduced urease and phosphatase enzyme activity in the soil and affected microbial community, which was studied by the random amplified polymorphic DNA (RAPD) analysis, where RAPD profiles of butachlor treated samples showed variation in appearance of new bands and loss of normal bands in comparison to control soil. Chen et al. (2009) also showed microbial community (general and nitrogen fixing bacteria) alteration on butachlor application.

On application of 1.5 kg a.i. ha^{-1} of butachlor to rice crops, a significant reduction in bacterial and fungal population was observed from 0-3 days of butachlor application. Actinomycetes showed a depressing effect till 10 days. After a period of 30 days, increase in population was observed for all bacteria, fungus and actinomycetes (Raut et al., 1997). When applied at a concentration of 5.5 to 22 µg g^{-1} dried soil, butachlor showed significant decline in number of actinomycetes along with stimulation of growth of sulfate-reducing bacteria, hydrolytic fermentative bacteria and denitrifying bacteria. Concentration dependent effect of butachlor was observed in methane-producing bacteria, where butachlor concentration upto 11 µg g^{-1} dried soil showed stimulatory effect, while higher concentration of 22 µg g^{-1} dried soil showed

inhibitory effect. Retardation of fungal growth was observed at higher butachlor concentrations (Min et al., 2001). Jena et al. (1987) reported reduced population of aerobic nitrogen fixers and *Azospirillium* in non-flooded soil. Inhibitory effects of butachlor were reported by Barman et al. (2009) on his study conducted in a black cotton soil, where significant decline in microbial population was observed on butachlor application. During a period of 45 days, soil was unable to regain its total fungal count and lost *Azotobacter* and phosphate solubilizing fungi.

2.2.4 Biodegradation of butachlor

Several treatment methods such as recycling, pyrolysis, incineration and filling of contaminated sites have been employed for treating soil pollution and soil toxicants in agricultural lands (Wang et al., 2005). Among them, biological methods involving effective use of micro-organisms such as bacteria, fungi and algae for enzymatic breakdown of toxic pesticides into simpler, less complex and less or non-toxic compounds is the most promising technique, which provides additional benefits of being effective, eco-friendly, cheaper and minimally hazardous (Porto et al., 2011; Finley et al., 2010). Remediation of chloroacetanilides by micro-organisms has been reported by several researchers.

Bacterial degradation of butachlor

Several reports describe the isolation and identification of bacteria such as *Stenotrophomonas acidaminiphila* JS-1 (Dwivedi et al., 2010), *Novosphingobium chloroacetimidivorans* sp. (Chen et al., 2014), *Ammoniphilus* sp. JF (Singh and Nandabalan, 2018), *Serratia ureitylica* strain AS1 and *Enterobacter cloacae* (Mohanty and Jena, 2018; 2019) capable of catabolizing butachlor (Table 2.5). Dwivedi et al. (2010) isolated *Stenotrophomonas acidaminiphila* JS-1, which utilized butachlor as sole carbon and energy source and could completely degrade 3.2 mmol l^{-1} butachlor in 20 days at a half-life of 4 days and rate constant of 0.17 day^{-1}, following first order rate kinetics. The strain was also capable of producing indole acetic acid at lower butachlor concentrations. Another bacterial strain *Paracoccus* sp. FLY-8 isolated from rice field soil effectively degraded butachlor as a result of aniline dioxygenase and catechol 1,2-dioxygenase enzymes (Zhang et al., 2011). The strain was potential enough to degrade five other chloroacetamide herbicides including alachlor, propisochlor, acetachlor, pretilachlor and metolachlor. A novel strain *Catellibacterium caeni* sp. DCA-1^T degraded 81.2 % butachlor (50 mg L^{-1}) in 84 h, at a broad range of temperature (15 - 35 °C) and pH (6.0 - 9.0), forming five major metabolites, that were identified using GC-MS and degradation pathway was proposed.

Table 2.5: Degradation of butachlor by bacteria

Bacterial strain	Gram character	Inoculum size	Degradation of butachlor	Metabolites produced	Reference
Stenotrophomonas acidaminiphila sp. JS-1	Gram -ive	0.1 mL	3.2 mmol l^{-1} in 20 days	-	Dwivedi et al., 2010
Paracoccus sp.FLY-8	Gram -ive	1 % v/v	65.2% of 100 mg L^{-1} in 5 days	Alachlor, 2-chloro-*N*-(2,6-dimethylphenyl) acetamide, 2,6-diethylaniline	Zhang et al., 2011
Catellibacterium caeni sp. nov DCA-1^T	Gram -ive	2%	81.2% of 50 mg L^{-1} in 84 h	*N*-hydroxymethyl-2-chloro-*N*-(2,6-diethyl-phenyl)-acctamide, 2-chloro-*N*-(2,6-diethyl-phenyl)-acetamide, (2,6-diethyl-phenyl)-ethoxymethyl-carbamic acid, *N*-(2,6-diethyl-phenyl)-*N*-hydroxymethylacetamide and *N*-(2,6-diethyl-phenyl)-*N*-hydroxymethyl-formamide	Zheng et al., 2012
Rhodococcus sp. strain B1	Gram +ive	1.4×10^6 cfu mL^{-1}	100 mg L^{-1} within 5 days	2-chloro-*N*-(2,6-dimethylphenyl) acetamide and butoxymethanol	Liu et al., 2012
Mycobacterium sp. J7A and *Sphingobium* sp. J7B	Gram +ive, Gram -ive	$OD_{600\ nm}$ = 0.004	100 mg L^{-1} in 24 h	2-chloro-*N*-(2,6-diethylphenyl) acetamide and 2,6-diethylaniline	Kim et al., 2013
Novosphingobium chloroacetimidivorans sp. BUT-14^T	Gram -ive	5 % (v/v)	90.5±14.1% of 100 mg L^{-1} in 5 days	-	Chen et al., 2014
Bacillus sp. hys-1	Gram +ive	OD_{600nm} =1.0	More than 90% of 100 mg L^{-1} in 7 days	2-chloro-*N*-(2,6-diethylphenyl)-*N*-methylacetamide, 2-chloro-*N*-(2,6-diethylphenyl)-acetamide, and 2,6-diethylaniline	Gao et al., 2015
Sphingomonas chloroacetimidivorans sp. $Y1^T$	Gram -ive	5 % (v/v)	68.5 ± 8.7 % of 100 mg L^{-1} in 7 days	-	Chen et al., 2015
Roseomonas chloroacetimidivorans sp. BUT-13^T	Gram -ive	5 % (v/v)	48.6 ± 6.5 % of 100 mg L^{-1} in 4 days	-	Chu et al., 2016
Ammoniphilus sp. JF	Gram variable	$OD_{600\ nm}$ = 0.002	100 mg L^{-1} within 24 h	1,2-benzenedicarboxylic acid, bis(2-methylpropyl) ester and 2,4-bis(1,1-dimethylethyl)-phenol	Singh and Nandabalan, 2018
Bacillus altitudinis A16	Gram +ive	$OD_{600\ nm}$ = 0.002	More than 90% of 50 mg L^{-1} in 5 days	*N*-(butoxymethyl)-*N*-(2-chloroethyl)-2,6-diethylaniline, (*N*-butoxymethyl)-2-chloro-*N*-(2-ethylphenyl) acetamide, *N*-(butoxymethyl)-2,6-diethyl-*N*-propylaniline, 2-chloro-*N*-(2,6-diethylphenyl) acetamide and 2,6-diethylaniline	Current study

Inoculation of the DCA-1^T cells into three different soils - sterile red soil (pH 4.8), sterile fluvo-aquic soil (pH 6.3) and high sandy soil (pH 8.2) with 50 mg L^{-1} butachlor significantly accelerated butachlor degradation (57.2% - 90.4%) as compared to control (5.4% - 36%), signifying effect of soil type on butachlor degradation (Zheng et al., 2012).

Liu et al. (2012) studied butachlor degradation using *Rhodococcus* sp. B1, where butoxymethanol and 2-chloro-*N*-(2,6-dimethylphenyl)-acetamide were produced as a result of hydrolysis of butachlor by hydrolase ChlH (optimum pH 7.0 - 7.5; temperature 30°C) through *N*- dealkylation. 2-chloro-*N*-(2,6-dimethylphenyl)-acetamide couldn't be degraded further, whereas, butoxymethanol was degraded and utilized as carbon source for bacterial growth. A syntrophic degradation of 100 mg L^{-1} butachlor within 24 h was achieved by *Mycobacterium* sp. J7A *and Sphingobium* sp. J7B at 28 °C. GC-MS analysis revealed production of 2-chloro-*N*-(2,6-diethylphenyl) acetamide (CDEPA) on butachlor degradation by strain J7A, which was further completely metabolized by strain J7B for its growth through production of 2,6-diethylaniline (Kim et al., 2013). *Novosphingobium chloroacetimidivorans* BUT-14^T and *Sphingomonas chloroacetimidivorans* Y1^T are another gram negative and non- spore forming bacterial isolates capable of effective chloroacetamide herbicide degradation (Chen et al., 2014; Chen et al., 2015).

Gao et al. (2015) isolated butachlor degrading *Bacillus* sp. hys-1, and cloned a novel 744 bp gene encoding debutoxylase Dbo, which led to complete mineralization of butachlor by debutoxylation and *N*-demethylation reactions, where 2-chloro-N-(2,6-diethylphenyl)-N-methylacetamide and 2-chloro-*N*-(2,6-diethylphenyl)acetamide were the major intermediate products produced. Singh and Nandabalan (2018) also isolated *Ammoniphilus* sp. JF from the agricultural fields of Punjab, which showed complete butachlor (100 mg L^{-1}) degradation within 24 h of incubation, where 1,2-benzenedicarboxylic acid, bis(2-methylpropyl) ester and 2,4-bis(1,1-dimethylethyl)-phenol were the two intermediate products obtained.

Fungal degradation of butachlor

Two soil fungi (*Fusarium solani* and *F. oxysporum*) effectively degraded 50 ppm butachlor in a 0.02 M KH_2PO_4 buffer solution (pH 5.2) via dechlorination, dehydrogenation, hydroxylation, debutoxymethylation, dealkylation and cyclization reactions, where 30-32 metabolites were detected by GC-MS as a result of butachlor degradation by *F. solani* (Chakraborty and Bhattacharya, 1991). In a similar experiment conducted by Raut and Kulshreshta (1997), fungal

isolates *F. solani* and *Chaetomium globosum* followed the same route of degradation and transformed butachlor into six and four products, respectively. *Trichoderma viride* can quickly degrade 98% of 50 mg kg^{-1} of butachlor in an incubation period of 15 days (Abd-Alrahman and Salem-Bekhit, 2013). Another two fungal isolates (*Neodeightonia subglobosa* IFM 63572 and *Sclerotium hydrophilum* IFM 63573) isolated from underwater wood and surface water collected from Taal Lake (Philippines) could efficiently degrade 94.68% and 89.64 % of 100 ppm of butachlor, respectively in five days of incubation and use it as a sole carbon source (Carascal et al., 2017).

Algal degradation of butachlor

Like bacteria and fungi, algae play very important role in biodegradation of pollutants (Quesnel et al., 2011). Anees et al. (2014) studied the butachlor degradation (5, 10, 20, 40 and 80 ppm) with cyanobacteria *Nostoc muscorum*. GC-MS analysis revealed *N. muscorum* could effectively degrade 5 ppm butachlor into phenols and benzene dicaroxylic acid, but with increase in butachlor concentration inhibitory effect on growth of *N. muscorum* was seen probably due to inhibition of photosynthesis, pigment synthesis and nitrogen metabolism. AKR17A1, an aldo-keto reductase, isolated from *Anabaena* sp. PCC 7120 catalyzed degradation of butachlor and resulted in the formation of 2,6-bis(1,1-dimethylethyl)-4-methylphenol and 1,2-benzene dicarboxylic acid as major degraded products, as confirmed by GC-MS analysis (Agrawal et al., 2015).

Products and metabolites of butachlor degradation

Large number of intermediate products or metabolites are obtained from butachlor degradation by diverse microbes, involving different degradation pathways (Zhang et al., 2011; Zheng et al., 2012; Kim et al., 2013; Singh and Nandabalan, 2018). Mineralization of butachlor occurs by combination of several reactions such as dechlorination, hydroxylation, dehydrogenation, debutoxymethylation, dealkylation and cyclization reactions (Chakraborty and Bhattacharya, 1991). 2-chloro-N-(2,6-dimethylphenyl) acetamide and 2,6-diethylaniline are the two major metabolites obtained during bacterial degradation of butachlor. Similar metabolites produced during butachlor degradation by *Paracoccus* sp. FLY-8 were reported by Zhang et al. (2011) as shown in the proposed degradation pathway (Fig. 2.4), where first step was formation of alachlor by partial C-dealkylation, which was then broken down into 2-chloro-N-(2,6-dimethylphenyl)acetamide (CDEPA) by N-dealkylation. CDEPA was further transformed to

2,6-diethylaniline, which was finally metabolized into CO_2 and H_2O via the metabolite aniline and catechol through an ortho-cleavage pathway.

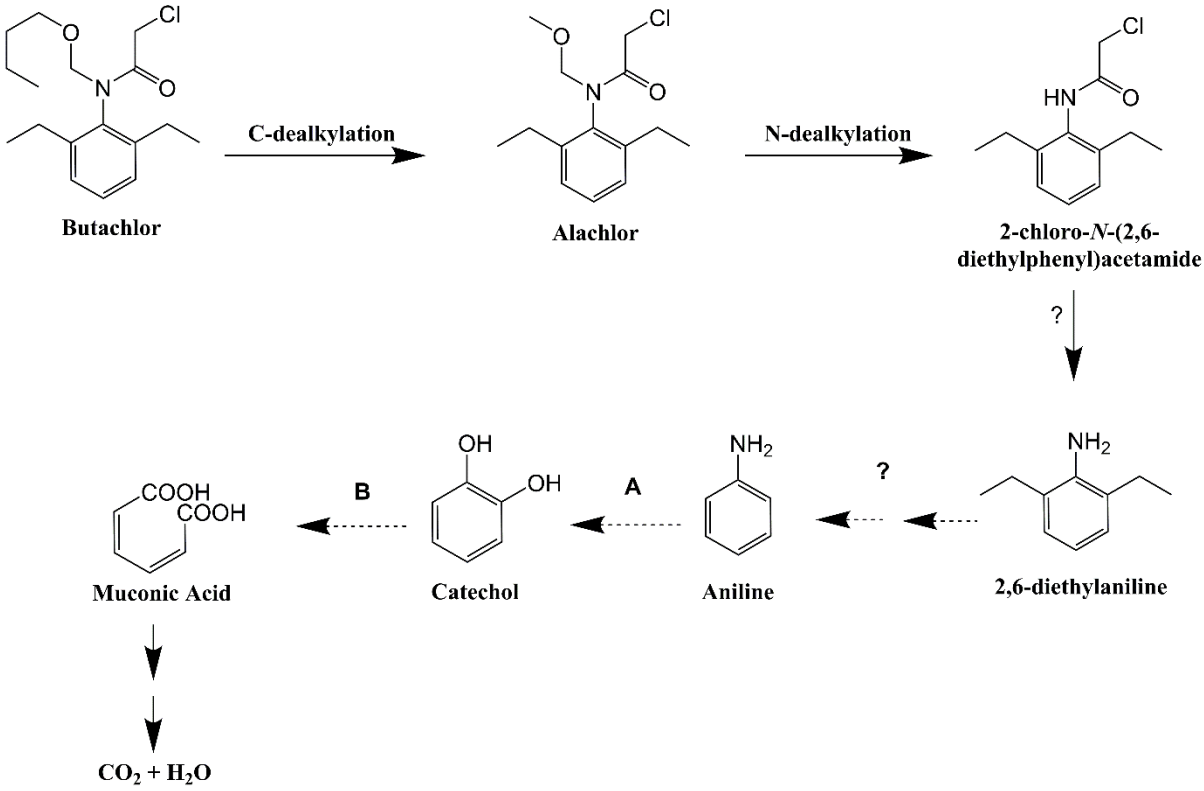


Fig. 2.4: Proposed metabolic pathway of butachlor degradation by *Paracoccus* sp. FLY-8 (Source: Zhang et al., 2011)

In similar study, conducted by Zheng et al. (2012), five metabolites *N*-hydroxymethyl-2-chloro-*N*-(2,6-diethyl-phenyl)-acctamide, (2,6-diethyl-phenyl)-ethoxymethyl-carbamic acid, *N*-(2,6-diethyl-phenyl)-*N*-hydroxymethyl-acetamide, 2-chloro-*N*-(2,6-diethyl-phenyl)-acetamide and *N*-(2,6-diethylphenyl)-*N*-hydroxymethyl-formamide were identified by GC-MS analysis and a plausible metabolic pathway was proposed (Fig. 2.5). Formation of *N*-hydroxymethyl-2-chloro-*N*-(2,6-diethyl-phenyl)-acctamide (A) by the hydrolysis of C-O ester bond of butachlor was the first step involved in the breakdown of butachlor, which was further transformed into 2-chloro-*N*-(2,6-diethylphenyl)-acetamide (B) by doff a hydroxymethyl. Metabolite A can also undergo dechlorination reaction, forming *N*-(2,6-diethyl-phenyl)-*N*-hydroxymethylacetamide (D), a common step in the mineralization of chloroacetamides. Intermediate D can further doff a methyl group to transform into *N*-(2,6-diethyl-phenyl)-*N*-hydroxymethyl-formamide (E). Dechlorination of butachlor can also form (2,6-diethylphenyl)-ethoxymethyl-carbamic acid (C) and de-ethane.

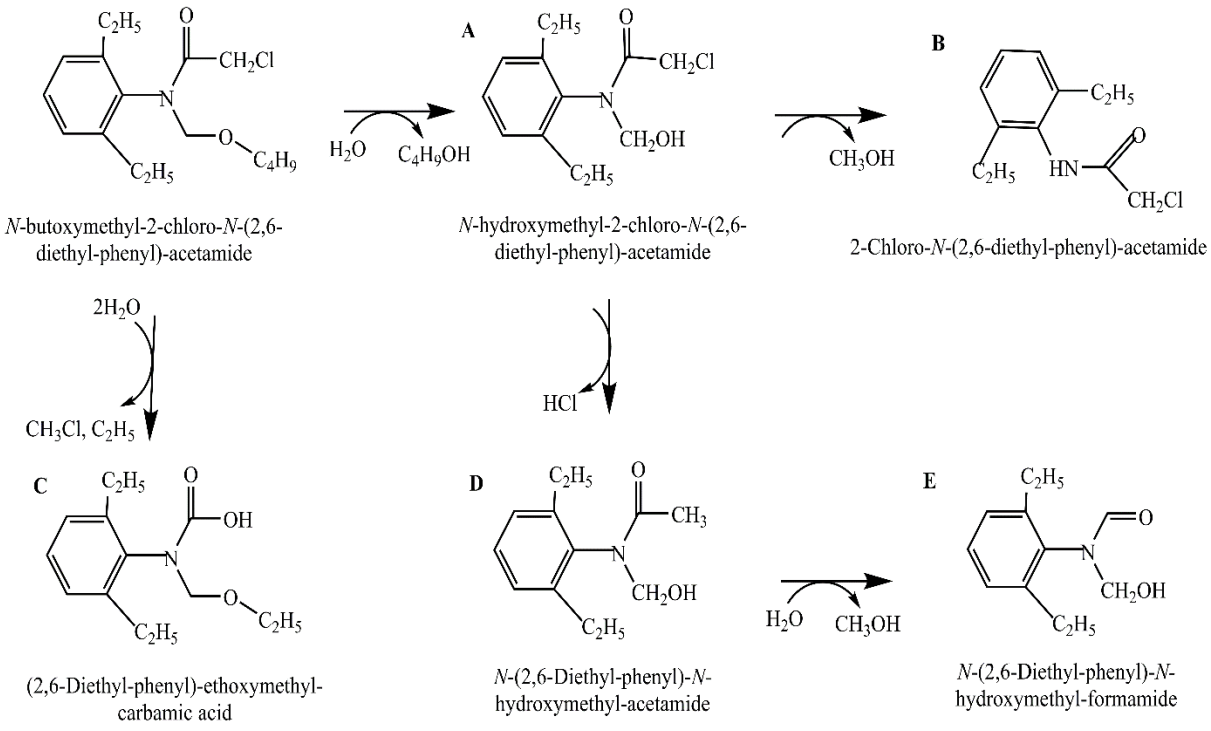


Fig. 2.5: Proposed degradation pathway of butachlor by *Catellibacterium caeni* sp. nov DCA-1^T (Source: Zheng et al., 2012)

In a syntrophic pathway proposed by Kim et al. (2013), butachlor was broken down into 2-chloro-*N*-(2,6-diethylphenyl) acetamide by *N*-dealkylation due to hydrolase activity and then further degraded to 2,6-diethyanaline by strain J7B (Fig. 2.6).

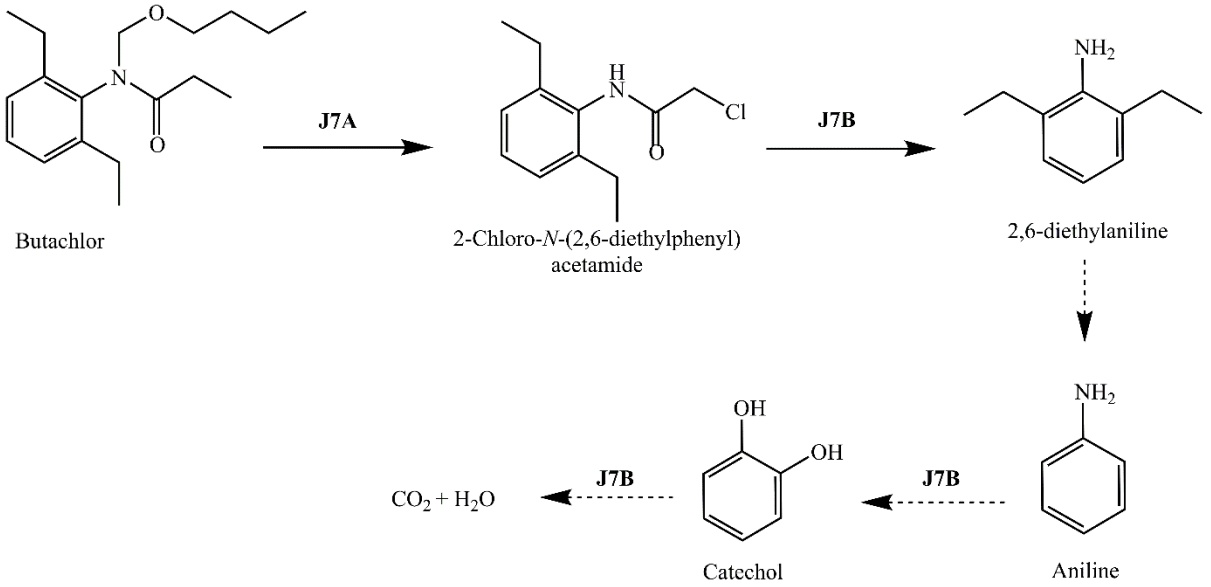


Fig. 2.6: Proposed butachlor degradation pathway by syntrophic pair J7 (Source: Kim et al., 2013)

Fig. 2.7 shows breakdown of butachlor into two compounds *N*-(Butoxymethyl)- 2,6-diethyl-*N*-propylaniline and *N*-(butoxymethyl)-2-ethylaniline by *Ammoniphilus* sp. JF.

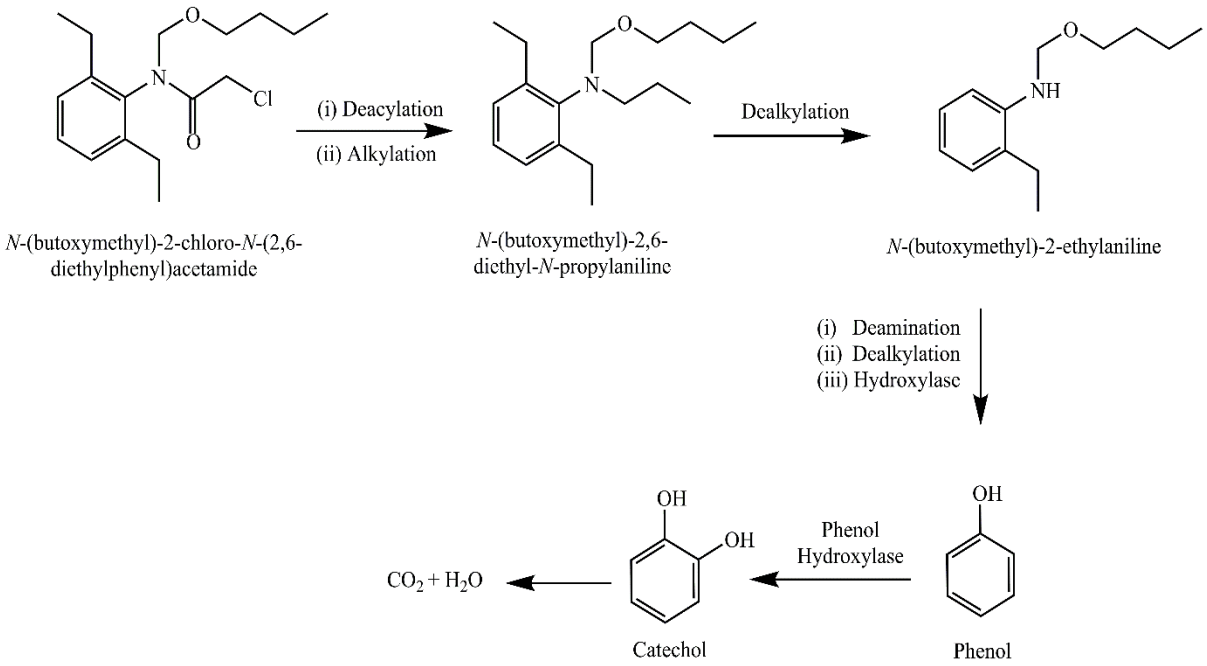


Fig. 2.7: Proposed metabolic pathway of butachlor by *Ammoniphilus* sp. JF (Source: Singh and Nandabalan, 2018)

GC-MS analysis confirmed the formation of 1,2-benzenedicarboxylic acid, 2,4-bis(1,1-dimethylethyl)-phenol, and bis(2-methylpropyl) ester which were the result of deacylation at butachlor's nitrogen group and replacement of acetyl group by alkyl group (alkylation) forming *N*-(butoxymethyl)-2,6-diethyl-*N*-propylaniline. *N*-(butoxymethyl)-2-ethylaniline is formed by dealkylation and deamination reactions producing butoxymethylanamine, which is subsequently dealkylated to phenol; catalyzed by hydroxylase. Phenol is further mineralized to carbon dioxide and water by its oxygenation by phenol hydroxylase forming intermediate catechol (Singh and Nandabalan, 2018).

2.3 Nanotechnology in remediation

Nanotechnology involves synthesis of materials with dimensions in the range of nanometers (10^{-9} m) by manipulating atoms and molecules (Thomé et al., 2015; Rawtani et al., 2018). There are different ways to classify nanomaterials (Fig. 2.8).

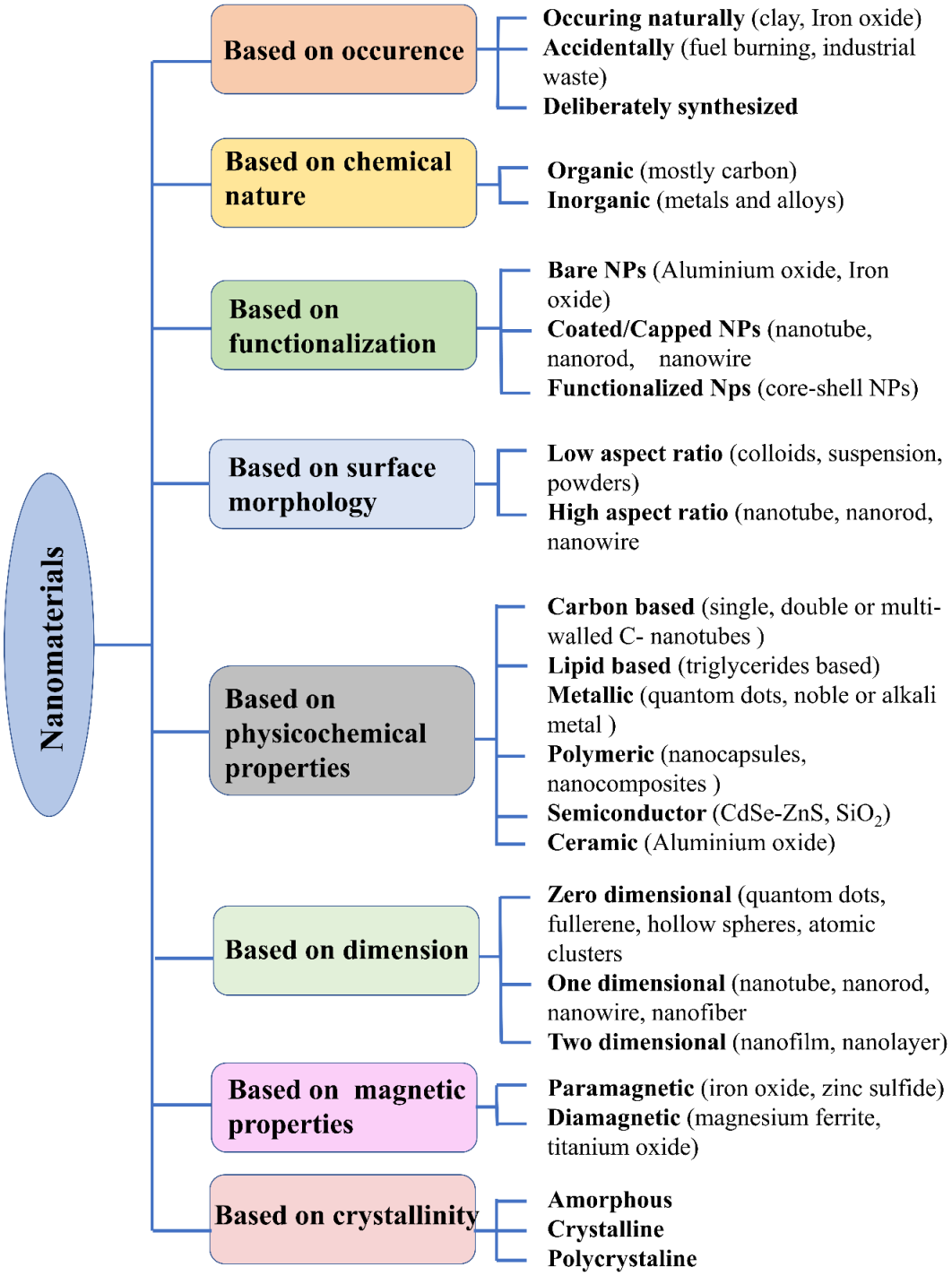


Fig. 2.8: Classification of nanomaterials

Comprehensive approaches available for synthesis of nanomaterials are top-down (i.e., part of the bulk material turns into something smaller) and bottom-up (self-assembly of atomic size particles to grow into nano-sized particles). (Thomé et al., 2015; Ahmad et al., 2019).

The quantum nature of energy state and high surface-to-volume ratio make nano materials of great importance in agriculture for a large number of applications in sensor development, soil remediation and agrochemical degradation. (Ghormade et al., 2011; Zhang et al., 2019). Nanotechnology plays significant role in slow release or delivery of agrochemicals (pesticides, fertilizers, biofertilizers) encapsulated in nanomaterials, delivery of genetic materials for crop improvement, soil conservation and development of nanosensors for plant pathogens and pesticide detection (Ghormade et al., 2011).

Application of nanotechnology in the field of decontamination of water began in 1990s, where Gillham (1996) presented the idea of utilizing zero valence iron (Fe^0) in permeable reactive barriers, on the basis of the work on decontaminating halogenated group containing water using zero valence iron (Gillham and O'Hannesin, 1994). However, the actual research on decontamination of groundwater contaminated with organochlorines using NPs was presented by Wand and Zang (1997). A rapid complete degradation of several aromatic chlorinated and organochlorine pollutants was observed using bimetallic NPs (Ni/Fe, Pt/Fe/Zn, Pd/Fe) stating elements Zn and Fe as electron donors and Pt, Pd and Ni as metal catalysts. Also, zero-valent iron NPs being 100 times more reactive than Fe^0 in the macro-scale form left no by-product on organochlorine degradation, similar to the degradation carried with macro-scale iron, concluding NPs a great approach for further research.

On the basis of chemical reaction involved, remediation using NPs can occur by two ways: (a) stabilization and sorption process, where NPs are used as sorbent or for precipitating the contaminant, and (b) Reduction that uses NPs as electron donors, decomposing the contaminant into a lesser toxic and less mobile form (Cundy et al., 2008; Thomé et al., 2015). Among different remediation techniques available for removal of pollutants, adsorption is considered a suitable approach because of high removal efficiency, relatively low cost, easy recyclability and simplicity of design. Owing to their high surface reactivity and large specific surface area, adsorbents using nano-adsorbents or NPs usually have advantages over their conventional bulk materials. Different kind of interactions such as, hydrogen bonding, hydrophobic effect, electrostatic interaction and ion exchange can take place between nano-adsorbents and adsorbates during the adsorption process (Du et al., 2014; Thomé et al., 2015). There are two

approaches available for degradation or detection/sensing of contaminants including pesticides from aqueous systems- (a) homogeneous; and (b) heterogeneous. Homogenous approach involves dispersing NPs in the water sample containing contaminant (pesticide). With the advantage of utilizing all the surface area of NPs for contaminant removal or detection, this approach possesses a drawback of NP separation from water, where NPs can themselves contaminate purified water. In heterogenous process, NPs are immobilized on different support materials. Further, these NP immobilized support materials are used for contaminant degradation or detection from water samples. The advantages associated with heterogenous approach are reusability of support systems and prevention of NP agglomeration upon their immobilization on solid support materials. However, post immobilization certain changes are noticed in the properties and behaviour of such NPs (Rawtani et al., 2018). Photocatalysis is an effective technique where, semiconductor-based NPs /photocatalysts are used for degradation of organic pollutants in the presence of sunlight or UV- light (Zhang et al., 2019).

2.3.1 Nano-based approaches for pesticide degradation

Nanomaterials such as metallic, bimetallic, metal oxides, nanotubes and nanocomposites have been employed for pesticide detection and their removal. Different nanomaterials employed for sensing, removal and degradation of pesticides have been summarised in Table 2.6, 2.7 and 2.8.

2.3.1.1 Metal nanoparticles

The NPs synthesized from noble metals (gold, silver, palladium and platinum) and some transition metals such as Iron, zinc and copper play significant role in environmental remediation. They offer a great advantage of low-cost precursor requirement along with simple, quick and easy fabrication techniques (Liu et al., 2008). The redox reactions occurring at the NP surface are responsible for degradation of pesticides into lesser toxic and smaller metabolites (Rawtani et al., 2018).

Iron nanoparticles

Iron nanoparticles (FeNPs) play significant role in degradation or removal of harmful contaminants such as heavy metals (Shahriari et al., 2014), dyes (Zhou et al., 2013), phosphates and arsenate (Zeng et al., 2008) and pesticides (San Román et al., 2013). Zero valent (ZV-

Table 2.6: Different nanomaterials for detection of pesticides in different matrix

Nanomaterial	Modification made	Matrix	Pesticide	Detection limit	Reference
AuNPs	Fusion with IgG antibody	Orange, tomato, cucumber and grapes	Kitazine	0.65 – 2.44 µL mL^{-1}	Malarkodi et al., 2017
	Conjugation with anti-DDT antibodies	Cauliflower, grapes, mango juice and milk	DDT	27 ng mL^{-1}	Lisa et al., 2009
AgNPs	Conjugation with Rhodamine B	River water, tomato, and apple	Carbaryl	0.023 ng L^{-1}	Luo et al., 2017
	Capping with citrate	Dipterex	Water	0.18 ng mL^{-1}	Li et al., 2014
SiO_2 NPs	Conjugated with anti-CLT and anti-FNT antibodies	FNT and CLT spiked solution	FNT and CLT	0.25 ng mL^{-1}	Wang et al., 2013b
	Immobilization of AChE and AuNPs	Paraoxan spiked solution	Paraoxan	500 nM	Luckham and Brennan, 2010
Carbon nanotubes	Immobilization of AgNPs	Lake water and orange	Dimethoate	0.01 µg mL^{-1}	Hsu et al., 2017
	Coated with silica & immobilization of phthalocyanine ruthenium	Orange juice	FNT	0.45 µg mL^{-1}	Canevari et al., 2016
Halloysite nanotubes	Immobilization of TiO_2 NPs	Agricultural water, apple, strawberry and celery	Parathion	0.03 µg L^{-1}	Saraji et al., 2016

AuNPs- gold NPs; AgNPs- silver NPs; SiO_2 – silica NPs; TiO_2 – titanium dioxide; DDT- Dichlorodiphenyl trichloroethane; AChE- Acetylcholinesterase; CLT- Chlorpyrifos- methyl; FNT- Fenitrothion

Table 2.7: Different nanomaterials for removal of pesticides

Nanomaterial	Nanomaterial type	Matrix	Pesticide	Degradation mechanism	Removal efficiency (%)	Reference
Metal oxide NP	ZnO NPs	Water	Naphthalene	Adsorption	100	Kaur et al., 2017b
	Fe_3O_4 NPs	Tap, pond and river water	Bifenthrin, deltamethrin, and cyhalothrin	Magnetic separation	80.2	Fan et al., 2017
	TiO_2 NPs	Lake water and rain water	HCB, cis-chlordane, trans-chlordane, o,p-DDT, p,p-DDT and mirex	Adsorption	81.2 (lake) 89.1 (river)	Liu et al., 2015
	Fe_2O_3 NPs	Water	Fenarimol	Magnetic separation and adsorption	70	Ouali et al., 2015
	SiO_2 NPs	Water	metsulfuron-methyl, Bensulfuron-methyl, pyrazosulfuron-methyl, triasulfuron and thifensulfuron-methyl	Adsorption	83.9	Lerma-Garcia et al., 2013
Bimetallic	Fe/Ni NPs	Water	Prefenofos	Adsorption	96	Mansouriieh et al., 2019
Nanotubes	Carbon nanotubes	Water	Fenuron	Adsorption	90	Ali et al., 2019
		Water	Malathion	Adsorption	100	Dehghani et al., 2017
		Fruits and vegetables	Carbofuran and carbaryl	Adsorption	75.7	Makkliang et al., 2016
		Tea	Chlorpyrifos, cypermethrin, buprofezin and pyridaben	Adsorption	70	Hou et al., 2014a

	Halloysite nanotubes	Water	Prometryn	Adsorption	100	Grabka et al., 2015
Nanocomposite	Graphene oxide/ TiO_2	Pesticide spiked water	Butachlor, 2,4-D, trifluralin and glyphosate	Filtration and adsorption	-	Hosseini and Toosi, 2019
	Graphene oxide with Fe_3O_4 NPs	Water	Simazine, Atrazine, simeton ametryn, and prometryn	Electrostatic interaction and magnetic separation	93.61	Boruah et al., 2017
	Montmorillonite with hexadimethrine	Water	2-methyl-4-chlorophenoxy acetic acid	Electrostatic Interaction	94	Gámiz et al., 2015
	Chitosan-ZnO NPs beads	Permethrin spiked water	Permethrin	Adsorption	99	Dehaghi et al., 2014
	Copper coated chitosan	Agricultural runoff	Malathion	Adsorption	>90	Jaiswal et al., 2012
	Chitosan- Ag NPs beads	Atrazine soiked water	Atrazine	Adsorption	98	Saifuddin et al., 2011

Table 2.8: Different nanomaterials for degradation of pesticides

Nanomaterial	Nanomaterial type	Matrix	Pesticide	Degradation mechanism	Degradation efficiency (%)	Reference
Metal NP	FeNPs	Chlorpyrifos spiked soluton	Chlorpyrifos	Enzyme-based catalysis	99	Das et al., 2017
		water	Lindane	Dichloroelimination and dehydrohalogenation	95	San Román et al., 2013
Bimetallic NP	Cu/ZnO Nps	Monocrotophos spiked solution	Monocrotophos	photocatalysis	-	Hanh et al., 2019
	Ag/Cu NPs	water	Chlorpyrifos	Catalytic reduction	-	Rosbero and Camacho, 2017
	Fe/Ni NPs	Sulfentrazone spiked solution	Sulfentrazone	Dechlorination	100	Nascimento et al., 2016
		Profenofos spiked solution	Profenofos	Catalytic reduction	94.5	Mansouriieh et al., 2019
Metal oxide NP	ZnO NPs	Water	Parathion and methyl parathion	photocatalysis	93	Sharma et al., 2016
	TiO_2 NPs	Carbendazim spiked solution	Carbendazim	photocatalysis	98	Kaur et al., 2016
		Borewell and pond water	Chlorpyrifos and monocrotophos	photocatalysis	>95	Amalraj and Pius, 2015
Nanotube	Halloysite Nanotubes	Pentachloro- phenol spiked solution	Pentachloro-phenol	Catalytic oxidation	100	Tsoufis et al., 2017
		4-n-nonylphenol spiked solution	4-n-nonylphenol	photocatalysis	>90	Bielska et al., 2015
Nanocomposites	GO and AgNPs	water	Chlorpyrifos, endosulfan and DDE	Catalytic dehalogenation	95	Koushik et al., 2016

FeNPs) have been used to study degradation of DDT and lindane (El-Temsah et al., 2016, San Román et al., 2013, Elliott et al., 2009). Complete reductive breakdown of pesticide lindane into chlorides and benzene within 24 h was observed by Elliott et al. (2009). In another work reported by San Román et al. (2013), degradation of lindane with ZV-FeNPs and polymer stabilized ZV-FeNPs was compared, where NP stabilization with the polymer prevented their aggregation and led to greater degradation of pollutant. Dechlorination and dehydrohalogenation led to formation of benzene, dichlorobenzene and chlorobenzene as metabolites of lindane. ZV-FeNPs effectively degraded DDT in water and soil, where degradation in water (92%) was higher than soil (22.4%).

Adsorption of 2,4-dichlorophenol was carried out using bio-synthesized FeNPs to facilitate degradation using hydrogen peroxide (Fenton-like oxidation), where FeNPs served as heterogenous catalyst and resulted in formation of acetic acid and acetone as initial intermediate products detected by GC-MS analysis (Guo et al., 2017). In another similar, Das et al. (2017) reported degradation of chlorpyrifos into 1,2 benzenedicarboxylic acid, bis(2-methyl propyl)ester and 2,4-bis(1,1 dimethylethyl)phenol using chitosan coated FeNPs with and without laccase enzyme immobilization.

Gold nanoparticles

Gold (Au) NPs have been extensively applied in detection of several contaminants due to their special optical properties. Their property to change colours with alteration in their shape and size make them useful in remediation of heavy metals (Darbha et al., 2008) and aromatic compounds (Gu et al., 2016). These unique properties have been utilized for detection of various organochlorine and organophosphate pesticides using sensors conjugated with AuNPs (Rawtani et al., 2018). AuNPs have successfully been employed for detection of DDT (Lisa et al., 2009), kitazine (Malarkodi et al., 2017), mathamidophos (Li et al., 2011), malathion (Bala et al., 2017) and parathion (Wu et al., 2017) from different fruits and vegetables.

Silver nanoparticles

Unique size and shape exhibited by silver nanoparticles (AgNPs) provide them various optical, magnetic and electrical properties, which enables their usage in pesticide detection (Siangproh et al., 2017), biosensors and as an antimicrobial agent (Rawtani et al., 2013). Citrate-stabilized AgNPs were used as an effective, analytical probe for detection of organophosphate pesticide,

dipterex, on the basis of acetylcholinesterase (AChE) inhibition, which is responsible for catalysing acetylthiocholine (ATCh) to produce thiocholine (TCh) which further causes aggregation of AgNPs. Since, organophosphates act by inhibiting AChE, therefore, the permanent inhibition of AChE activity induced by dipterex, prevents AgNP aggregation. Hence, the amount of dipterex could be estimated with the colour and UV-Vis spectra changes (Li et al., 2014). Based on similar concept, Luo et al. (2017) detected pesticide carbaryl in river water, apple and tomato, using rhodamine B (RB) modified AgNPs. The enzymatic action of acetylcholinesterase led to color change of RB-AgNPs from yellow to gray. The presence of carbaryl was confirmed when no variation in color was observed. Ly et al. (2019) used AgNPs for adsorption of an insecticide fipronil, and developed a surface-enhanced Raman scattering method for sensing of adsorbed fipronil, with a detection limit of 0.001 mg L^{-1}.

2.3.1.2 Bimetallic nanoparticles

As the name suggests, bimetallic nanoparticles (BNPs) are composed of two metals. BNPs have gained a huge attention due to their fascinating and remarkable characteristics developed due to synergistic effects upon combination of two metals (Rawtani et al., 2018). Several BNPs have proved very effective in degradation of pesticides, especially Ni/Fe NPs. Ni/Fe BNPs efficiently degraded DDT at alkaline or weakly acidic medium (Tian et al., 2009b). In another study, Fe/Ni BNPs successfully degraded 94.51% of 1.4 mg L^{-1} profenofos, where zero valent iron NPs served as reducing agent for profenofos degradation and Ni saved the surface of iron NPs from corrosion, thereby, increasing the reaction rate (Mansouriieh et al., 2019). They are also effective in dechlorination of pesticides sulfentrazone and 4-chorophenol (Nascimento et al., 2016; Shen et al., 2017). 100% dechlorination of sulfentrazone was carried out by 1 g L^{-1} of Fe/Ni BNPs within 30 min (Nascimento et al., 2016). Superoxide radicals produced while the catalytic reaction were accountable for degradation of 4-chorophenol, where phenol and chlorides were identified as degraded products by GC-MS (Shen et al., 2017). Joo and Zhao (2008) reported 65% and 100% degradation of Lindane using Fe-Pd BNPs by aerobic (Fenton-like process) and anaerobic (reduction process), respectively. In another work, bio-synthesized Ag/Cu BNPs were used as nano-catalysts for degradation of chlorpyrifos into trichloropyridinol and diethyl-thiophosphate (Rosbero and Camacho, 2017).

2.3.1.3 Metal oxide nanoparticles

Due to their superconducting nature, different kinds of metal oxide NPs such as titanium oxide (TiO_2) NPs, iron oxide (Fe_3O_4 or Fe_2O_3) NPs, zinc oxide (ZnO) NPs and silica (SiO_2) NPs have been widely used for the sensing, removal and degradation of pesticides. The metal oxide NPs possess specific photocatalytic activity, which make them efficient agents for degradation of contaminants.

Titanium oxide nanoparticles

Due to their exceptional photocatalytic activity at wide range of temperature and pH, non-toxicity, stability towards chemicals and low-cost, titanium oxide NPs (TiO_2) have extensively been studied in remediation of contaminants from the environment. Liu et al. (2015) worked on microextraction of six organochlorine pesticides (cis-chlordane, trans-chlordane, p,p-DDT, o,p-DDT, hexachlororbenzene and mirex) from lake and river water samples by fabricating solid-phase microextraction fiber using mesoporous TiO_2 NPs. In a study conducted by Yu et al. (2008), TiO_2 NPs completely mineralized dicofol in 2h under UV light irradiation. Monocrotophos and chlorpyrifos present in borewell and pond water were effectively degraded by TiO_2 when irradiated with UV light source, where photodegradation efficiency was elevated with increase in illumination time (Amalraj and Pius, 2015). The photocatalytic efficiency of TiO_2 NPs is enhanced by doping them with different metal ions. TiO_2 NPs doped with Si and Fe ions resulted in 98% decomposition of carbendazim under solar radiations (Kaur et al., 2016). In another study, cobalt- doped TiO_2 NPs were employed for degrading 2,4-dichlorophenol during advanced oxidation process in visible light (Hoseini et al., 2017).

Zinc oxide nanoparticles

Zinc oxide nanoparticles (ZnO NPs) possess higher density at the edge-points on their surface, contributing to unique physical and chemical properties. Their surface functionalization enhances the detection and photocatalytic properties (Rawtani et al., 2018). The significance of surface functionalization of ZnO NPs have been studied by utilizing them as nano-adsorbents after functionalization with 1-butyl-3-methylimidazolium tetrafluoroborate (BMTF-IL) and cetyltrimethyl ammonium bromide (CTAB) for the elimination of naphthalene from liquid solutions, where BMTF-IL functionalized NPs exhibited higher adsorption capacity (148.3 mg g^{-1}) for the naphthalene in comparison to CTAB functionalized NPs (89.96

mg g^{-1}) as well as bare ZnO NPs (66.8 mg g^{-1}) (Kaur et al., 2017b). ZnO NPs were used as nano-photocatalyst for breakdown of methyl parathion and parathion from water samples after irradiation with the UV-light. 93% degradation of pesticides was achieved under optimum conditions (Sharma et al., 2016).

Silica nanoparticles

Silica (SiO_2) NPs are sphere-shaped, porous particles (microporous, mesoporous or hollow porous), which can be synthesized by biological or chemical ways (Bapat et al., 2016; Rawtani et al., 2018). They have been widely utilized for remediation of pollutants after chemical or physical modification, after conjugating with diverse biological and/or chemical molecules. SiO_2 NPs possess large surface area, making them useful in preparation of sorbents used in solid-phase extraction (SPE) of pollutants from several samples. They were functionalized with *N*-methylimidazole and used for extraction of a polar pesticide, sulfonylurea present in water (Lerma-Garcia et al., 2013). Ibrahim et al. (2013) used SiO_2 NPs for extraction of organophosphates (mathamidophos, chlorpyrifos, dicrotophos, methidathion, malathion, and diazinon) after co-functionalization with non-polar methyltrimethoxysilane and polar cyanopropyltriethoxysilane.

Iron oxide nanoparticles

Nanosized iron oxides namely hematite (α-Fe_2O_3), maghemite (γ-Fe_2O_3) and magnetite (Fe_3O_4) are widely studied nano-adsorbents in the environmental remediation due to their high pollutant removal capacity. Their fast reaction kinetics and easy removal from the system due to their magnetism ability make them advantageous over other NPs. The specificity and effectiveness of iron oxide NPs can be enhanced by surface modifications and controlling shape and size of NPs. Ouali et al. (2015) utilized palygorskite immobilized Fe_2O_3 NPs for adsorption of a fungicide, fenarimol. This magnetically modified clay was stable for 2 weeks and showed 70% removal of fenarimol. Its retention capacity was significantly enhanced by immobilized Fe_2O_3 NPs. In similar study, silica entrapped iron oxide NPs were used for adsorption of glyphosate from water (Fiorilli et al., 2017). Fan et al. (2017) reported the removal of 4 different types of pyrethroid pesticides from various water samples by combining Fe_3O_4 NPs treatment with liquid-liquid extraction.

2.3.1.4 Nanotubes

Nanotubes are hollow, long, cylinderical NMs having diameters of about 1-100nm. Carbon nanotubes (CNTs) along with Halloysite Nanotubes (HNTs) have gained huge attention in detection and removal of different contaminants from the environment due to their large aspect ratio and surface area.

Carbon nanotubes **(CNTs)**

CNTs are graphene-based NMs, exhibiting excellent chemical stability and thermal properties with significant optical, electrical and mechanical properties. They can be single walled (SWCNTs), or multi-walled with concentric SWCNTs possessing a common longitudinal axis (Rawtani et al., 2018). CNTs have been used for detection and remediation of pesticides, heavy metals and toxic dyes. Hou et al. (2014a) used MWCNTS for adsorption of seventy-eight pesticides from spiked tea samples by SPE method, which were later sensed with GC-MS/MS. This technique proved beneficial and efficient in detection and removal of several pesticides from real tea samples, where cypermethrin, buprofezin, chlorpyrifos and pyridaben had a detection rate of 50.9 %, 49.1%, 54.5% and 50.9%, respectively. Using a similar approach, poly(3,4-ethylenedioxythiophene)-doped CNTs, functionalized with ionic-liquid polymer were used for carbamates' removal (Wu et al., 2016). Canevari et al. (2016) used SiO_2-coated MWCNTs immobilized with phthalocyanine ruthenium to determine fenitrothion present in orange juice samples. This NM exhibited great specificity for fenitrothion with limit of detection of 0.45 mg L^{-1}. MWCNTs could also successfully remove malathion from water samples (Dehghani et al., 2017).

Halloysite nanotubes **(HNTs)**

HNTs are the nanotubular clay minerals present as aluminosilicate, with thin mesoporous lumen in nanometer range. Because of their huge surface area, low-cost, non-toxic nature and biocompatibility, HNTs have gained huge popularity in different applications such as removal of toxic dyes, as a nano-support to immobilize drugs, enzymes, NPs and hormones and detection and degradation of pesticides (Rawtani et al., 2018). Excellent adsorption capacity of HNTs was utilized by Grabka et al. (2015) for removal of prometryn from water. An environment-friendly solid-phase micro-extraction fiber coating was fabricated using HNTs along with TiO_2 NPs, which was utilized for detection and extraction of parathion (Saraji et al., 2016). Incorporation of Fe_2O_3 NPs in HNTs enhanced the catalytic breakdown of

pentachlotophenol, suggesting HNTs improve the catalytic property of iron oxide NPs (Tsoufis et al., 2017).

2.3.1.5 Nanocomposites

Nanocomposites are a mixture of hybrid/heterogenous materials, composed of at least one nanoscale phase (nanofiller) dispersed in another phase called matrix to obtain properties that are combination of its constituents. These properties offer great application in remediation of pesticides. Nanocomposite prepared from montmorillonite and a cationic polymer hexadimethrine was used to remove anionic herbicide 2-methyl-4-chlorophenoxyacetic acid based on the mechanism of electrostatic interaction between ammonium group of polymer nanocomposite and herbicide, proving it an outstanding adsorbent for anionic pesticides (Gámiz et al., 2015). An oxidized form of graphene, graphene oxide (GO) has been widely used for synthesis of several nanocomposites with different metal/metal oxide NPs, which play great role in pollutant remediation. The process behind solid adsorptive nature of GO towards several pesticides is a strong π-π interaction of pollutants with its aromatic ring (Rawtani et al., 2018). A nanocomposite of reduced GO (rGO) with Fe_3O_4 NPs effectively adsorbed 93.61% of pesticide triazine by the electrostatic interactions between them (Boruah et al., 2017). Koushik et al. (2016) used rGO-AgNPs nanocomposites for degradation of organochlorine pesticides (endosulfan, chlorpyrifos and dichlorodiphenyldichloroethylene), where rGO adsorbed the products degraded by AgNPs by dehalogenation reaction.

2.3.2. Chitosan based nanocomposites in nanoremediation

Chitosan (β-1,4-linked polysaccharide) is a cationic polymer produced in bulk from chitin (crustaceans shells) as a by-product (Agnihotri et al., 2012; Gholamali et al., 2020). Fig. 2.9 shows the general structure of chitosan. Because of its extraordinary properties, such as gel forming capability, low toxicity, biodegradability, biocompatibility, eco-friendliness and adsorption capacity, chitosan is used as a sorbent for removal of contaminants (Agnihotri et al., 2012; Habiba et al., 2019). Its sorption efficiency is attributed to the presence of amino and hydroxyl groups on the glucosamine unit (Dwivedi et al., 2014). The limitation linked to chitosan hydrogel is its poor mechanical strength on swelling and sensitivity to pH, which can be minimized by chemical crosslinking it with another polymer possessing greater mechanical strength and addition of cross-connecting agents such as glutaraldehyde, formaldehyde glyoxalin and isocyanides etc (Agnihotri et al., 2012; Habiba et al., 2019). Polyvinyl alcohol

(PVA) is a water soluble, vinyl type polymer, extensively studied due to its hydrophilicity, excellent chemical stability, gel and film forming ability, biocompatibility, greater mechanical strength and non-toxic nature (Agnihotri et al., 2012; Krstić et al., 2014; Gholamali et al., 2020). To enhance the adsorption properties and complete elimination of the contaminants, nanoparticles are incorporated within the crosslinked and swollen networks to form nanocomposite hydrogels (Habiba et al., 2019; Gholamali et al., 2020).

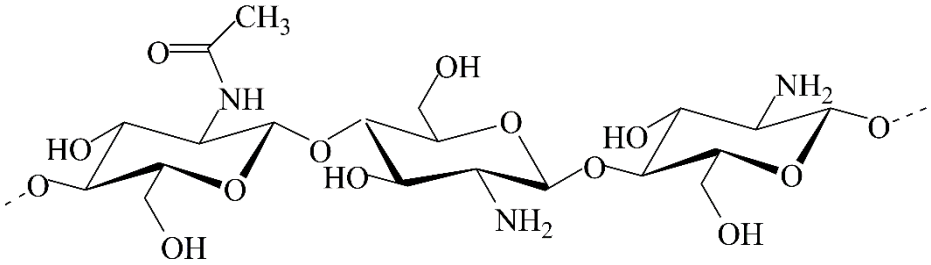


Fig. 2.9: Chemical structure of chitosan

Chitosan nanocomposites with different metal NPs have proved to be great adsorbents for removal of different pesticides. Dwivedi et al. (2014) synthesized gold nanoparticles (GNP) embedded in a cross-linked chitosan polymer matrix and used the nanocomposite for removal of the pesticide methyl parathion. In another similar study, chitosan-ZnO nanocomposite beads successfully removed 99% of permethrin (Dehaghi et al., 2014). Chitosan when complexed with magnesium, calcium, iron (III), and zinc was effective in degradation of four organophosphorous pesticides (dichlorvos, omethoate, dimethoate, chlorpyrifos) by solid phase extraction method (Zhang et al., 2015). Lu et al. (2011) used chitosan beads along with crab shell powder for removal of organochlorines.

2.3.3 Hydrogel as an immobilizing matrix for nanoparticle synthesis

Hydrogel is a gel-like, water-insoluble polymeric network which has a potential to retain water and shows swelling properties due to the presence of several functional groups such as hydroxyl, amino, amide, carboxyl and sulphonic in the polymers of the hydrogel forming network (Agnihotri et al., 2012). Common techniques available for synthesis of hydrogels are cross-linking by chemical agents, physical means or radiations such as UV and electron beam irradiation (Nangia et al., 2018).

2.3.3.1 Fabrication of chitosan-based hydrogel

Fabrication of chitosan-based composites can be done by physical as well as chemical mechanisms, where physical measures lead to formation of electrostatic bonds forming a weak network and chemical measures enhance the strength of the matrix (Nangia et al., 2018). Sol-gel method can be used for preparing chitosan based hydrid hydrogels such as chitosan/PVA hydrogel using crosslinkers such as glutaraldehyde. Macromolecular chains present in the preliminary material such as chitosan or PVA are linked together forming large branched but soluble polymer called sol. As this linking continues, with increase in size, decrease in solubility occurs, resulting in the formation of 'network' or 'gel'. This transition of the structure is called sol-gel transition or gelation (Rubinstein and Colby, 2003). Chemical crosslinking method is quite popular for achieving permanent hydrogel with higher mechanical strength which involves the use of linking two polymers with a cross-linking agent such as glutaraldehyde. Further, freeze- drying methods are also used where the hydrogels are frozen at very low temperature and then thawing is done at room temperature. Repetitive free-thawing leads to generation of highly porous hydrogels (Agnohotri et al., 2012; Nangia et al., 2018).

2.3.3.2 Silver nanoparticle-polymer hydrogel nanocomposite

Recent studies make use of *in-situ* synthesis of metal NPs inside the polymeric hydrogel networks. After the fabrication of hydrogels, AgNPs are synthesized within the hydrogel by chemical or biological means of nanoparticle synthesis. Such hydrogels contain the characteristics of both AgNPs and the polymers involved. Nithya et al. (2015) synthesized chitosan-silver nanocomposite without using a chemical-reducing agent which possessed photocatalytic activity and degrade 81% of methyl red dye. GO-AgNP hydrogel synthesized by Zeng et al. (2015) displayed antibacterial activity and could also be used for water disinfection. Another nanocomposite, PVA/gum acacia hydrogel produced by γ-radiation stimulated cross-linking with *in-situ* synthesized AgNPs also showed antibacterial activity, which could be decreased with increase in gum acacia concentration. This hydrogel could also be applied for disinfection of water (Juby et al., 2012).

2.3.3.3 Characterization of synthesized silver nanoparticles and chitosan-based hydrogel

The main characteristics of nanocomposite that must be determined are its morphology, size distribution of synthesized AgNPs within it, optical properties, specific surface area, crystallographic characterization and thermal properties. Fig. 2.10 shows schematic

representation of different characterization techniques used to study chitosan-based metal nanocomposites.

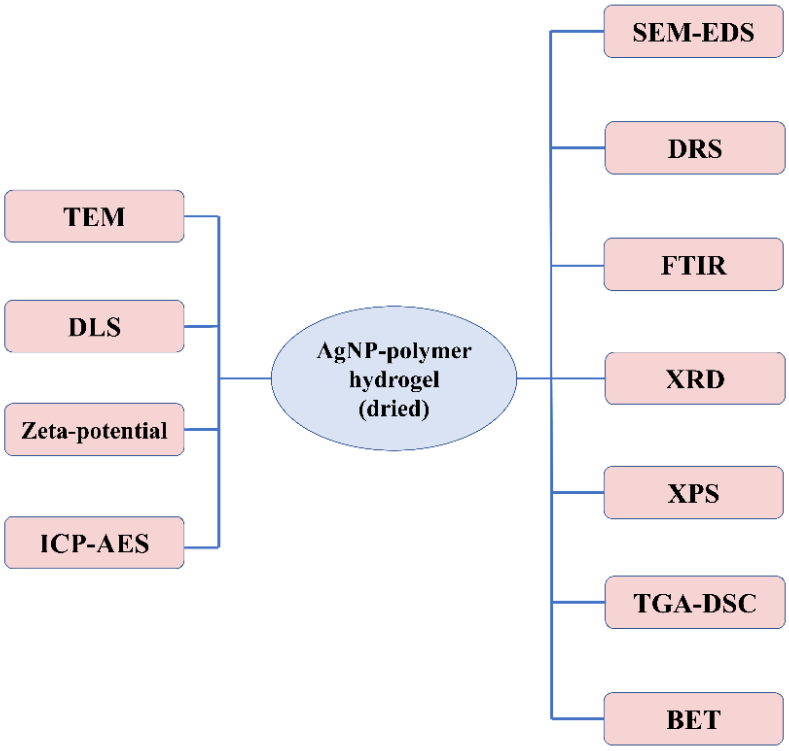


Fig. 2.10: Schematic representation of different characterization techniques

For determining morphology of synthesized hydrogel nanocomposite, imaging equipment is used, the most common equipment used for the purpose are scanning electron microscopy (SEM) and transmission electron microscopy (TEM). The freeze-dried hydrogel sample is mounted on a sample holder with the conductive tape along with conductive metal (gold or platinum) coating with a sputter coater and scanned with SEM. To determine size and shape of synthesized NPs in the hydrogel, the hydrogel discs are dispersed in distilled water overnight and a suspension is produced using ultrasonic water bath, followed by centrifugation to separate large particles (Elbarbary and El-sawy, 2017). Then this suspension is subjected to and Dynamic light scattering (DLS), along with zeta-sizer to know hydrodynamic size and surface charge on the synthesized metal nanoparticles.

The optical properties of nanocomposite are analyzed from the optical band gap energy obtained from diffused reflectance spectra (DRS) analysis. To estimate the amount of silver present the hydrogel, a pre weighed hydrogel is subjected to nitric acid digestion and diluted, followed by filtration. The filtrate is then subjected to ICP-AES (Agnihotri et al., 2012).

Presence of silver NP is also confirmed by subjecting the hydrogel to EDX ananlysis. To determine the cross-linking between the polymers and studying the interaction of the functional groups in hydrogel synthesis along with incorporation of AgNPs within it, FTIR analysis is done (Elbarbary and El-sawy, 2017).

Crystallography of the fabricated hydrogel is determined using X-ray diffraction (XRD), which tells the crystalline or amorphous structure of the metal NPs synthesized within the nanocomposite (Thomé et al., 2015). The diffractogram of nanocomposite containing AgNPs showed five peaks at 2θ values of 38.02°, 44.3°, 64.6°, 77.5° and 81.9° corresponding to Bragg's reflections from (1 1 1), (2 0 0), (2 2 0), (3 1 1) and (2 2 2) planes of the face centered cubic (FCC) crystal structure of AgNPs (ICDD card no. 03-065-2871), confirming crystalline structure of AgNPs (Mishra et al., 2015).

X-ray photoelectron spectroscopy (XPS) analysis is carried out to study the chemical state of metal NP in nanocomposite (Nivethaa et al., 2015). Brunauer–Emmett–Teller (BET) and the gas adsorption isotherms method are commonly used to study the pore size and specific surface area of fabricated nanocomposite. To determine thermal properties of the nanocomposite, dried sample is subjected to TGA-DSC in a nitrogen atmosphere.

2.4 Conclusion

Extensive use of pesticides such as butachlor and monocrotophos have not only contaminated top soil, but also groundwater, causing several harmful effects to non-target organisms. Several microbes have also been studied to degrade different pesticides. In this study, degradation of pesticides was carried out using bacterial isolates and suitable degradation pathways were proposed based on the metabolites obtained from GC-MS analysis. Also, adsorption and photo-degradation of butachlor was carried out using nanocomposites, and degraded products were studied using LC-MS analysis and a plausible pathway was proposed. Based on this, following objectives were designed:

Objectives

1. Screening of bacterial isolates for degradation of pesticides.
2. Fabrication and characterization of Hydrogel-nanoparticulate system for degradation of pesticide.
3. Removal of butachlor from synthetic water using hydrogel-nanoparticulate system.

Chapter III- Materials and methods

3.1 Materials required

3.1.1 Chemicals and glassware

General (analytical) chemicals

Certified standard analytical grade herbicide butachlor with 97.7% purity and monocrotophos with 99% purity were procured from Sigma Aldrich and their stock solutions were made in acetone and ethyl alcohol (HPLC grade), filtered and stored in dark bottles. Chitosan, in powder form (>90 % deacetylation degree) was procured from Marine Hydrocolloids, Cochin, Kerala and was used without any treatment. PVA (MW 1,60,000), sodium hydroxide and sodium borohydride were purchased from Himedia. Silver nitrate ($AgNO_3$) was obtained from Sigma Aldrich. Other analytical grade chemicals, such as glacial acetic acid and glutaraldehyde solution (25 wt%) were obtained from SD Fine Ltd. All other reagents such as dichloromethane were of high purity and analytical grade. Deionized water was used in the entire study.

Bacteriological media

Nutrient broth (NB) used for growth of bacterial cultures and Minimal salt media Bushnell Hass (BH) used to study butachlor degradation by bacterial isolates were purchased from Himedia (Appendix 1). Mueller Hinton (MH) media used for studying monocrotophos degradation was also procured from Himedia. Solid agar medium used in the study was prepared by mixing 1.8% (w/v) agar (purchased from Himedia) to the respective liquid broth.

Bacterial strains

Eleven different bacterial strains were procured from Research Lab III, Department of Biotechnology, TIET, Patiala. Four other bacterial isolates were screened and identified from soil samples collected earlier from coal tar contaminated soil of Patiala, located at 30.3530° N, 76.3710° E, 310 m above the sea level.

Glassware and plasticware

Glassware used in the entire study was of borosil or JSGW make and the plasticware used was procured from Tarsons, India.

3.1.2 Sterilization techniques

All the glasswares used the entire study were washed properly with detergent solution and oven dried at 40-50 °C. After drying, they were treated with Aqua Regia (Appendix 1) or acid wash to remove all the accumulated metals and salts, followed by washing with distilled water. For all the bacterial studies, glasswares, solutions, deionized water and nutrient media were autoclaved for 15 min at 121 °C.

3.2 Screening of bacterial isolates for degradation of pesticides

Different bacterial strains (Table 3.1) such as *Bacillus subtilis* (NA15), *Bacillus licheniformis* (NA8, NA9, NA11, NA14, DGB, DGC), *Lysinibacillus fusiformis* (DGA), *Citrobacter* sp. (CT5, CS8) previously isolated from paper pulp, compost, sugarcane bagasse, tannary effluent and chrome sludge respectively, along with *E.coli* and un-identified bacterial isolates (A12, A14, A15, A16) from coal tar contaminated soil were screened for their potential for effective degradation of two pesticides monocrotophos and butachlor.

Table 3.1: Bacterial isolates used in the study

S.No	Identification	Bacterial Isolate	Source
1	*Bacillus licheniformis* LZBL8	T8	Paper Pulp
2	*Bacillus licheniformis* X2	NA9	Paper Pulp
3	*Bacillus licheniformis* CK1	NA11	Compost
4	*Bacillus licheniformis* BPRIST030	NA14	Compost
5	*Bacillus subtilis* HB1	NA15	Compost
6	*Lysinibacillus fusiformis* N139	DGA	Sugarcane bagasse
7	*Bacillus licheniformis* BAB1836	DGB	Sugarcane bagasse
8	*Bacillus licheniformis* MS514	DGC	Sugarcane bagasse
9	*Bacillus* sp.	A12	Soil
10	*Bacillus* sp.	A14	Soil
11	*Bacillus* sp.	A15	Soil
12	*Bacillus sp.*	A16	Soil
13	*Citrobacter* sp. IS2	CT5	Tannery effluent
14	*Citrobacter freundii* IS4	CS8	Chrome sludge
15	*E. coli* DH5α	DH5α	MTCC (1652)

3. 2.1 Isolation of monocrotophos degrading bacteria

All the purified bacterial isolates were tested for their capability to grow in the presence of monocrotophos. The degradation experiment was conducted by standard disc/well diffusion method. Autoclaved MH Agar media was poured in disposable petri plates and left undisturbed to let it solidify. The MH agar plates were inoculated with bacterial isolates (10^8 cfu mL^{-1}) with the help of sterile cotton swab or glass spreader to form an even bacterial lawn. The even sized wells generated with cork borer were filled with 100 µL of different concentrations (0.5, 1, 2, 4, 8, 16, 32, 64, 128, 250 and 500 mg L^{-1}) of commercial grade monocrotophos and left undisturbed for proper diffusion/leaching of the insecticide. The petri plates were then sealed with parafilm, followed by 24 h incubation at 37 °C. Each set was carried out in triplicates and a negative control was prepared using same solvent (autoclaved distilled water) used to prepare monocrotophos working concentrations. Plates were observed after 24 h and Zone of inhibition (ZOH) produced due to inhibited bacterial growth caused by leaching of monocrotophos was measured. Bacterial isolate showing smallest/no ZOH at highest monocrotophos concentration (i.e. higher tolerance) was further studied (Bauer et al., 1966; Buvaneswari et al., 2017; Khurana et al., 2016).

3.2.2 Biodegradation of monocrotophos by *Bacillus licheniformis* BPRIST030 and identification of metabolites

Bacterial cells grown in Bushnell Hass broth containing 50 mg L^{-1} monocrotophos (analytical grade) were separated in the late log phase by centrifuging at 4 °C and 8000 rpm. Cell pellet was washed thrice with BH broth; inoculum size was adjusted to 0.01 (OD_{600nm}) with BH broth spiked with 50 mg L^{-1} monocrotophos and was then incubated for 5 days (120 h) at 37 °C, 120 rpm in an incubator shaker. After time intervals of 24 h, aliquots of culture were collected and cell density (OD_{600nm}) was determined along with cfu mL^{-1}. A control devoid of the bacteria was run under the same conditions.

Monocrotophos and its degraded metabolites in the liquid medium were analysed after 120 h. 2mL of the sample aliquot was sonicated and centrifuged for 8 min at 12,000 rpm; the supernatant was subjected to solvent extraction using double volume of acetonitrile - dichloromethane (2:1) in a separating funnel. The resultant extract obtained was dried over anhydrous sodium sulphate and evaporated. The insecticide residue obtained was dissolved in dichloromethane, filtered (pore size - 0.22 µm) and stored until gas chromatography- mass spectrometry (GC–MS) analysis was done. The analysis was conducted in electron ionization

mode (ionization energy-70 eV) on Thermo Trace 1300GC device coupled with Thermo TSQ 800 Triple Quadrupole MS, equipped with BP 5MS capillary column (30m length × 0.25mm inner diameter × 0.25µm film thickness), using helium as a carrier gas at a constant flow rate of 1 mL min^{-1}. The column temperature was programmed at 50 °C (2.0 min hold) to 100 °C at 20 °C min^{-1}, then increased to 180 °C at 8 °C min^{-1}, and finally programmed to 260 °C (1.0 min hold) at 50 °C min^{-1} with injection temperature set at 220 °C. The samples were injected in split mode (20:1) and detected in the mass range (m/z) 30 to 650. Based on the GC-MS analysis degradation pathway was proposed.

NOTE: In the mid of study, monocrotophos was banned in India, hence unavailable for further study. So, the entire work was conducted on another pesticide, butachlor.

3.2.3 Isolation of butachlor degrading bacteria

Isolation of bacterial isolates capable of degrading butachlor was carried out as per section **3.2.1**, followed by selective enrichment technique using butachlor spiked minimal media Bushnell Haas (BH) broth. Bacterial isolates were individually added to a 250 ml conical flask containing 100 mL BH broth spiked with 20 mg L^{-1} butachlor as a sole carbon source and incubated for 5 days (120 h) in an incubator shaker at 120 rpm, 37 °C. 5mL of the enrichment culture were sub-cultured into fresh BH, spiked with 50 mg L^{-1} butachlor. The residual concentration of butachlor in broth was measured by UV scan in the range of 200-800nm (λ_{max} for butachlor was 265nm) (Haq et al., 2019; Kim et al., 2013). Calibration curve (OD_{265nm}) from known concentrations of butachlor in BH was prepared to calculate its residual concentration (Appendix II).

Percent degradation (χ) was calculated as per the following equation

$$\chi = \frac{C_0 - C_1}{C_0} \times 100 \quad (1)$$

where, C_1 is the concentration of butachlor after 120 h and C_0 is the concentration of butachlor at zero-time interval.

3.2.4 Identification of bacterial isolate by 16S rRNA analysis

Genomic DNA from bacterial strain was isolated using DNA Extraction Solution (Cat No. 2120600021730), followed by amplification of its 16S rRNA gene by polymerase chain reaction (PCR) using enzyme Taq DNA Polymerase, dNTPs and primers (27F (5′-AGAGTTTGATCCTGGCTCAG -3′) & 1492R (5′-TACGGCTACCTTGTTACGACTT -3′). Total volume of reaction mixture used for PCR was 50µL and the Thermal cycler was run for 35 cycles. Bacterial isolate was sequenced (16S rRNA gene sequencing) at Genei Laboratories

Pvt Ltd. In order to identify the bacterial strain, sequences closely related to its 16S rRNA gene were downloaded from the NCBI website (16S ribosomal RNA sequences (Bacteria and Archaea) database) using an algorithm Basic Local Alignment Search Tool (BLAST). Identification of 16S rRNA sequence was confirmed using available DNA data in EzTaxon-e database (https://eztaxon-e.ezbiocloud.net/) introduced by Kim et al. (2012). Closely related sequences obtained were subjected to pairwise alignment (CLUSTALW) and a phylogenetic tree was generated by MEGA X software, using neighbour-joining method with Kimura two-parameter distance model for calculating evolutionary distances (Kumar et al., 2018). Bootstrap analysis with 1000 replications was performed to assess the statistical support for the phylogenetic tree.

3.2.5 Biodegradation of butachlor by *Bacillus altitudinis* A16

Bacterial cells grown in Bushnell Hass broth containing 50 mg L^{-1} butachlor were separated in the late log phase by centrifuging at 4 °C and 8000 rpm. Cell pellet was washed thrice with BH broth; inoculum size was adjusted to 0.02 (OD_{600nm}) with BH broth spiked with 50 mg L^{-1} butachlor and was then incubated for 5 days (120 h) at 37 °C, 120 rpm in an incubator shaker. After time intervals of 24 h, aliquots of culture were collected and cell density (OD_{600nm}) was determined along with cfu mL^{-1}. To determine residual concentrations of butachlor, supernatant obtained after centrifuging (12,000 rpm for 8 min) culture aliquot was subjected to UV scan in the range of 200-800nm on Elisa reader with additional cuvette port (Thermo Fischer Scientific) (Liu et al., 2012; Kim et al., 2013; Haq et al., 2019). A control devoid of the bacteria was run under the same conditions. Percent degradation and residual concentration was calculated using equation (1) and calibration curve (Appendix II) obtained from butachlor standard.

3.2.6 Degradation Kinetics

The kinetics of butachlor degradation by strain A16 was studied by testing four different kinetic models: first order, pseudo-first order, second order, and pseudo-second order (Agnihotri et al., 2018). These models were expressed by the following equations:

First order: $$\ln C = \ln C_0 - kt \quad (2)$$

Pseudo-first order: $$\ln[C_0 - C] = \ln C - kt \quad (3)$$

Second order: $$\frac{1}{C} = \frac{1}{C_0} + kt \quad (4)$$

Pseudo-second order: $$\frac{t}{C} = \frac{t}{C_0} + \frac{1}{kC_0^2} \quad (5)$$

where, C_0 is the initial butachlor concentration at time zero; C is butachlor concentration at time, t and k is the kinetic rate constant.

3.2.7 Chemical analysis and identification of intermediates

Butachlor and its degraded metabolites in the liquid medium were analysed after a time interval of 48 h and 120 h. 2mL of the sample aliquot was sonicated and centrifuged for 8 min at 12,000 rpm; the supernatant was subjected to solvent extraction using double volume of dichloromethane in a separating funnel. The extract containing degraded metabolites was dried over anhydrous sodium sulphate and evaporated. The herbicide residue obtained was dissolved in acetonitrile, filtered (pore size-0.22 µm) and stored until gas chromatography- mass spectrometry (GC–MS) analysis was done. The analysis was carried out in electron ionization mode (ionization energy-70 eV) on Perkin-Elmer clarus 500 GC device, equipped with Elite-5MS capillary column (25m length × 0.20mm inner diameter × 0.33µm film thickness), using helium as a carrier gas at a constant flow rate of 1 mL min^{-1}. The column temperature was programmed at 100 °C for 2 min, then increased to 280 °C at 10 °C min^{-1} (20 min hold), with injection temperature set at 250 °C. The samples were injected in split mode (1: 20) and detected in the mass range (m/z) 30 to 650. Based on the GC-MS analysis degradation pathway was proposed.

3.3 Fabrication and characterization of hydrogel-nanoparticulate system for degradation of pesticide

3.3.1 Preparation of crosslinked Chitosan/PVA hydrogel

Chitosan solution was prepared by dissolving chitosan (2% w/v) in glacial acetic acid (2% v/v) at room temperature under continuous stirring, while aqueous solution of PVA (4% w/v) was made by dissolving PVA in deionized water at 60 °C for 5 h. The viscous chitosan solution was filtered to remove impurities and mixed with the PVA solution. This chitosan/PVA blend was stirred at 60 °C for 2 h and then left overnight for continuous stirring to obtain a homogenous polymeric mixture. Cross-linking agent glutaraldehyde (30 mM) was added drop-wise to the resulting mixture and mixed well for 5 min to achieve polymeric network formation.

The resultant solution was casted in the test tubes and kept in oven at 60 °C for about 6 h to obtain hydrogel membranes. The hydrogels were removed from the test tubes by precipitating with aqueous NaOH (12% w/v) at room temperature, rinsed thrice with deionized water, followed by 24 h soaking in deionized water and lyophilization. Finally, to obtain porous semi-interpenetrating networks, the hydrogel formed was subjected to repeated freeze-thaw cycles at -20 °C for 6 h and room temperature for 2 h, respectively. In this way, Ch/PVA hydrogel was prepared.

3.3.2 Preparation of Ch/PVA-Ag Nanocomposite Hydrogels

Ch/PVA hydrogel was cut into circular discs (10 mm diameter) and introduced into silver ion precursor i.e. silver nitrate ($AgNO_3$) solution (5mM) for 24 h to load silver ions (Ag^+) within the hydrogel. The Ag^+ loaded Ch/PVA discs were washed thrice with deionized water to achieve removal of the unbound Ag^+ and were further subjected to reduction by $NaBH_4$ solution (10 mM) for 30 min. Following complete reduction, Ag^0 immobilized discs were again rinsed with deionized water several times, lyophilized and stored for further analysis.

3.3.3 Swelling studies of the crosslinked Ch/PVA hydrogel discs

Ch/PVA and Ch/PVA-Ag hydrogel discs (10 mm) were vacuum dried for about 72 h to find out their dry weight (DW). To calculate the swelling ratio of the hydrogels, the dried hydrogel discs were soaked in deionised water at room temperature for 2.5 h and their wet weight (WW) was measured after removing the surface water using a blotting paper. Swelling ratio (S%) was determined in terms of absorbed water content as per the following eq.

$$S\% = \frac{WW - DW}{WW} \times 100 \quad (6)$$

3.3.4 Characterization and analysis of hydrogel composites

Surface morphology and size

The morphology of dried hydrogels and presence of silver in Ch/PVA-Ag hydrogel was studied using JEOL JSM-6510LV Scanning electron microscope (SEM) coupled with Energy dispersive spectroscopy (EDS) and FE-SEM (Carl Zeiss Supra 55). The average size and shape of the AgNPs inside the fabricated hydrogel was measured using Tecnai T20 transmission electron microscope (TEM) at an acceleration voltage of 200 kV. Incorporation of AgNPs in the Ch/PVA-Ag nanocomposite was determined with inductively coupled plasma-atomic emission spectrometer (ICP-AES; ARCOS ICP spectrophotometer, Germany) as mentioned by

Agnihotri et al. (2012). The average hydrodynamic size of AgNPs within the hydrogel was determined by Malvern (ZEN3600) particle size analyzer.

Fourier transform infrared (FTIR)

The FTIR spectra of Ch/PVA hydrogels with and without AgNPs, before and after adsorption were recorded in the wave range of 4000- 400 cm^{-1}, with a resolution of 2 cm^{-1} with FTIR-Spectrophotometer (Perkin Elmer Spectrum Version 10.4.00) using KBr pellet.

X-ray diffraction (XRD)

To determine various crystalline phases of nanosilver particles within the hydrogel, the X-ray diffraction pattern was studied using Pan Analytical (X'Pert-pro) diffractometer with Cu-Kα (1.54 A°) at 45 kV and scan range (2θ) 5° to 90°, with a step size of 0.02.

X-ray photoelectron spectroscopy (XPS)

Chemical states of the functional groups were studied by XPS. The complex peaks obtained using XPS (Physical Electronics, PHI 5000 VersaProbe III) were deconvulated into component Gaussian peaks using origin software.

Thermal analysis and BET analysis

Thermal stability of the hydrogels was studied using thermogravimetric analysis and differential scanning calorimetry (TGA-DSC) on Mettler Toledo Instrument under N_2 atmosphere, over a temperature range of 25-1000 °C and heating rate of 10 °C min^{-1}. To determine surface area and pore size distribution of the hydrogels, BET (Brunauer Emmett Teller) analysis was done using Quanta Chrome Novae-2200 instrument based on N_2 adsorption-desorption method after degassing at 150 °C for 6 h.

3.4 Removal of butachlor from synthetic water using hydrogel-nanoparticulate system

3.4.1 Adsorption

Adsorption studies for removal of butachlor by Ch/PVA and Ch/PVA-Ag hydrogels from water were performed in batch mode under dark conditions. The experiments were performed in the month of April 2019 with average temperature of 30 °C. 50 mL of butachlor with its varying initial concentrations (10- 100 mg L^{-1}) was stirred at 200 rpm on a magnetic stirrer, with a known amount of sorbent (Ch/PVA & Ch/PVA-Ag) in 100 mL Erlenmeyer flask. The pH of the working solution was adjusted with 0.1 M HCl/ 0.1 M NaOH. At regular time intervals,

sample aliquots were withdrawn, centrifuged for 2 min at 5000 rpm and analyzed for absorbance change at λ_{max} (265_{nm}) on Thermo Fischer Scientific Elisa reader with additional cuvette port. Calibration curve at $\lambda = 265_{nm}$ was used to calculate residual concentration of butachlor (Appendix II). Different parameters affecting butachlor removal were studied, including pH (3-11), butachlor initial concentration (10-100 mg L^{-1}), sorbent dosage (50 – 1000 mg), temperature (303 – 338 K) and contact time. Different adsorption isotherm models (Langmuir linear, Langmuir non-linear, Freundlich linear and Freundlich non-linear) along with multiple error functions were analyzed. The percentage removal and amount of butachlor adsorption per unit mass of Ch/PVA and Ch/PVA-Ag were evaluated as:

$$\text{Removal } \% = \left(\frac{C_0 - C_e}{C_0}\right) \times 100 \quad (7)$$

$$q_e = \left(\frac{C_0 - C_e}{m}\right) \times V \quad (8)$$

where, C_0 and C_e are the initial and final butachlor concentrations (mg L^{-1}), q_e is the amount of butachlor adsorbed (mg g^{-1}), m is the mass of Ch/PVA or Ch/PVA-Ag (g) and V is the total volume of the solution (L).

3.4.2 Photocatalytic degradation

Photocatalytic degradation was performed in batch mode, with the optimized parameters of adsorption. 50 mL of 10 mg L^{-1} butachlor was stirred on a magnetic stirrer at 200 rpm, with 100 mg Ch/PVA-Ag hydrogel in 100 mL Erlenmeyer flask at pH 3 and temperature 30 °C. The pH of the working solution was adjusted with 0.1 M NaOH / 0.1 M HCl. After 30 min of dark adsorption by Ch/PVA-Ag hydrogel, the reaction was examined for degradation with continuous stirring under UV-radiation (125 W Hg arc lamp) in a photoreactor with water circulation system. At regular time intervals, sample aliquots were withdrawn, centrifuged for 2 min at 5000 rpm and analyzed for absorbance change at λ_{max} (265_{nm}) on Elisa reader with additional cuvette port (Thermo Fischer Scientific). From the UV data, four different kinetic models (first order, pseudo-first order, second order, and pseudo-second order) were studied to analyze the photocatalytic degradation of butachlor by AgNPs present within Ch/PVA-Ag. Reusability of the nanocomposite was tested for three consecutive cycles using the steps above.

The reaction products were also analyzed by Liquid chromatography- mass spectroscopy (LC-MS) equipped with an electrospray ionization (ESI). The metabolites were ionized in ESI

positive mode set at a capillary voltage of 2.5 kV, a source temperature of 110 °C and a desolvation temperature of 450 °C. C_{18} column was used for the analysis, with argon as the collision gas and nitrogen as the desolvation gas. The cone gas and desolvation gas flow were maintained at 50 and 1000 L h^{-1}, respectively. Full scan signals were recorded from m/z 30 to 320. A possible degradation pathway was proposed using intermediate product obtained from LC-ESI-Q-TOF-MS analysis.

4.1 Screening of bacterial isolates for degradation of monocrotophos

Previously isolated 15 bacterial isolates were examined for their ability to grow in the presence of monocrotophos using disc/well diffusion assay (Fig. 4.1). Bacteria grown on MHA media with different concentrations of monocrotophos (0.5, 1, 2, 4, 8, 16, 32, 64,128, 250 and 500 mg L^{-1}) were screened for isolating best strain capable of tolerating higher concentration of monocrotophos. All the bacterial strains tolerated monocrotophos upto 64 mg L^{-1}. After an incubation of 24 h at 37 °C, zone of inhibition (ZOH) was observed in the petri plates with 128, 250 and 500 mg L^{-1} monocrotophos. ZOH in plates (Fig. 4.1) with 500 mg L^{-1} monocrotophos was observed and the bacterial isolate showing minimum ZOH, was considered best bacterial strain possessing higher tolerance (Fig. 4.2) and was further analysed for degradation capacity.

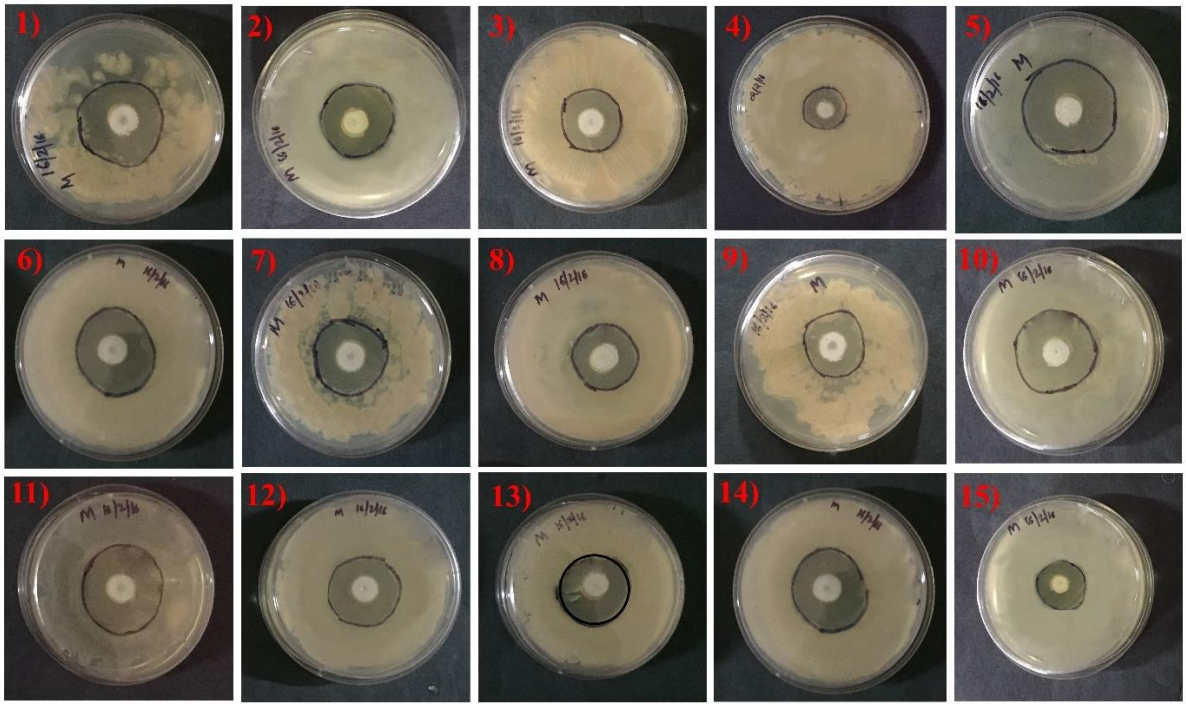


Fig. 4.1: Tolerance of 500 mg L^{-1} monocrotophos by different bacterial isolates judged by zone of inhibition at 37 °C: 1) T8, 2) NA9, 3) NA11, 4) NA14, 5) NA15, 6) DGA, 7) DGB, 8) DGC, 9) A12, 10) A14, 11) A15, 12) A16, 13) CT5, 14) CS8 and 15) *E. coli*

Table 4.1: *In vitro* zone of inhibition activity of bacteria in the presence of 500 mg L^{-1} monocrotophos

S.No	Bacteria	Source	Zone of inhibition (mm)
1	*Bacillus licheniformis* LZBL8 (T8)	Paper Pulp	19.50 ± 0.50
2	*Bacillus licheniformis* X2 (NA9)	Paper Pulp	18.17 ± 0.29
3	*Bacillus licheniformis* CK1 (NA11)	Compost	15.83 ± 0.29
4	*Bacillus licheniformis* BPRIST030 (NA14)	Compost	10.67 ± 0.58
5	*Bacillus subtilis* HB1 (NA15)	Compost	20.67 ± 0.58
6	*Lysinibacillus fusiformis* N139 (DGA)	Sugarcane bagasse	18.33 ± 0.58
7	*Bacillus licheniformis* BAB1836 (DGB)	Sugarcane bagasse	17.67 ± 0.58
8	*Bacillus licheniformis* MS514 (DGC)	Sugarcane bagasse	15.00 ± 1.00
9	*Bacillus* sp. (A12)	Soil	17.33 ± 2.52
10	*Bacillus* sp. (A14)	Soil	19.67 ± 1.53
11	*Bacillus* sp. (A15)	Soil	19.33 ± 0.58
12	*Bacillus altitudinis* (A16)	Soil	17.00 ± 0.50
13	*Citrobacter* sp. IS2 (CT5)	Tannery effluent	17.00 ± 0.50
14	*Citrobacter freundii* IS4 (CS8)	Chrome sludge	18.67 ± 0.58
15	*E. coli* DH5α	MTCC	14.67 ± 0.58

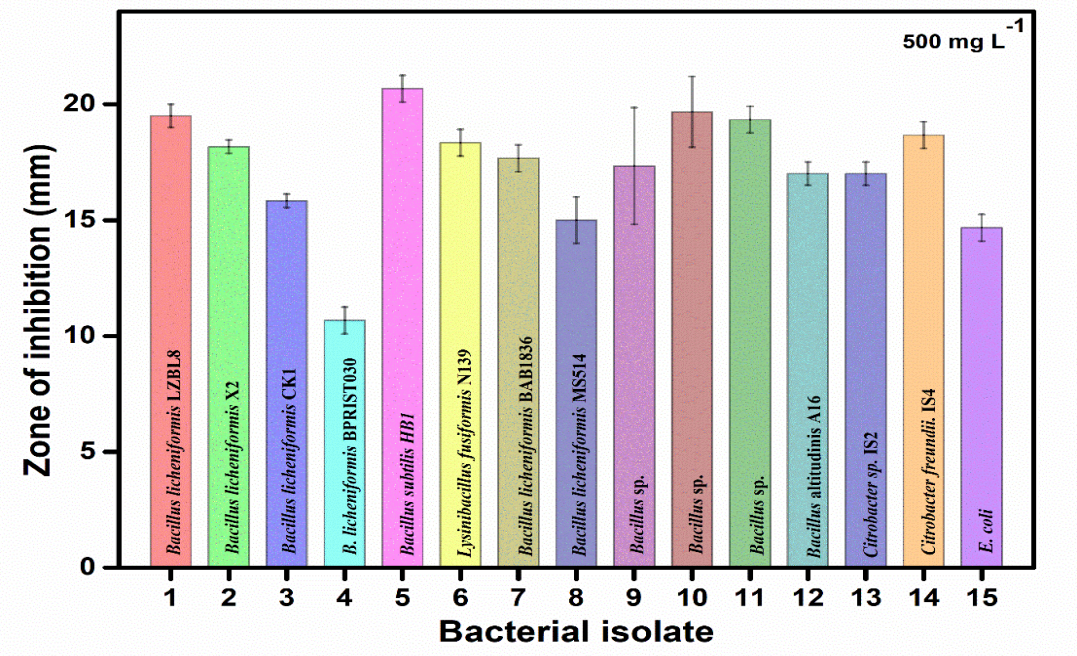


Fig. 4.2: Tolerance of bacterial isolates against of 500 mg L^{-1} monocrotophos as judged by Zone of inhibition on petri plates at 37 °C

Table 4.1 shows comparative data of different ZOH obtained with 500 mg L^{-1} monocrotophos. *Bacillus licheniformis* BPRIST030 (NA14) showed minimum ZOH (10.67 ± 0.58), indicating it is capable of tolerating even higher concentrations of monocrotophos. In a similar research reported by Buvaneshwari et al. (2017), effect of different concentration of monocrotophos using well diffusion assay was studied, where a bacterial isolate *Bacillus tequilensis* BSGP006 showed highest monocrotophos degradation at 500 ppm. Majority of bacterial strains capable of degrading monocrotophos belong to *Bacillus, Enterobacter and Pseudomonas* sp. (Buvaneshwari et al., 2017). Different *Bacillus* sp. including *Bacillus licheniformis*, *Bacillus subtilis* (Acharya et al., 2015; Sidhu et al., 2015; Buvaneswari et al., 2017), *Bacillus coagulans*, *Bacillus brevis* (Bhadbhade et al., 2002a), *Bacillus megaterium* MCM B-423 (Bhadbhade et al., 2002b) and *Lactobacillus bulgaricus* (Zhao and Wang, 2012) have been widely studied to metabolize monocrotophos present in the soil. Mineralization of monocrotophos by various *Pseudomonas* strains, *viz*. *Pseudomonas stutzeri* (Barathidasan and Reetha, 2013; Buvaneswari et al., 2017), *Pseudomonas moraviensis* JAS18 (Abraham et al., 2014), *Pseudomonas synxantha* (Sidhu et al., 2015), *Pseudomonas aeruginosa* (Subhas and Singh, 2003; Balamurugan et al., 2010) and *Pseudomonas mendocina* (Bhadbhade et al., 2002a) has been widely reported.

4.1.1 Biodegradation of monocrotophos by *Bacillus licheniformis* BPRIST030 and identification of the metabolites

Bacillus licheniformis BPRIST030 is a rod shaped, Gram positive, mesophilic, cellulose degrading bacteria, isolated from compost. They formed creamy-white, irregular shaped colonies (Fig. 4.3).

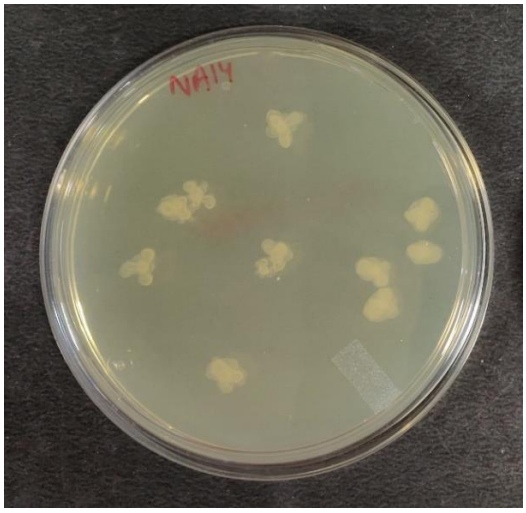


Fig. 4.3: Colony morphology of *Bacillus licheniformis* BPRIST030 (NA14)

Since, recommended field dosage of monocrotophos is 1.5 – 2.5 kg ha^{-1} (Kaur and Goyal, 2019), which is much lesser than 5 mg L^{-1}, so the degradation of monocrotophos by *Bacillus licheniformis* BPRIST030 was studied using BH medium spiked with 50 mg L^{-1} monocrotophos as sole carbon source for 5 days (120 h) at 37 °C. Bacteria was able to grow in monocrotophos supplemented minimal BH media, however no growth was seen in control medium without monocrotophos. Increase in cell/optical density (OD_{600nm}) from 0.014 ± 0.004 to 0.864 ± 0.020 was observed, with corresponding increase in viable cell count from 5.9 to 13.73 (log cfu mL^{-1}) over a period of five days (Fig. 4.4).

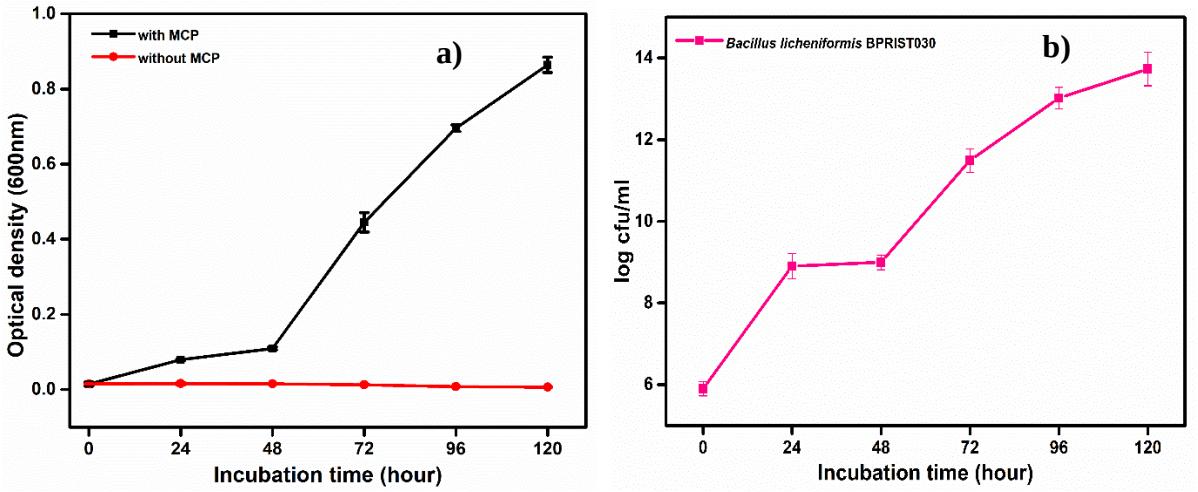


Fig. 4.4: Growth of *Bacillus licheniformis* BPRIST030 in 50 mg L^{-1} monocrotophos supplemented BH media **a)** Absorbance at 600 nm in presence and absence of monocrotophos **b)** cell count in presence of monocrotophos

Monocrotophos degradation has been studied using several bacterial isolates. Jia et al. (2006) isolated *Paracoccus* sp. M1 that was able to mineralize 300 mg L^{-1} of monocrotophos along with other OP insecticides and amide herbicides under different culture conditions. Another bacterial isolate, YW6, characterized as *Starkeya novella*, degraded 0.2 mM monocrotophos with no lag period within 36 h, utilizing it for its growth as the sole nitrogen and carbon source (Sun et al., 2016). Subhas and Singh (2003) studied two bacterial isolates *Pseudomonas aeruginosa* F10B and *Clavibacter michiganense* subsp. *Insidiosum* SBL 11 capable of degrading 98.9% and 86.9% technical monocrotophos, respectively, under laboratory conditions and 79% and 80% of pure monocrotophos within 24 h at 37 °C, where 500 ppm was the optimal monocrotophos concentration required for their normal growth. Similar research was conducted by a research group, where they isolated 17 bacterial isolates (16 different *Bacillus* sp. and *Arthrobacter atrocyaneus*) (Bhadbhade et al., 2002b). Among them, *Bacillus*

megaterium and *Arthrobacter atrocyaneus* degraded monocrotophos within 8 days to an amount of 93% and 83%, respectively, from media spiked with 1000 mg L^{-1} monocrotophos.

4.1.2 Elucidation of metabolic pathway of monocrotophos degradation by *Bacillus licheniformis* BPRIST030

Monocrotophos supplemented BH media inoculated with *Bacillus licheniformis* BPRIST030 was subjected to GC-MS analysis after centrifugation and solvent extraction, which showed approximately 70% reduction in concentration of monocrotophos after five days of incubation, whereas no significant change in control was detected (Fig. 4.5).

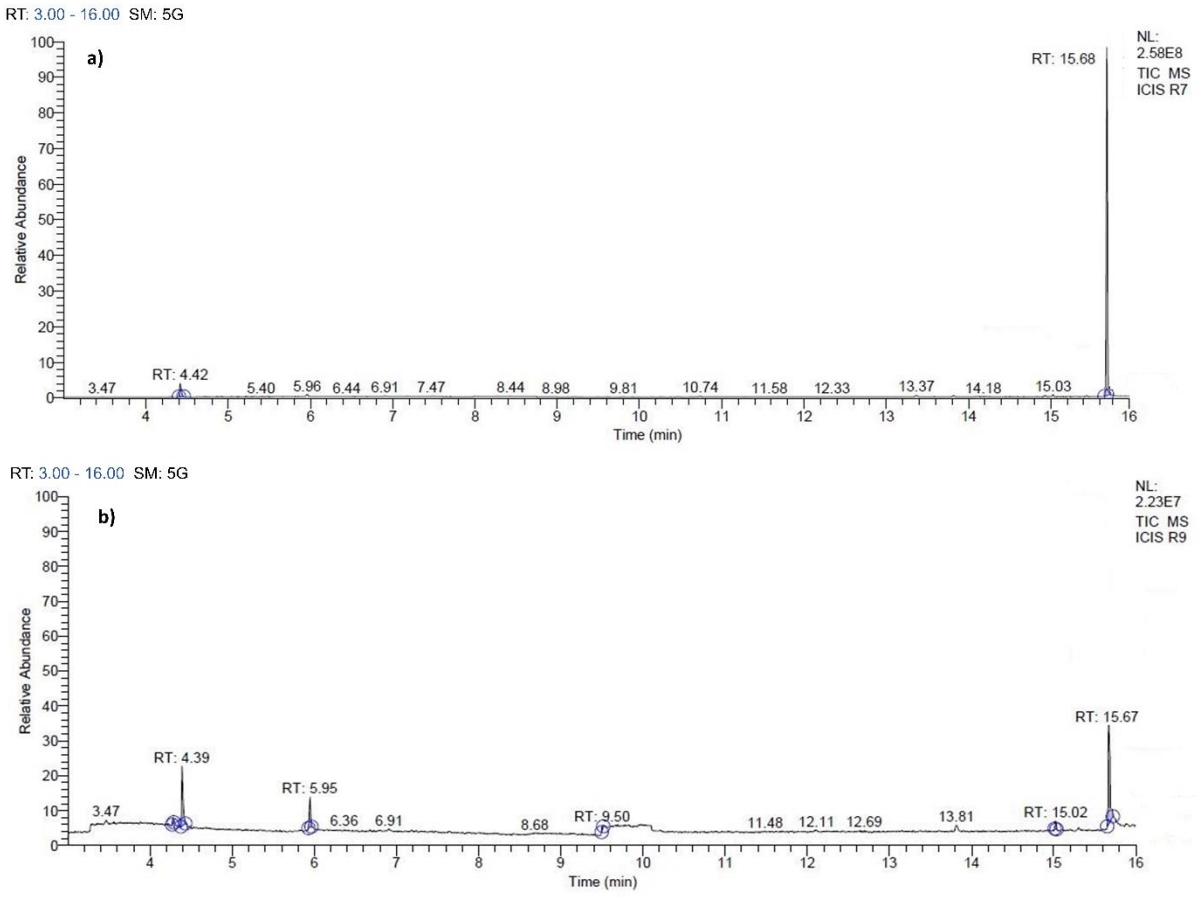
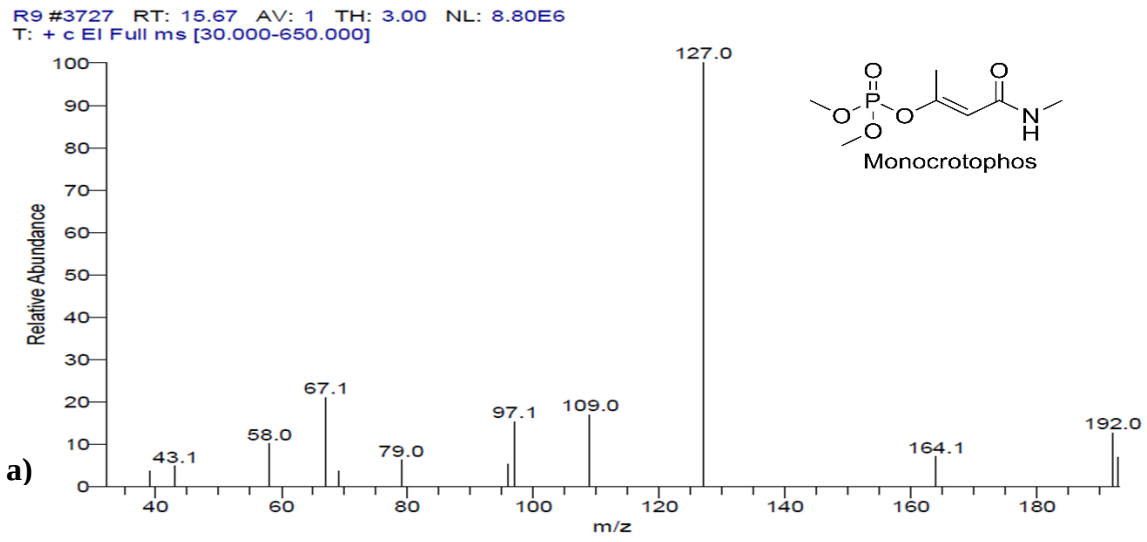


Fig. 4.5: GC-MS analysis of residual monocrotophos in **a)** control **b)** culture broth at 120 h. Peaks with RT 15.67 min,15.02 min, 9.50 min, 5.95 min, 4.39 min and 4.28 min showing breakdown into different metabolites

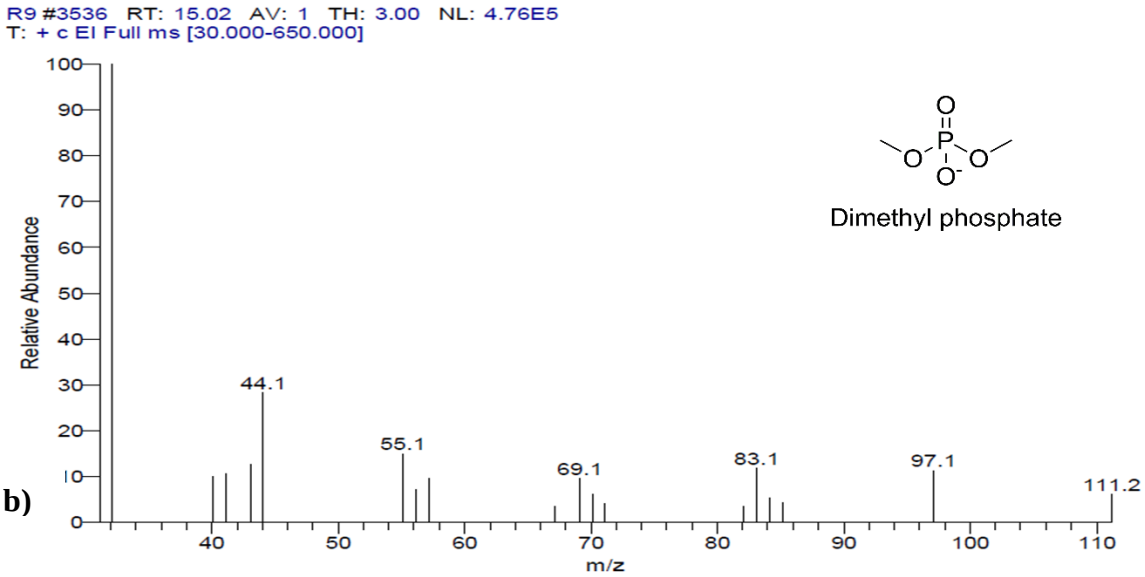
The detected metabolites were determined by matching with the electron ionization mass spectra provided by National Institute of Standards and Technology (NIST) library. The characteristic fragment ion peaks were also matched with earlier reports. Single peak with RT= 15.68 min found in control sample was identified as monocrotophos by NIST library. Sample

collected after 120 h of degradation process gave a peak (A) with RT (15.67 min), but lower intensity/area than control suggesting partial degradation of monocrotophos. Fig. 4.6 shows GC-MS masses of five different intermediates along with monocrotophos (RT 15.67). Monocrotophos has a molecular weight of 223.16 and showed characteristic fragment ion peaks at m/z 192.0, 164.1, 127.0, 109.0, 97.1, 79.0, 67.1, 58.0 and 43.1 (Fig. 4.6 (a)). Five major metabolites corresponding to B (RT- 15.02 min), C (RT- 9.50 min), D (RT-5.95 min), E (RT-4.39 min) and F (4.28 min) were detected in sample collected after 120 h (Fig. 4.5 (b)).

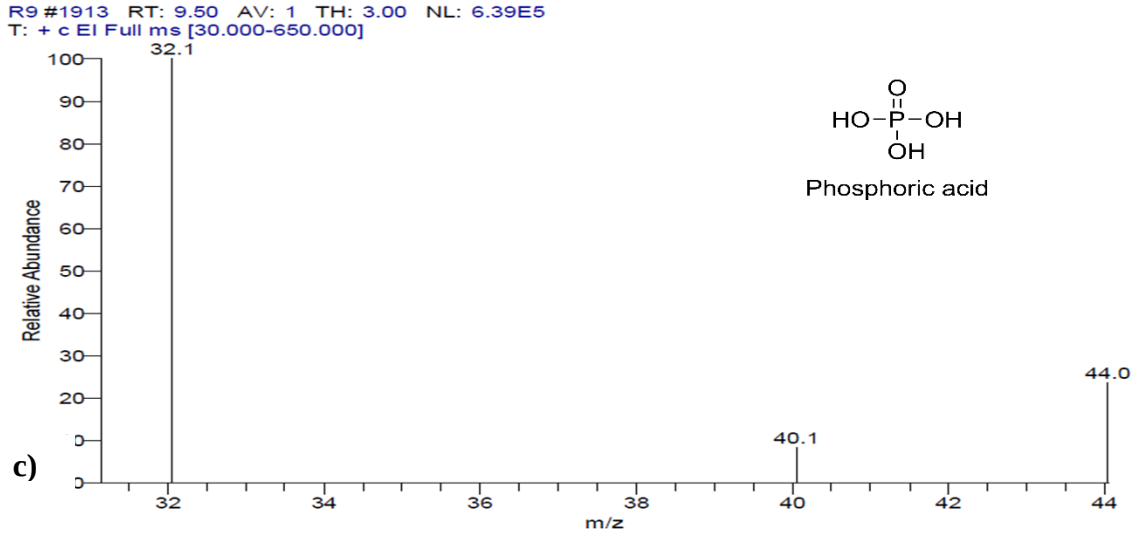
Peak B with RT 15.02 min was supposed to be dimethyl phosphate, which showed a fragment ion peaks at m/z at 111.2, 97.1, 83.1, 69.1, 55.1 and 44.1 (Fig. 4.6 (b)). Peak C (RT 9.50 min) was observed to be phosphoric acid with molecular weight 97.28 and ion fragments at m/z 44.0, 40.1and 32.1 (Fig. 4.6 (c)). Peak D (RT 5.95 min) was identified as *N*-methyl acetoacetamide and has a molecular weight of 115.06. It showed fragment ions at m/z 94.0, 66.1, 63.0, 55.1, 50.0, 44.0 and 39.1 (Fig. 4.6 (d)). Peak E (RT 4.39) displayed fragment ions at m/z 101, 98.1, 83.1, 59.1 and 43.1 and was identified as malonic acid, dihydrazide. Molecular weight of the identified compound is 132. (Fig. 4.6 (e)). The molecular weight of compound having RT 4.28 min (peak F) is 113.08. Based on the molecular weight and its fragment ion peaks (96.1, 67.1, 44.0 and 39.1), the compound was identified as *N*,3-dimethylbut-2-enamide (Fig. 4.6 (f)).



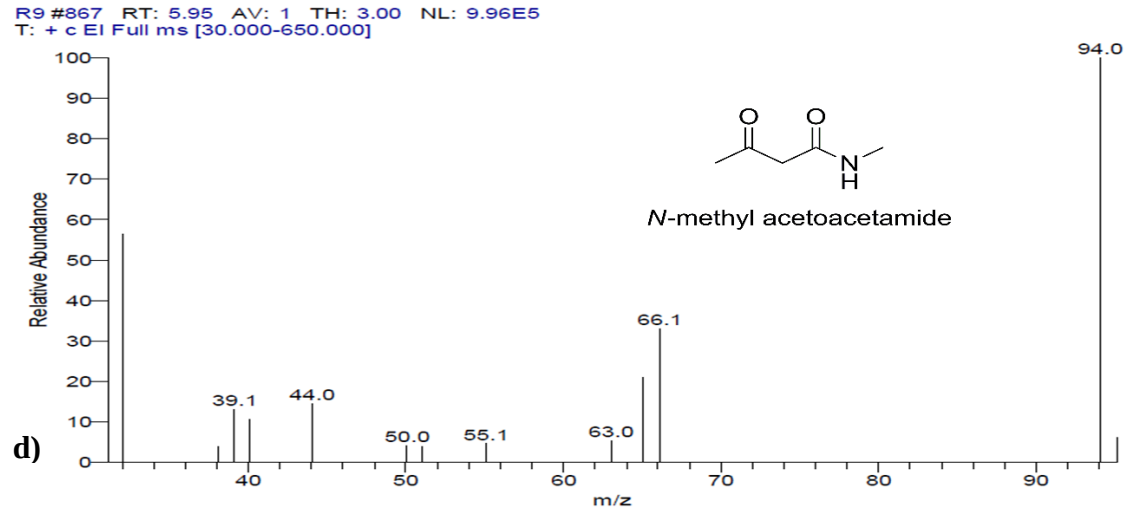
a)


R9 #3536 RT: 15.02 AV: 1 TH: 3.00 NL: 4.76E5
T: + c EI Full ms [30.000-650.000]
Relative Abundance
m/z
44.1
55.1
69.1
83.1
97.1
111.2
Dimethyl phosphate

b)


R9 #1913 RT: 9.50 AV: 1 TH: 3.00 NL: 6.39E5
T: + c EI Full ms [30.000-650.000]
Relative Abundance
m/z
32.1
40.1
44.0
Phosphoric acid

c)


R9 #867 RT: 5.95 AV: 1 TH: 3.00 NL: 9.96E5
T: + c EI Full ms [30.000-650.000]
Relative Abundance
m/z
94.0
66.1
39.1
44.0
50.0
55.1
63.0
N-methyl acetoacetamide

d)

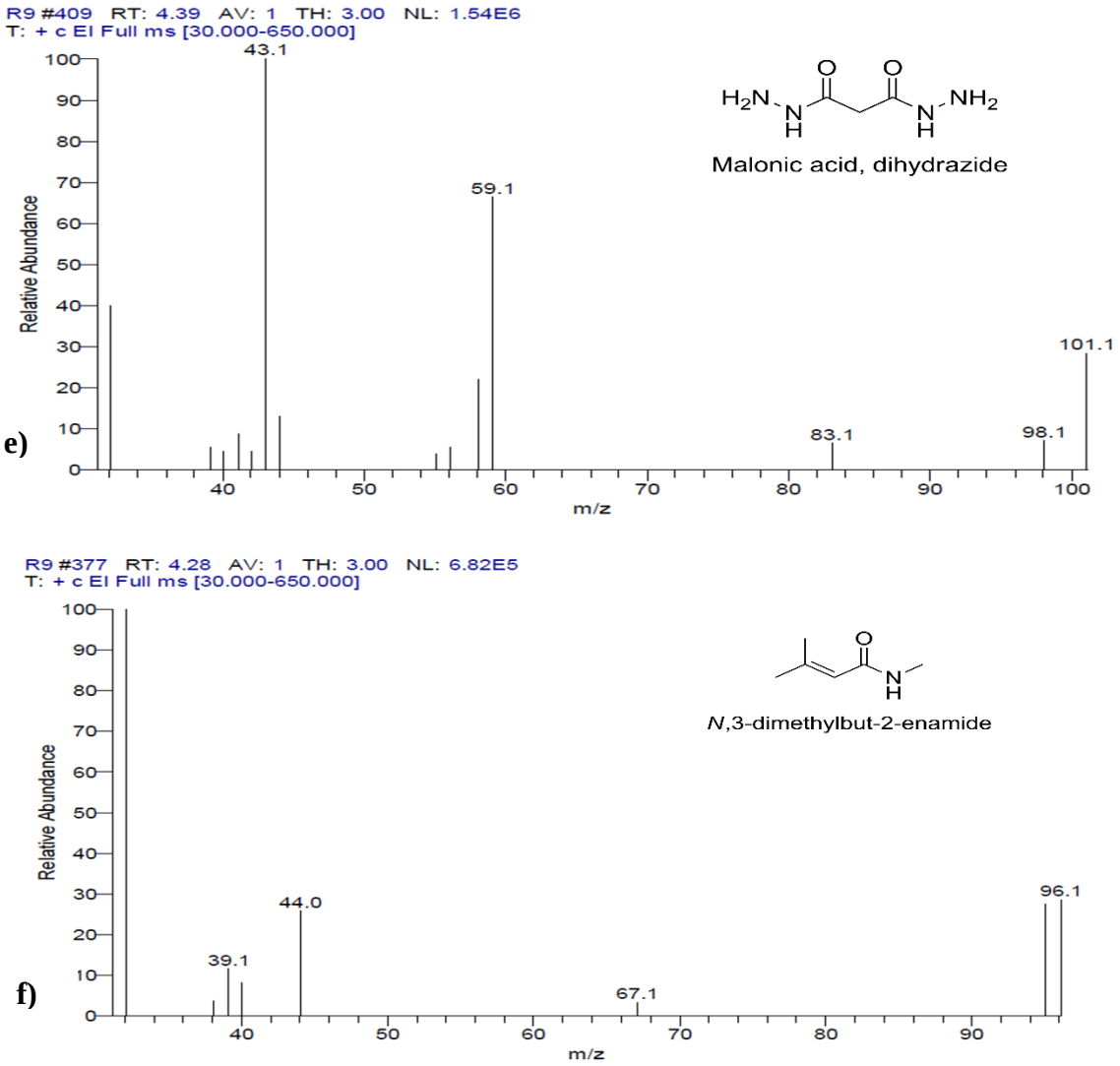


Fig. 4.6: Mass spectra analysis for peaks **a)** RT- 15.67 (monocrotophos), **b)** RT- 15.02 (dimethyl phosphate), **c)** RT- 9.50 (phosphoric acid), **d)** RT- 5.95 (*N*-methyl acetoacetamide), **e)** RT- 4.39 (malonic acid, dihydrazide) and **f)** RT- 4.28 (*N*,3-dimethylbut-2-enamide)

Monocrotophos metabolization by different bacteria has been reported through catabolic mechanisms, where monocrotophos provides carbon or phosphorus source to the growing micro-organisms (Singh and Walker, 2006). GC-MS analysis showed 5 metabolites (dimethyl phosphate, phosphoric acid, *N*-methyl acetoacetamide, malonic acid, dihydrazide and *N*,3-dimethylbut-2-enamide) among which malonic acid, dihydrazide and *N*,3-dimethylbut-2-enamide were not previously reported. Monocrotophos is characterized by an amide bond and P–O–C linkage. The first step of monocrotophos degradation involves hydrolysis, producing *N*-methyl acetoacetamide along with dimethyl phosphate, which was analogous to the study conducted by Beynon et al. (1973). In the next step, *N*-methyl acetoacetamide could have

possibly been degraded to *N*,3-dimethylbut-2-enamide whereas, dimethyl phosphate may have led to the generation of phosphoric acid. Malonic acid, dihydrazide was another metabolite produced, which could have directly resulted by dephosphorylation and amination of monocrotophos. All the metabolites were further mineralized to phosphates, carbon dioxide and ammonia (Fig. 4.7). Phosphatases (mono and dimethyl) and esterases are the enzymes involved in the biodegradation of monocrotophos into ammonia, carbon dioxide, and phosphates through formation of intermediate compounds as valeric acid or acetic acid, methylamine and other metabolites (Bhadbhade et al., 2002b).

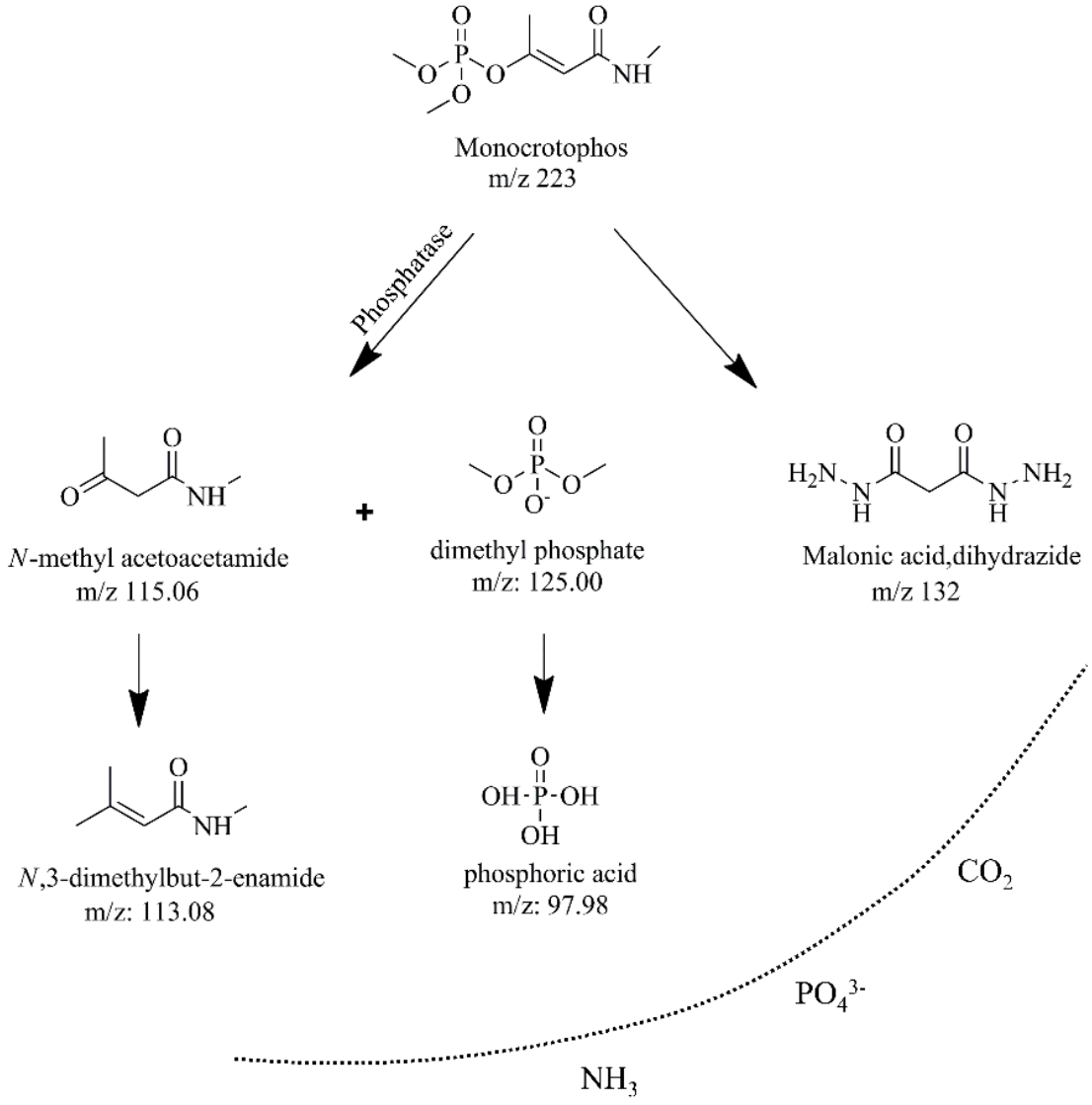


Fig. 4.7: Proposed possible metabolic pathways of monocrotophos degradation by *Bacillus licheniformis* BPRIST030

Rhodococcus phenolicus MCP1 along with *Rhodococcus ruber* MCP-2, isolated from groundnut soils, were able to utilize monocrotophos as a carbon source by hydrolysis leading to the formation of *N*-methylacetoacetamide, indicating decomposition of the parent compound (Srinivasulu et al., 2017). Degradation of *N*-methyl acetoacetamide produces valeric acid in *Arthrobacter atrocyaneus* and acetic acid in *Bacillus megaterium* (Bhadbhade et al., 2002b).

4.2 Screening of bacterial isolates for degradation of butachlor

For the preliminary studies, 15 bacterial isolates were screened for their ability to grow in the presence of butachlor using disc/well diffusion assay (Fig. 4.8). Bacteria grown on MHA media with different concentrations of butachlor (0 – 64 mg L^{-1}) were screened for isolating best strain capable of degrading butachlor. Since, no ZOH was observed in any petri plate, therefore, all the bacterial were able to tolerate 64 mg L^{-1}.

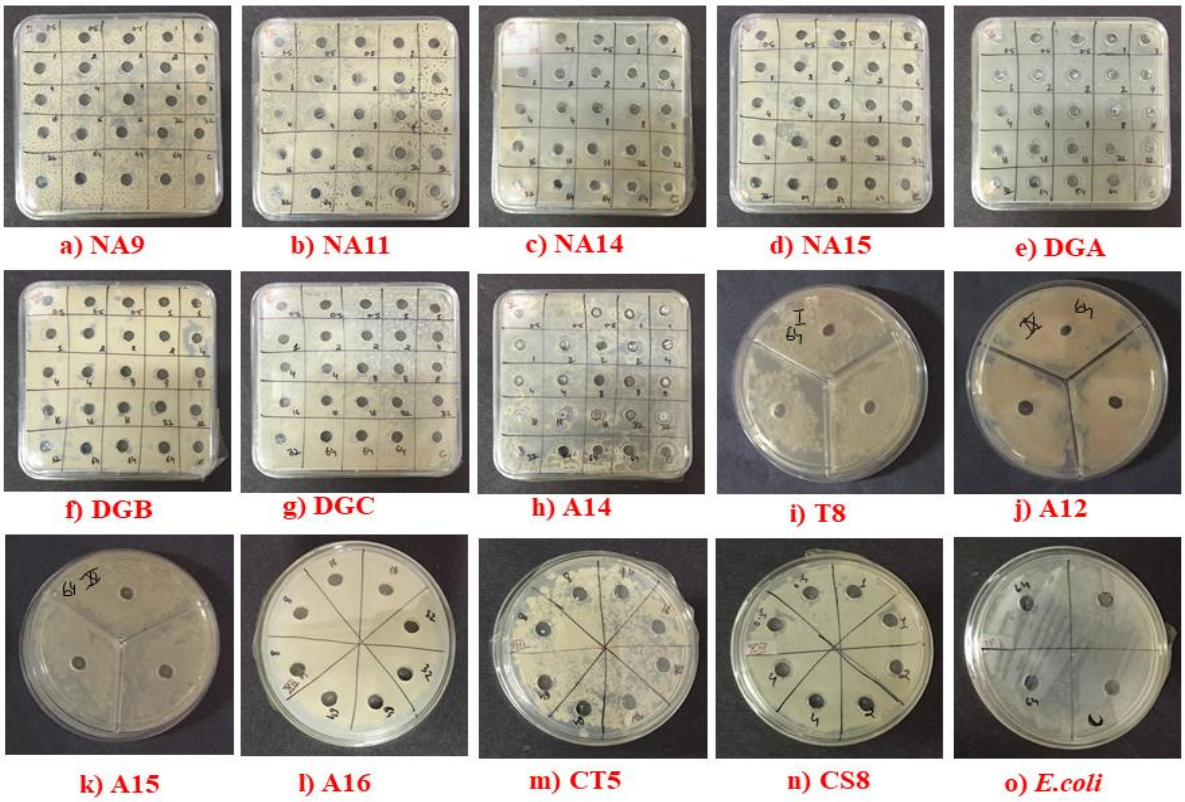


Fig. 4.8: Tolerance of 64 mg L^{-1} butachlor by different bacterial isolates judged by zone of inhibition at 37 °C

In order to get the best butachlor degrading bacterial isolate, butachlor degradation was further studied in butachlor spiked Bushnell Hass minimal medium using broth dilution assay. Since, recommended field dosage of butachlor is 10-150 µM (≈ 3 - 46 mg L^{-1}) (Abigail et al., 2015), therefore, degradation experiments were carried out with 50 mg L^{-1} butachlor. Bacteria grown on BH media spiked with 50 mg L^{-1} butachlor were screened for isolating best strain capable of degrading butachlor with higher efficiency and yielding minimum or no butachlor residues. Table 4.2 shows residual concentration of butachlor obtained from standard curve (Appendix II) using UV-Vis spectrophotometer. Bacterial isolate A16 showed highest degradation of butachlor with 5.53 ± 0.21 mg L^{-1} residual concentration, followed by *Bacillus licheniformis*

MS514 (DGC). The isolate A16 was further identified and studied for degradation kinetics and metabolic pathway.

Table 4.2: Butachlor degradation (50 mg L^{-1}) by different bacteria

S.No	Bacteria	Source	Residual butachlor (mg L^{-1})
1	*Bacillus licheniformis* LZBL8 (T8)	Paper Pulp	23.96 ± 2.40
2	*Bacillus licheniformis* X2 (NA9)	Paper Pulp	31.57 ± 1.26
3	*Bacillus licheniformis* CK1 (NA11)	Compost	33.82 ± 1.52
4	*Bacillus licheniformis* BPRIST030 (NA14)	Compost	21.26 ± 0.64
5	*Bacillus subtilis* HB1 (NA15)	Compost	34.31 ± 2.74
6	*Lysinibacillus fusiformis* N139 (DGA)	Sugarcane bagasse	16.03 ± 0.80
7	*Bacillus licheniformis* BAB1836 (DGB)	Sugarcane bagasse	21.19 ± 1.38
8	*Bacillus licheniformis* MS514 (DGC)	Sugarcane bagasse	6.42 ± 0.16
9	*Bacillus* sp. (A12)	Soil	19.91 ± 1.17
10	*Bacillus* sp. (A14)	Soil	16.61 ± 0.66
11	*Bacillus* sp. (A15)	Soil	16.16 ±0.71
12	***Bacillus altitudinis* (A16)**	**Soil**	**5.53 ± 0.21**
13	*Citrobacter* sp. IS2 (CT5)	Tannery effluent	10.29 ± 0.30
14	*Citrobacter freundii* IS4 (CS8)	Chrome sludge	9.40 ± 0.47
15	*E. coli* DH5α	MTCC	11.73 ± 0.36

4.2.1 Degradation of butachlor by bacterial isolate A16

Bacterial isolate from coal tar contaminated soil was rod shaped, aerobic, spore forming and Gram-positive capable of utilizing sucrose, glucose and fructose as carbon source. Colonies after 24 hr of growth on nutrient agar were white coloured, round and convex with an average diameter of 1.5-3 mm (Fig. 4.9).

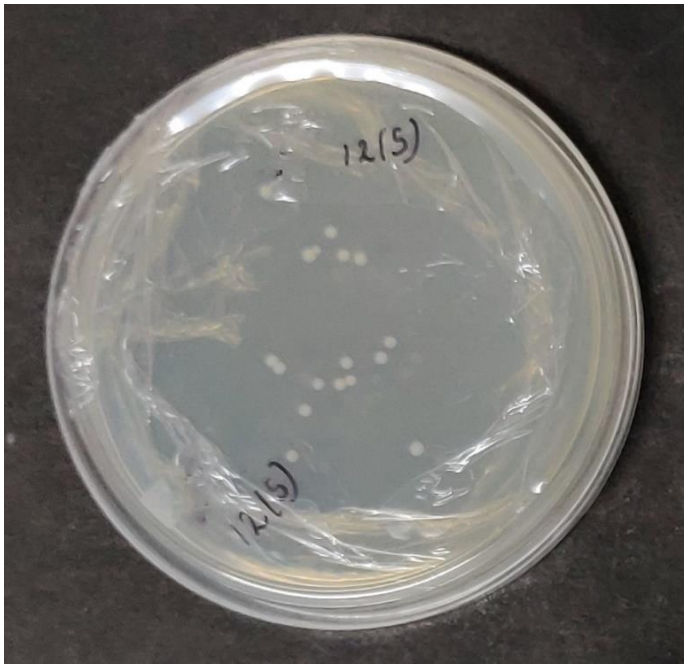


Fig. 4.9: Colony morphology of bacterial isolate *Bacillus altitudinis* A16

The 1450 bp 16S rRNA gene sequence of *B. altitudinis* A16 was assigned an accession number MN595198 after submission to the Genbank database (Appendix III) and phylogenetic analysis showed 99.38% similarity with *Bacillus altitudinis* 41KF2b^{T} (Fig. 4.10).

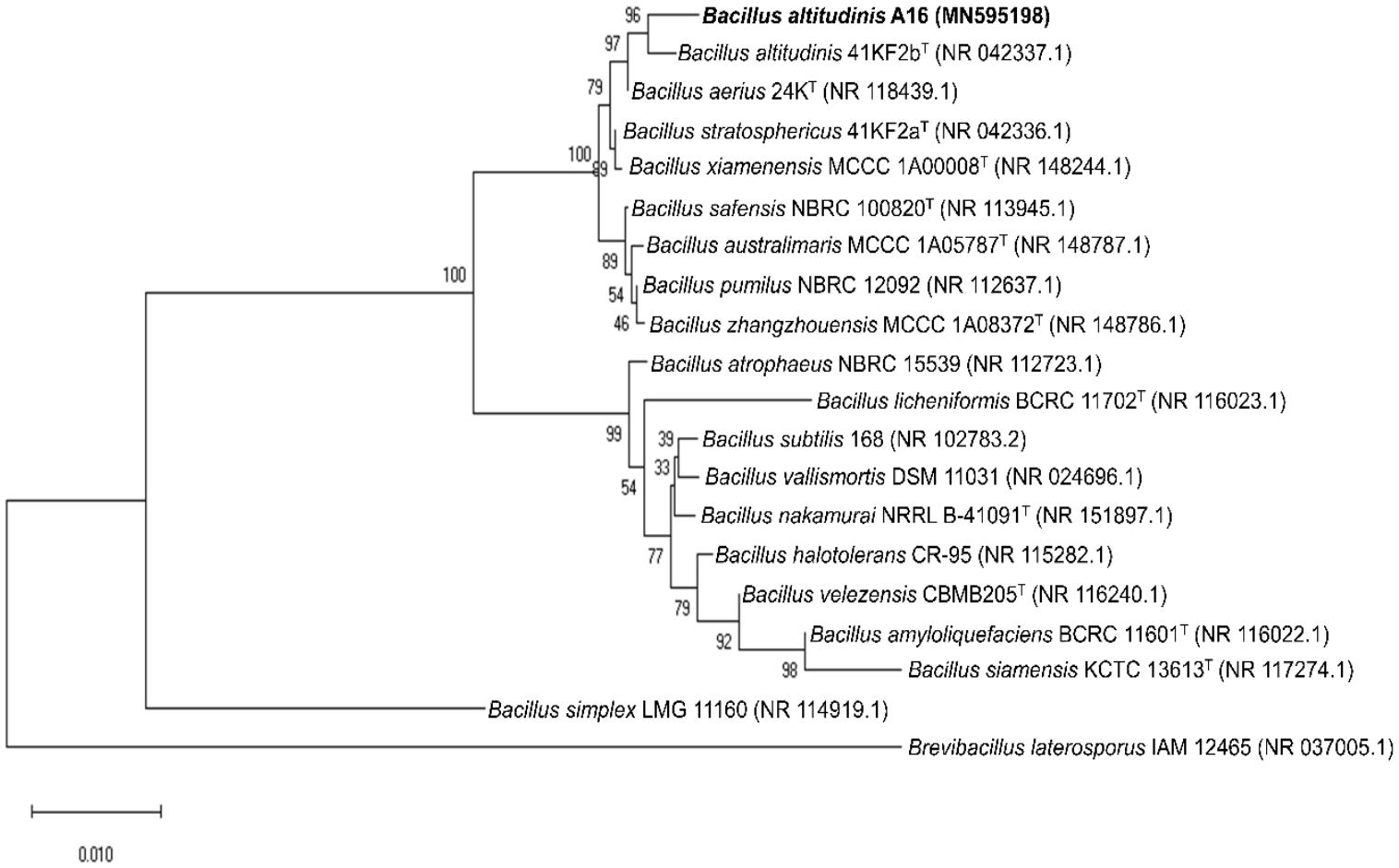


Fig. 4.10: Neighbour- joining tree depicting the phylogenetic relationship between *Bacillus altitudinis* A16 with other related bacterial species based on 16S rRNA gene sequences. Bootstrap values are expressed as percentage of 1000 replications. *Brevibacillus laterosporus* IAM 12465 was used as an outgroup. Scale bar represents an evolutionary distance of 0.01 substitutions per nucleotide position.

Bacillus altitudinis A16 did not grow in BH media (control), however it utilized butachlor as a sole source of carbon (Fig. 4.11) for its growth which was associated with increase in cell density (OD_{600nm}) from 0.02 to 0.33, and corresponding increase in viable cell count from 2.87 × 10^6 to 36.01 × 10^6 cfu mL^{-1} in 120 h (Fig. 4.12). There was almost 50% reduction in the concentration of butachlor after 48 h and after 120 h more than 90% butachlor was catabolized, with control showing no significant change in residual concentration. Degradation of butachlor occurred at mesophilic temperature range (25-40 °C) and pH (5-9). Maximum degradation was observed at 37 °C and pH 7 with inoculum density of 0.02 (OD_{600nm}), however with increase in cell density to 0.2-0.4 (OD_{600nm}) it showed rapid removal of butachlor from media.

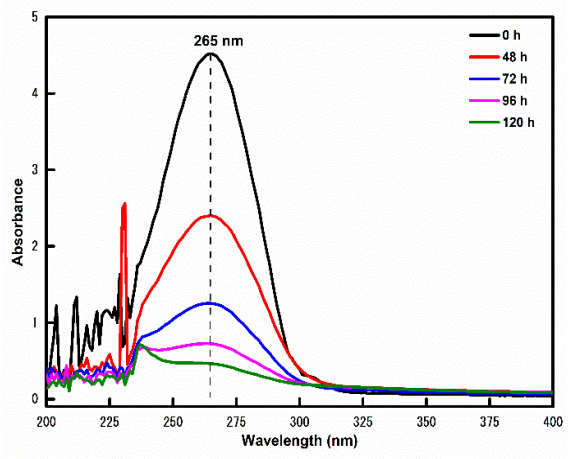


Fig. 4.11: Change in absorption spectra of time course degradation of butachlor by *Bacillus altitudinis* A16

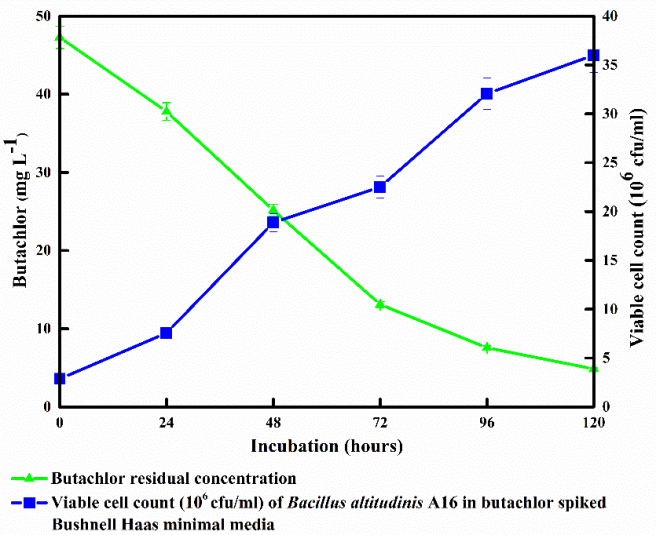


Fig. 4.12: Growth of *Bacillus altitudinis* A16 in presence of 50 mg L^{-1} of butachlor in Bushnell Haas broth at different time intervals

Biodegradation of different chloroacetamide herbicides by several bacteria has been reported, where most of the reports are based on degradation by Gram-negative bacteria. Xu et al. (2013) isolated *Achromobacter* sp., which could effectively degrade about 95% of 10 mg L^{-1} acetochlor in a period of 5 days. *Paracoccus* sp. strain FLY-8 showed 65.2% degradation of butachlor (100 mg L^{-1}) in minimal salt medium within incubation period of 5 days (Zhang et al., 2011). *Catellibacterium caeni* sp. nov DCA-1^T could also degrade 81.2% of butachlor (50 mg L^{-1}) in 84 h (Zheng et al., 2012). *Ammoniphilus* sp. JF could completely mineralize butachlor (100 mg L^{-1}) within 24 h of incubation (Singh and Nandabalan, 2018). Gao et al. (2015) isolated *Bacillus* sp. hys-1 which degraded 90% of 100 mg L^{-1} butachlor in 7 days at 30 °C and pH 6.5 with cell density of 0.21 to 0.92 (OD_{600} nm). However, strain A16 degraded 90% of butachlor in 5 days at minimum cell density (OD_{600nm} = 0.02) at 37 °C and pH 7.

4.2.2 Butachlor degradation kinetics

Butachlor degradation rate kinetics was studied using different kinetic models (Table 4.3). The best fit reaction kinetics was obtained in a first-order model for degradation of butachlor by the bacterium in BH broth, based on highest regression coefficient (R^2) which was 0.979 (Fig. 4.13).

Table 4.3: Kinetic models of butachlor degradation by *Bacillus altitudinis* A16

Kinetic Models	**Equation**	**Rate Constant (k)**	**R^2 values**
First order	$\ln C = \ln C_0 - kt$	2×10^{-2} h^{-1}	0.979
Pseudo-first order	$\ln[C_0 - C] = \ln C - kt$	2.16×10^{-2} h^{-1}	0.755
Second order	$1/C = 1/C_0 + kt$	0.1×10^{-2} mg L^{-1} h^{-1}	0.851
Pseudo-second order	$t/C = t/C_0 + 1/kC_0^2$	19.46×10^{-2} mg L^{-1} h^{-1}	0.781

The degradation was characterized by a rate constant (k) of 0.02 h^{-1} and half-life ($t_{1/2}$) of 34.65 h, within which the initial concentration of butachlor was mineralized to 50% by strain A16. R^2 values for other three kinetic models were far from unity (Table 4.3) and were not suitable to explain butachlor degradation. Dwivedi et al. (2010) reported first order kinetic model for the complete biodegradation of 3.2 mmol L^{-1} butachlor in soil, with a half-life and a rate constant of 4 days and 0.17 day^{-1}, respectively. In other similar studies conducted in soil, kinetics of butachlor degradation was also best fitted to its first order kinetics model (Yu et al., 2003; Yang et al., 2012).

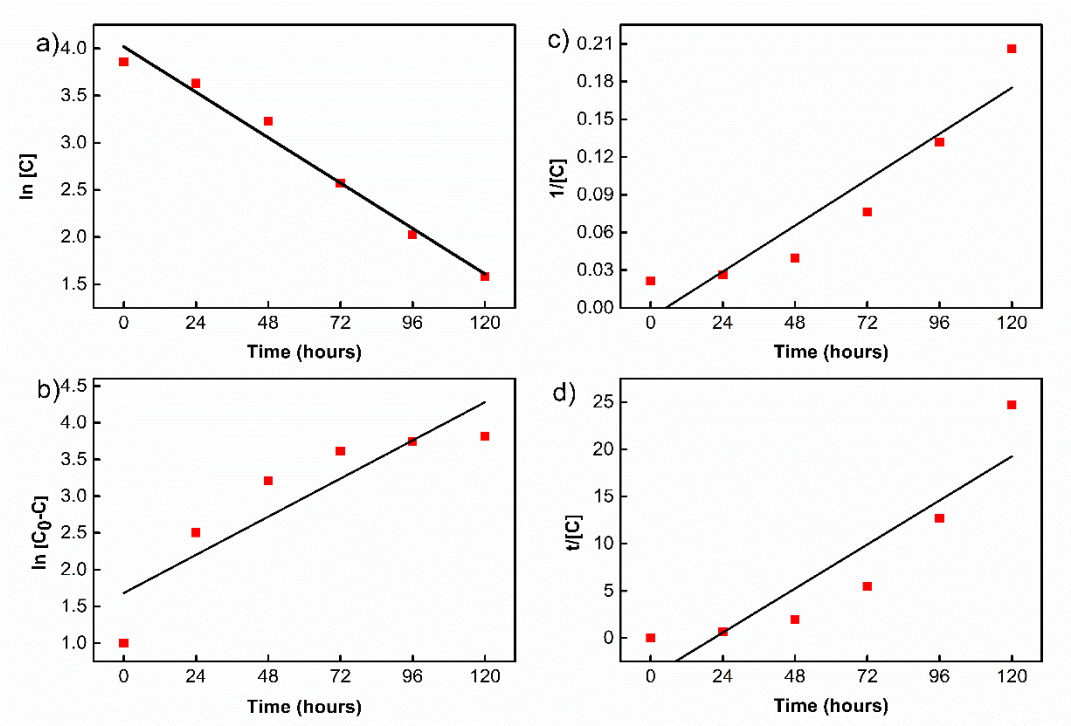


Fig. 4.13: Kinetic model fitting for rate of degradation of butachlor by strain A16 - **a)** first order **b)** pseudo-first order **c)** second order **d)** pseudo-second order

4.2.3 Identification of metabolites and degradation pathway

The intermediate compounds formed during butachlor degradation by bacterial isolate A16 were identified by GC-MS analysis at 0 h, 48 h and 120 h. The detected metabolites were determined by matching with the electron ionization mass spectra provided by National Institute of Standards and Technology (NIST) library. The characteristic fragment ion peaks were also matched with earlier reports. Single peak with RT= 17.22 min found in control sample was identified as butachlor by NIST library. Sample collected after 48 h of degradation process gave a peak (A) with RT (17.26 min), but lower intensity/area than control suggesting partial degradation of butachlor (Fig. 4.14). Butachlor has a molecular weight of 311.17 and showed characteristic fragment ion peaks at m/z 281.16, 251.99, 207.17, 176.22, 160.14, 77.02, 57.13 (Fig. 4.15 (a)). Five major metabolites corresponding to B (RT- 16.91 min), C (RT- 16.61 min), D (RT-15.86 min), E (RT-15.17 min) and F (14.51 min) were detected in sample collected after 120 h (Fig. 4.14 (c)).

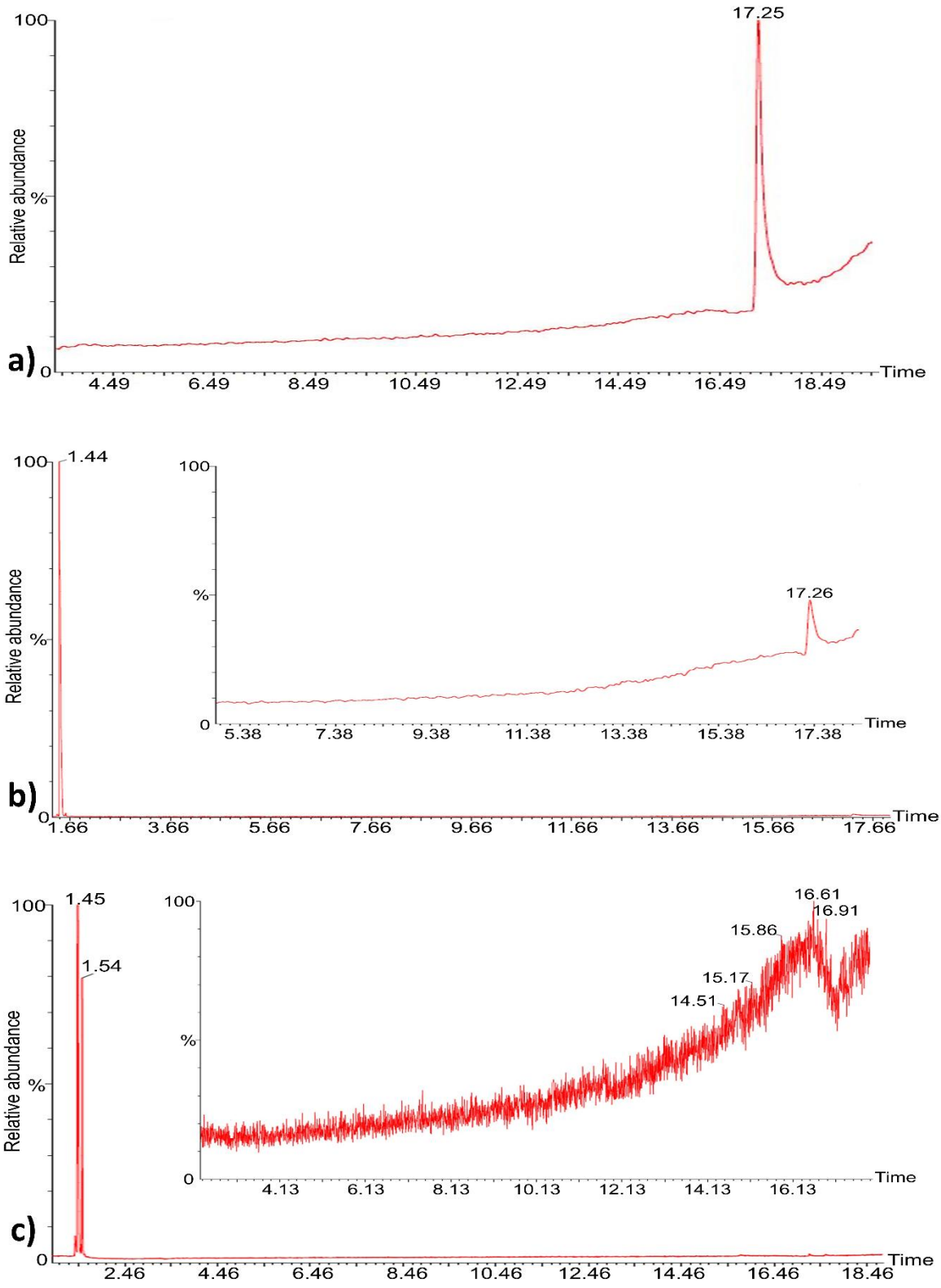


Fig. 4.14: GC-MS analysis of residual butachlor in **a)** control and culture broth at **b)** 48h, **c)** 120 h. Peaks with RT 17.26 min,16.91min, 16.61 min, 15.86 min, 15.17 min and 14.51 min showing breakdown into different metabolites

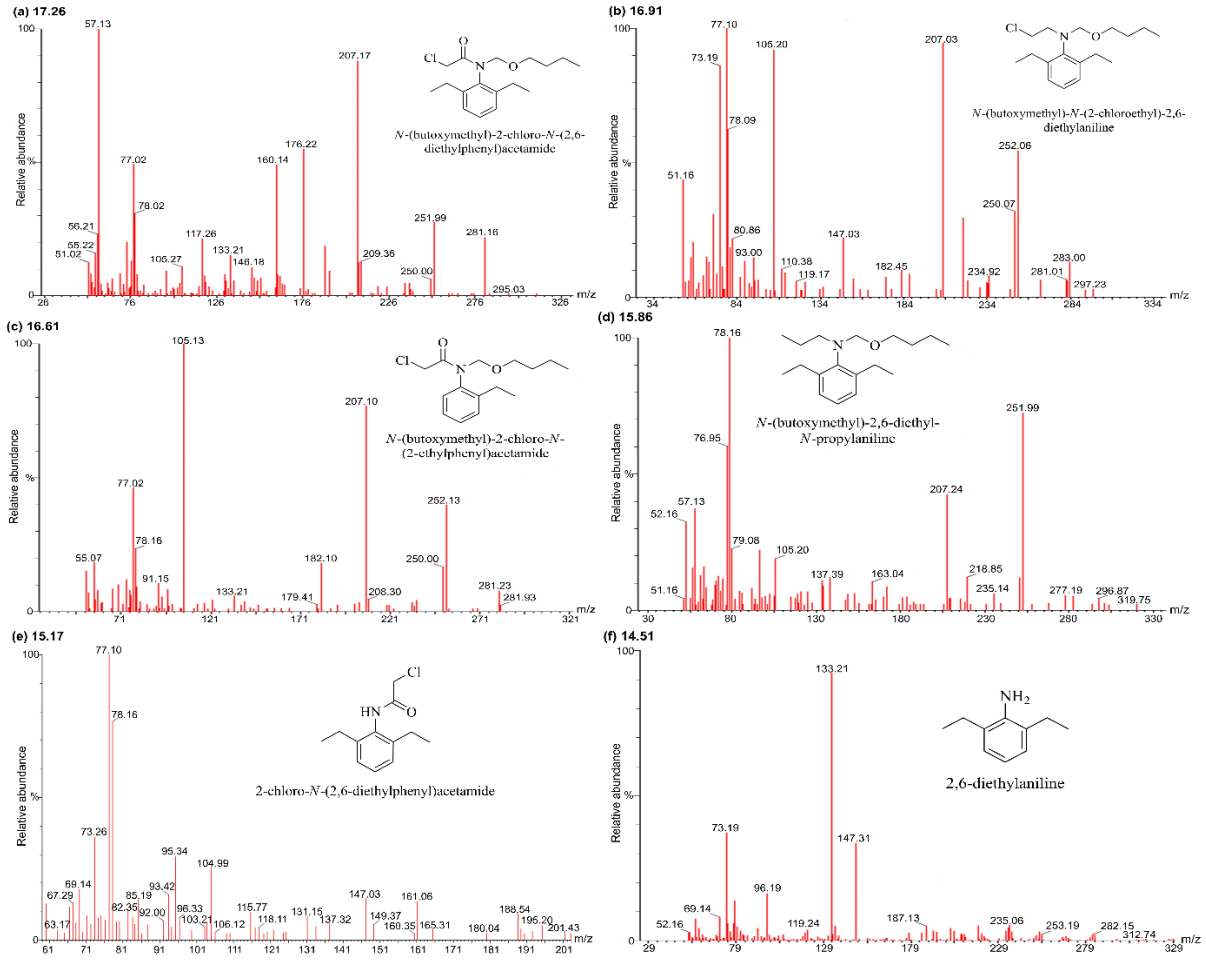


Fig. 4.15: A mass spectra analysis for peaks a) RT- 17.26 (butachlor), b) RT- 16.91 (*N*-butoxymethyl)-*N*-(2-chloroethyl)-2,6-diethylaniline), c) RT- 16.61 (*N*-(butoxymethyl)-2-chloro-*N*-(2-ethylphenyl) acetamide), d) RT- 15.86 (*N*-(butoxymethyl)-2,6-diethyl-*N*-propylaniline), e) RT- 15.17 (2-chloro-*N*-(2,6-diethylphenyl) acetamide) and f) RT- 14.51 (2,6-diethylaniline)

Peak B with RT 16.91 min was supposed to be *N*-(butoxymethyl)-*N*-(2-chloroethyl)-2,6-diethylaniline, which showed a positive ion chemical ionization at 297.23 and fragment ion peaks at m/z at 283, 252.06, 207,182.45, 147.03, 119.17, 105.20, 77.10, 51.16 (Fig. 4.15 (b)). Peak C (RT 16.61 min) was observed to be *N*-(butoxymethyl)-2-chloro-*N*-(2-ethylphenyl) acetamide with molecular weight 283.13 and ion fragments at m/z 281.23, 252.13, 207,10, 182.10, 105.13, 91.15, 77.02 (Fig. 4.15 (c)). Peak D (RT 15.86 min) was identified as *N*-(butoxymethyl)-2,6-diethyl-*N*-propylaniline and has a molecular weight of 277.44. It showed a positive ion chemical ionization at 277.19 and fragment ions at m/z at 251.99, 235.19, 218.85, 207.24,163.04, 137.39,105.20, 78.16,76.95,57.13 (Fig. 4.15 (d)). Peak E (RT 15.17) displayed fragment ions at m/z 201.43, 195.20, 188.54, 161.06, 147.03,131.15, 118.11, 104.99,95.34, 93.42,77.10 and was identified as 2-chloro-*N*-(2,6-diethylphenyl) acetamide. Molecular weight

of the identified compound is 225.09. (Fig. 4.15 (e)). The molecular weight of compound having RT 14.51 min (peak F) is 149.12. Based on the molecular weight and its fragment ion peaks (147.31, 133.21,119.24,96.19,73.19,69.14), the compound was identified as 2,6-diethylaniline (Fig. 4.15 (f)).

GC-MS analysis gave 5 metabolites, among which *N*-(butoxymethyl)-*N*-(2-chloroethyl)-2,6-diethylaniline and *N*-(butoxymethyl)-2-chloro-*N*-(2-ethylphenyl) acetamide were not previously reported. Butachlor could possibly be degraded into *N*-(butoxymethyl)-*N*-(2-chloroethyl)-2,6-diethylaniline by deacylation at nitrogen group of butachlor which further underwent dechlorination to form *N*-(butoxymethyl)-2,6-diethyl-*N*-propylaniline. Dealkylation of *N*-(butoxymethyl)-2,6-diethyl-*N*-propylaniline led to the formation of *N*-(butoxymethyl)-2-ethylaniline, which was comparable with the pathway reported by Singh and Nandabalan (2018). The major compounds found were 2-chloro-*N*-(2,6-diethylphenyl) acetamide and 2,6-diethylaniline, which were previously reported in several butachlor degradation studies (Zhang et al., 2011; Liu et al., 2012; Hou et al., 2014b; Gao et al., 2015). Formation of 2-chloro-*N*-(2,6-diethylphenyl) acetamide was the result of debutoxylation and dealkylation reactions. Liu et al. (2012) proposed hydrolysis of butachlor through N-dealkylation resulting in the formation of butoxymethanol and 2-chloro-*N*-(2,6-dimethylphenyl)-acetamide where, hydrolase Ch1H was the enzyme involved the degradation process. Zhang et al. (2011) detected oxygenases (aniline dioxygenase and catechol 1, 2-dioxygenase) during butachlor degradation by *Paracoccus* sp., which were induced by butachlor and 2,6-diethylaniline. Detection of metabolite 2,6-diethylaniline in our study indicates 2,6-diethylaniline was subsequently metabolized into CO_2 and H_2O *via* oxidation of aniline and catechol through ortho/meta-cleavage pathway. In another research conducted by Zheng et al. (2012), a Gram-negative bacterium *Catellibacterium caeni* sp. nov DCA-1^T degraded butachlor into five different metabolites. Hydrolases and oxygenases (aniline dioxygenase, catechol 1,2-dioxygenase, catechol 2,3-dioxygenase) in crude cell extracts of *Bacillus* sp. Hys-1 (Gao et al., 2015), *Rhodococcus* (Liu et al., 2012), and *Paracoccus* (Zhang et al., 2011) are involved in degradation of butachlor and no enzyme activity was detected in cell extracts when glucose was used as substrate. In our study we report growth of *Bacillus altitudinis* A16 from coal tar contaminated soil in presence of butachlor as sole carbon source and its utilization through degradation by cell extract with the formation of similar metabolites following three possible initial steps (Fig. 4.16) based on previous reports and our findings.

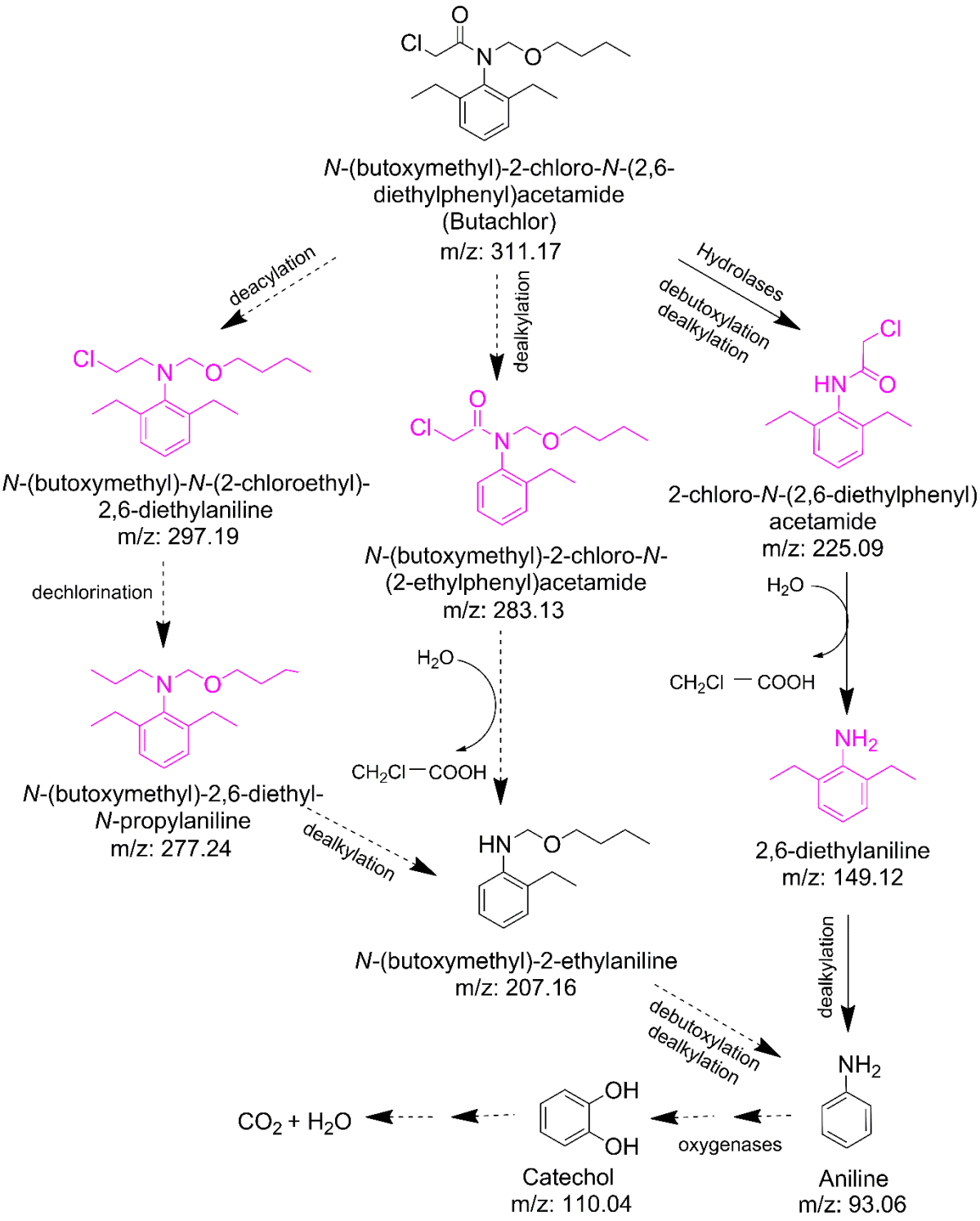


Fig. 4.16: Proposed possible metabolic pathways of butachlor degradation by *Bacillus altitudinis* A16

4.3 Fabrication and characterization of hydrogel-nanoparticulate system for degradation of pesticide

4.3.1 Fabrication of Ch/PVA hydrogel-nanoparticulate system

Presence of amino (-NH_2) and hydroxyl (-OH) groups in the chitosan and polyvinyl alcohol (PVA) contributes to their excellent absorption capacities (Agnihotri et al., 2012). Mechanism of synthesis of Ch/PVA hydrogel which acts as a nanoreactor and a template for immobilization of AgNPs is given in Fig. 4.17 (Vimala et al., 2011; Agnihotri et al., 2012).

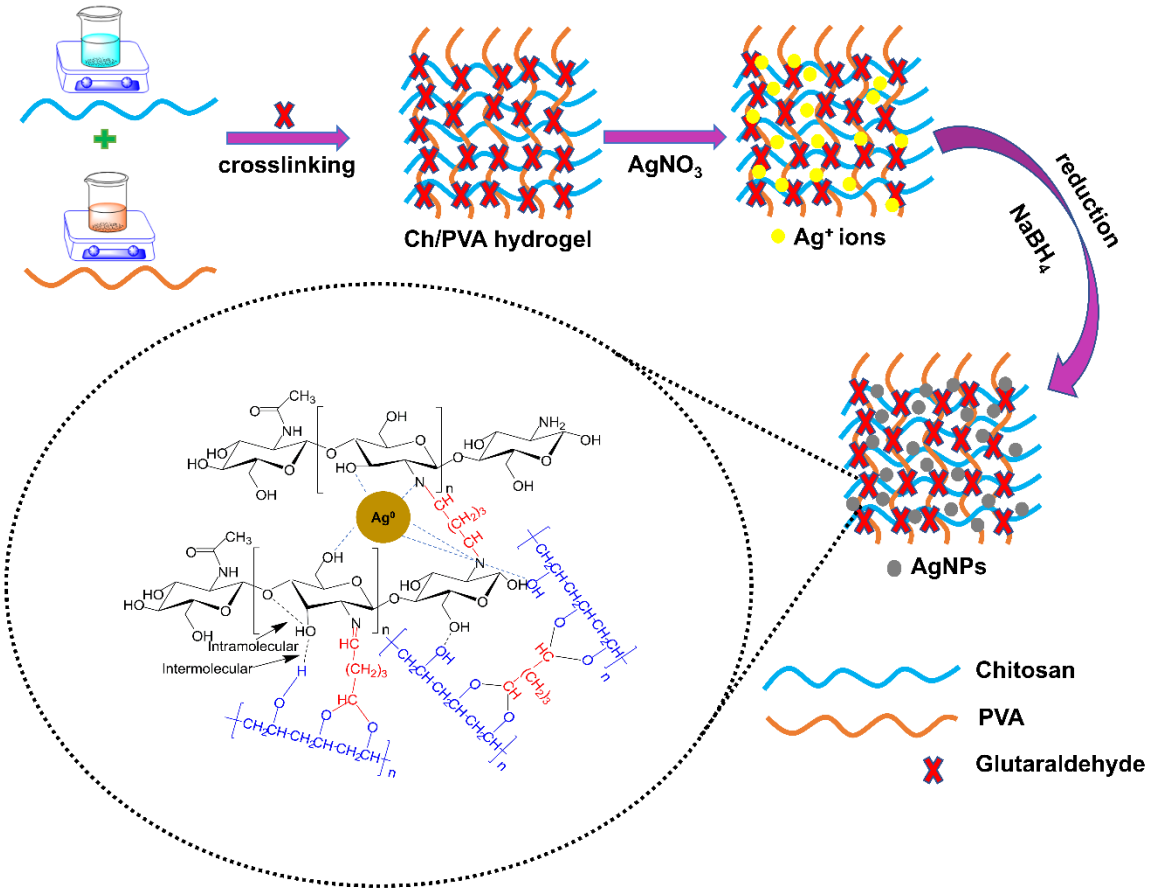


Fig. 4.17: Scheme for fabrication of Ch/PVA-Ag nanocomposite with *in situ* synthesis of AgNPs

On addition of the entirely swollen Ch/PVA hydrogel discs to $AgNO_3$ solution (precursor), some of the Ag^+ ions get entrapped in the free spaces within the crosslinked polymeric hydrogel networks and others are absorbed by a number of hydrophilic hydroxides and amines present in the hydrogel *via* electrostatic interactions (Agnihotri et al., 2012; Gholamali et al., 2020). Ag^+ ions present in the hydrogel were reduced *in situ* by strong reducing agent sodium borohydride ($NaBH_4$), which was confirmed by quick color change of the discs to deep-yellow

within 10 s, indicating the generation of Ag nuclei. However, further gradual color change from yellow to light-brown and lastly to deep-brown over time of 30 min indicated the formation of AgNPs (Ag^0). Synthesized AgNPs had a tendency to establish complex and/or non-covalent interactions with Ag^+ ions and the functional moieties (–OH, $–NH_2$, –C=O) present in the hydrogel network (Agnihotri et al., 2012) and hence, were uniformly distributed within the hydrogel, forming a hydrogel nanocomposite Ch/PVA-Ag (Fig. 4.18).

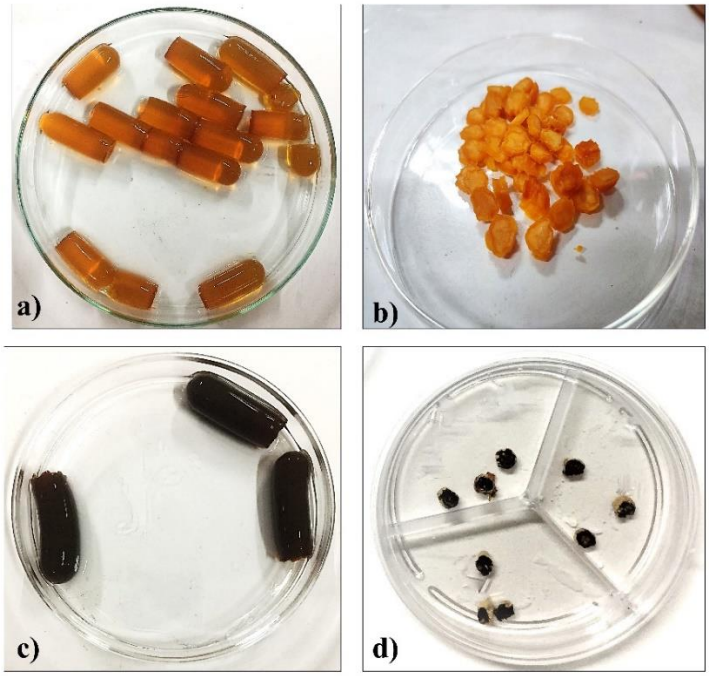


Fig. 4.18: a) Ch/PVA hydrogel, **b)** Ch/PVA hydrogel discs, **c)** Ch/PVA-Ag hydrogel and **d)** Ch/PVA-Ag hydrogel discs

4.3.2 Swelling studies

Precursor hydrogels with different amounts of glutaraldehyde crosslinker (10mM-50mM) were synthesized (Table 4.4). Increase in swelling ratio was observed with increase in crosslinker concentration. Considering its toxic effects, 30mM glutaraldehyde was used for hydrogel synthesis. Wang and Gunasekaran (2006) investigated the effect of quantity of crosslinker on the swelling percentage of the synthesized hydrogel and concluded that increase in swelling ratio with higher crosslinker amount was the result of higher degree of localization of water molecules within the polymeric hydrogel network. Swelling ratio is directly proportional to the increase in chitosan content, which is attributed to the presence of more hydrophilic moities (Vimala et al., 2011). Compared to pristine Ch/PVA hydrogel cross-linked with 30 mM glutaraldehyde, the swelling ratio of silver incorporated Ch/PVA-Ag hydrogel decreased from

Table 4.4: Swelling ratio of Ch/PVA hydrogel with different amount of chitosan, PVA and glutaraldehyde

Chitosan (%)	PVA (%)	Glutaraldehyde-Crosslinker (mM)	Swelling Ratio (%)
2	3	30	67.10 ± 0.61
2	3	40	65.89 ± 1.09
2	3	50	70.19 ± 0.56
2	4	30	66.58 ± 0.12
2	4	40	67.64 ± 0.35
2	4	50	68.10 ± 1.22
2	5	30	64.94 ± 0.82
2	5	40	67.99 ± 0.35
2	5	50	42.99 ± 2.06
2.5	3	30	73.24 ± 1.11
2.5	3	40	67.52 ± 0.96
2.5	3	50	75.36 ± 0.66
2.5	**4**	**30**	**74.39 ±0.01**
2.5	4	40	70.86 ± 2.70
2.5	4	50	polymerized
2.5	5	30	69.20 ± 1.85
2.5	5	40	68.65 ± 0.37
2.5	5	50	69.42 ± 0.26
3	3	30	polymerized
3	3	40	polymerized
3	3	50	polymerized
3	4	30	polymerized
3	4	40	polymerized
3	4	50	polymerized
3	5	30	polymerized
3	5	40	polymerized

* polymerized – Hydrogel polymerized immediately on addition of glutaraldehyde; hydrogel was not homogenous.

74.39 ± 0.01 % to 52.35 ± 0.58 %, probably due to extra cross-linking between AgNPs and the electron-rich O and N atoms of -OH and NH_2 present in the Ch/PVA hydrogel, which restricts the penetration of water within the hydrogel nanocomposite, thereby reducing the swelling behaviour (Vimala et al., 2011). Also, the flexibility of silver loaded hydrogel is enhanced with

the formation of AgNPs due to the interaction between Ag and hydroxyl groups, resulting in decreased hydrophilicity of the nanocomposite and reduced swelling behaviour (Ma et al., 2009).

4.3.3 Characterization and analysis of hydrogel composites

Structural and morphological properties

To study the cross-sectional morphology and confirm the *in-situ* formation of AgNPs in the Ch/PVA hydrogel, both the hydrogels were examined by SEM and FE-SEM with EDX technique. Fig. 4.19 (a) and (b) show the structural morphology of chitosan and PVA. Fig. 4.19 (c) (SEM) and (2e) (FE-SEM) shows the morphology of Ch/PVA hydrogel, where a porous structure was seen, with no metal nanoparticles within it. Fig. 4.19 (d) (SEM) and (f) (FE-SEM) shows evenly distributed nanoparticles within the hydrogel and confirms that *in situ* loading of AgNPs did not affect the structural morphology and integrity of the hydrogel. EDX analysis (Fig. 4.19 (g)) also confirmed that Ch/PVA-Ag nanocomposite contained 0.97 % of silver within it, which corroborates well with the elemental mapping of Ch/PVA-Ag, where Ag was homogenously distributed throughout the nanocomposite network, though with a very less proportion (Fig. 4.19 (i) - (k)).

To determine size of the synthesized AgNPs, TEM analysis was done. TEM image (Fig. 4.19 (h) indicates the presence of spherical nanoparticles (~5-20 nm in size) with no signs of lumps or aggregates. Average hydrodynamic size of the synthesized nanoparticles measured by dynamic light scattering using zetasizer nano was 61.89 nm. The amount of silver loaded in the Ch/PVA-Ag hydrogel was determined by ICP-AES. Pre-weighed (0.5g) hydrogel discs were crushed and sonicated to retrieve AgNPs from hydrogel matrix and further nitric acid digestion was carried out for their dissolution following further dilution. The total amount of silver content present in Ch/PVA-Ag hydrogel was calculated as 2.73 ± 0.36 mg g^{-1} of hydrogel.

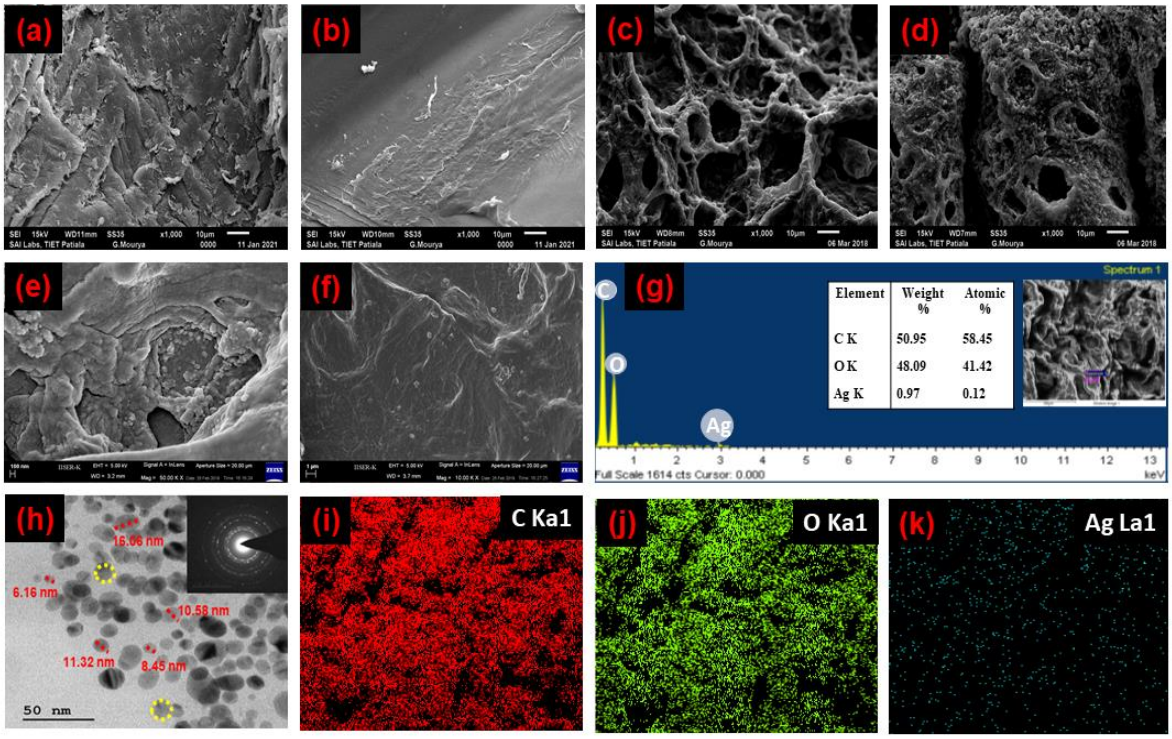


Fig. 4.19: SEM images of **(a)** chitosan, **(b)** PVA, **(c)** pure Ch/PVA hydrogel, **(d)** AgNP loaded Ch/PVA-Ag hydrogel, FE- SEM images of **(e)** pure Ch/PVA hydrogel and **(f)** AgNP loaded Ch/PVA-Ag hydrogel, **(g)** EDX spectra confirming presence of silver within the hydrogel, **h)** TEM image of synthesized AgNPs within the Ch/PVA-Ag hydrogel and **(i-k)** elemental mapping of Ch/PVA-Ag hydrogel

FTIR

FTIR spectra of pristine Ch/PVA and silver incorporated Ch/PVA-Ag hydrogels were evaluated to examine the cross-linking between the polymers and studying the interaction of the functional groups in hydrogel synthesis along with incorporation of AgNPs within it. Significant changes occurred after synthesis of AgNPs within Ch/PVA hydrogel (Fig. 4.20).

Although there's a possibility of overlapping between O-H and N-H stretching, presence of sharp, broad peaks at 3340 and 3344 cm^{-1} in Ch/PVA and Ch/PVA-Ag hydrogels indicate O-H stretching vibration (Nguyen et al., 2011; Elbarbary and El-sawy, 2017). The C-H stretching in the hydrogels has strong peak at 2950-2850 cm^{-1} (Elbarbary and El-sawy, 2017). The peaks at 1642, 1416 and 1076 cm^{-1} are attributed to absorption of $NHCOCH_3$ groups, presence of C-H bonds and the stretching vibration of C-O-C in glucose unit, respectively (Yang et al., 2004; Agnihotri et al., 2012; Nithya et al., 2015). The appearance of a new bands 1734 cm^{-1} and 1218 cm^{-1} in fingerprint region of Ch/PVA-Ag hydrogel at 1218 cm^{-1} indicates presence of AgNPs.

1734 cm^{-1} corresponds to carbonyl group, indicating $–NH_2$ of chitosan and free –OH group of PVA as the ideal places for binding of silver ions and AgNP immobilization (Agnihotri et al., 2012; Elbarbary and El-sawy, 2017). Additionally, band at 1416 cm^{-1} corresponding to C- H bonds was shifted to 1368 cm^{-1} after synthesis of AgNPs which was probably due to co-ordination bond formation between the silver atom and the electron rich groups of chitosan (Vimala et al., 2011).

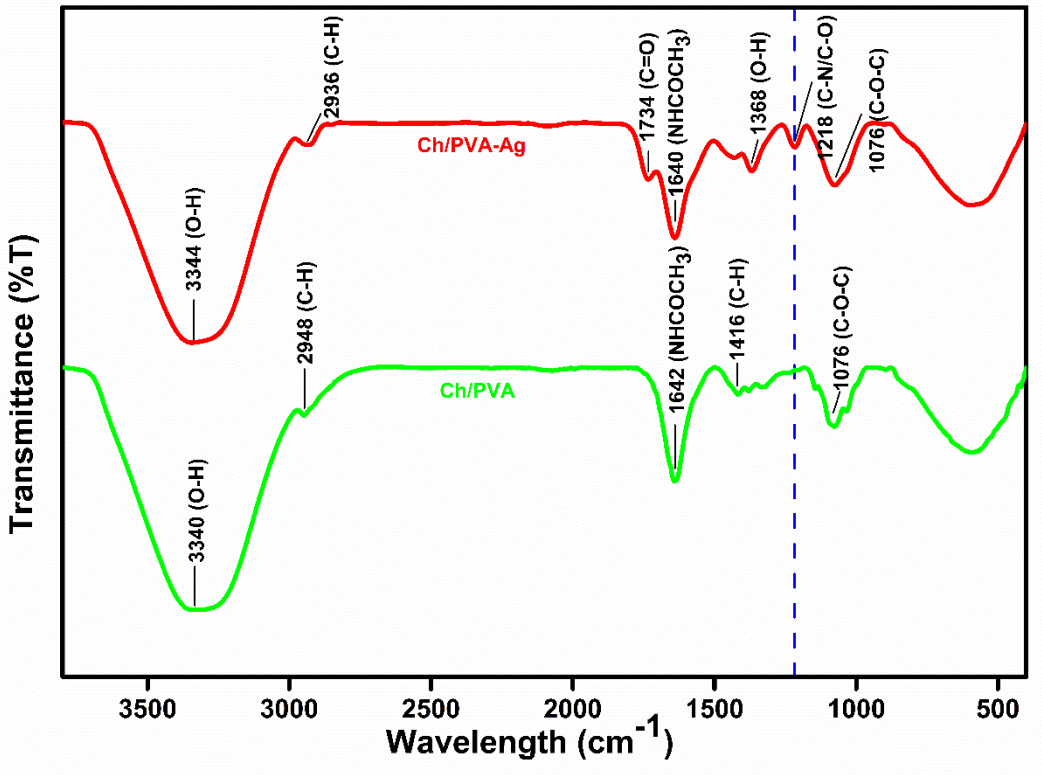


Fig. 4.20: FTIR spectra of Ch/PVA hydrogel with and without AgNP loading

XRD

Fig. 4.21 (d) shows the XRD pattern for Ch/PVA hydrogel incorporated with AgNPs. Chitosan showed characteristic diffraction peaks at 2θ = 10.8° and 20.12°, corresponding to the respective equatorial (100) and (020) reflections (Fig. 4.21 (a)). Three peaks at 19.81°, 23.11° and 40.90° were observed in PVA, indicating its semicrystalline structure (Fig 4.21 (b)). After crosslinking both the polymers, peaks at 20.02°, 22.8°and 40.8° were seen, with reduced intensity, probably due to reduction in crystallinity. Significant peak at diffraction angle of 20.02 and 40.67° in Ch/PVA-Ag hydrogel indicated the polymeric Ch/PVA matrix (Mishra et al., 2015). The diffractogram of Ch/PVA-Ag hydrogel showed five peaks at 2θ values of

38.02°, 44.3°, 64.6°, 77.5° and 81.9° corresponding to Bragg's reflections from (1 1 1), (2 0 0), (2 2 0), (3 1 1) and (2 2 2) planes of the face centered cubic (FCC) crystal structure of AgNPs (ICDD card no. 03-065-2871), confirming crystalline structure of AgNPs.

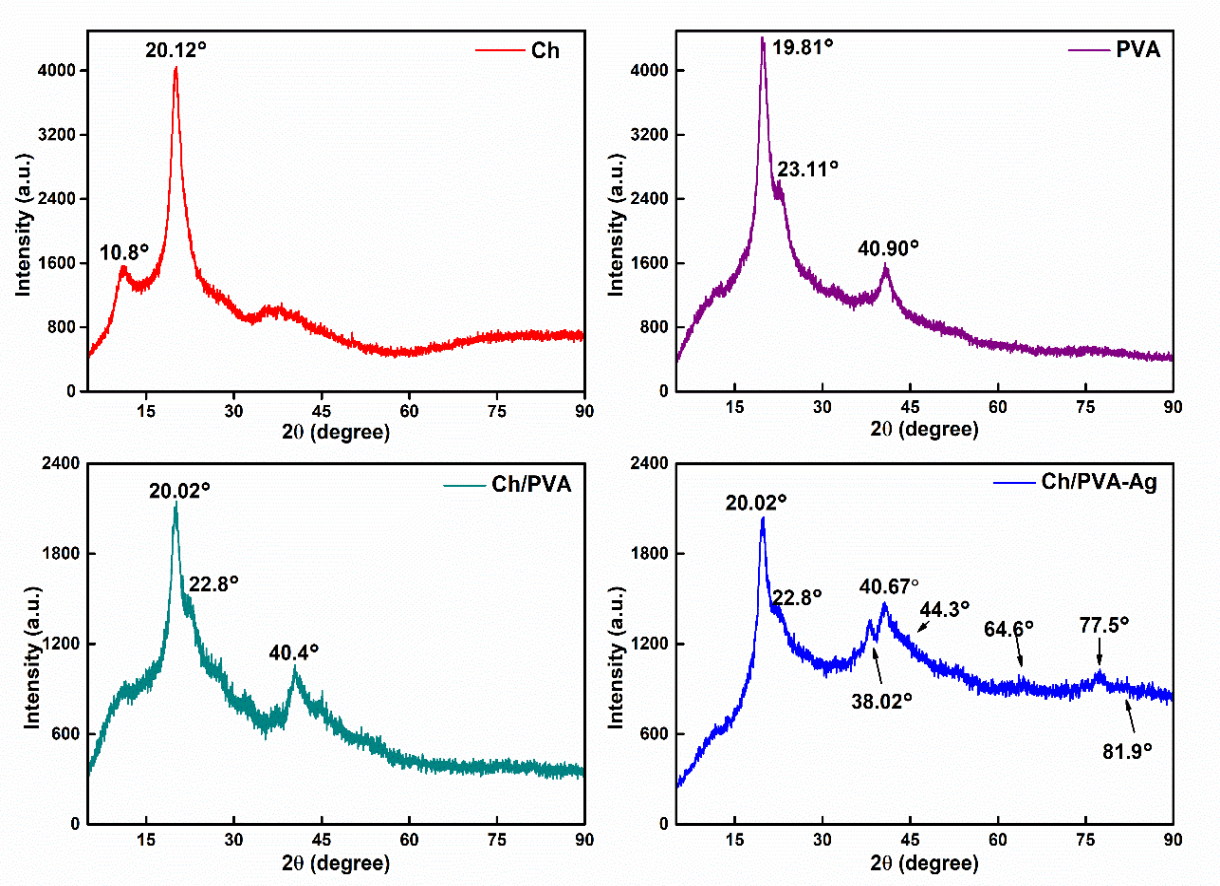


Fig. 4.21: XRD a) chitosan b) PVA c) Ch/PVA hydrogel d) Ch/PVA-Ag hydrogel

XPS

XPS analysis was carried out as survey and narrow region spectra to confirm the formation of AgNPs in Ch/PVA-Ag nanocomposite. The survey spectrum was fitted by multiple Gaussians and confirmed the presence of carbon, oxygen, silver, and nitrogen in the nanocomposite (Fig. 4.22 (a)). The high- resolution spectra of Ag 3d and O 1s were calibrated to the binding energy of C 1s at 284.8 eV and deconvoluted using gaussian function and Levenberg-Marquardt iteration algorithm. The C 1s peak was deconvoluted into two peaks with binding energy (BE) 284.8 eV and 286.2 eV corresponding to C-C/C-H and C-O/C–OH, respectively (Nivethaa et al., 2015) (Fig. 4.22 (c)). In Fig 4.22 (d) O 1s spectra shows two peaks at the BE 530.5 eV and 531.5 eV corresponding to C-O and C-OH, respectively. Fig 4.22 (b) corresponds to Ag 3d core levels deconvoluted to get characteristic peaks for Ag $3d_{5/2}$ and Ag $3d_{3/2}$ with a spin energy

separation of 6.0 eV. The peaks at the BE of 369.1 eV and 375.1 eV confirms the presence of metallic silver in the nanocomposite, whereas two peaks with the lower BE 367.5 eV and 373.5 eV indicates the presence of Ag ions (Arjunan et al., 2016). Presence of silver ions could be the result of interaction/reaction of AgNPs either with chitosan or the oxygen present in the solution or air (An et al., 2011).

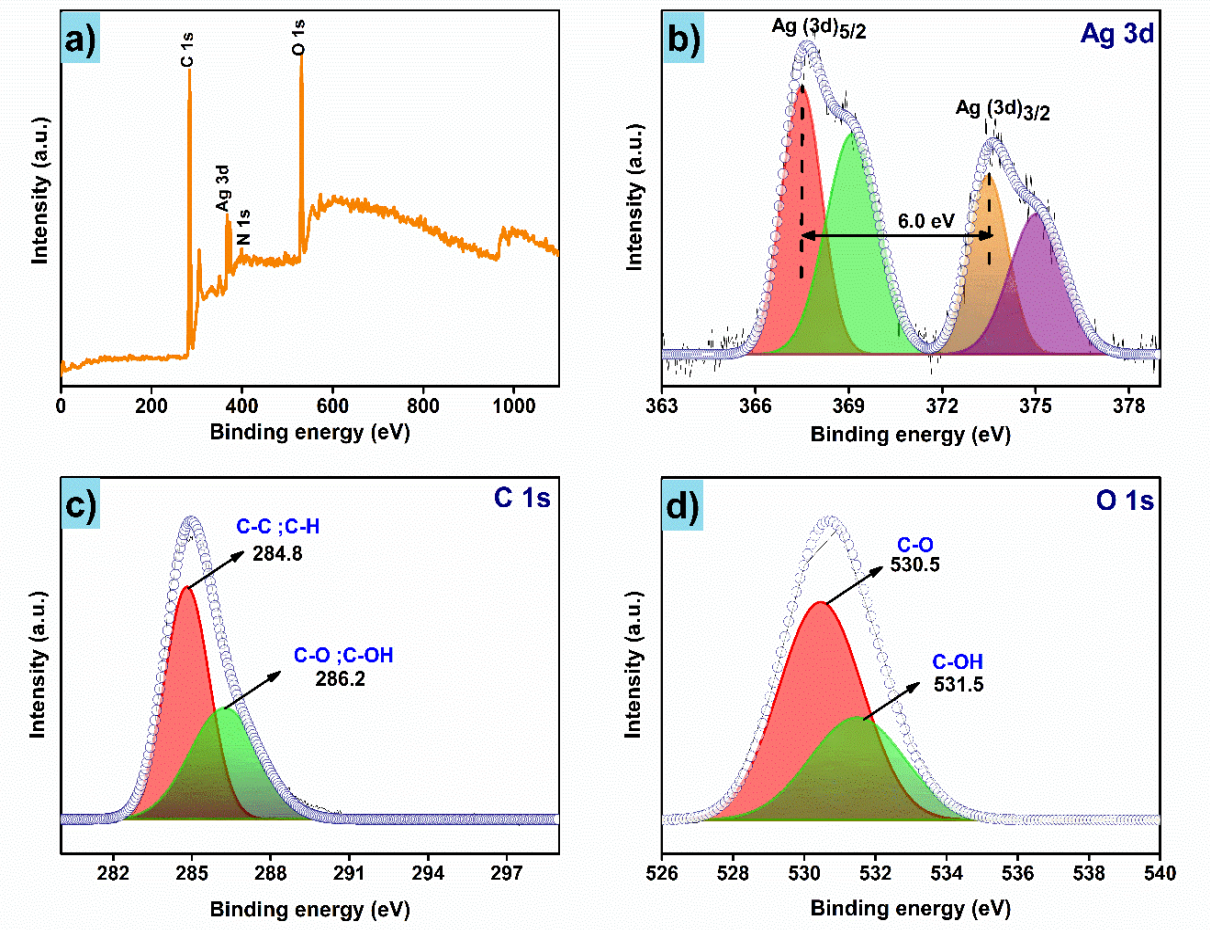


Fig. 4.22: XPS analysis **a)** survey XPS spectra of Ch/PVA-Ag nanocomposite, **b)** Ag (3d), **c)** C (1s) and **d)** O (1s)

Thermal behaviour and BET surface area analysis

TGA and derivative weight loss (DTG) analyses were done to evaluate the thermal decomposition of Ch-PVA nanocomposite before and after immobilization of nano-silver (Fig. 4.23).

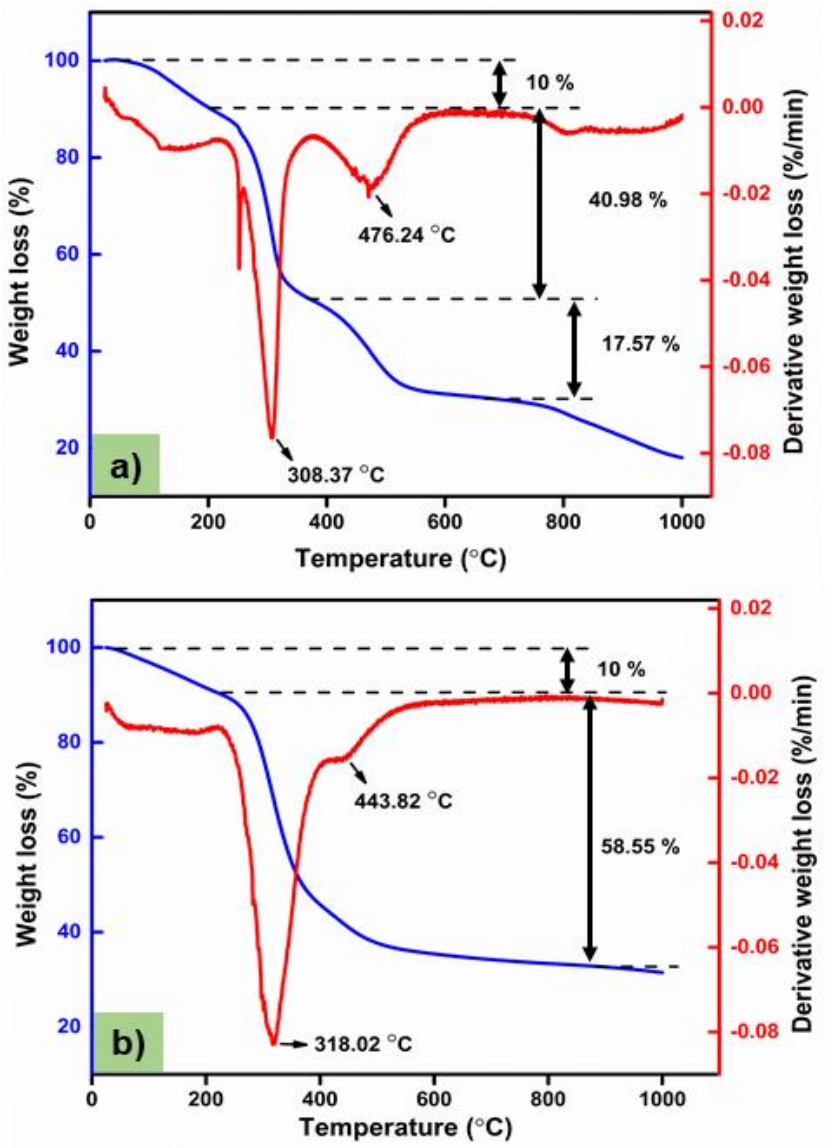


Fig. 4.23: TGA and DTG curves for **a)** Ch/PVA and **b)** Ch/PVA-Ag hydrogel

A known mass of the hydrogel discs was heated in alumina crucible in non-oxidized conditions (nitrogen atmosphere) from ambient temperature to 1000 °C. The first thermal event occurred at a temperature range 80-150°C and is accompanied by a significant weight loss (10%) in the sample. This loss accounts for the majority of residual water present in the sample, either physically adsorbed or weakly/strongly H-bonded, which get evaporated within this range. Furthermore, an initial thermal decomposition of the polymeric structures appeared at 204 – 375°C and 229 – 410°C for Ch/PVA and Ch/PVA-Ag, respectively. Interestingly, while Ch-PVA showed its characteristic exothermic peak at 308°C, which is ascribed to the decomposition of chitosan, the corresponding peak was shifted to 318°C for Ch/PVA-Ag nanocomposite. It clearly indicates that the addition of silver nanoparticles increased the

thermal stability of the resulting nanocomposite, as also evidenced in previous analyses. The next thermal decomposition of polymeric networks occurred in between 375–550 °C (Ch/PVA) and 410–500 °C (Ch/PVA-Ag) due to the complete depolymerisation of polymer chains and their subsequent degradation through deamination and dehydration reactions. At 1000 °C, ~18% char residue was seen in case of Ch/PVA, whereas, for Ch/PVA-Ag ~31% char residue was recorded.

The Nitrogen adsorption-desorption isotherms were generated using N_2 adsorption-desorption analyzer (Fig. 4.24).

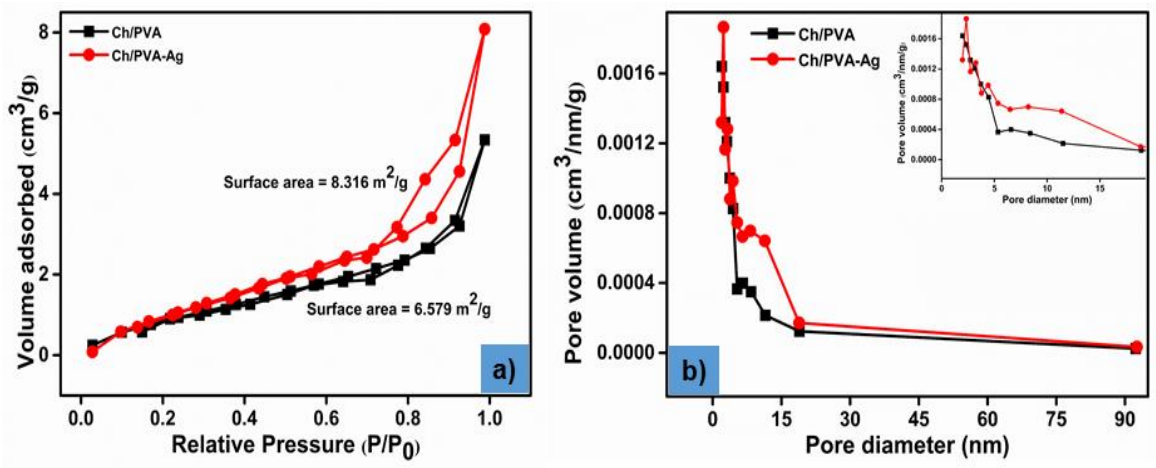


Fig. 4.24: BET analysis **a)** Nitrogen adsorption-desorption plots **b)** pore size distribution (BJH curve)

The surface area and pore volume of pristine Ch/PVA hydrogel and silver loaded Ch/PVA hydrogel were calculated by employing multi-point BET analysis and Barrett– Joyner–Halenda (BJH) method, respectively. Fig. 4.24 (a) shows hysteresis loops and a type III isotherm for both the hydrogels, stating the formation of micropores as shown by Arjunan et al. (2016). For Ch/PVA, the surface area and pore diameter were found to be 6.579 m^2 g^{-1} and 1.98 nm, with pore volume of 0.011 cc g^{-1}. Under similar conditions, surface area, pore diameter and pore volume for Ch/PVA-Ag hydrogel were determined as 8.316 m^2 g^{-1}, 2.33 nm and 0.016 cc g^{-1}, respectively. This increased surface area of the Ch/PVA-Ag hydrogel could be due to the presence of AgNPs. Loading of metal NPs in the polymeric matrix enhances the crosslinking density, resulting in the appearance of nano porosity and the increased surface area in the polymer gel (Dwivedi et al., 2014). The BET analysis was carried out with the dried hydrogel, which swells during the experimentation while adsorption. So, the actual surface area of the hydrogel in the swollen state is expected to be much higher.

4.4 Removal of butachlor from synthetic water using hydrogel- nanoparticulate system

4.4.1 Removal of butachlor

Removal of butachlor from aqueous solution using fabricated Ch/PVA-Ag nanocomposite was studied by conducting adsorption experiments, where distilled water spiked with butachlor (10 -100 mg L^{-1}) was used as a test pollutant. Comparative adsorption potential of both pristine Ch/PVA and silver immobilized Ch/PVA-Ag hydrogel was carried out in dark until adsorption-desorption equilibrium was achieved. FTIR spectra of the pristine Ch/PVA and Ch/PVA-Ag hydrogels before and after adsorption of butachlor is shown in Fig. 4.25.

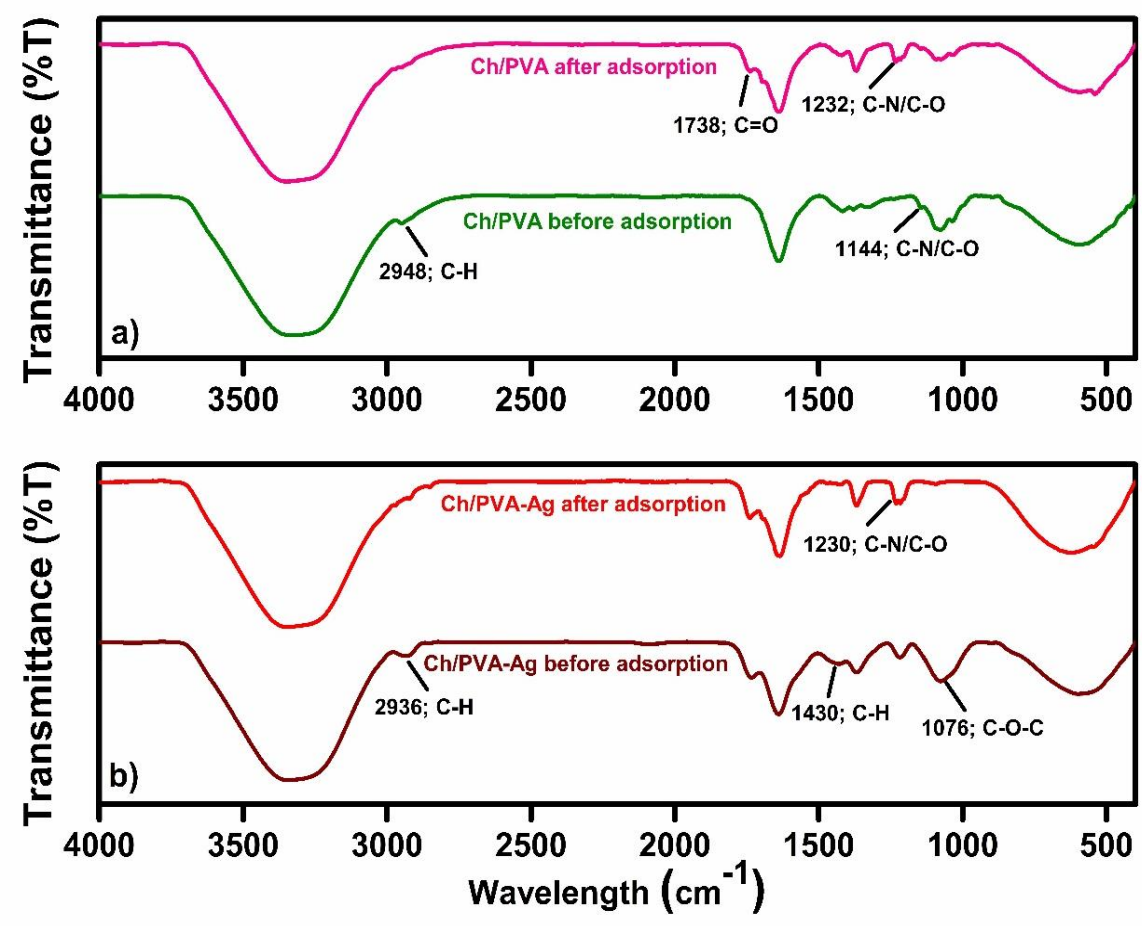
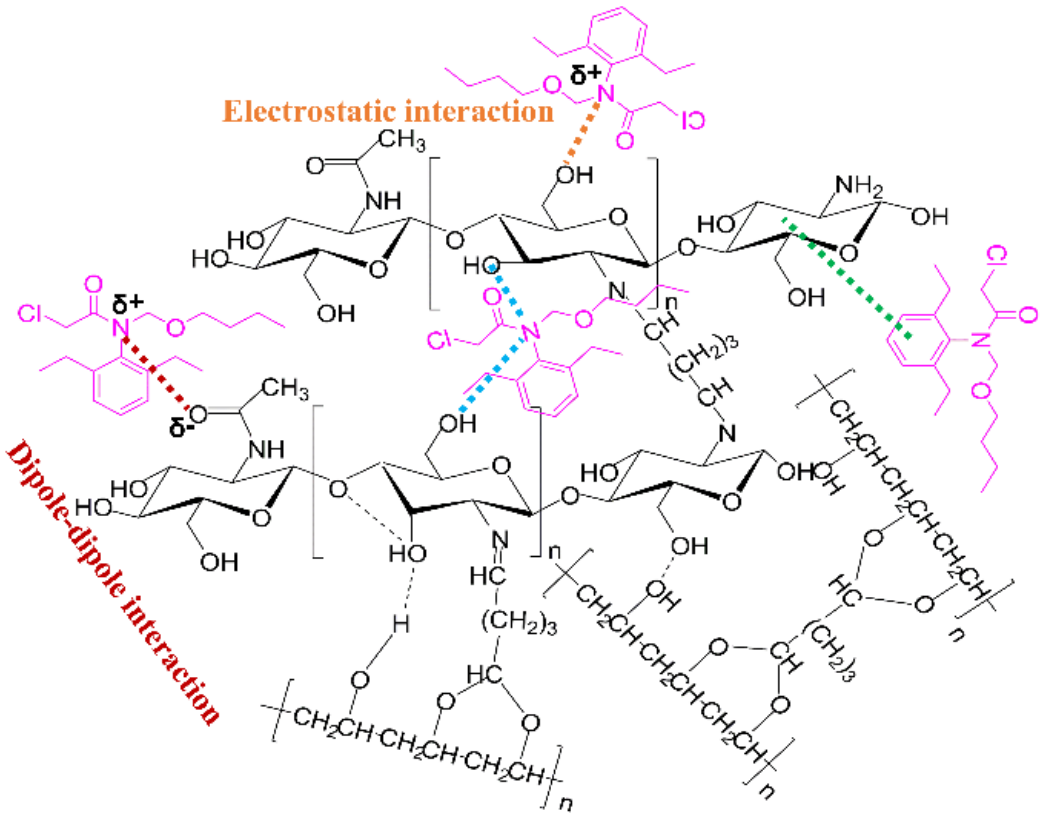


Fig. 4.25: FTIR analysis of **(a)** Ch/PVA hydrogel and **(b)** Ch/PVA-Ag hydrogel, before and after adsorption of butachlor

After adsorption of butachlor, change in position and intensities of some of the peaks was observed in both the hydrogel systems, indicating successful sorption of butachlor. Peaks at 2948 cm^{-1} and 2936 cm^{-1} corresponding to C-H bond in both the hydrogels were lost after butachlor adsorption. The bands at 1232 cm^{-1} and 1230 cm^{-1} in Ch/PVA and Ch/PVA-Ag hydrogels formed after adsorption of butachlor were ascribed to occurrence of C-N/C-O bonds

(Jin and Bai, 2002). A peak at 1144 cm^{-1} (C-N/ C-O stretching) was shifted to 1232 cm^{-1} after adsorption by Ch/PVA hydrogel and a new peak corresponding to C=O stretching at 1738 cm^{-1} was formed (Elbarbary and El-sawy, 2017; Jin and Bai, 2002) (Fig. 4.25 (a)). As shown in Fig. 4.25 (b), two peaks at 1430 cm^{-1} and 1076 cm^{-1} assigned to C-H bending and the stretching vibration of C-O-C were lost after butachlor adsorption in Ch/PVA-Ag nanocomposite (Nguyen et al., 2011; Nithya et al., 2015). The electron rich O and N atoms present in the synthesized hydrogel networks help in efficient adsorption of butachlor by the hydrogels. Ch/PVA-Ag hydrogel showed approximately 10% higher butachlor adsorption than Ch/PVA probably due to additional cross-links between AgNPs and the hydrogel (Agnihotri et al., 2012). A schematic representation of possible interaction of butachlor with both the hydrogels is presented in Fig. 4.26.



Ch/PVA

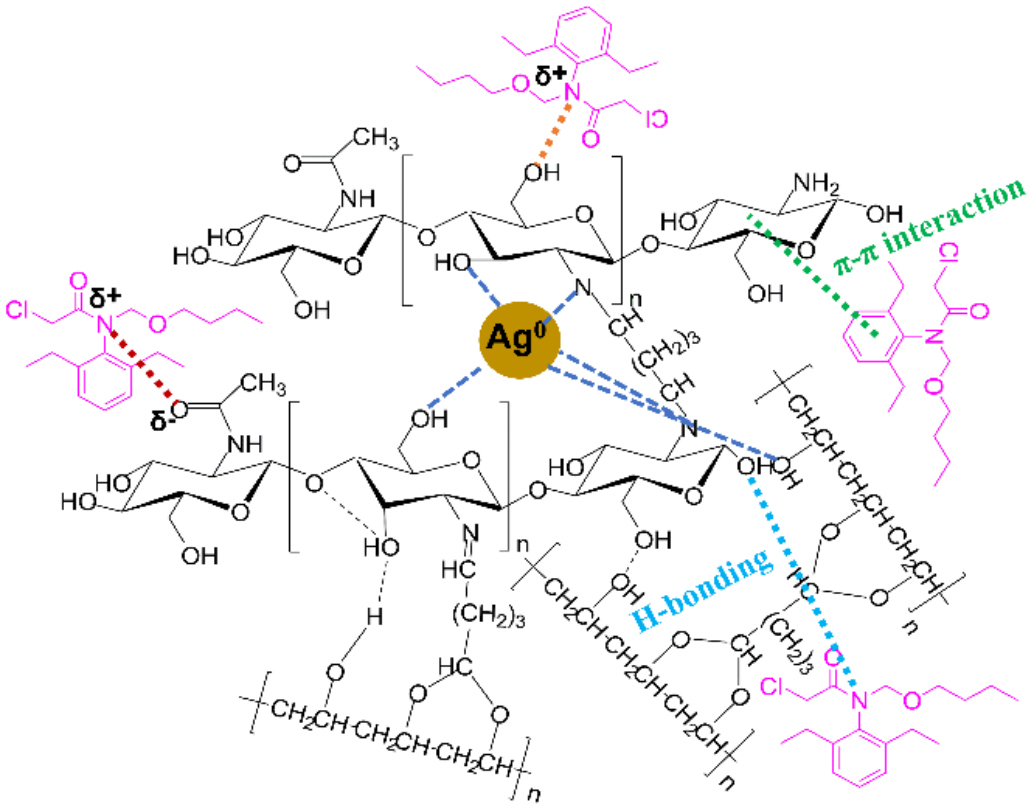


Fig. 4.26: Possible interaction between butachlor and the hydrogels

4.4.1.1 Effect of pH

Effect of pH, butachlor initial concentration, hydrogel dosage, temperature and contact time on sorption efficiency of hydrogels with and without AgNPs was studied. pH is one of the vital parameters, which plays asignificant role in adsorption process as it monitors the electrostatic interactions between adsorbate and adsorbent (Sharma et al., 2017). To examine the adsorption capacity of pristine Ch/PVA and Ch/PVA-Ag hydrogels for butachlor, a set of experiments was performed at different pH (3-11), with 50 mL distilled water spiked with 10 mg L^{-1} butachlor and 100 mg hydrogels discs for 270 min (4.5 h) at room temperature. Maximum removal of butachlor by hydrogels was observed at pH 3 (Fig. 4.27), where after % removal was declined from 86.55% to 81.17% for Ch/PVA and 96.87% to 90.52% for Ch/PVA-Ag.

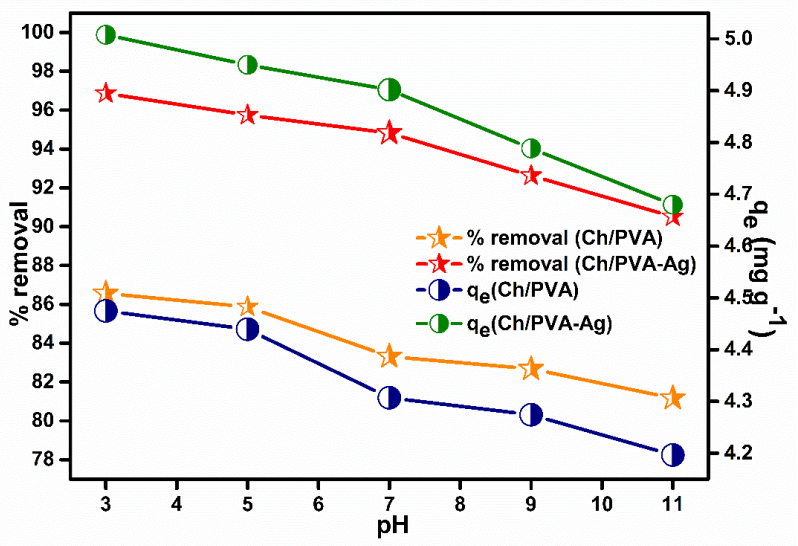


Fig. 4.27: Effect of pH on butachlor removal (Butachlor concentration- 10 mg L^{-1}; hydrogel dosage- 2 g L^{-1}; temp- 30°C)

The predicted pKa value for butachlor is 1.20 ± 0.50 (https://www.chemicalbook.com/ChemicalProductProperty_EN_CB2693046.htm), therefore, at a pH lower than pKa value, butachlor is positively charged, while at a higher pH, it is negatively charged (Hanh et al., 2019). The point of zero charge (pH_{PZC}) of Ch/PVA and Ch/PVA-Ag obtained by the protocol given by Brouers and Al-Musami (2015) was 11.02 and 9.77, respectively, indicating positively charged surface at pH < pH_{PZC} and negatively charged surface at pH > pH_{PZC} (Fig. 4.28). Therefore, at acidic pH, the electrostatic interaction between butachlor and hydrogels lead to better adsorption efficiency than basic pH. Since, adsorption was also observed at higher pH, suggesting strong involvement of physical forces such as Vander waals forces and hydrogen bonding in the adsorption process (Sun et al., 2008).

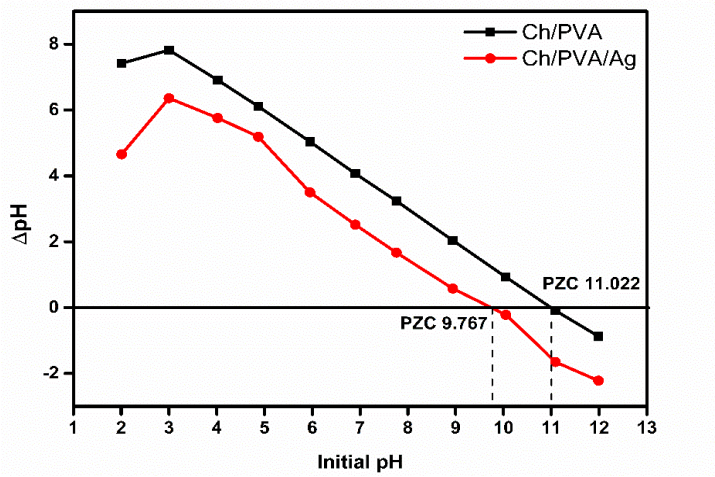


Fig. 4.28: PZC plot for the hydrogels

4.4.1.2 Effect of sorbent dosage

Fig. 4.29 depicts the effect of sorbent dosage on percentage removal of butachlor from the solution.

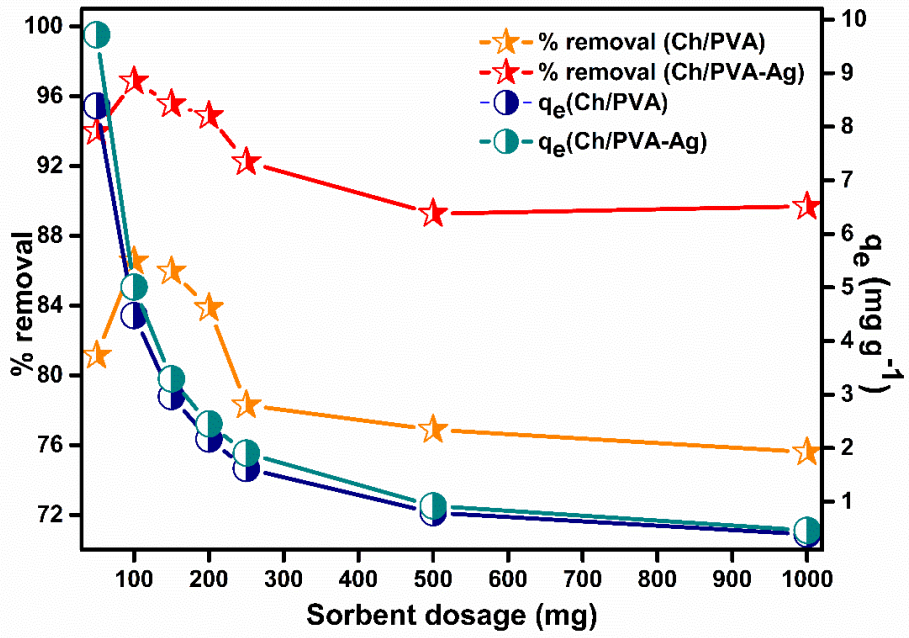


Fig. 4.29: Effect of sorbent dosage on butachlor removal (Butachlor concentration- 10 mg L^{-1}; pH-3; temp- 30°C)

The effect of Ch/PVA and Ch/PVA-Ag hydrogels dosage was studied in the range of 50-1000 mg in 50 mL butachlor solution of concentration 10 mg L^{-1}, keeping other parameters constant. With an increase in mass of hydrogel discs from 50-100 mg, the percentage adsorption was found to increase from 81.14% to 86.55% for Ch/PVA and 93.97% to 96.87% for Ch/PVA-Ag hydrogel discs. Afterwards, a decrease in percentage adsorption values was observed in both hydrogel discs, which was 85.98% to 75.61% for Ch/PVA and 95.54 to 89.26% for Ch/PVA-Ag. The initial increase in butachlor uptake with increase in hydrogel dosage was due to more active sites and optimal surface area supplying more functional groups for bonding with butachlor, boosting adsorption process. Later, decrease in adsorption might be due to increase in steric hindrance due to overcrowding of more active sites within constant volume leading to decrease in butachlor adsorption (Sharma et al., 2018). On contrary, a decrease in sorption capacity (8.39 - 0.39 mg g^{-1} for Ch/PVA and 9.72 - 0.46 mg g^{-1} for Ch/PVA-Ag) was observed with increase in sorbent dosage. Similar effect was studied by Haq et al. (2019), where relatively greater number of the active sites remain unsaturated with high sorbent dosage

leading to decreased sorption capacity at a fixed butachlor concentration. Therefore, an optimum dosage of 100mg (i.e. 2 g L^{-1}) was selected for subsequent set of experiments.

4.4.1.3 Effect of initial concentration of butachlor

The effect of butachlor initial concentration on the sorption capacity of the hydrogel and percentage removal was investigated by varying its concentration from 5 – 100 mg L^{-1}, keeping other factors constant. Percentage removal of butachlor was maximum at concentration 10 mg L^{-1} for both the hydrogels (Fig. 4.30).

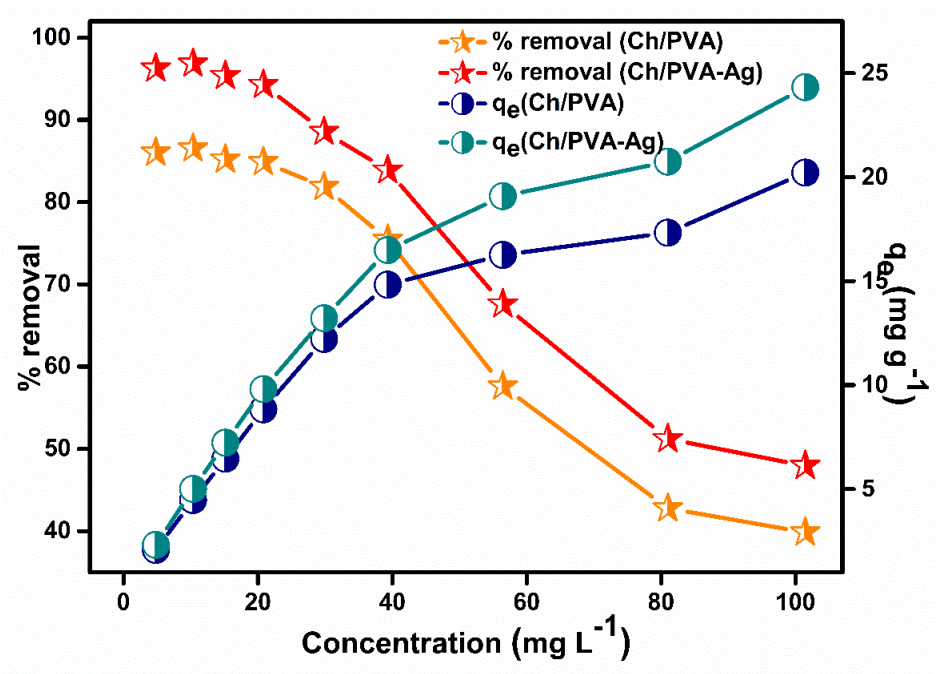


Fig. 4.30: Effect of initial concentration on butachlor removal (Hydrogel dosage 2 g L^{-1}; pH-3; temp- 30°C)

With increase in butachlor concentration from 10 – 100 mg L^{-1}, percentage removal of butachlor declined from 86.55 to 39.85% for Ch/PVA and 96.86 to 47.95 % for Ch/PVA-Ag. At butachlor concentration 5 and 10 mg L^{-1}, adsorption was higher because the number of butachlor molecules in comparison to active sites on the Ch/PVA and Ch/PVA-Ag was small, leading to a good interaction between butachlor and active sites of hydrogels, therefore, increasing the removal of butachlor. As the concentration increases, the competition between butachlor molecules for interaction with the active sites on the hydrogel also intensifies, leading to decrease in butachlor uptake because of lesser availability of vacant sites (Dwivedi et al., 2014; Haq et al., 2019). On the other hand, a gradual rise in sorption capacity (q_e) for both the hydrogels was observed with increase in butachlor concentration.

4.4.1.4 Effect of temperature

Butachlor is broken down at temperature ≥ 165 °C and gets disintegrated on heating, emitting harmful fumes of nitrous oxides and hydrogen chloride (Abigail et al., 2015). So, butachlor removal was studied by varying the magnetic stirrer temperature from 303.15 – 338.15 K (30-65 °C), under optimized conditions of pH of solution, adsorbent dosage and butachlor concentration (Fig. 4.31).

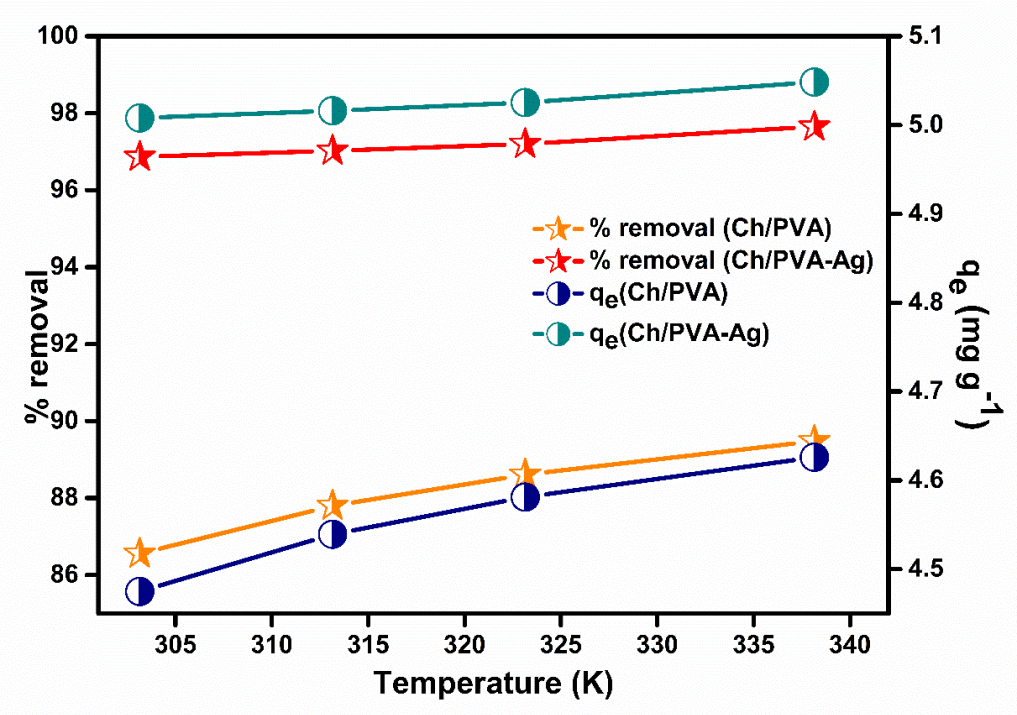


Fig. 4.31: Effect of temperature on butachlor removal (Butachlor concentration- 10 mg L^{-1}; hydrogel dosage 2 g L^{-1}; pH-3)

Increase in temperature from 303.15 – 338.15 K does not exert a much stronger influence on the adsorption process. For blank Ch/PVA hydrogel, increase in percentage removal from 86.55 – 89.47 % was observed, with sorption capacity (q_e) going down from 4.47 – 4.62 mg g^{-1}. In contrast, a very small increase in percentage removal of butachlor by Ch/PVA-Ag (96.86 – 97.64 %) was observed, with negligible change in q_e values i.e. 5.01 – 5.05 mg g^{-1}. So, based on the results, experiments were conducted at room temperature.

4.4.1.5 Effect of contact time

Time of agitation i.e. contact time between Ch/PVA / Ch/PVA-Ag hydrogels and butachlor molecules helps in establishing adsorption- desorption relation between the two and determining maximum adsorption. With 100 mg hydrogel in 50 ml of 10 mg L^{-1} butachlor (pH

3; 30 °C), the time effect was studied in the range of 30-270 min, where increase in the percentage removal of butachlor was observed with the passage of time (Fig. 4.32). At the beginning of the adsorption process, more vacant active sites were available for butachlor uptake, but with the passage of time, repulsive forces between solute molecules on the hydrogel and liquid phase make it difficult to occupy remaining vacant sites. Therefore, the time of agitation was optimized at 270 min.

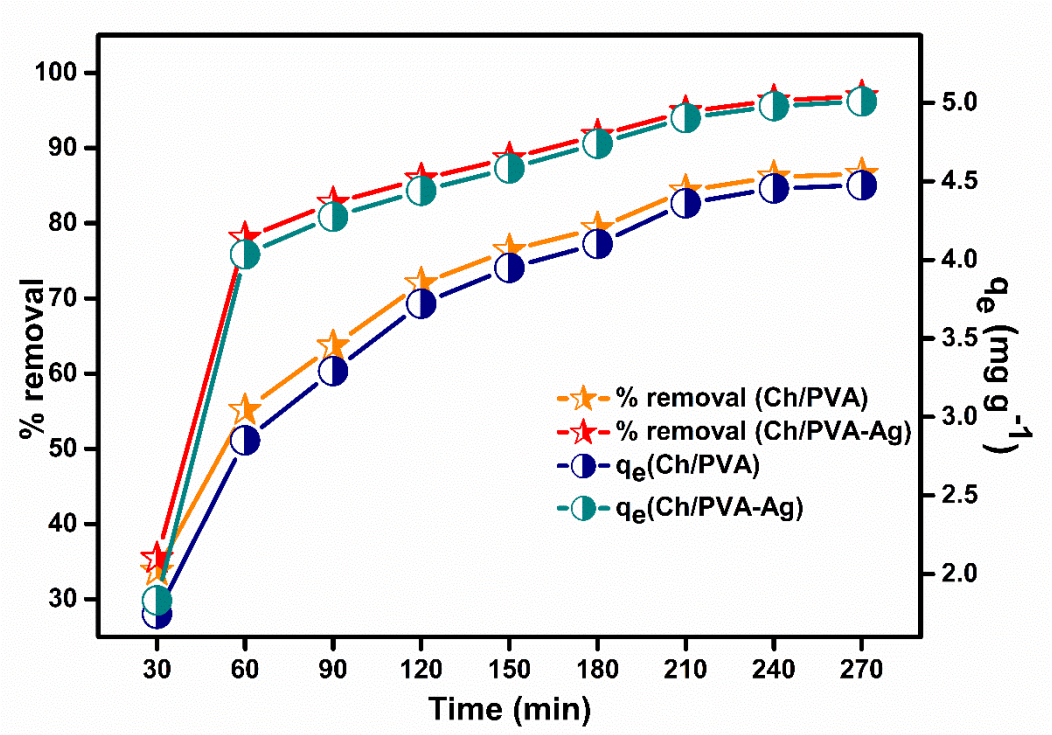


Fig. 4.32: Effect of contact time on butachlor removal (Butachlor concentration- 10 mg L^{-1}; hydrogel dosage 2 g L^{-1}; pH-3; temp- 30°C)

4.4.1.6 Adsorption isotherms

In order to understand the interaction between solute molecules and the sorbent, adsorption isotherms play an important role. Therefore, the experimental data obtained was fitted to Langmuir (linear and non-linear) and Freundlich (linear and non-linear) isotherm models (Fig. 4.33).

Langmuir isotherm

Langmuir isotherm is based on an assumption of monolayer adsorption on the homogenous surface with finite number of active sites (Dwivedi et al., 2014; Haq et al., 2019). The linearized form of Langmuir isotherm model can be expressed as:

$$\frac{C_e}{q_e} = \frac{1}{q_m K_L} + \frac{C_e}{q_m} \quad (9)$$

where, C_e (mg g^{-1}) is the equilibrium concentration, q_e (mg g^{-1}) is the amount of butachlor adsorbed per unit mass of Ch/PVA / Ch/PVA-Ag, K_L (mg g^{-1}) and q_m (L mg^{-1}) are the Langmuir constants related to energy of adsorption and maximum adsorption capacity. As depicted by Fig. 4.33, the intercept and slope of the linear regression plot between C_e/q_e versus C_e gives the values of K_L and q_m, which are shown in Table 4.5.

The isotherm is further studied by another dimensionless constant known as equilibrium parameter or separation factor (R_L), which is defined by the equation below:

$$R_L = \frac{1}{1 + K_L C_0} \quad (10)$$

where, C_0 is the initial butachlor concentration (5, 10, 15, 20, 30, 40, 60, 80 and 100 mg L^{-1}). Value of R_L determines the nature of isotherm to be irreversible ($R_L = 0$), linear ($R_L = 1$), favourable ($0 < R_L < 1$) or unfavourable ($R_L > 1$). The calculated R_L values for whole range of initial butachlor concentrations for Ch/PVA (0.50 – 0.048) and Ch/PVA-Ag (0.32 – 0.03) signifies favourable adsorption.

The nonlinear form of langmuir isotherm is represented by the following equation:

$$q_e = q_m \frac{K_L C_e}{1 + K_L C_e} \quad (11)$$

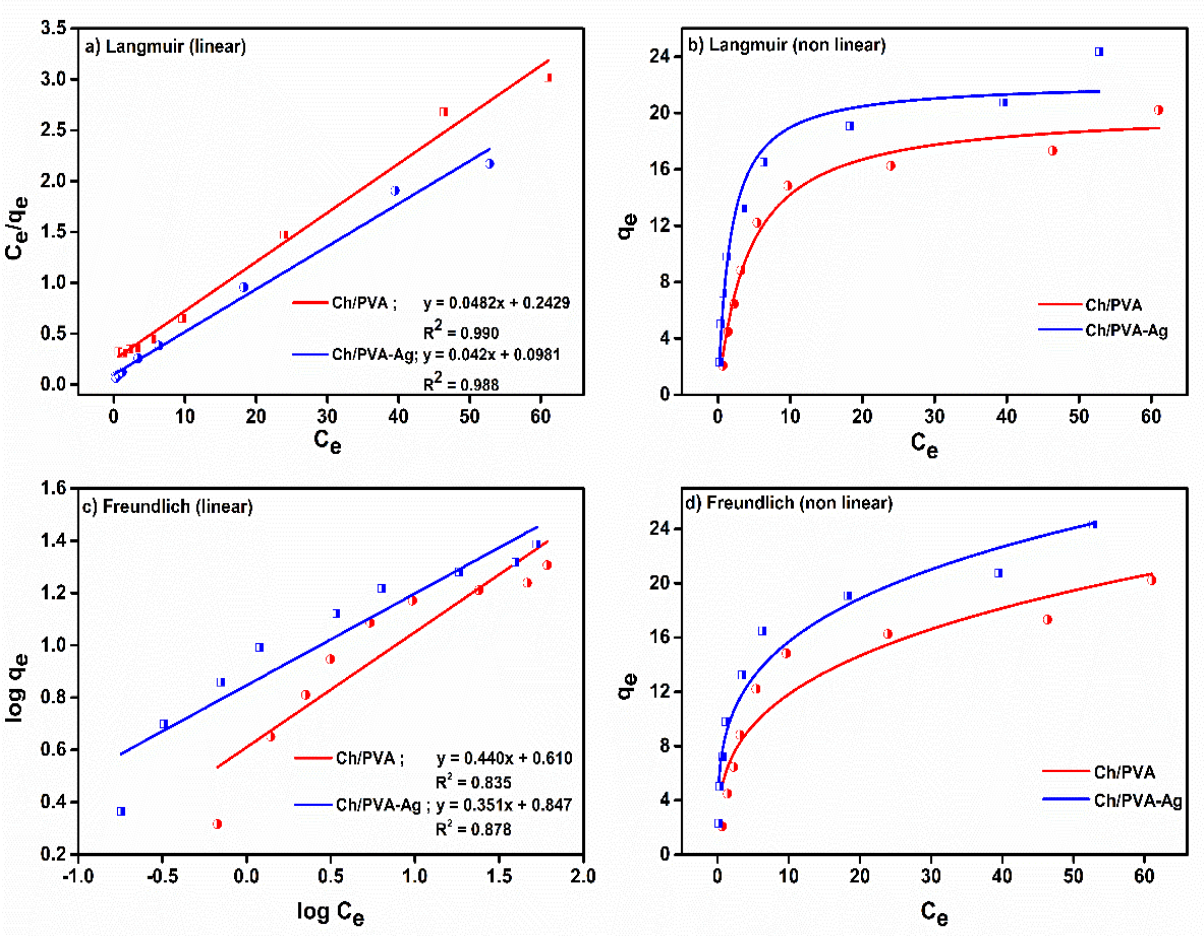


Fig. 4.33: Adsorption isotherms **(a)** Langmuir (linear), **(b)** Langmuir (non-linear), **(c)** Freundlich (linear) and **(d)** Freundlich (non-linear)

Freundlich isotherm

Freundlich isotherm model represents multilayer adsorption mechanism occurring on heterogeneous surfaces, assuming all the active sites on the sorbent are unequal and the stronger binding sites are occupied first. Also, with the increase in degree of site occupation, the binding strength decreases (Dwivedi et al., 2014).

The linearized form of Freundlich model is given as below:

$$\log q_e = \log K_F + \frac{1}{n} \log C_e \qquad (12)$$

Also, freundlich model in nonlinear form can be expressed as:

$$q_e = K_F C_e^{\frac{1}{n}} \qquad (13)$$

where, K_F and n are freundlich constants signifying adsorption capacity and adsorption intensity or surface heterogeneity. The value of n indicates nature of adsorption. Adsorption is poor, relatively difficult or excellent when $n < 1$, $1 < n < 2$ and $2 < n < 10$, respectively.

The use of R^2 (correlation coefficient) alone for data validation is not satisfactory, because experimental data may result in high R^2 values. So, in order to validate isotherm models (linear and nonlinear), five different error functions (Adjusted R-squared – R^2_{adj}, reduced Chi-square - χ^2, Root-mean square error – RMSE and Residual sum of squares – RSS), including R^2 were employed. Higher value of R^2 and R^2_{adj} (close to 1), and smaller value of RSME, χ^2 and RSS indicates higher fit by the model. Table 4.5 shows the isotherm parameters along with error function values obtained using a curve fitting tool origin. It can be clearly seen from the experimental data that the high R^2 and R^2_{adj} values and smaller RSME, χ^2 and RSS values of langmuir isotherm for both Ch/PVA and Ch/PVA-Ag hydrogel indicates good correlation between langmuir model and the experimental data, referring to monolayer adsorption of butachlor. Comparison between linear and nonlinear error functions shows the adsorption favours linear model. Hence, removal of butachlor by Ch/PVA / Ch/PVA-Ag should be investigated using Langmuir linear model, where Ch/PVA and Ch/PVA-Ag give maximum monolayer capacity of 20.75 mg g^{-1} and 23.81 mg g^{-1}, respectively. From the literature survey, we found that similar kind of polymeric sorbent systems follow Langmuir isotherm (Dwivedi et al., 2014; Vilela et al., 2019).

Table 4.5: Adsorption isotherm parameters for butachlor adsorption by Ch/PVA and Ch/PVA-Ag hydrogel

Isotherm model	Isotherm constants **Ch/PVA**							Isotherm constants **Ch/PVA-Ag**						
Langmuir	**q_m (mg g^{-1})**	**K_L (Lmg^{-1})**	**R^2**	**Adj R^2**	**RMSE**	**χ^2**	**RSS**	**q_m (mg g^{-1})**	**K_L (Lmg^{-1})**	**R^2**	**Adj R^2**	**RMSE**	**χ^2**	**RSS**
linear	20.75	0.198	0.991	0.989	0.109	0.012	0.083	23.81	0.428	0.989	0.988	0.09	0.008	0.056
Nonlinear	20.25	0.235	0.979	0.976	0.961	0.923	6.46	22.23	0.582	0.964	0.959	1.532	2.347	16.43
Freundlich	**n**	**K_f (Lmg^{-1})**	**R^2**	**Adj R^2**	**RMSE**	**χ^2**	**RSS**	**n**	**K_f (Lmg^{-1})**	**R^2**	**Adj R^2**	**RMSE**	**χ^2**	**RSS**
linear	2.27	4.07	0.856	0.835	0.132	0.017	0.123	2.85	7.03	0.894	0.878	0.117	0.014	0.095
Nonlinear	3.23	5.79	0.893	0.877	2.197	4.829	33.80	3.76	8.51	0.946	0.938	1.887	3.559	24.915

4.4.2 Photocatalytic degradation and kinetic studies

Photodegradation capability of Ch/PVA-Ag nanocomposite was investigated by the degradation of butachlor under UV light. Fig. 4.34 shows adsorption-coupled-photocatalysis and the UV-Vis absorption spectra of butachlor (10 mg L^{-1}) with 100 mg Ch/PVA-Ag under continuous exposure to UV light, at different time intervals.

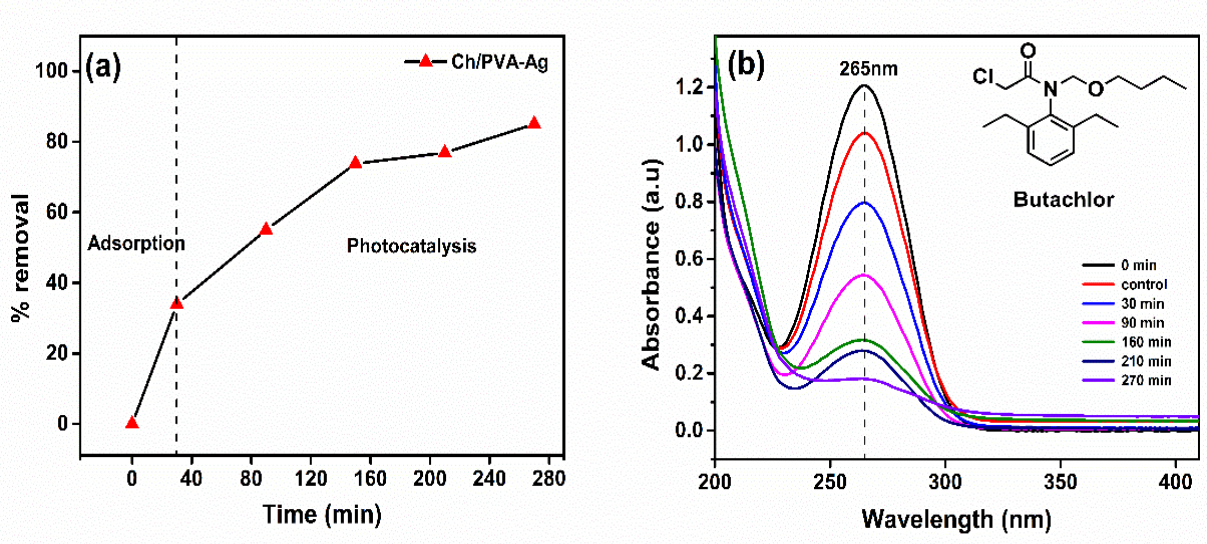


Fig. 4.34: (a) Adsorption coupled photocatalysis of butachlor, **(b)** UV-Vis spectra showing butachlor degradation

With increase in illumination time, the absorption maxima (265nm) gradually decreases and 85% of degradation is observed after 270 min. Approximately, 33.97% of butachlor was adsorbed by hydrogel prior to exposure to UV-light, facilitating faster degradation, as adsorbed molecules are prone to faster attack by free radicals. A control devoid of nanocomposite, kept under same conditions did not show significant decrease in absorption maxima. In previous studies, several nanoparticles such as zero valent iron (Fe^0), (TiO_2) and Zinc oxide (ZnO) were utilized for butachlor degradation in the presence of sunlight or UV-irradiation. Fe^0 could effectively degrade 90% of 20 mg L^{-1} butachlor (Macet EC 58.5%) in 24 h (Kim et al., 2006). Nozhat et al. (2018) studied butachlor degradation (10 mg L^{-1}) with UV-irradiation, where 97.6% and 100% removal efficiency were achieved with 1.4 g L^{-1} TiO_2 and 0.2 g L^{-1} ZnO.

Fig. 4.35 (a-d) shows the four different kinetic models evaluated to understand degradation of butachlor and its mechanism (Kaur and Goyal, 2020). Respective equations with their corresponding rate constant (k) and correlation coefficient (R^2) are presented in Table 4.6. The kinetic models are expressed by the following equations:

First order: $\ln C = \ln C_0 - kt$ (14)

Pseudo-first order: $\ln [C_0 - C] = \ln C - kt$ (15)

Second order: $$\frac{1}{C} = \frac{1}{C_0} + kt$$ (16)

Pseudo-second order: $$\frac{t}{C} = \frac{t}{C_0} + \frac{1}{kC_0^2}$$ (17)

where, C is butachlor concentration at time t, C_0 is the initial butachlor concentration at time zero and k is the kinetic rate constant.

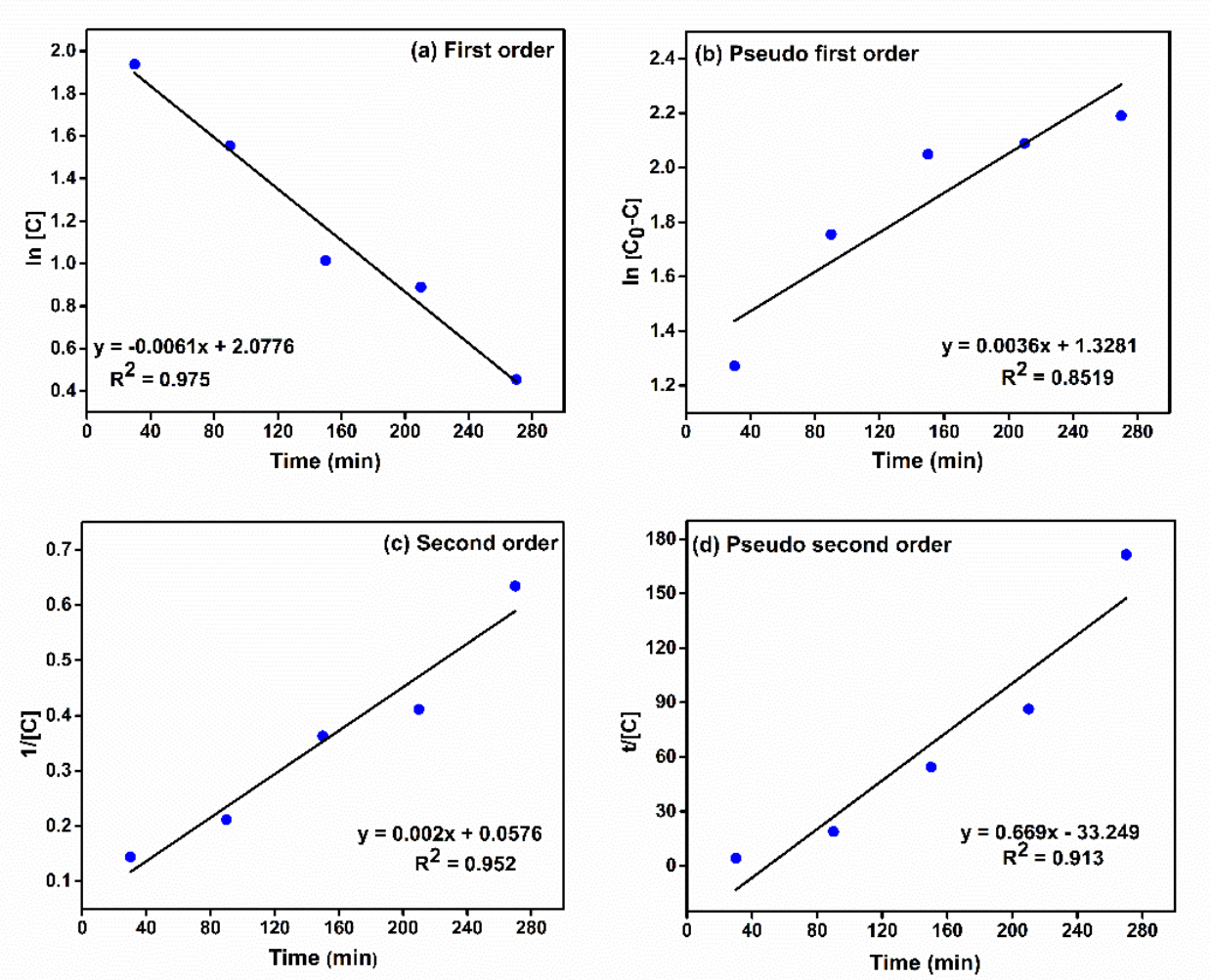


Fig. 4.35: Degradation kinetics **(a)** first order kinetics, **(b)** pseudo-first order kinetics, **(c)** second order kinetics and **(d)** pseudo-second order kinetics

Table 4.6: Kinetic models of photocatalytic degradation of butachlor by silver immobilized Ch/PVA-Ag hydrogel

Kinetic Models	Equation	Rate Constant (k)	R^2 values
First order	$\ln C = \ln C_0 - kt$	6.05×10^{-3} min^{-1}	0.975
Pseudo-first order	$\ln [C_0 - C] = \ln C - kt$	3.6×10^{-3} min^{-1}	0.852
Second order	$1/C = 1/C_0 + kt$	1.9×10^{-3} mg L^{-1} min^{-1}	0.952
Pseudo-second order	$t/C = t/C_0 + 1/kC_0^2$	66.90×10^{-2} mg L^{-1} min^{-1}	0.913

The fitted linear regression plot showed that the butachlor degradation data was best fitted to first order kinetic model with highest R^2 value of 0.975, suggesting the rate of reaction is proportional to substrate depletion. Similar first order kinetics model was reported by PushpaMalini et al. (2018), where 20 µg mL^{-1} butachlor in ground water was completely degraded by 0.5 g L^{-1} TiO_2 (Degussa P-25) in 30 h at 40 °C.

4.4.2.1 Degradation pathway

Degradation using a UV-light source is based on the principle of photo-excitation of the catalyst due to the absorption of electromagnetic radiation and involves the action of hydroxyl radicals, superoxide radicals and holes generated due to excitation of electrons (Wu et al., 2020). As shown in Fig. 4.37 (b), when irradiated with the UV-light, electrons from the valence band (VB) of AgNPs present in the nanocomposite are excited to its conduction band (CB), generating holes in the VB. These photogenerated electrons react with O_2 to form $\bullet O_2^-$, which is capable enough to degrade any contaminant to stable products. Also, the holes generated after electron excitation can directly cause degradation or oxidize surface water or hydroxide ion forming hydroxyl radical (•OH), a strong oxidant, which further reacts with butachlor causing its photodegradation. Following equations describe the degradation of butachlor using free radical mechanism (Kaur and Goyal, 2019).

$$AgNP + h\nu \rightarrow AgNP\ (e_{cb}^- + h_{vb}^+) \quad (18)$$

$$AgNP\ (h_{vb}^+) + H_2O \rightarrow AgNP + \bullet OH + H^+ \quad (19)$$

$$AgNP\ (h_{vb}^+) + OH^- \rightarrow AgNP + \bullet OH \quad (20)$$

$$AgNP(e_{cb}^-) + O_2 \rightarrow AgNP + \bullet O_2^- \quad (21)$$

$$\bullet O_2^- + H^+ \rightarrow HO_2\bullet \quad (22)$$

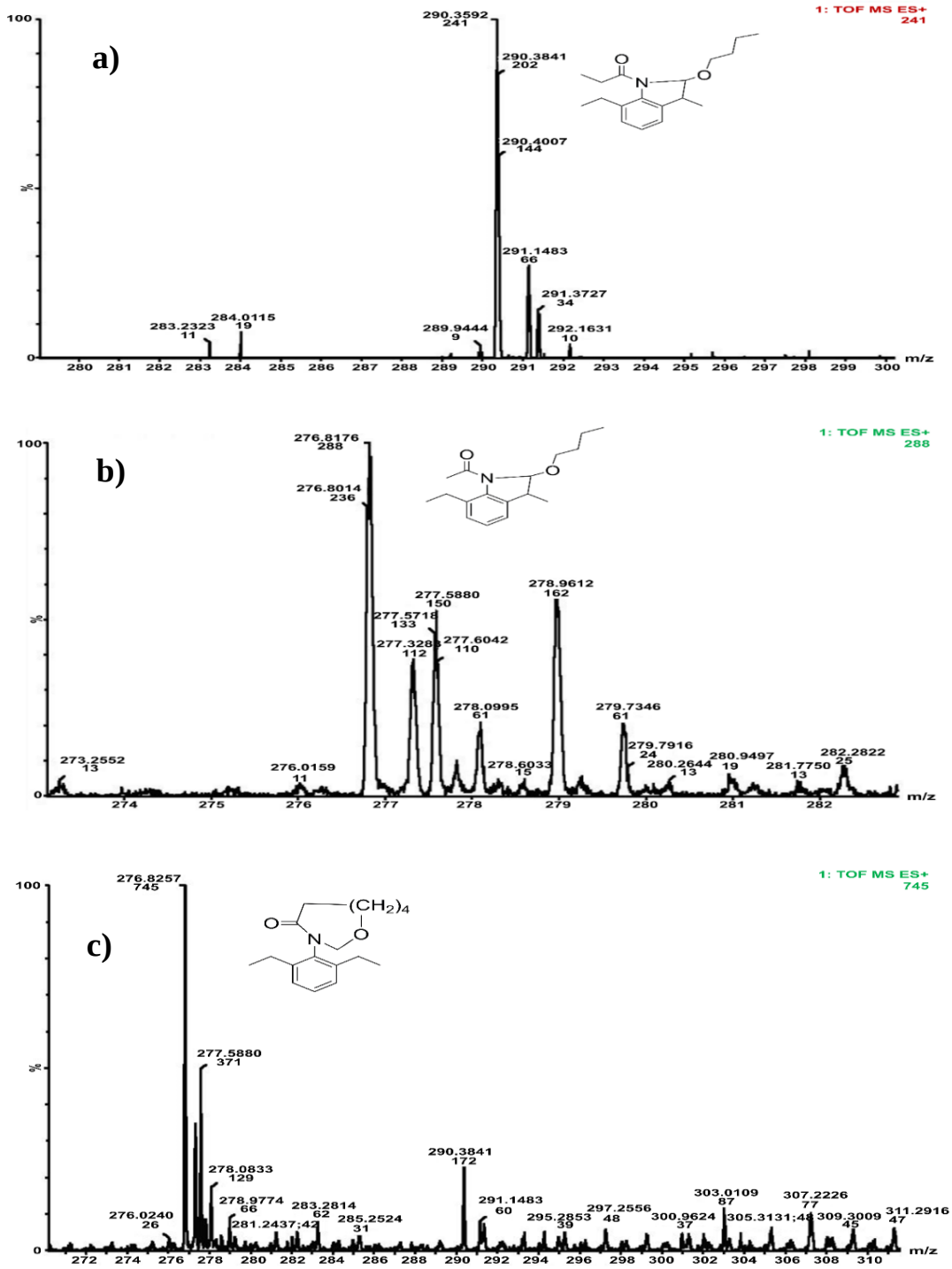
$$\bullet O_2^- + HO_2\bullet \rightarrow \bullet OH + O_2 + H_2O_2 \quad (23)$$

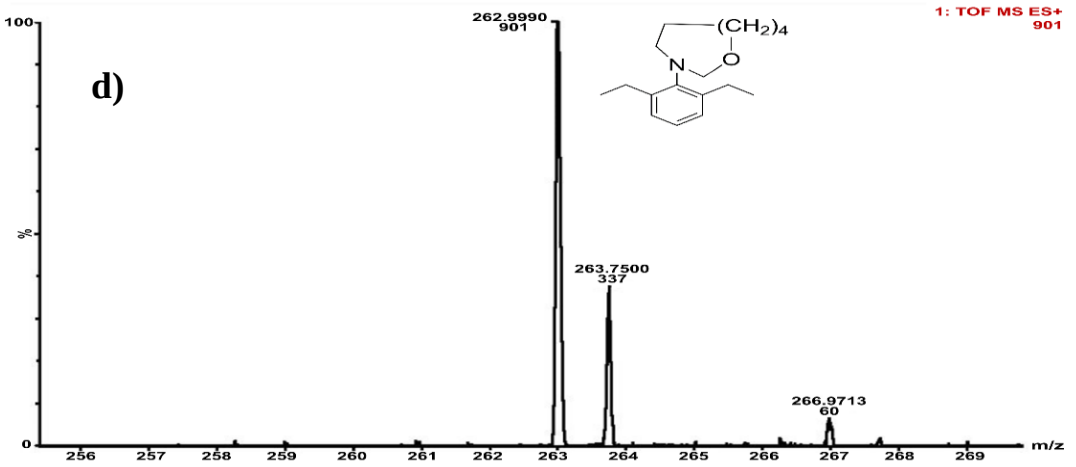
$$2HO_2\bullet \rightarrow O_2 + H_2O_2 \quad (24)$$

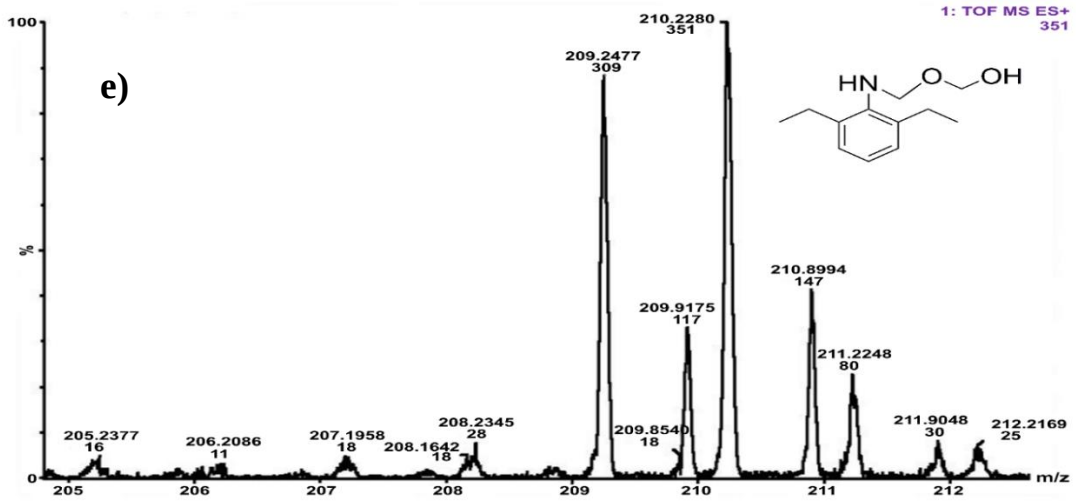
$$AgNP(e^-_{cb}) + H_2O_2 \rightarrow AgNP + OH^- + \bullet OH \quad (24)$$

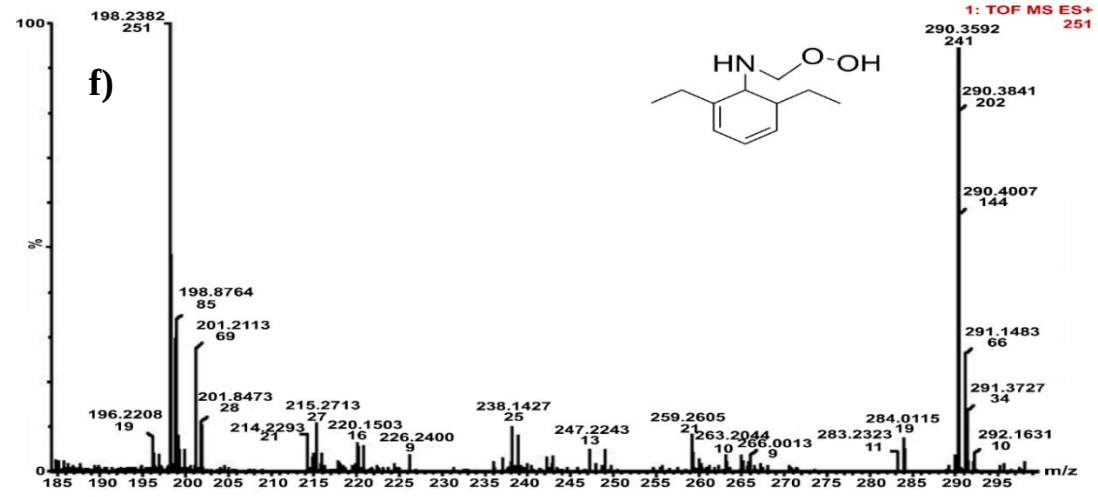
$$\bullet OH + \text{Butachlor} \rightarrow \text{intermediate metabolites} \rightarrow\rightarrow CO_2 + H_2O + Cl^- \quad (26)$$

In order to study the photocatalytic degradation and mineralization of the pollutant butachlor, the samples were subjected to LC-ESI-Q-TOF-MS analysis at different time intervals. The LC-MS chromatograms of the samples extracted at different time intervals confirm the presence of 8 major intermediates (Fig. 4.36).




d)
1: TOF MS ES+
901
262.9990
901
263.7500
337
266.9713
60
(CH2)4
N
O
100
%
0
256 257 258 259 260 261 262 263 264 265 266 267 268 269
m/z


e)
1: TOF MS ES+
351
210.2280
351
209.2477
309
209.9175
117
210.8994
147
211.2248
80
205.2377
16
206.2086
11
207.1958
18
208.1642
18
208.2345
28
209.8540
18
211.9048
30
212.2169
25
HN
O
OH
100
%
0
205 206 207 208 209 210 211 212
m/z


f)
1: TOF MS ES+
251
198.2382
251
290.3592
241
290.3841
202
290.4007
144
198.8764
85
201.2113
69
291.1483
66
291.3727
34
292.1631
10
196.2208
19
201.8473
28
214.2293
21
215.2713
27
220.1503
16
226.2400
9
238.1427
25
247.2243
13
259.2605
21
263.2044
10
266.0013
9
283.2323
11
284.0115
19
HN
O
OH
100
%
0
185 190 195 200 205 210 215 220 225 230 235 240 245 250 255 260 265 270 275 280 285 290 295
m/z

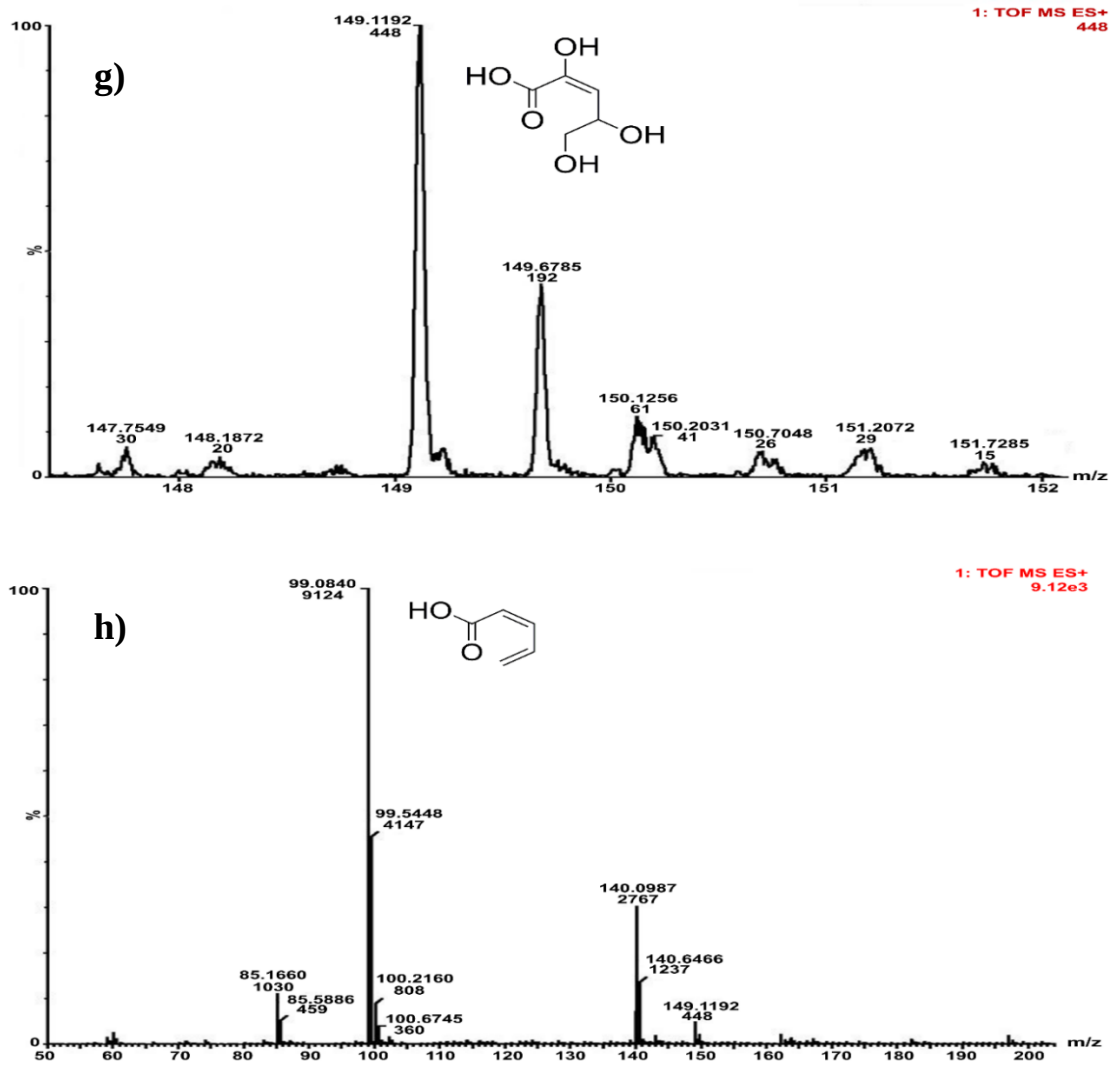
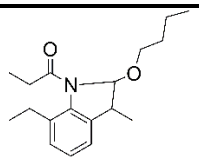
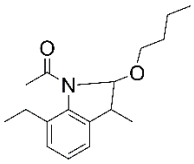
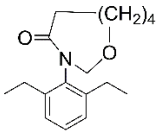
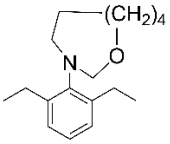
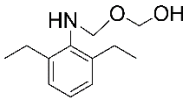
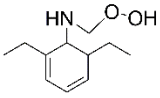
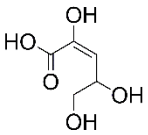
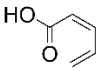


Fig. 4.36: LC-MS mass spectra of eight major metabolites **a)** ((1-(2-butoxy-7-ethyl-3-methylindolin-1-yl)propan-1-one, **b)** 1-(2-butoxy-7-ethyl-3-methylindolin-1-yl)ethenone, **c)** 3-(2,6-diethylphenyl)-1,3-oxazonan-4-one, **d)** 3-(2,6-diethylphenyl)-1,3-oxazonane, **e)** (((2,6-diethylphenyl)amino)methoxy)methanol, **f)** 2,6-diethyl-N-(hydroperoxymethyl) cyclohexa-2,4-dienamine, **g)** (E)-2,4,5-trihydroxypent-2-enoic acid and **h)** (Z)-penta-2,4-dienoic acid)

The resultant intermediates obtained along with the m/z ratio, elemental composition and proposed structure are presented in Table 4.7.

Table 4.7: Structures of butachlor intermediates detected by LC-ESI-Q-TOF-MS.

S.No.	m/z $[M+H]^+$	Elemental composition and name	Predicted structure
1.	290	$C_{18}H_{27}NO_2$ (1-(2-butoxy-7-ethyl-3-methylindolin-1-yl)propan-1-one	
2.	276	$C_{17}H_{25}NO_2$ 1-(2-butoxy-7-ethyl-3-methylindolin-1-yl)ethanone	
3.	276	$C_{17}H_{25}NO_2$ 3-(2,6-diethylphenyl)-1,3-oxazonan-4-one	
4.	262	$C_{17}H_{27}NO$ 3-(2,6-diethylphenyl)-1,3-oxazonane	
5.	210	$C_{12}H_{19}NO_2$ (((2,6-diethylphenyl)amino)methoxy)methanol	
6.	198	$C_{11}H_{19}NO_2$ 2,6-diethyl-N-(hydroperoxymethyl)cyclohexa-2,4-dienamine	
7.	149	$C_5H_8O_5$ (E)-2,4,5-trihydroxypent-2-enoic acid	
8.	99	$C_5H_6O_2$ (Z)-penta-2,4-dienoic acid	

Based on the identified metabolites, a plausible degradation scheme is presented in Fig. 4.37. Degradation begins with dechlorination reaction, where •OH radical attacks chlorine atom, resulting in the formation of 1-(2-butoxy-7-ethyl-3-methylindolin-1-yl)propan-1-one and 3-(2,6-diethylphenyl)-1,3-oxazonan-4-one with m/z 289 and 275. Kim et al. (2006) reported dehalogenation as one of the major mechanisms behind butachlor degradation. Subsequent removal of methyl group and hydroxylation reactions lead to the formation of aliphatic compound (E)-2,4,5-trihydroxypent-2-enoic acid with m/z 148, further breaking down into (Z)-penta-2,4-dienoic acid (m/z 98). Finally, oxidation of aliphatic compounds to CO_2 and H_2O lead to complete mineralization of butachlor.

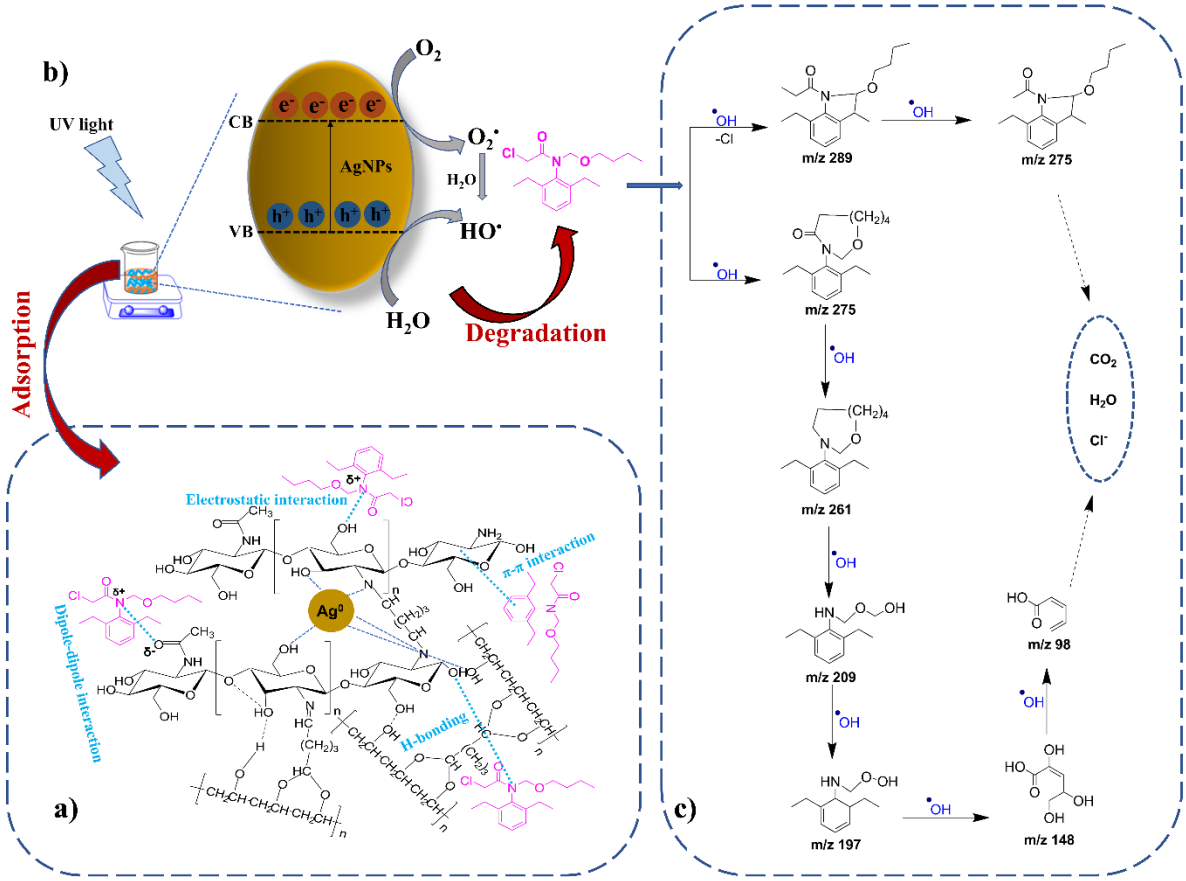


Fig. 4. 37: UV- induced degradation of butachlor by Ch/PVA-Ag hydrogel

4.4.2.2 Reusability

The reusability of the hydrogel was studied for three consecutive cycles/runs with 10 mg L^{-1} butachlor and 100 mg hydrogel (2 g L^{-1}). The photodegradation capacity (reusability) of the nanocomposite dropped from 85% to 73 % after 3 cycles of testing, where the degradation percentages for every run was about 85 % (Run 1), 81.23% (Run 2) and 73% (Run 3) respectively (Fig. 4.38). The nanocomposite exhibited great stability and could be reused again for butachlor degradation.

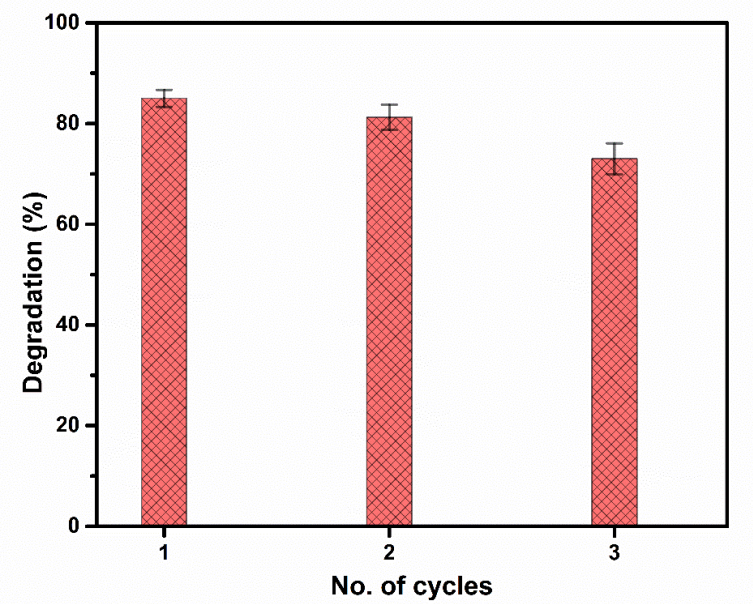


Fig. 4.38: Reusability of the Ch/PVA-Ag hydrogel

Summary

Among fifteen bacterial isolates used for monocrotophos degradation, *Bacillus licheniformis* BPRIST030 (NA14) degraded about 70% monocrotophos in 5 days (120 h) with an increase in viable cell count from 5.9 to 13.73 log cfu mL^{-1} and OD_{600nm} from 0.014 ± 0.004 to 0.864 ± 0.020. The isolate could tolerate 500 mg L^{-1} monocrotophos. GC-MS analysis gave five major metabolites (dimethyl phosphate, phosphoric acid, malonic acid, dihydrazide, *N*-3-dimethylbut-2-enamide and *N*-methyl acetoacetamide) and degradation pathway was proposed.

Butachlor degrading bacterial strain A16 was isolated from coal tar contaminated soil, which showed 99.38% similarity with *Bacillus altitudinis* 41KF2b^T as revealed by 16S rRNA analysis. *B. altitudinis* strain A16 utilised butachlor as a sole source of carbon and degraded 90% of 50 mg L^{-1} butachlor in 5 days at a rate constant and half-life ($t_{1/2}$) of 0.02 h^{-1} and 34.65 h, respectively, following the first-order reaction kinetics. Five metabolites (*N*-(butoxymethyl)-*N*-(2-chloroethyl)-2,6-diethylaniline, (*N*-(butoxymethyl)-2-chloro-*N*-(2-ethylphenyl) acetamide, *N*-(butoxymethyl)-2,6-diethyl-*N*-propylaniline, 2-chloro-*N*-(2,6-diethylphenyl) acetamide and 2,6-diethylaniline) were produced during the breakdown of butachlor by *B. altitudinis* A16 as identified by GC-MS analysis, which are further mineralized to carbon dioxide and water. A metabolic pathway is proposed and compared with other bacteria.

Silver nanoparticle (AgNP) incorporated chitosan-PVA (Ch/PVA) hydrogel nanocomposite was fabricated by repeated freeze-thaw treatment using glutaraldehyde as crosslinker for removal of herbicide butachlor from aqueous solution. Ch/PVA hydrogel acted as a nanoreactor in providing a matrix for *in-situ* immobilization of AgNPs and was characterized by FTIR, SEM-EDS, TEM, ICP-AES, XRD, XPS, TDA-DSC and BET analysis. Incorporation of AgNPs led to increase in thermal stability and surface area and possessed crystalline structure with a size of about 5-20 nm. Effect of adsorption parameters such as pH, butachlor concentration, sorbent dosage, temperature and contact time on removal of butachlor was investigated. Comparative adsorption capacity of Ch/PVA hydrogel showed a maximum adsorption of 86.55%, while Ch/PVA-Ag showed an increased adsorption of about 96.87%. Linear and non-linear forms of Langmuir and Freundlich models with different error functions (R^2, R^2_{adj}, RSME, χ^2 and RSS) confirmed monolayer adsorption of butachlor, favouring linear Langmuir model.

The study also reveals the impact of Ch/PVA hydrogel with *in-situ* synthesized AgNPs on degradation of herbicide butachlor under UV irradiation. Ch/PVA-Ag nanocomposite was employed for adsorption-coupled-photocatalytic removal of butachlor proved to be a promising photocatalyst, degrading 85% of 10 mg L^{-1} butachlor in the presence of UV-light following first order kinetic model with a half-life of 114.54 min. Activity of nanocomposite hydrogel was due to synergism effect taking place between biopolymer nanocomposite hydrogel part acting as adsorbent and AgNPs as photocatalyst. Based on eight major metabolites ((1-(2-butoxy-7-ethyl-3-methylindolin-1-yl)propan-1-one, 1-(2-butoxy-7-ethyl-3-methylindolin-1-yl)ethenone, 3-(2,6-diethylphenyl)-1,3-oxazonan-4-one, 3-(2,6-diethylphenyl)-1,3-oxazonane, (((2,6-diethylphenyl)amino)methoxy)methanol, 2,6-diethyl-N-(hydroperoxymethyl)cyclohexa-2,4-dienamine, (E)-2,4,5-trihydroxypent-2-enoic acid and (Z)-penta-2,4-dienoic acid) obtained from LC-ESI-Q-TOF-MS analysis, a plausible degradation pathway was proposed. Reusability of nanocomposite and break-down of butachlor with no release of Ag ions in the solution makes it highly suitable for photocatalytic degradation of pesticides.

Comparing both the techniques used for butachlor removal, biodegradation is slower yet cost effective, whereas, hydrogel-based removal of butachlor is much faster and expensive in comparison to bacterial setup. Bacteria directly utilize the pesticides and use them as sole carbon source, so no further contamination is caused. They can be directly applied to soil for remediation of pollutants. Nano hydrogel is equally effective as no further contamination with the nanoparticles is caused, since they are immobilized within the hydrogel, but their degradation in the soil is time consuming. Hence, nanocomposites are the best for degradation of contaminants from liquid samples.

Future scope of the work

Since only 0.1% of the total pesticide applied reaches their target and the rest remains in the soil. Therefore, repetitive application of pesticides leads to their accumulation in soil, worsening the soil quality, contaminating ground water and entering the food chain affecting all living systems. Bacterial isolates *Bacillus licheniformis* BPRIST030 and *Bacillus altitudinis* A16 being potential biodegraders of monocrotophos and butachlor respectively, can also be employed for degradation of other organophosphorus and chloroacetanilide pesticides. These bacteria can be used for faster bioremediation of pesticides in soils where their bioavailability is low by mass culturing and soil inoculation, therefore, minimizing negative impact of pesticides on health and environment. The Ch/PVA-Ag nanocomposite can be also be effectively used for the remediation/clean-up of groundwater and agricultural run-off water which is contaminated with harmful pesticides and agro-chemicals. Apart from this, mutagenesis study will be conducted to confirm the proposed metabolic pathways.

Salient Findings

1. *Bacillus licheniformis* BPRIST030 (NA14) degraded about 70% monocrotophos in 5 days (120 h) with an increase in viable cell count from 5.9 to 13.73 log cfu mL^{-1} and OD_{600nm} from 0.014 ± 0.004 to 0.864 ± 0.020.
2. Five major metabolites (dimethyl phosphate, phosphoric acid, malonic acid, dihydrazide, *N*-3-dimethylbut-2-enamide and *N*-methyl acetoacetamide) were obtained from GC-MS analysis and degradation pathway was proposed.
3. Out of 15 bacterial isolates studied, *Bacillus altitudinis* A16 showed maximum degradation of butachlor in 5 days. Phylogenetic analysis revealed A16 showed maximum similarity (99.38%) with *Bacillus altitudinis* 41KF2b^{T}.
4. *B. altitudinis* A16 utilized butachlor as a sole source of carbon and degraded 90% of 50 mg L^{-1} butachlor in 5 days at a rate constant and half-life ($t_{1/2}$) of 0.02 h-1 and 34.65 h, respectively, following the first-order reaction kinetics.
5. Five major metabolites ((*N*-(butoxymethyl)-*N*-(2-chloroethyl)-2,6-diethylaniline, (*N*-(butoxymethyl)-2-chloro-*N*-(2-ethylphenyl) acetamide, *N*-(butoxymethyl)-2,6-diethyl-*N*-propylaniline, 2-chloro-*N*-(2,6-diethylphenyl) acetamide and 2,6-diethylaniline)) produced during butachlor degradation by *B. altitudinis* A16 were confirmed by GC-MS analysis.
6. The synthesized Ch/PVA hydrogel behaved as a nanoreactor and immobilizing matrix for silver nanoparticles and was characterized by FTIR, DRS, SEM-EDS, FE-SEM, TEM, ICP-AES, DLS, XRD, XPS, TGA-DSC and BET analysis.
7. Ch/PVA hydrogel showed a maximum butachlor adsorption of about 86.55% while Ch/PVA-Ag showed an increased adsorption rate of about 96.87 %, where both the hydrogels followed Langmuir isotherm model, confirming monolayer adsorption.
8. Ch/PVA-Ag hydrogel also proved to be a promising photocatalyst and degraded 85% of 10 mg L^{-1} butachlor in the presence of UV-light following first order kinetic model with a half-life of 114.54 min.
9. A plausible degradation pathway for butachlor degradation in the presence of UV-light was proposed based on 8 major intermediates obtained by LC-ESI-Q-TOF-MS analysis.
10. The photodegradation capacity (reusability) of the nanocomposite dropped from 85% to 73 % after 3 cycles of testing.

References

1). Abd-Alrahman, S. H., Salem-Bekhit, M. M. (2013). Microbial biodegradation of butachlor pollution (obsolete pesticide Machete 60% EC). *African Journal of Microbiology Research*, *7*(4), 330-335. https://doi.org/10.5897/AJMR12.1605

2). Abigail, M. E. A., Samuel, S. M., Ramalingam, C. (2015). Addressing the environmental impacts of butachlor and the available remediation strategies: a systematic review. *International journal of environmental science and technology*, *12*(12), 4025-4036. https://doi.org/10.1007/s13762-015-0866-2

3). Abraham, J., Mukherjee, P., Bose, D., Dutta, A. (2016). Utilization of monocrotophos by *Aspergillus sojae* strain JPDA1 isolated from sugarcane fields of Vellore district in India. *Research Journal of Pharmacy and Technology*, *9*(12), 2155-2160. https://doi.org/10.5958/0974-360X.2016.00437.6

4). Abraham, J., Silambarasan, S. (2015). Bacterial degradation of monocrotophos and phyto-and cyto-toxicological evaluation of metabolites. *Toxicological & Environmental Chemistry*, *97*(9), 1202-1216. https://doi.org/10.1080/02772248.2015.1092541

5). Abraham, J., Silambarasan, S., Logeswari, P. (2014). Simultaneous degradation of organophosphorus and organochlorine pesticides by bacterial consortium. *Journal of the Taiwan Institute of Chemical Engineers*, *45*(5), 2590-2596. https://doi.org/10.1016/j.jtice.2014.06.014

6). Acharya, K. P., Shilpkar, P., Shah, M. C., Chellapandi, P. (2015). Biodegradation of insecticide monocrotophos by *Bacillus subtilis* KPA-1, isolated from agriculture soils. *Applied biochemistry and biotechnology*, *175*(4), 1789-1804. https://doi.org/10.1007/s12010-014-1401-5

7). Agnihotri, N. P., Pandey, S. Y., Jain, H. K., Srivastava, K. P. (1981). Persistence, leaching and movement of chlorfenvinphos, chlorpyriphos, disulfoton, fensulfothion, monocroiophos and tetrachlorvinphos in soil. *Indian Journal of Agricultural Chemistry (India)*. *14*, 27-31.

8). Agnihotri, S., Mukherji, S., Mukherji, S. (2012). Antimicrobial chitosan–PVA hydrogel as a nanoreactor and immobilizing matrix for silver nanoparticles. *Applied Nanoscience*, *2*(3), 179-188. https://doi.org/10.1007/s13204-012-0080-1

9). Agnihotri, S., Sillu, D., Sharma, G., Arya, R. K. (2018). Photocatalytic and antibacterial potential of silver nanoparticles derived from pineapple waste: process optimization and modeling kinetics for dye removal. *Applied Nanoscience*, *8*(8), 2077-2092. https://doi.org/10.1007/s13204-018-0883-9

10). Agrahari, S., Pandey, K. C., Gopal, K. (2007). Biochemical alteration induced by monocrotophos in the blood plasma of fish, *Channa punctatus* (Bloch). *Pesticide Biochemistry and Physiology*, *88*(3), 268-272. https://doi.org/10.1016/j.pestbp.2007.01.001

11). Agrawal, A., Pandey, R.S., Sharma, B. (2010). Water Pollution with Special Reference to Pesticide Contamination in India. *Journal of Water Resource and Protection, 2(5),* 432-448. https://doi.org/10.4236/jwarp.2010.25050

12). Agrawal, C., Sen, S., Singh, S., Rai, S., Singh, P. K., Singh, V. K., Rai, L. C. (2014). Comparative proteomics reveals association of early accumulated proteins in conferring butachlor tolerance in three N_2-fixing *Anabaena* spp. *Journal of proteomics, 96,* 271-290. https://doi.org/10.1016/j.jprot.2013.11.015

13). Agrawal, C., Sen, S., Yadav, S., Rai, S., Rai, L. C. (2015). A novel aldo-keto reductase (AKR17A1) of *Anabaena* sp. PCC 7120 degrades the rice field herbicide butachlor and confers tolerance to abiotic stresses in *E. coli*. *PloS one, 10*(9), e0137744. https://doi.org/10.1371/journal.pone.0137744

14). Ahmad, M. A., Alrozi, R. (2010). Optimization of preparation conditions for mangosteen peel-based activated carbons for the removal of Remazol Brilliant Blue R using response surface methodology. *Chemical Engineering Journal, 165*(3), 883-890. https://doi.org/10.1016/j.cej.2010.10.049

15). Ahmad, M. A., Alrozi, R. (2011). Optimization of rambutan peel based activated carbon preparation conditions for Remazol Brilliant Blue R removal. *Chemical Engineering Journal, 168*(1), 280-285. https://doi.org/10.1016/j.cej.2011.01.005

16). Ahmad, S., Munir, S., Zeb, N., Ullah, A., Khan, B., Ali, J., Bilal, M., Omer, M., Alamzeb, M., Salman, S.M., Ali, S. (2019). Green nanotechnology: a review on green synthesis of silver nanoparticles—an ecofriendly approach. *International journal of nanomedicine, 14,* 5087. https://doi.org/ 10.2147/IJN.S200254

17). Ali, I., Alharbi, O. M., ALOthman, Z. A., Al-Mohaimeed, A. M., Alwarthan, A. (2019). Modeling of fenuron pesticide adsorption on CNTs for mechanistic insight and removal in water. *Environmental research, 170,* 389-397. https://doi.org/10.1016/j.envres.2018.12.066

18). Alla, M. N., Badawi, A. M., Hassan, N. M., El-Bastawisy, Z. M., Badran, E. G. (2008). Effect of metribuzin, butachlor and chlorimuron-ethyl on amino acid and protein formation in wheat and maize seedlings. *Pesticide Biochemistry and Physiology, 90*(1), 8-18. https://doi.org/10.1016/j.pestbp.2007.07.003

19). Amalraj, A., Pius, A. (2015). Photocatalytic degradation of monocrotophos and chlorpyrifos in aqueous solution using TiO_2 under UV radiation. *Journal of Water Process Engineering, 7,* 94-101. https://doi.org/10.1016/j.jwpe.2015.06.002

20). An, J., Luo, Q., Yuan, X., Wang, D., Li, X. (2011). Preparation and characterization of silver-chitosan nanocomposite particles with antimicrobial activity. *Journal of Applied Polymer Science, 120*(6), 3180-3189. https://doi.org/10.1002/app.33532

21). Anbumani S, Mohankumar M. N. (2015) Cytogenotoxicity assessment of monocrotophos and butachlor at single and combined chronic exposures in the fish *Catla catla* (Hamilton). Environ Sci Pollut R 22(7):4964-4976. https://doi.org/10.1007/s11356-014-3782-y

22). Anees, S., Suhail, S., Pathak, N., Zeeshan, M. (2014). Potential use of rice field cyanobacterium *Nostoc muscorum* in the evaluation of butachlor induced toxicity and their degradation. *Bioinformation*, *10*(6), 365-370. https://doi.org/10.6026/97320630010365

23). Anitha, S., Das, S. S. M. (2011). Mycoremediation of Monocrotophos. *International Journal of Pharma and Bio Sciences*, *2*(1), 342.

24). Arjunan, N., Kumari, H. L. J., Singaravelu, C. M., Kandasamy, R., Kandasamy, J. (2016). Physicochemical investigations of biogenic chitosan-silver nanocomposite as antimicrobial and anticancer agent. *International journal of biological macromolecules*, *92*, 77-87. https://doi.org/10.1016/j.ijbiomac.2016.07.003

25). Arora, S. (2009). Analysis of insecticides in okra and brinjal from IPM and non-IPM fields. *Environmental monitoring and assessment*, *151*(1-4), 311-315. https://doi.org/10.1007/s10661-008-0272-z

26). Asi, M. R. (2003). Solid-phase extraction and chromatographic determination of pesticides in food and water samples. Dissertation, Institutue of Chemistry University of the Punjab Lahore, Pakistan

27). Ateeq, B., Farah, M. A., Ahmad, W. (2005). Detection of DNA damage by alkaline single cell gel electrophoresis in 2, 4-dichlorophenoxyacetic-acid-and butachlor-exposed erythrocytes of *Clarias batrachus*. *Ecotoxicology and environmental safety*, *62*(3), 348-354. https://doi.org/10.1016/j.ecoenv.2004.12.011

28). Ayranci, E., Hoda, N. (2005). Adsorption kinetics and isotherms of pesticides onto activated carbon-cloth. *Chemosphere*, *60*, 1600–1607. https://doi.org/10.1016/j.chemosphere.2005.02.040

29). Bai, S., Li, Z., Zang, X., Wang, C., Wang, Z. (2013). Graphene-based magnetic solid phase extraction dispersive liquid-liquid microextraction combined with gas chromatographic method for determination of five acetanilide herbicides in water and green tea samples. *Chinese Journal of Analytical Chemistry*, *41*(8), 1177-1182. https://doi.org/10.1016/S1872-2040(13)60672-6

30). Bala, R., Dhingra, S., Kumar, M., Bansal, K., Mittal, S., Sharma, R. K., Wangoo, N. (2017). Detection of organophosphorus pesticide–malathion in environmental samples using peptide and aptamer based nanoprobes. *Chemical Engineering Journal*, *311*, 111-116. https://doi.org/10.1016/j.cej.2016.11.070

31). Balagurusamy, N. (2005). Anaerobic bioremediation-an untapped potential. *Revista Mexicana de Ingeniería Química*, 4(3), 273-287.

32). Balamurugan, K., Ramakrishnan, M., Senthilkumar, R., Ignacimuthu, S. (2010). Research article Biodegradation of methyl parathion and monochrotophos by *Pseudomonas aeruginosa* and *Trichoderma viridae. Asian Journal of Science and Technology, 6*, 123-126

33). Banu, B. S., Devi, K. D., Mahboob, M., Jamil, K. (2001). In vivo genotoxic effect of zinc sulfate in mouse peripheral blood leukocytes using comet assay. *Drug and chemical toxicology*, *24*(1), 63-73. https://doi.org/10.1081/DCT-100103086

34). Bapat, G., Labade, C., Chaudhari, A., Zinjarde, S. (2016). Silica nanoparticle based techniques for extraction, detection, and degradation of pesticides. *Advances in colloid and interface science*, *237*, 1-14. https://doi.org/10.1016/j.cis.2016.06.001

35). Barathidasan, K., Reetha, D. (2013). Microbial degradation of monocrotophos by *Pseudomonas stutzeri*. *Indian Streams Research Journal*, *3*(5), 1-7.

36). Barman, K. K., Shrivastava, E., Varshney, J. G. (2009). Effect of butachlor on total microbial activity, Azotobacter and phosphate solubilizing fungal population. *Indian J Weed Sci*, *41*, 27-31.

37). Bauer, A. W., Kirby, W. M. M., Sherris, J. C., Turck, M. (1966). Antibiotic susceptibility testing by a standardized single disk method. *American Journal of Clinical Pathology*, 45(4), 493-6. https://doi.org/10.1093/ajcp/45.4_ts.493

38). Beynon, K. I., Hutson, D. H., Wright, A. N. (1973). The metabolism and degradation of vinyl phosphate insecticides. *Residue Rev*, *47*, 55-142. Springer, New York, NY. https://doi.org/10.1007/978-1-4615-8488-9_2

39). Bhadbhade, B. J., Dhakephalkar, P. K., Sarnaik, S. S., Kanekar, P. P. (2002a). Plasmid-associated biodegradation of an organophosphorus pesticide, monocrotophos, by *Pseudomonas mendocina*. *Biotechnology letters*, *24*(8), 647-650. https://doi.org/10.1023/A:1015099409563

40). Bhadbhade, B. J., Sarnaik, S. S., Kanekar, P. P. (2002b). Biomineralization of an organophosphorus pesticide, Monocrotophos, by soil bacteria. *Journal of applied microbiology*, *93*(2), 224-234. https://doi.org/10.1046/j.1365-2672.2002.01680.x

41). Bhadbhade, B. J., Sarnaik, S. S., Kanekar, P. P. (2002c). Bioremediation of an industrial effluent containing monocrotophos. *Current microbiology*, *45*(5), 346-349. https://doi.org/10.1007/s00284-002-3681-1

42). Bhalerao, T. S., Puranik, P. R. (2009). Microbial degradation of monocrotophos by *Aspergillus oryzae*. *International Biodeterioration & Biodegradation*, *63*(4), 503-508. https://doi.org/10.1016/j.ibiod.2008.11.011

43). Bhushan, C., Bhardwaj, A., Misra, S. S. (2013). State of pesticide regulations in India. *Centre for Science and Environment, New Delhi*, 1-72.

44). Bielska, D., Karewicz, A., Lachowicz, T., Berent, K., Szczubiałka, K., Nowakowska, M. (2015). Hybrid photosensitizer based on halloysite nanotubes for phenol-based pesticide photodegradation. *Chemical Engineering Journal*, *262*, 125-132. https://doi.org/10.1016/j.cej.2014.09.081

45). Binukumari, S., Devi, K. A., Vasanthi, J. (2016). Applications in environmental risk assessment of biochemical analysis on the Indian fresh water fish, *Labeo rohita* exposed

to monocrotophos pesticide. *Environmental Toxicology and Pharmacology*, *47*, 200-205. https://doi.org/10.1016/j.etap.2016.08.014

46). Boruah, P. K., Sharma, B., Hussain, N., Das, M. R. (2017). Magnetically recoverable Fe_3O_4/graphene nanocomposite towards efficient removal of triazine pesticides from aqueous solution: investigation of the adsorption phenomenon and specific ion effect. *Chemosphere*, *168*, 1058-1067. https://doi.org/10.1016/j.chemosphere.2016.10.103

47). Brouers, F., Al-Musawi, T. J. (2015). On the optimal use of isotherm models for the characterization of biosorption of lead onto algae. *Journal of Molecular Liquids*, *212*, 46-51. https://doi.org/10.1016/j.molliq.2015.08.054

48). Buvaneswari, G., Thenmozhi, R., Nagasathya, A., Thajuddin, N. (2017). Screening of efficient monocrotophos degrading bacterial isolates from paddy field soil of Sivagangai district, Tamil Nadu, India. *Journal of Environmental Science and Technology*, *10*(1), 13-24. https://doi.org/10.3923/jest.2017.13.24

49). Buvaneswari, G., Thenmozhi, R., Nagasathya, A., Thajuddin, N., Kumar, P. (2018). GC-MS and molecular analyses of Monocrotophos Biodegradation by Selected Bacterial Isolates. *African Journal of Microbiology Research*, *12*(3), 52-61. https://doi.org/10.5897/AJMR2017.8696

50). Canevari, T. C., Prado, T. M., Cincotto, F. H., Machado, S. A. (2016). Immobilization of ruthenium phthalocyanine on silica-coated multi-wall partially oriented carbon nanotubes: electrochemical detection of fenitrothion pesticide. *Materials Research Bulletin*, *76*, 41-47. https://doi.org/10.1016/j.materresbull.2015.12.007

51). Carascal, M. B., del Rosario, M. J. G., Notarte, K. I. R., Huyop, F., Yaguchi, T., dela Cruz, T. E. E. (2017). Butachlor biodegradation potential of fungi isolated from submerged wood and surface water collected in Taal Lake, Philippines. *Philipp Sci Lett*, *10*, 81-88.

52). Chakraborty, S. K., Bhattacharyya, A. (1991). Degradation of butachlor by two soil fungi. *Chemosphere*, *23*(1), 99-105. https://doi.org/10.1016/0045-6535(91)90119-X

53). Chakravarthi, B. K., Naravaneni, R., Philip, G. H., Redddy, C. S. (2009). Investigation of monocrotophos toxic effects on human lymphocytes at cytogenetic level. *African Journal of Biotechnology*, *8*(10).

54). Chang, J., Liu, S., Zhou, S., Wang, M., Zhu, G. (2013). Effects of butachlor on reproduction and hormone levels in adult zebrafish (*Danio rerio*). *Experimental and toxicologic pathology*, *65*(1-2), 205-209. https://doi.org/10.1016/j.etp.2011.08.007

55). Chang, S. S., Ashton, F. M., Bayer, D. E. (1985). Butachlor influence on selected metabolic processes of plant cells and tissues. *Journal of Plant Growth Regulation*, *4*, 1-9. https://doi.org/10.1007/BF02266938

56). Chaudhry, S., Luhach, J., Mittal, P., Panwar, H., Sharma, C. (2013). Biodegradation potential of indigenous *Bacillus* strains isolated from oil and sludge contaminated sites.

Asian Journal of Microbiology, Biotechnology & Environmental Sciences, *15*(1), 85-92.

57). Chauhan, P. S., Jha, B. (2018). Pilot scale production of extracellular thermo-alkali stable laccase from *Pseudomonas* sp. S2 using agro waste and its application in organophosphorous pesticides degradation. *Journal of Chemical Technology & Biotechnology*, *93*(4), 1022-1030. https://doi.org/10.1002/jctb.5454

58). Chen, K., Chen, Q., Wang, G. X., Ni, H. Y., He, J., Yan, X., Gu, J., Li, S. P. (2015). *Sphingomonas chloroacetimidivorans* sp. nov., a chloroacetamide herbicide-degrading bacterium isolated from activated sludge. *Antonie Van Leeuwenhoek*, *108*(3), 703-710. https://doi.org/10.1007/s10482-015-0526-z

59). Chen, Q., Zhang, J., Wang, C. H., Jiang, J., Kwon, S. W., Sun, L. N., Shen, W., He, J. (2014). *Novosphingobium chloroacetimidivorans* sp. nov., a chloroacetamide herbicide–degrading bacterium isolated from activated sludge. *International journal of systematic and evolutionary microbiology*, *64*(8), 2573-2578. https://doi.org/10.1099/ijs.0.062950-0

60). Chen, W. C., Yen, J. H., Chang, C. S., Wang, Y. S. (2009). Effects of herbicide butachlor on soil microorganisms and on nitrogen-fixing abilities in paddy soil. *Ecotoxicology and environmental Safety*, *72*(1), 120-127. https://doi.org/10.1016/j.ecoenv.2008.03.013

61). Chen, Z., Juneau, P., Qiu, B. (2007). Effects of three pesticides on the growth, photosynthesis and photoinhibition of the edible cyanobacterium Ge-Xian-Mi (*Nostoc*). *Aquatic Toxicology*, *81*(3), 256-265. https://doi.org/10.1016/j.aquatox.2006.12.008

62). Chu, C. W., Chen, Q., Wang, C. H., Wang, H. M., Sun, Z. G., He, Q., He, J., Gu, J. G. (2016). *Roseomonas chloroacetimidivorans* sp. nov., a chloroacetamide herbicide-degrading bacterium isolated from activated sludge. *Antonie van Leeuwenhoek*, *109*(5), 611-618. https://doi.org/10.1007/s10482-016-0664-y

63). Cundy, A. B., Hopkinson, L., Whitby, R. L. (2008). Use of iron-based technologies in contaminated land and groundwater remediation: A review. *Science of the total environment*, *400*(1-3), 42-51. https://doi.org/10.1016/j.scitotenv.2008.07.002

64). Darbha, G. K., Singh, A. K., Rai, U. S., Yu, E., Yu, H., Chandra Ray, P. (2008). Selective detection of mercury (II) ion using nonlinear optical properties of gold nanoparticles. *Journal of the American Chemical Society*, *130*(25), 8038-8043. https://doi.org/10.1021/ja801412b

65). Darko, G., Akoto, O. (2008). Dietary intake of organophosphorus pesticide residues through vegetables from Kumasi, Ghana. *Food and Chemical Toxicology*, *46*(12), 3703-3706. https://doi.org/10.1016/j.fct.2008.09.049

66). Das, A., Singh, J., Yogalakshmi, K. N. (2017). Laccase immobilized magnetic iron nanoparticles: fabrication and its performance evaluation in chlorpyrifos degradation. *International Biodeterioration & Biodegradation*, *117*, 183-189. https://doi.org/10.1016/j.ibiod.2017.01.007

67). Das, G. P., Pasha Shaik, A., Jamil, K. (2006). Estimation of apoptosis and necrosis caused by pesticides in vitro on human lymphocytes using DNA diffusion assay. *Drug and Chemical Toxicology*, *29*(2), 147-156. https://doi.org/10.1080/01480540600561387

68). Das, N. P., Kumar, A., Singh, P. K. (2015). Cyanobacteria, pesticides and rice interaction. *Biodiversity and Conservation*, *24*(4), 995-1005. https://doi.org/10.1007/s10531-015-0886-8

69). Das, S., Singh, DK (2006). Purification and characterization of phosphotriesterases from *Pseudomonas aeruginosa* F10B and *Clavibacter michiganense* subsp. *insidiosum* SBL11. *Canadian journal of microbiology*, *52* (2), 157-168. https://doi.org/10.1139/w05-113

70). Dehaghi, S. M., Rahmanifar, B., Moradi, A. M., Azar, P. A. (2014). Removal of permethrin pesticide from water by chitosan–zinc oxide nanoparticles composite as an adsorbent. *Journal of Saudi Chemical Society*, *18*(4), 348-355. https://doi.org/10.1016/j.jscs.2014.01.004

71). Dehghani, M. H., Niasar, Z. S., Mehrnia, M. R., Shayeghi, M., Al-Ghouti, M. A., Heibati, B., McKay, G., Yetilmezsoy, K. (2017). Optimizing the removal of organophosphorus pesticide malathion from water using multi-walled carbon nanotubes. *Chemical Engineering Journal*, *310*, 22-32. https://doi.org/10.1016/j.cej.2016.10.057

72). Delgado, M., Mendez, J., Rodríguez-Herrera, R., Aguilar, C. N., Cruz-Hernández, M., Balagurusamy, N. (2014). Characterization of phosphate-solubilizing bacteria isolated from the arid soils of a semi-desert region of north-east Mexico. *Biological agriculture & horticulture*, *30*(3), 211-217. https://doi.org/10.1080/01448765.2014.909742

73). Deng, S., Chen, Y., Wang, D., Shi, T., Wu, X., Ma, X., Li, X., Hua, R., Tang, X., Li, Q. X. (2015). Rapid biodegradation of organophosphorus pesticides by *Stenotrophomonas* sp. G1. *Journal of hazardous materials*, *297*, 17-24. https://doi.org/10.1016/j.jhazmat.2015.04.052

74). Dolas, H., Sahin, O., Saka, C., Demir, H. (2011). A new method on producing high surface area activated carbon: the effect of salt on the surface area and the pore size distribution of activated carbon prepared from pistachio shell. *Chemical engineering journal*, *166*(1), 191-197. https://doi.org/10.1016/j.cej.2010.10.061

75). Du, Z., Deng, S., Bei, Y., Huang, Q., Wang, B., Huang, J., Yu, G. (2014). Adsorption behavior and mechanism of perfluorinated compounds on various adsorbents—A review. *Journal of hazardous materials*, *274*, 443-454. https://doi.org/10.1016/j.jhazmat.2014.04.038

76). Dureja, P. (1989). Photodecomposition of monocrotophos in soil, on plant foliage, and in water. *Bulletin of environmental contamination and toxicology*, *43*(2), 239-245. https://doi.org/10.1007/BF01701754

77). Dutton, A. J., Roberts, T. R., Stoydin, G. (1974). The degradation of Azodrin in soil. Shell-Report WKGR. 0053.74

78). Dwivedi, C., Gupta, A., Chaudhary, A., Nandi, C. K. (2014). Gold nanoparticle chitosan composite hydrogel beads show efficient removal of methyl parathion from waste water. *RSC advances*, *4*(75), 39830-39838. https://doi.org/10.1039/C4RA03870C

79). Dwivedi, S., Saquib, Q., Al-Khedhairy, A. A., Musarrat, J. (2012). Butachlor induced dissipation of mitochondrial membrane potential, oxidative DNA damage and necrosis in human peripheral blood mononuclear cells. *Toxicology*, *302*(1), 77-87. https://doi.org/10.1016/j.tox.2012.07.014

80). Dwivedi, S., Singh, B. R., Al-Khedhairy, A. A., Alarifi, S., Musarrat, J. (2010). Isolation and characterization of butachlor-catabolizing bacterial strain *Stenotrophomonas acidaminiphila* JS-1 from soil and assessment of its biodegradation potential. *Letters in applied microbiology*, *51*(1), 54-60. https://doi.org/10.1111/j.1472-765X.2010.02854.x

81). Elbarbary, A. M., El-Sawy, N. M. (2017). Radiation synthesis and characterization of polyvinyl alcohol/chitosan/silver nanocomposite membranes: antimicrobial and blood compatibility studies. *Polymer Bulletin*, *74*(1), 195-212. https://doi.org/10.1007/s00289-016-1708-1

82). Elliott, D. W., Lien, H. L., Zhang, W. X. (2009). Degradation of lindane by zero-valent iron nanoparticles. *Journal of Environmental Engineering*, *135*(5), 317-324. https://doi.org/10.1061/(ASCE)0733-9372(2009)135:5(317)

83). El-Temsah, Y. S., Sevcu, A., Bobcikova, K., Cernik, M., Joner, E. J. (2016). DDT degradation efficiency and ecotoxicological effects of two types of nano-sized zero-valent iron (nZVI) in water and soil. *Chemosphere*, *144*, 2221-2228. https://doi.org/10.1016/j.chemosphere.2015.10.122

84). Eurostat. (2007). The use of plant protection products in the European Union, data 1992–2003. Office for Official publications of the European Communities, Luxembourg

85). Fan, C., Liang, Y., Dong, H., Ding, G., Zhang, W., Tang, G., Yang, J., Kong, D., Wang, D., Cao, Y. (2017). In-situ ionic liquid dispersive liquid-liquid microextraction using a new anion-exchange reagent combined Fe_3O_4 magnetic nanoparticles for determination of pyrethroid pesticides in water samples. *Analytica Chimica Acta*, *975*, 20-29. https://doi.org/10.1016/j.aca.2017.04.036

86). Farombi, E. O., Ajimoko, Y. R., Adelowo, O. A. (2008). Effect of butachlor on antioxidant enzyme status and lipid peroxidation in fresh water African catfish, (*Clarias gariepinus*). *International journal of environmental research and public health*, *5*(5), 423-427. https://doi.org/10.3390/ijerph5050423

87). Finley, S. D., Broadbelt, L. J., Hatzimanikatis, V. (2010). In silico feasibility of novel biodegradation pathways for 1, 2, 4-trichlorobenzene. *BMC systems biology*, *4*(1), 7.

88). Fiorilli, S., Rivoira, L., Calì, G., Appendini, M., Bruzzoniti, M. C., Coïsson, M., Onida, B. (2017). Iron oxide inside SBA-15 modified with amino groups as reusable adsorbent for highly efficient removal of glyphosate from water. *Applied Surface Science*, *411*, 457-465. https://doi.org/10.1016/j.apsusc.2017.03.206

89). Franke, C., Studinger, G., Berger, G., Böhling, S., Bruckmann, U., Cohors-Fresenborg, D., Jöhncke, U. (1994). The assessment of bioaccumulation. *Chemosphere*, *29*(7), 1501-1514. https://doi.org/10.1016/0045-6535(94)90281-X

90). Gámiz, B., Hermosín, M. C., Cornejo, J., Celis, R. (2015). Hexadimethrine-montmorillonite nanocomposite: characterization and application as a pesticide adsorbent. *Applied Surface Science*, *332*, 606-613. https://doi.org/10.1016/j.apsusc.2015.01.179

91). Gao, Y., Jin, L., Shi, H., Chu, Z. (2015). Characterization of a novel butachlor biodegradation pathway and cloning of the debutoxylase (Dbo) gene responsible for debutoxylation of butachlor in *Bacillus* sp. hys-1. *Journal of agricultural and food chemistry*, *63*(38), 8381-8390. https://doi.org/10.1021/acs.jafc.5b03326

92). Gavrilescu, M. (2005). Fate of pesticides in the environment and its bioremediation. *Engineering in life sciences*, *5*(6), 497-526. https://doi.org/10.1002/elsc.200520098

93). Gholamali, I., Asnaashariisfahani, M., Alipour, E. (2020). Silver nanoparticles incorporated in pH-sensitive nanocomposite hydrogels based on carboxymethyl chitosan-poly (vinyl alcohol) for use in a drug delivery system. *Regenerative Engineering and Translational Medicine*, *6*(2), 138-153. https://doi.org/10.1007/s40883-019-00120-7

94). Ghormade, V., Deshpande, M. V., Paknikar, K. M. (2011). Perspectives for nano-biotechnology enabled protection and nutrition of plants. *Biotechnology advances*, *29*(6), 792-803. https://doi.org/10.1016/j.biotechadv.2011.06.007

95). Gill, J. P. K., Sethi, N., Mohan, A., Datta, S., Girdhar, M. (2018). Glyphosate toxicity for animals. *Environmental Chemistry Letters*, *16*(2), 401-426. https://doi.org/10.1007/s10311-017-0689-0

96). Gillham, R. W. (1996). In situ treatment of groundwater: Metal-enhanced degradation of chlorinated organic contaminants. In *Advances in groundwater pollution control and remediation* (pp. 249-274). Springer, Dordrecht. https://doi.org/10.1007/978-94-009-0205-3_13

97). Gillham, R. W., O'Hannesin, S. F. (1994). Enhanced degradation of halogenated aliphatics by zero-valent iron. *Ground water*, *32*(6), 958-969.

98). Goldstein, M. I., Lacher, T. E., Woodbridge, B., Bechard, M. J., Canavelli, S. B., Zaccagnini, M. E., Cobb, G. P., Scollon, E. J., Tribolet, R., Hopper, M. J. (1999). Monocrotophos-induced mass mortality of Swainson's Hawks in Argentina, 1995–96. *Ecotoxicology*, *8*(3), 201-214. https://doi.org/10.1023/A:1026496331396

99). Govindarajan, B. (2014). Toxic effect of insecticide (monocrotophos) on protein content of *Eudrilus Eugeniae* under experimental conditions. *Int J Pharm Ther*, *5*(1), 01-02.

100). Grabka, D., Raczyńska-Żak, M., Czech, K., Słomkiewicz, P. M., Jóźwiak, M. A. (2015). Modified halloysite as an adsorbent for prometryn from aqueous solutions. *Applied Clay Science*, *114*, 321-329. https://doi.org/10.1016/j.clay.2015.06.012

101). Gu, H. X., Hu, K., Li, D. W., Long, Y. T. (2016). SERS detection of polycyclic aromatic hydrocarbons using a bare gold nanoparticles coupled film system. *Analyst*, *141*(14), 4359-4365. https://doi.org/10.1039/C6AN00319B

102). Gundi, V. A., Reddy, B. R. (2006). Degradation of monocrotophos in soils. *Chemosphere*, *62*(3), 396-403. https://doi.org/10.1016/j.chemosphere.2005.04.076

103). Guo, M., Weng, X., Wang, T., Chen, Z. (2017). Biosynthesized iron-based nanoparticles used as a heterogeneous catalyst for the removal of 2, 4-dichlorophenol. *Separation and Purification Technology*, *175*, 222-228. https://doi.org/10.1016/j.seppur.2016.11.042

104). Gupta, M., Bagchi, G., Bandyopadhyay, S., Sasmal, D., Chatterjee, T., Dey, S. N. (1982). Hematological changes produced in mice by Nuvacron or Furadan. *Toxicology*, *25*(2-3), 255-260. https://doi.org/10.1016/0300-483X(82)90034-8

105). Habiba, U., Joo, T. C., Shezan, S. K. A., Das, R., Ang, B. C., Afifi, A. M. (2019). Synthesis and characterization of chitosan/TiO_2 nanocomposite for the adsorption of Congo red. *Desalination and Water Treatment*, 164, 361-367. https://doi.org/10.5004/dwt.2019.24391

106). Hanh, N. T., Tri, N. L. M., Thuan, D. V., Tung, M. H. T., Pham, T. D., Minh, T. D., Trang, H. T., Binh, M.T., Nguyen, M. V. (2019). Monocrotophos pesticide effectively removed by novel visible light driven Cu doped ZnO photocatalyst. *Journal of Photochemistry and Photobiology A: Chemistry*, *382*, 111923. https://doi.org/10.1016/j.jphotochem.2019.111923

107). Haq, A.U., Saeed, M., Usman, M., Muneer, M., Adeel, S., Abbas, S., Iqbal, A. (2019). Removal of butachlor from aqueous solution using cantaloupe seed shell powder: kinetic, equilibrium and thermodynamic studies. *Int. J. Environ. Sci. Technol.*, *16*(10), 6029-6042. https://doi.org/10.1007/s13762-018-1992-4

108). Hasnain, S., Ali, S. S., Uddin, Z., Zafar, R. (2013). Application of nanotechnology in health and environmental research: a review. *Research Journal of Environmental and Earth Sciences*, *5*(3), 160-166.

109). He, H., Chen, G., Yu, J., He, J., Huang, X., Li, S., Guo, Q., Tu, T., Li, H. (2013). Individual and joint toxicity of three chloroacetanilide herbicides to freshwater

cladoceran *Daphnia carinata*. *Bulletin of environmental contamination and toxicology*, *90*(3), 344-350. https://doi.org/10.1007/s00128-012-0898-y

110). Hernandez, H., Stearns, S. M., Fukuto, J. M. (1986). Anaerobic soil metabolism of SD 9129. Shell-Report RIR-22-018-86

111). Hoseini, S. N., Pirzaman, A. K., Aroon, M. A., Pirbazari, A. E. (2017). Photocatalytic degradation of 2, 4-dichlorophenol by Co-doped TiO_2 (Co/TiO_2) nanoparticles and Co/TiO_2 containing mixed matrix membranes. *Journal of water process engineering*, *17*, 124-134. https://doi.org/10.1016/j.jwpe.2017.02.015

112). Hosseini, N., Toosi, M. R. (2019). Removal of 2, 4-D, glyphosate, trifluralin, and butachlor herbicides from water by polysulfone membranes mixed by graphene oxide/TiO_2 nanocomposite: study of filtration and batch adsorption. *Journal of Environmental Health Science and Engineering*, *17*(1), 247-258. https://doi.org/10.1007/s40201-019-00344-3

113). Hou, X., Lei, S., Qiu, S., Guo, L., Yi, S., Liu, W. (2014a). A multi-residue method for the determination of pesticides in tea using multi-walled carbon nanotubes as a dispersive solid phase extraction absorbent. *Food chemistry*, *153*, 121-129. https://doi.org/10.1016/j.foodchem.2013.12.031

114). Hou, Y., Dong, W., Wang, F., Li, J., Shen, W., Li, Y., Cui, Z. (2014b). Degradation of acetochlor by a bacterial consortium of *Rhodococcus* sp. T3-1, *Delftia* sp. T3-6 and *Sphingobium* sp. MEA 3-1. *Letters in applied microbiology*, *59*(1), 35-42. https://doi.org/10.1111/lam.12242

115). Hsu, C. W., Lin, Z. Y., Chan, T. Y., Chiu, T. C., Hu, C. C. (2017). Oxidized multiwalled carbon nanotubes decorated with silver nanoparticles for fluorometric detection of dimethoate. *Food chemistry*, *224*, 353-358. https://doi.org/10.1016/j.foodchem.2016.12.095

116). Hsu, K. Y., Lin, H. J., Lin, J. K., Kuo, W. S., Ou, Y. H. (2005). Mutagenicity study of butachlor and its metabolites using *Salmonella typhimurium*. *Journal of Microbiology, Immunology and Infection*, *38*(6), 409-416.

117). Huang, Y., Shi, T., Luo, X., Xiong, H., Min, F., Chen, Y., Nie, S., Xie, M. (2019). Determination of multi-pesticide residues in green tea with a modified QuEChERS protocol coupled to HPLC-MS/MS. *Food chemistry*, *275*, 255-264. https://doi.org/10.1016/j.foodchem.2018.09.094

118). Hussain, S., Masud, T., Ahad, K. (2002). Determination of pesticides residues in selected varieties of mango. *Pak. J. Nutr*, *1*(1), 41-42.

119). Ibrahim, W. A. W., Ismail, W. N. W., Sanagi, M. M. (2013). Selective and Simultaneous Solid Phase Extraction of Polar and NonPolar Organophosphorus Pesticides Using Sol-Gel Hybrid Silica-Based Sorbent. *Jurnal Teknologi*, 62(3), 83–87.

120). Imran, A., hussain, T., Nadeem, A. (2016). Chromatographic determination of residual contents of pesticides in rice samples from different geographical regions of Punjab. *FUUAST Journal of Biology*, *6*(2), 155-160.

121). Iyer, R., Iken, B., Damania, A. (2013). A comparison of organophosphate degradation genes and bioremediation applications. *Environmental microbiology reports*, *5*(6), 787-798. https://doi.org/10.1111/1758-2229.12095

122). Jain, R., Garg, V. (2013). Enzymatic degradation of monocrotophos by extracellular fungal OP hydrolases. *Applied biochemistry and biotechnology*, *171*(6), 1473-1486. https://doi.org/10.1007/s12010-013-0438-1

123). Jain, R., Garg, V. (2014). Comparative Analysis of Chemical, Fungal and Enzymatic Degradation of MCP. *SAJ Biotechnology*, *2*(2), 1. https://doi.org/10.18875/2375-6713.1.101

124). Jain, R., Garg, V. (2015). Degradation of monocrotophos in soil, microbial versus enzymatic method. *Journal of Environmental and Occupational Health*, *4*(1), 44-52. https://doi.org/10.5455/jeos.20141214124733

125). Jain, R., Garg, V., Dangwal, K., Lily, M. K. (2013a). Comparative purification and characterization of two distinct extracellular monocrotophos hydrolases secreted by *Penicillium aculeatum* and *Fusarium pallidoroseum* isolated from agricultural fields. *Bioscience, biotechnology, and biochemistry*, *77*(5), 961-965. https://doi.org/10.1271/bbb.120907

126). Jain, R., Garg, V., Dangwal, K., Lily, M. K. (2013b). Purification and characterization of acid phosphatase from monocrotophos (MCP) hydrolyzing *Aspergillus niger* ITCC 7782.10 Isolated from Local Agricultural Field. *Turkish Journal of Biochemistry/Turk Biyokimya Dergisi*, *38*(4). https://doi.org/10.5505/tjb.2013.19870

127). Jain, R., Garg, V., Saxena, J. (2015). Effect of an organophosphate pesticide, monocrotophos, on phosphate-solubilizing efficiency of soil fungal isolates. *Applied biochemistry and biotechnology*, *175*(2), 813-824. https://doi.org/10.1007/s12010-014-1309-0

128). Jain, R., Garg, V., Yadav, D. (2014). In vitro comparative analysis of monocrotophos degrading potential of *Aspergillus flavus*, *Fusarium pallidoroseum* and *Macrophomina* sp. *Biodegradation*, *25*(3), 437-446. https://doi.org/10.1007/s10532-013-9672-z

129). Jaiswal, M., Chauhan, D., Sankararamakrishnan, N. (2012). Copper chitosan nanocomposite: synthesis, characterization, and application in removal of organophosphorous pesticide from agricultural runoff. *Environmental Science and Pollution Research*, *19*(6), 2055-2062. https://doi.org/10.1007/s11356-011-0699-6

130). Jamil, K., Shaik, A. P., Mahboob, M., Krishna, D. (2004). Effect of organophosphorus and organochlorine pesticides (monochrotophos, chlorpyriphos, dimethoate, and endosulfan) on human lymphocytes in-vitro. *Drug and chemical toxicology*, *27*(2), 133-144. https://doi.org/10.1081/DCT-120030725

131). Jena, P. K., Adhya, T. K., Rajaramamohan Rao, V. (1987). Influence of carbaryl on nitrogenase activity and combinations of butachlor and carbofuran on nitrogen-fixing micro-organisms in paddy soils. *Pesticide science*, *19*(3), 179-184. https://doi.org/10.1002/ps.2780190303

132). Jia, K. Z., Cui, Z. L., He, J., Guo, P., Li, S. P. (2006). Isolation and characterization of a denitrifying monocrotophos-degrading *Paracoccus* sp. M-1. *FEMS microbiology letters*, *263*(2), 155-162. https://doi.org/10.1111/j.1574-6968.2006.00389.x

133). Jiang, R., Zhu, H. Y., Fu, Y. Q., Zong, E. M., Jiang, S. T., Li, J. B., Zhu, J. Q., Zhu, Y. Y. (2021). Magnetic $NiFe_2O_4$/MWCNTs functionalized cellulose bioadsorbent with enhanced adsorption property and rapid separation. *Carbohydrate Polymers*, *252*, 117158. https://doi.org/10.1016/j.carbpol.2020.117158

134). Jin, L., Bai, R. (2002). Mechanisms of lead adsorption on chitosan/PVA hydrogel beads. *Langmuir*, *18*(25), 9765-9770. https://doi.org/10.1021/la025917l

135). Joint FAO/WHO meeting on Pesticide Residues (JMPR 1972). 244. Monocrotophos (WHO Pesticide Residues Series 2). http://www.inchem.org/documents/jmpr/jmpmono/v072pr22.htm. Last accessed on December 04, 2020

136). Joo, S. H., Zhao, D. (2008). Destruction of lindane and atrazine using stabilized iron nanoparticles under aerobic and anaerobic conditions: effects of catalyst and stabilizer. *Chemosphere*, *70*(3), 418-425. https://doi.org/10.1016/j.chemosphere.2007.06.070

137). Jose, A., Selvakumar, R., Peter, J. V., Karthik, G., Fleming, D. H., Fleming, J. J. (2015). Estimation of Monocrotophos renal elimination half-life in humans. *Clinical Toxicology*, *53*(7), 629-632. https://doi.org/10.3109/15563650.2015.1054500

138). Joshi, A. K. R., Rajini, P. S. (2012). Hyperglycemic and stressogenic effects of monocrotophos in rats: evidence for the involvement of acetylcholinesterase inhibition. *Experimental and toxicologic pathology*, *64*(1-2), 115-120. https://doi.org/10.1016/j.etp.2010.07.003

139). Juby, K. A., Dwivedi, C., Kumar, M., Kota, S., Misra, H. S., Bajaj, P. N. (2012). Silver nanoparticle-loaded PVA/gum acacia hydrogel: Synthesis, characterization and antibacterial study. *Carbohydrate polymers*, *89*(3), 906-913. https://doi.org/10.1016/j.carbpol.2012.04.033

140). Kalyani, S, S., Sharma, J., Singh, S., Dureja, P., Lata. (2009). Enrichment and isolation of endosulfan-degrading microorganism from tropical acid soil. *Journal of Environmental Science and Health Part B*, *44*(7), 663-672. https://doi.org/10.1080/03601230903163665

141). Kanekar, P. P., Bhadbhade, B. J., Deshpande, N. M., Sarnaik, S. S. (2004). Biodegradation of organophosphorus pesticides. *Proc Indian Natl Sci Acad* B70(1):57-70.

142). Kang, Y., Zhang, G., Sheng, G., Fu, J. (2000). Analysis of organophosphorous pesticides from source water using solid-phase extraction technique. *China Environmental Science*, *20*(1), 1-4.

143). Karpouzas, D. G., Singh, B. K. (2006). Microbial degradation of organophosphorus xenobiotics: metabolic pathways and molecular basis. *Advances in microbial physiology*, *51*, 119-225. https://doi.org/10.1016/S0065-2911(06)51003-3

144). Kaur, P., Randhawa, S. K., Duhan, A., Bhullar, M. S. (2017a). Influence of long term application of butachlor on its dissipation and harvest residues in soil and rice. *Bulletin of Environmental Contamination and Toxicology*, *98*(6), 874-880. https://doi.org/10.1007/s00128-017-2070-1.

145). Kaur, R., Goyal, D. (2019). Toxicity and degradation of the insecticide monocrotophos. *Environmental Chemistry Letters*, *17*(3), 1299-1324. https://doi.org/10.1007/s10311-019-00884-y

146). Kaur, R., Goyal, D. (2020). Biodegradation of Butachlor by *Bacillus altitudinis* and Identification of Metabolites. *Current Microbiology*, *77*, 2602-2612 https://doi.org/10.1007/s00284-020-02031-1

147). Kaur, T., Sraw, A., Wanchoo, R. K., Toor, A. P. (2016). Visible–light induced photocatalytic degradation of fungicide with Fe and Si doped TiO_2 nanoparticles. *Materials Today: Proceedings*, *3*(2), 354-361. https://doi.org/10.1016/j.matpr.2016.01.020

148). Kaur, Y., Bhatia, Y., Chaudhary, S., Chaudhary, G. R. (2017b). Comparative performance of bare and functionalize ZnO nanoadsorbents for pesticide removal from aqueous solution. *Journal of Molecular Liquids*, *234*, 94-103. https://doi.org/10.1016/j.molliq.2017.03.069

149). KaviKarunya, S., Reetha, D. (2012). Biological degradation of chlorpyrifos and monocrotophos by bacterial isolates. *Int J Pharm Biol Arch*, *3*(3), 685-691.

150). Khan, A. B. (2005) Studies on the residues of commonly used insecticides on fruits and vegetables grown in NWFP-Pakistan Dissertation, NWFP Agriculture University, Peshawar

151). Khurana, C., Vala, A. K., Andhariya, N., Pandey, O. P., Chudasama, B. (2016). Influence of antibiotic adsorption on biocidal activities of silver nanoparticles. *IET nanobiotechnology*, *10*(2), 69-74. https://doi.org/10.1049/iet-nbt.2015.0005

152). Kim, H. Y., Kim, I. K., Han, T., Shim, J. H., Kim, I. S. (2006). Degradation of the Herbicide Butachlor by Laboratory-synthesized Nanoscale Fe^0 in Batch Experiments. *Agricultural Chemistry and Biotechnology*, *49*(3), 101.

153). Kim, J. R., Ahn, Y. J. (2009). Identification and characterization of chlorpyrifos-methyl and 3, 5, 6-trichloro-2-pyridinol degrading *Burkholderia* sp. strain KR100. *Biodegradation*, *20*(4), 487-497. https://doi.org/10.1007/s10532-008-9238-7

154). Kim, N. H., Kim, D. U., Kim, I., Ka, J. O. (2013). Syntrophic biodegradation of butachlor by *Mycobacterium* sp. J7A and *Sphingobium* sp. J7B isolated from rice paddy soil. *FEMS microbiology letters*, *344*(2), 114-120. https://doi.org/10.1111/1574-6968.12163

155). Kim, O. S., Cho, Y. J., Lee, K., Yoon, S. H., Kim, M., Na, H., Park, S.C., Jeaon, Y. S., Lee, J., Yi, H., Won, S., Chun, J. (2012). Introducing EzTaxon-e: a prokaryotic 16S rRNA gene sequence database with phylotypes that represent uncultured species. *International journal of systematic and evolutionary microbiology*, *62*(3), 716-721. https://doi.org/10.1099/ijs.0.038075-0

156). Kim, S., Park, M. Y., Kim, H. J., Shin, J. Y., Ko, K. Y., Kim, D. G., Kim, M., Kang, H., So, B., Park, S. W. (2016). Analysis of insecticides in dead wild birds in Korea from 2010 to 2013. *Bulletin of environmental contamination and toxicology*, *96*(1), 25-30. https://doi.org/10.1007/s00128-015-1688-0

157). Kodandaram, M. H., Saha, S., Rai, A. B., Naik, P. S. (2013). Compendium on pesticide use in vegetables. IIVR Extension Bulletin (50):133

158). Koushik, D., Gupta, S. S., Maliyekkal, S. M., Pradeep, T. (2016). Rapid dehalogenation of pesticides and organics at the interface of reduced graphene oxide–silver nanocomposite. *Journal of hazardous materials*, *308*, 192-198. https://doi.org/10.1016/j.jhazmat.2016.01.004

159). Krstić, J., Spasojević, J., Radosavljević, A., Šiljegović, M., Kačarević-Popović, Z. (2014). Optical and structural properties of radiolytically in situ synthesized silver nanoparticles stabilized by chitosan/poly (vinyl alcohol) blends. *Radiation Physics and Chemistry*, *96*, 158-166. https://doi.org/10.1016/j.radphyschem.2013.09.013

160). Kumar, N. H., Jagannath, S. (2015). Cytological Effects of Herbicide Butachlor 50 EC on Somatic cells of *Triticum aestivum* L. *Journal of Applied Biology & Biotechnology*, *3*(02), 030-034. https://doi.org/10.7324/JABB.2015.3206

161). Kumar, S., Stecher, G., Li, M., Knyaz, C., Tamura, K. (2018). MEGA X: molecular evolutionary genetics analysis across computing platforms. *Molecular biology and evolution*, *35*(6), 1547-1549. https://doi.org/10.1093/molbev/msy096

162). Kumar, V., Upadhyay, N., Kumar, V., Kaur, S., Singh, J., Singh, S., Datta, S. (2014). Environmental exposure and health risks of the insecticide monocrotophos—a review. *J Biodivers Environ Sci*, *5*(1), 111-120.

163). Kumari, B., Madan, V. K., Kathpal, T. S. (2007). Pesticide residues in rain water from Hisar, India. *Environmental monitoring and assessment*, *133*(1-3), 467-471. https://doi.org/10.1007/s10661-006-9601-2

164). Kumari, B., Madan, V. K., Singh, J., Singh, S., Kathpal, T. S. (2004). Monitoring of pesticidal contamination of farmgate vegetables from Hisar. *Environmental Monitoring and Assessment*, *90*(1-3), 65-71. https://doi.org/10.1023/B:EMAS.0000003566.63111.f6

165). Lee, P. W., Fukuto, J. M., Hernandez, H., Stearns, S. M. (1990). Fate of monocrotophos in the environment. *Journal of Agricultural and Food Chemistry*, *38*(2), 567-573.

166). Lee, P. W., Vanderlinden, H. F., Stackhouse, S. C. (1980). Comparative aerobic metabolism of SD 9129 in sterilized and unsterilized Hanford sandy loam soil. ShellReport RIR-22-014-80.

167). Lerma-García, M. J., Simó-Alfonso, E. F., Zougagh, M., Ríos, Á. (2013). Use of gold nanoparticle-coated sorbent materials for the selective preconcentration of sulfonylurea herbicides in water samples and determination by capillary liquid chromatography. *Talanta*, *105*, 372-378. https://doi.org/10.1016/j.talanta.2012.10.056

168). Li, H., Guo, J., Ping, H., Liu, L., Zhang, M., Guan, F., Sun, C., Zhang, Q. (2011). Visual detection of organophosphorus pesticides represented by mathamidophos using Au nanoparticles as colorimetric probe. *Talanta*, *87*, 93-99. https://doi.org/10.1016/j.talanta.2011.09.046

169). Li, S., Li, M., Wang, Q., Gui, W., Zhu, G. (2016). Exposure to butachlor causes thyroid endocrine disruption and promotion of metamorphosis in *Xenopus laevis*. *Chemosphere*, *152*, 158-165. https://doi.org/10.1016/j.chemosphere.2016.02.098

170). Li, Z., Wang, Y., Ni, Y., Kokot, S. (2014). Unmodified silver nanoparticles for rapid analysis of the organophosphorus pesticide, dipterex, often found in different waters. *Sensors and Actuators B: Chemical*, *193*, 205-211. https://doi.org/10.1016/j.snb.2013.11.096

171). Lisa, M., Chouhan, R. S., Vinayaka, A. C., Manonmani, H. K., Thakur, M. S. (2009). Gold nanoparticles based dipstick immunoassay for the rapid detection of dichlorodiphenyltrichloroethane: an organochlorine pesticide. *Biosensors and Bioelectronics*, *25*(1), 224-227. https://doi.org/10.1016/j.bios.2009.05.006

172). Liu, H. M., Cao, L., Lu, P., Ni, H., Li, Y. X., Yan, X., Hong, Q., Li, S. P. (2012). Biodegradation of butachlor by *Rhodococcus* sp. strain B1 and purification of its hydrolase (ChlH) responsible for N-dealkylation of chloroacetamide herbicides. *Journal of agricultural and food chemistry*, *60*(50), 12238-12244. https://doi.org/10.1021/jf303936j

173). Liu, S., Xie, L., Zheng, J., Jiang, R., Zhu, F., Luan, T., Ouyang, G. (2015). Mesoporous TiO_2 nanoparticles for highly sensitive solid-phase microextraction of organochlorine pesticides. *Analytica Chimica Acta*, *878*, 109-117. https://doi.org/10.1016/j.aca.2015.03.054

174). Liu, S., Yuan, L., Yue, X., Zheng, Z., Tang, Z. (2008). Recent advances in nanosensors for organophosphate pesticide detection. *Advanced Powder Technology*, *19*(5), 419-441. https://doi.org/10.1016/S0921-8831(08)60910-3

175). Liu, W. Y., Wang, C. Y., Wang, T. S., Fellers, G. M., Lai, B. C., Kam, Y. C. (2011). Impacts of the herbicide butachlor on the larvae of a paddy field breeding frog

(*Fejervarya limnocharis*) in subtropical Taiwan. *Ecotoxicology*, *20*(2), 377-384. https://doi.org/10.1007/s10646-010-0589-6

176). Lu, L. C., Wang, C. I., Sye, W. F. (2011). Applications of chitosan beads and porous crab shell powder for the removal of 17 organochlorine pesticides (OCPs) in water solution. *Carbohydrate Polymers*, *83*(4), 1984-1989. https://doi.org/10.1016/j.carbpol.2010.11.003

177). Luckham, R. E., Brennan, J. D. (2010). Bioactive paper dipstick sensors for acetylcholinesterase inhibitors based on sol–gel/enzyme/gold nanoparticle composites. *Analyst*, *135*(8), 2028-2035. https://doi.org/10.1039/C0AN00283F

178). Luo, Q. J., Li, Y. X., Zhang, M. Q., Qiu, P., Deng, Y. H. (2017). A highly sensitive, dual-signal assay based on rhodamine B covered silver nanoparticles for carbamate pesticides. *Chinese Chemical Letters*, *28*(2), 345-349. https://doi.org/10.1016/j.cclet.2016.10.024

179). Ly, N. H., Nguyen, T. H., Nghi, N. Đ., Kim, Y. H., Joo, S. W. (2019). Surface-enhanced Raman scattering detection of fipronil pesticide adsorbed on silver nanoparticles. *Sensors*, *19*(6), 1355. https://doi.org/10.3390/s19061355

180). Ma, Y. Q., Yi, J. Z., Zhang, L. M. (2009). A facile approach to incorporate silver nanoparticles into dextran-based hydrogels for antibacterial and catalytical application. *Journal of Macromolecular Science, Part A: Pure and Applied Chemistry*, *46*(6), 643-648. https://doi.org/10.1080/10601320902852031

181). Mackay, D., Shiu, W.Y., Ma, K. C., Lee, S. C. (2006). Handbook of physical-chemical properties and environmental fate for organic chemicals. CRC press

182). Makkliang, F., Kanatharana, P., Thavarungkul, P., Thammakhet, C. (2016). A novel miniaturized zinc oxide/hydroxylated multiwalled carbon nanotubes as a stir-brush microextractor device for carbamate pesticides analysis. *Analytica Chimica Acta*, *917*, 27-36. https://doi.org/10.1016/j.aca.2016.02.040

183). Malarkodi, C., Rajeshkumar, S., Annadurai, G. (2017). Detection of environmentally hazardous pesticide in fruit and vegetable samples using gold nanoparticles. *Food Control*, *80*, 11-18. https://doi.org/10.1016/j.foodcont.2017.04.023

184). Mamun, M. I. R., Park, J. H., Choi, J. H., Kim, H. K., Choi, W. J., Han, S. S., Hwang, K., Jang, N., Assayed, M. E., Shin, H. C. (2009). Development and validation of a multiresidue method for determination of 82 pesticides in water using GC. *Journal of separation science*, *32*(4), 559-574. https://doi.org/10.1002/jssc.200800606

185). Mandhane, S. N., Chopde, C. T. (1995). Neurobehavioural effects of acute monocrotophos administration in rats and mice. *Indian Journal of Pharmacology*, *27*(4), 245-249.

186). Mansouriieh, N., Sohrabi, M. R., Khosravi, M. (2019). Optimization of profenofos organophosphorus pesticide degradation by zero-valent bimetallic nanoparticles using

response surface methodology. *Arabian Journal of Chemistry*, *12*(8), 2524-2532. https://doi.org/10.1016/j.arabjc.2015.04.009

187). Maqbool, Z., Hussain, S., Imran, M., Mahmood, F., Shahzad, T., Ahmed, Z., Azeem, F., Muzammil, S. (2016). Perspectives of using fungi as bioresource for bioremediation of pesticides in the environment: a critical review. *Environmental Science and Pollution Research*, *23*(17), 16904-16925. https://doi.org/10.1007/s11356-016-7003-8

188). Megharaj, M., Ramakrishnan, B., Venkateswarlu, K., Sethunathan, N., Naidu, R. (2011). Bioremediation approaches for organic pollutants: a critical perspective. *Environment international*, *37*(8), 1362-1375. https://doi.org/10.1016/j.envint.2011.06.003

189). Megharaj, M., Venkateswarlu, K., Rao, A. S. (1986a). Effect of monocrotophos and quinalphos on soil algae. *Environmental Pollution Series A, Ecological and Biological*, *40*(2), 121-126. https://doi.org/10.1016/0143-1471(86)90079-6

190). Megharaj, M., Venkateswarlu, K., Rao, A. S. (1986b). Growth response of four species of soil algae to monocrotophos and quinalphos. *Environmental Pollution Series A, Ecological and Biological*, *42*(1), 15-22. https://doi.org/10.1016/0143-1471(86)90041-3

191). Megharaj, M., Venkateswarlu, K., Rao, A. S. (1987). Metabolism of monocrotophos and quinalphos by algae isolated from soil. *Bulletin of environmental contamination and toxicology*, *39*(2), 251-256. https://doi.org/10.1007/BF01689414

192). Megharaj, M., Venkateswarlu, K., Rao, A. S. (1988). Microbial degradation and algal toxicity of monocrotophos and quinalphos in flooded soil. *Chemosphere*, *17*(5), 1033-1039. https://doi.org/10.1016/0045-6535(88)90073-2

193). Mendelssohn, H., Paz, U. (1977). Mass mortality of birds of prey caused by Azodrin, an organophosphorus insecticide. *Biological Conservation*, *11*(3), 163-170. https://doi.org/10.1016/0006-3207(77)90001-5

194). Meylan, W. M., Howard, P. H. (1993). Computer estimation of the atmospheric gas-phase reaction rate of organic compounds with hydroxyl radicals and ozone. *Chemosphere*, *26*(12), 2293-2299. https://doi.org/10.1016/0045-6535(93)90355-9

195). Min, H., Ye, Y. F., Chen, Z. Y., Wu, W. X., Du, Y. F. (2002). Effects of butachlor on microbial enzyme activities in paddy soil. *Journal of Environmental Sciences*, *14*(3), 413-417.

196). Min, H., Ye, Y. F., Chen, Z. Y., Wu, W. X., Yufeng, D. (2001). Effects of butachlor on microbial populations and enzyme activities in paddy soil. *Journal of Environmental Science and Health, Part B*, *36*(5), 581-595. https://doi.org/10.1081/PFC-100106187

197). Mishra, S. K., Ferreira, J. M. F., Kannan, S. (2015). Mechanically stable antimicrobial chitosan–PVA–silver nanocomposite coatings deposited on titanium implants. *Carbohydrate polymers*, *121*, 37-48. https://doi.org/10.1016/j.carbpol.2014.12.027

198). Mohanty, S. S., Jena, H. M. (2018). Process optimization of butachlor bioremediation by *Enterobacter cloacae* using Plackett Burman design and response surface methodology. *Process Safety and Environmental Protection*, *119*, 198-206. https://doi.org/10.1016/j.psep.2018.08.009

199). Mohanty, S. S., Jena, H. M. (2019). Evaluation of butachlor biodegradation efficacy of Serratia ureilytica strain AS1: a statistical optimization approach. *International Journal of Environmental Science and Technology*, *16*(10), 5807-5816. https://doi.org/10.1007/s13762-018-1958-6

200). Muley, D. V., Karanjkar, D. M., Maske, S. V. (2007). Impact of industrial effluents on the biochemical composition of fresh water fish *Labeo rohita*. *Journal of Environmental Biology*, *28*(2), 245-249.

201). Mundhe, A. Y., Bhilwade, H., Pandit, S. V. (2016). Genotoxicity and oxidative stress as biomarkers in fresh water mussel, *Lamellidens marginalis* (Lam.) exposed to monocrotophos. *J Exp Biol*, *54*, 822-28.

202). Muthukaruppan, G., Janardhanan, S., Vijayalakshmi, G. (2005). Sublethal Toxicity of the Herbicide Butachlor on the Earthworm *Perionyx sansibaricus* and its Histological Changes (5 pp). *Journal of Soils and Sediments*, *5*(2), 82-86. https://doi.org/10.1065/jss2004.09.111

203). Nagaraju, R., Joshi, A. K. R., Rajini, P. S. (2015). Organophosphorus insecticide, monocrotophos, possesses the propensity to induce insulin resistance in rats on chronic exposure Inducing insulin resistance. *Journal of diabetes*, *7* (1), 47-59. https://doi.org/10.1111/1753-0407.12158

204). Nagaraju, R., Rajini, P. S. (2016). Adaptive response of rat pancreatic β-cells to insulin resistance induced by monocrotophos: Biochemical evidence. *Pesticide biochemistry and physiology*, *134*, 39-48. https://doi.org/10.1016/j.pestbp.2016.04.009

205). Nangia, S., Warkar, S., Katyal, D. (2018). A review on environmental applications of chitosan biopolymeric hydrogel based composites. *Journal of Macromolecular Science, Part A*, *55*(11-12), 747-763. https://doi.org/10.1080/10601325.2018.1526041

206). Narang, G., Mahajan, N. K., Jadhav, V. J., Mittal, D., Mishra, A. C. (2016). Monocrotophos toxicity in peafowl in Haryana. *Haryana Veterinarian*, *55*(1), 73-75.

207). Nascimento, M. A., Lopes, R. P., Cruz, J. C., Silva, A. A., Lima, C. F. (2016). Sulfentrazone dechlorination by iron-nickel bimetallic nanoparticles. *Environmental Pollution*, *211*, 406-413. https://doi.org/10.1016/j.envpol.2015.12.043

208). National Center for Biotechnology Information. PubChem Database. Butachlor, CID=31677, https://pubchem.ncbi.nlm.nih.gov/compound/Butachlor (accessed on Oct. 22, 2019)

209). Nguyen, T. T. T., Tae, B., Park, J. S. (2011). Synthesis and characterization of nanofiber webs of chitosan/poly (vinyl alcohol) blends incorporated with silver nanoparticles. *J Mater Sci*, *46*(20), 6528-6537. https://doi.org/10.1007/s10853-011-5599-0

210). Nithya, A., JeevaKumari, H. L., Rokesh, K., Ruckmani, K., Jeganathan, K., Jothivenkatachalam, K. (2015). A versatile effect of chitosan-silver nanocomposite for surface plasmonic photocatalytic and antibacterial activity. *Journal of Photochemistry and Photobiology B: Biology*, *153*, 412-422. https://doi.org/10.1016/j.jphotobiol.2015.10.020

211). Nivethaa, E. A. K., Narayanan, V., Stephen, A. (2015). Synthesis and spectral characterization of silver embedded chitosan matrix nanocomposite for the selective colorimetric sensing of toxic mercury. *Spectrochimica Acta Part A: Molecular and Biomolecular Spectroscopy*, *143*, 242-250. https://doi.org/10.1016/j.saa.2015.01.075

212). Nozhat, S., Fazilati, M., Hassani, A. H. (2018). Butachlor and Diazinon Elimination from Aqueous Solution using TiO_2/ZnO nano-photocatalysts.

213). Ok, J., Doan, N. H., Watanabe, H., Thuyet, D. Q., Boulange, J. (2012). Behavior of butachlor and pyrazosulfuron-ethyl in paddy water using micro paddy lysimeters under different temperature conditions in spring and summer. *Bulletin of environmental contamination and toxicology*, *89*(2), 306-311. https://doi.org/10.1007/s00128-012-0700-1

214). Ou, Y. H., Chung, P. C., Chang, Y. C., Ngo, F. Q., Hsu, K. Y., Chen, F. D. (2000). Butachlor, a suspected carcinogen, alters growth and transformation characteristics of mouse liver cells. *Chemical research in toxicology*, *13*(12), 1321-1325. https://doi.org/10.1021/tx990076c

215). Ouali, A., Belaroui, L. S., Bengueddach, A., Galindo, A. L., Peña, A. (2015). Fe_2O_3–palygorskite nanoparticles, efficient adsorbates for pesticide removal. *Applied Clay Science*, *115*, 67-75. https://doi.org/10.1016/j.clay.2015.07.026

216). Pain, D. J., Gargi, R., Cunningham, A. A., Jones, A., Prakash, V. (2004). Mortality of globally threatened Sarus Cranes *Grus antigon* from monocrotophos poisoning in India. *Science of the Total Environment*, *326*(1-3), 55-61. https://doi.org/10.1016/j.scitotenv.2003.12.004

217). Pam, A. A. (2015). Sorption Kinetics Study of Monocrotophos (MCP) Pesticide in Unsterilized Soil. *Am Chem Sci J*, *7*(3), 183-192. https://doi.org/10.9734/ACSj/2015/17495

218). PAN UK. (2001). Pesticide Action Network UK. A catalogue of lists of pesticides identifying those associated with particularly harmful health or environmental impacts. http://www.pan-uk.org

219). Pandey, B., Baghel, P. S., Shrivastava, S. (2014). To study the bioremediation of monocrotophos and to analyze the kinetics effect of Tween 80 on fungal growth. *Indo Amer J Pharm Res*, *4*, 925-930.

220). Parveen, Z., Khuhro, M. I., Rafiq, N. (2005). Monitoring of pesticide residues in vegetables (2000–2003) in Karachi, Pakistan. *Bulletin of environmental contamination and toxicology*, *74*(1), 170-176. https://doi.org/10.1007/s00128-004-0564-0

221). Patil, S. S., Jena, H. M., Susmita, M. (2018). Kinetic modeling and metabolite identification of dimethyl phthalate biodegradation by *Bacillus* sp. KS1 isolated from municipal wastewater contaminated soil. *Desalination and Water Treatment*, *102*, 349-358. https://doi.org/10.5004/dwt.2018.21795

222). Phale, P. S., Gautam, K., Sharma, A. (2020). Microbial Degradation of Pesticides in the Environment. *Microbes for Sustainable Development and Bioremediation*. Chapter 4, Boca Raton: CRC Press, https://doi.org/10.1201/9780429275876

223). Porto, A. L. M., Melgar, G. Z., Kasemodel, M. C., Nitschke, M. (2011). Biodegradation of pesticides. *Pesticides in the Modern World–Pesticides Use and Management, Stoytcheva M.(Ed.)//Tech*, *1*, 407-438.

224). PushpaMalini, T., Ramesh, A., Arthanareeswari, M., Kamaraj, P., Selvi, J. P. A. (2018). TiO_2 assisted photocatalytic decomposition of butachlor in aqueous solution, ground water and effluent. *Materials Today: Proceedings*, *5*(2), 8844-8851. https://doi.org/10.1016/j.matpr.2017.12.316

225). Qiao, C. L., Huang, J., Li, X., Shen, B. C., Zhang, J. L. (2003). Bioremediation of organophosphate pollutants by a genetically-engineered enzyme. *Bulletin of environmental contamination and toxicology*, *70*(3), 0455-0461. https://doi.org/10.1007/s00128-003-0008-2

226). Quesnel, D. M., Bhaskar, I. M., Gieg, L. M., Chua, G. (2011). Naphthenic acid biodegradation by the unicellular alga *Dunaliella tertiolecta*. *Chemosphere*, *84*(4), 504-511. https://doi.org/10.1016/j.chemosphere.2011.03.012

227). Ragnarsdottir, K. V. (2000). Environmental fate and toxicology of organophosphate pesticides. *Journal of the Geological Society*, *157*(4), 859-876. https://doi.org/10.1144/jgs.157.4.859

228). Rajput, V., Singh, S. K., Arpita, Kirti, Abhishek. (2012) Comparative toxicity of Butachlor, Imidacloprid and Sodium fluoride on protein profile of the walking cat fish *Clarias batrachus*. J Appl Pharm Sci 02(06):121–124

229). Rangaswamy, V., Venkateswarlu, K. (1992). Degradation of selected insecticides by bacteria isolated from soil. *Bulletin of environmental contamination and toxicology*, *49*(6), 797-804. https://doi.org/10.1007/BF00203150

230). Rani, K., Dhania, G. (2014). Bioremediation and Biodegradation of Pesticide from Contaminated Soil and Water - A Noval Approach. *International Journal of Current Microbiology and Applied Sciences*, *3*(10): 23-33.

231). Rao, C. H. S., Venkateswarlu, V., Surender, T., Eddleston, M., Buckley, N. A. (2005a). Pesticide poisoning in south India: opportunities for prevention and improved medical management. *Tropical Medicine & International Health*, *10*(6), 581-588. https://doi.org/10.1111/j.1365-3156.2005.01412.x

232). Rao, J. V., Kavitha, P. (2004). Toxicity of azodrin on the morphology and acetylcholinesterase activity of the earthworm *Eisenia foetida*. *Environmental research*, *96*(3), 323-327. https://doi.org/10.1016/j.envres.2004.02.014

233). Rao, J. V., Parvathi, K., Kavitha, P., Jakka, N. M., Pallela, R. (2005b). Effect of chlorpyrifos and monocrotophos on locomotor behaviour and acetylcholinesterase activity of subterranean termites, *Odontotermes obesus*. *Pest Management Science: formerly Pesticide Science*, *61*(4), 417-421. https://doi.org/10.1002/ps.986

234). Rasool, N., Reshi, Z. A., Shah, M. A. (2014). Effect of butachlor (G) on soil enzyme activity. *European journal of soil biology*, *61*, 94-100. https://doi.org/10.1016/j.ejsobi.2014.02.002

235). Raut, A. K., Kulshrestha, G. (1997). Biotransformation of butachlor by soil fungi. *Toxicological & Environmental Chemistry*, *61*(1-4), 109-116. https://doi.org/10.1080/02772249709358477

236). Raut, A. K., Kulshrestha, G., Chhonkar, P. K. (1997). Effect of butachlor on microbial soil populations in rice fields. *Toxicological & Environmental Chemistry*, *59*(1-4), 145-149. https://doi.org/10.1080/02772249709358431

237). Rawtani, D., Agrawal, Y. K., Prajapati, P. (2013). Interaction behavior of DNA with halloysite nanotube–silver nanoparticle-based composite. *BioNanoScience*, *3*(1), 73-78. https://doi.org/10.1007/s12668-012-0071-4

238). Rawtani, D., Khatri, N., Tyagi, S., Pandey, G. (2018). Nanotechnology-based recent approaches for sensing and remediation of pesticides. *Journal of environmental management*, *206*, 749-762. https://doi.org/10.1016/j.jenvman.2017.11.037

239). Reddy, J. D., Rao, N. B., Sultan, A. M. (2000). Insecticide residues in market samples of grape berries. *Pesto*, *16*(9), 17-22.

240). Revankar, P. R., Shyama, S. K. (2009). Genotoxic effects of monocrotophos, an organophosphorous pesticide, on an estuarine bivalve, *Meretrix ovum*. *Food and chemical Toxicology*, *47*(7), 1618-1623. https://doi.org/10.1016/j.fct.2009.04.010

241). Rodrigues, D. F., Sakata, S. K., Comasseto, J. V., Bicego, M. C., Pellizari, V. H. (2009). Diversity of hydrocarbon-degrading *Klebsiella* strains isolated from hydrocarbon-contaminated estuaries. *Journal of applied microbiology*, *106*(4), 1304-1314. https://doi.org/10.1111/j.1365-2672.2008.04097.x

242). Rosbero, T. M. S., Camacho, D. H. (2017). Green preparation and characterization of tentacle-like silver/copper nanoparticles for catalytic degradation of toxic chlorpyrifos in water. *Journal of environmental chemical engineering*, *5*(3), 2524-2532. https://doi.org/10.1016/j.jece.2017.05.009

243). Roy, A., Singh, S., Bajpai, J., Bajpai, A. (2014). Controlled pesticide release from biodegradable polymers. *Open Chemistry*, *12*(4), 453-469. https://doi.org/10.2478/s11532-013-0405-2

244). Rubinstein, M., Colby, R. H. (2003). Polymer Physics, Oxford University Press, Oxford.

245). Saha, S., Dutta, D., Karmakar, R., Ray, D. P. (2012). Structure–toxicity relationship of chloroacetanilide herbicides: relative impact on soil microorganisms. *Environmental Toxicology and Pharmacology*, *34*(2), 307-314. https://doi.org/10.1016/j.etap.2012.04.014

246). Saifuddin, N., Nian, C. Y., Zhan, L. W., Ning, K. X. (2011). Chitosan-silver nanoparticles composite as point-of-use drinking water filtration system for household to remove pesticides in water. *Asian Journal of Biochemistry*, *6*(2), 142-159. https://doi.org/10.3923/ajb.2011.142.159

247). Salim, C., Rajini, P. S. (2017). Glucose-rich diet aggravates monocrotophos-induced dopaminergic neuronal dysfunction in *Caenorhabditis elegans*. *Journal of Applied Toxicology*, *37*(6), 772-780. https://doi.org/10.1002/jat.3426

248). Samal, B., Kotiyal, P. B. (2013). Bioremediation of Monocrotophos and Malathion by *Bacillus* sp. *Environmental sustainability: concepts, principles, evidences and innovations*, 88-93.

249). San Román, I., Alonso, M. L., Bartolomé, L., Galdames, A., Goiti, E., Ocejo, M., Moragues, M., Alonso, R.M., Vilas, J. L. (2013). Relevance study of bare and coated zero valent iron nanoparticles for lindane degradation from its by-product monitorization. *Chemosphere*, *93*(7), 1324-1332. https://doi.org/10.1016/j.chemosphere.2013.07.050

250). Sankhwar, M. L., Yadav, R. S., Shukla, R. K., Singh, D., Ansari, R. W., Pant, A. B., Parmar, D., Khanna, V. K. (2016). Monocrotophos induced oxidative stress and alterations in brain dopamine and serotonin receptors in young rats. *Toxicology and Industrial Health*, *32*(3), 422-436. https://doi.org/10.1177/0748233713500834

251). Saraji, M., Jafari, M. T., Mossaddegh, M. (2016). Halloysite nanotubes-titanium dioxide as a solid-phase microextraction coating combined with negative corona discharge-ion mobility spectrometry for the determination of parathion. *Analytica chimica acta*, *926*, 55-62. https://doi.org/10.1016/j.aca.2016.04.034

252). Sawaya, W. N., Al-Awadhi, F. A., Saeed, T., Al-Omair, A., Ahmad, N., Husain, A., Khalafawi, S., Al-Zenki, S., Al-Amiri, H., Al-Otaibi, J., Al-Saqer, J. (1999). Dietary intake of pesticides: State of Kuwait total diet study. *Food Additives & Contaminants*, *16*(11), 473-480. https://doi.org/10.1080/026520399283768

253). Schuler, J. F., Held, H. J. (1964). Soil stability of C1414. Ciba-Geigy-Report of 5 November 1964.

254). Shahriari, T., Bidhendi, G. N., Mehrdadi, N., Torabian, A. (2014). Effective parameters for the adsorption of chromium (III) onto iron oxide magnetic nanoparticle. *International Journal of Environmental Science and Technology*, *11*(2), 349-356. https://doi.org/10.1007/s13762-013-0315-z

255). Sharma, A. K., Tiwari, R. K., Gaur, M. S. (2016). Nanophotocatalytic UV degradation system for organophosphorus pesticides in water samples and analysis by Kubista model. *Arabian journal of chemistry*, *9*, S1755-S1764. https://doi.org/10.1016/j.arabjc.2012.04.044

256). Sharma, A., Gill, J. P. S., Bedi, J. S. (2015). Monitoring of pesticide residues in human blood from Punjab, India. *Bulletin of environmental contamination and toxicology*, *94*(5), 640-646. https://doi.org/10.1007/s00128-015-1522-8

257). Sharma, A., Gill, J. P. S., Bedi, J. S., Pooni, P. A. (2014). Monitoring of pesticide residues in human breast milk from Punjab, India and its correlation with health associated parameters. *Bulletin of environmental contamination and toxicology*, *93*(4), 465-471. https://doi.org/10.1007/s00128-014-1326-2

258). Sharma, A., Kumar, V., Kohli, S. K., Kaur, R., Kaur, T., Arora, S., Thukral, A. K., Bhardwaj, R. (2020). Pesticide Metabolism in Plants, Insects, Soil Microbes and Fishes: An Overview. *Pesticides in Crop Production: Physiological and Biochemical Action*, 35-53. https://doi.org/10.1002/9781119432241.ch3

259). Sharma, G., Kumar, A., Naushad, M., García-Peñas, A., Ala'a, H., Ghfar, A. A., Sharma, V., Ahamad, T., Stadler, F. J. (2018). Fabrication and characterization of Gum arabic-cl-poly (acrylamide) nanohydrogel for effective adsorption of crystal violet dye. *Carbohydrate polymers*, *202*, 444-453. https://doi.org/10.1016/j.carbpol.2018.09.004

260). Sharma, G., Naushad, M., Ala'a, H., Kumar, A., Khan, M. R., Kalia, S., Shweta., Bala, M., Sharma, A. (2017). Fabrication and characterization of chitosan-crosslinked-poly (alginic acid) nanohydrogel for adsorptive removal of Cr (VI) metal ion from aqueous medium. *International journal of biological macromolecules*, *95*, 484-493. https://doi.org/10.1016/j.ijbiomac.2016.11.072

261). Shen, W., Mu, Y., Wang, B., Ai, Z., Zhang, L. (2017). Enhanced aerobic degradation of 4-chlorophenol with iron-nickel nanoparticles. *Applied Surface Science*, *393*, 316-324. https://doi.org/10.1016/j.apsusc.2016.10.020

262). Siangproh, W., Somboonsuk, T., Chailapakul, O., Songsrirote, K. (2017). Novel colorimetric assay for paraquat detection on-silica bead using negatively charged silver nanoparticles. *Talanta*, *174*, 448-453. https://doi.org/10.1016/j.talanta.2017.06.045

263). Siddiqui, M. K. J., Rahman, M. F., Mustafa, M. (1993). Target enzyme inhibition by novel thion analogues of monocrotophos: an acute in vivo study in the rat. *Bulletin of environmental contamination and toxicology*, *51*(3), 409-415. https://doi.org/10.1007/BF00201760

264). Siddiqui, M. K. J., Rahman, M. F., Mustafa, M. Bhalerao, U. T. (1991). A comparative study of blood changes and brain acetylcholinesterase inhibition by monocrotophos and its analogues in rats. *Ecotoxicology and environmental safety*, *21*(3), 283-289. https://doi.org/10.1016/0147-6513(91)90067-Y

265). Sidhu, P. K., Dhanjal, N. I. K., Cameotra, S. S., Sud, D. (2015). Persistence and biodegradation of monocrotophos using soil microbes. *Desalination and Water Treatment*, *54*(8), 2293-2298. https://doi.org/10.1080/19443994.2014.899516

266). Singh, B. K., Walker, A. (2006). Microbial degradation of organophosphorus compounds. *FEMS microbiology reviews*, *30*(3), 428-471. https://doi.org/10.1111/j.1574-6976.2006.00018.x

267). Singh, D. P., Khattar, J. S., Alka, G. K., Singh, Y. (2016). Toxicological effect of pretilachlor on some physiological processes of cyanobacterium *Synechocystis* sp. strain PUPCCC 64. *Journal of Applied Biology & Biotechnology Vol*, *4*(01), 012-019. https://doi.org/10.7324/JABB.2016.40103

268). Singh, J., Nandabalan, Y. K. (2018). Prospecting *Ammoniphilus* sp. JF isolated from agricultural fields for butachlor degradation. *3 Biotech*, *8*(3), 164. https://doi.org/10.1007/s13205-018-1165-7

269). Sogorb, M. A., Vilanova, E. (2002). Enzymes involved in the detoxification of organophosphorus, carbamate and pyrethroid insecticides through hydrolysis. *Toxicology letters*, *128*(1-3), 215-228. https://doi.org/10.1016/S0378-4274(01)00543-4

270). Sood, A., Pabbi, S., Uniyal, P. L. (2011). Effects of paraquat on lipid peroxidation and antioxidant enzymes in aquatic fern *Azolla microphylla*. *Russian Journal of Plant Physiology*, *58*(4), 667-673. https://doi.org/10.1134/S1021443711040170

271). Srinivasulu, M., Nilanjan, P. C., Chakravarthi, B. V. S. K., Jayabaskaran, C., Jaffer, M. G., Naga, R. M., Manjunatha, B., Darwin, R. O., Juan, O. T., Rangaswamy, V. (2017). Biodegradation of monocrotophos by bacteria isolated from soil. *African Journal of Biotechnology*, *16*(9), 408-417. https://doi.org/10.5897/AJB2015.14885

272). Subhas, Singh, D. K. (2003). Utilization of monocrotophos as phosphorus source by *Pseudomonas aeruginosa* F10B and *Clavibacter michiganense* subsp. *insidiosum* SBL 11. *Canadian journal of microbiology*, *49*(2), 101-109. https://doi.org/10.1139/w03-013

273). Subramanian, G., Sekar, S., Sampoornam, S. (1994). Biodegradation and utilization of organophosphorus pesticides by cyanobacteria. *International biodeterioration & biodegradation*, *33*(2), 129-143. https://doi.org/10.1016/0964-8305(94)90032-9

274). Sun, L., Liu, H., Gao, X., Chen, W., Huang, K., Zhang, S. (2018). Isolation of monocrotophos-degrading strain *Sphingobium* sp. YW16 and cloning of its TnopdA. *Environmental Science and Pollution Research*, *25*(5), 4942-4950. https://doi.org/10.1007/s11356-017-0718-3

275). Sun, L., Zhu, S., Yang, Z., Chen, Q., Liu, H., Zhang, J., Hu, G., Li, S., Hong, Q. (2016). Degradation of monocrotophos by *Starkeya novella* YW6 isolated from paddy soil. *Environmental Science and Pollution Research*, *23*(4), 3727-3735. https://doi.org/10.1007/s11356-015-5606-0

276). Sun, X. F., Wang, S. G., Liu, X. W., Gong, W. X., Bao, N., Ma, Y. (2008). The effects of pH and ionic strength on fulvic acid uptake by chitosan hydrogel beads. *Colloids and Surfaces A: Physicochemical and Engineering Aspects*, *324*(1-3), 28-34. https://doi.org/10.1016/j.colsurfa.2008.03.023

277). Swann, R. L., Laskowski, D. A., McCall, P. J., Vander Kuy, K., Dishburger, H. J. (1983). A rapid method for the estimation of the environmental parameters octanol/water partition coefficient, soil sorption constant, water to air ratio, and water solubility. In *Residue reviews, 85,* 17–28. Springer, New York, NY.

278). Tariq, M. I., Afzal, S., Hussain, I. (2004). Pesticides in shallow groundwater of bahawalnagar, Muzafargarh, DG Khan and Rajan Pur districts of Punjab, Pakistan. *Environment International*, *30*(4), 471-479. https://doi.org/10.1016/j.envint.2003.09.008

279). Thirugnanam, J., Senthilkumar, R. (2016). Degradation of Pesticide by Using Geofungi from Thanjavur District. *Ijsrm.Human*, *4*(3), 225-230.

280). Thomé, A., Reddy, K. R., Reginatto, C., Cecchin, I. (2015). Review of nanotechnology for soil and groundwater remediation: Brazilian perspectives. *Water, Air, & Soil Pollution*, *226*(4), 121. https://doi.org/10.1007/s11270-014-2243-z

281). Tian, H., Li, J., Mu, Z., Li, L., Hao, Z. (2009b). Effect of pH on DDT degradation in aqueous solution using bimetallic Ni/Fe nanoparticles. *Separation and Purification Technology*, *66*(1), 84-89. https://doi.org/10.1016/j.seppur.2008.11.018

282). Tian, H., Li, Y., Wang, W., Wu, P., Ru, S. (2012). Exposure to monocrotophos pesticide during sexual development causes the feminization/demasculinization of the reproductive traits and a reduction in the reproductive success of male guppies (*Poecilia reticulata*). *Toxicology and applied pharmacology*, *263*(2), 163-170. https://doi.org/10.1016/j.taap.2012.06.006

283). Tian, H., Ru, S., Bing, X., Wang, W. (2010). Effects of monocrotophos on the reproductive axis in the male goldfish (*Carassius auratus*): Potential mechanisms underlying vitellogenin induction. *Aquatic toxicology*, *98*(1), 67-73. https://doi.org/10.1016/j.aquatox.2010.01.011

284). Tian, H., Ru, S., Wang, Z., Cai, W., Wang, W. (2009a). Estrogenic effects of monocrotophos evaluated by vitellogenin mRNA and protein induction in male goldfish (*Carassius auratus*). *Comparative Biochemistry and Physiology Part C: Toxicology & Pharmacology*, *150*(2), 231-236. https://doi.org/10.1016/j.cbpc.2009.04.014

285). Tomlin, C. (1994). The Pesticide Manual, British Crop Protection Council. Farnham, Surrey, UK, 1250

286). Tripathi, V. K., Kumar, V., Pandey, A., Vatsa, P., Dhasmana, A., Singh, R. P., Appikonda, S. H. C., Hwang, I., Lohani, M. (2017). Monocrotophos induces the expression of xenobiotic metabolizing cytochrome P450s (CYP2C8 and CYP3A4) and

neurotoxicity in human brain cells. *Molecular neurobiology*, *54*(5), 3633-3651. https://doi.org/10.1007/s12035-016-9938-7

287). Tsoufis, T., Katsaros, F., Kooi, B. J., Bletsa, E., Papageorgiou, S., Deligiannakis, Y., Panagiotopoulos, I. (2017). Halloysite nanotube-magnetic iron oxide nanoparticle hybrids for the rapid catalytic decomposition of pentachlorophenol. *Chemical Engineering Journal*, *313*, 466-474. https://doi.org/10.1016/j.cej.2016.12.056

288). Tu, W., Niu, L., Liu, W., Xu, C. (2013). Embryonic exposure to butachlor in zebrafish (*Danio rerio*): endocrine disruption, developmental toxicity and immunotoxicity. *Ecotoxicology and environmental safety*, *89*, 189-195. https://doi.org/10.1016/j.ecoenv.2012.11.031

289). Vaishampayan, A. (1985). Mutagenic activity of alachlor, butachlor and carbaryl to a N_2-fixing cyanobacterium *Nostoc muscorum*. *The Journal of Agricultural Science*, *104*(3), 571-576. https://doi.org/10.1017/S0021859600044336

290). Vandana, P., Rai, L. C. (2002). Interactive effects of UV-B and pesticides on photosynthesis and nitrogen fixation of *Anabaena doliolum*. *Journal of microbiology and biotechnology*, *12*(3), 423-430.

291). Velmurugan, B., Selvanayagam, M., Cengiz, E. I., Unlu, E. (2007). The effects of monocrotophos to different tissues of freshwater fish *Cirrhinus mrigala*. *Bulletin of Environmental Contamination and Toxicology*, *78*(6), 450-454. https://doi.org/10.1007/s00128-007-9190-y

292). Velmurugan, G., Babu, D. V., Ramasamy, S. (2013). Prolonged monocrotophos intake induces cardiac oxidative stress and myocardial damage in rats. *Toxicology*, *307*, 103-108. https://doi.org/10.1016/j.tox.2012.11.022

293). Verma, J. P., Jaiswal, D. K., Sagar, R. (2014). Pesticide relevance and their microbial degradation: a-state-of-art. *Reviews in Environmental Science and Bio/Technology*, *13*, 429–466. https://doi.org/10.1007/s11157-014-9341-7

294). Verma, S., Saxena, J., Prasanna, R., Sharma, V., Nain, L. (2012). Medium optimization for a novel crude-oil degrading lipase from *Pseudomonas aeruginosa* SL-72 using statistical approaches for bioremediation of crude-oil. *Biocatalysis and Agricultural Biotechnology*, *1*(4), 321-329. https://doi.org/10.1016/j.bcab.2012.07.002

295). Vilela, P. B., Dalalibera, A., Duminelli, E. C., Becegato, V. A., Paulino, A. T. (2019). Adsorption and removal of chromium (VI) contained in aqueous solutions using a chitosan-based hydrogel. *Environmental Science and Pollution Research*, *26*(28), 28481-28489. https://doi.org/10.1007/s11356-018-3208-3

296). Vimala, K., Yallapu, M. M., Varaprasad, K., Reddy, N. N., Ravindra, S., Naidu, N. S., Raju, K. M. (2011). Fabrication of curcumin encapsulated chitosan-PVA silver nanocomposite films for improved antimicrobial activity. *Journal of Biomaterials and Nanobiotechnology*, *2*(01), 55. https://doi.org/10.4236/jbnb.2011.21008

297). Wang, C. B., Zhang, W. X. (1997). Synthesizing nanoscale iron particles for rapid and complete dechlorination of TCE and PCBs. *Environmental science & technology*, *31*(7), 2154-2156. https://doi.org/10.1021/es970039c

298). Wang, J., Lu, Y., Shen, G. (2007). Combined effects of cadmium and butachlor on soil enzyme activities and microbial community structure. *Environmental Geology*, *51*(7), 1221-1228. https://doi.org/10.1007/s00254-006-0414-y

299). Wang, S., Li, H., Lin, C. (2013a). Physiological, biochemical and growth responses of Italian ryegrass to butachlor exposure. *Pesticide biochemistry and physiology*, *106*(1-2), 21-27. https://doi.org/10.1016/j.pestbp.2013.03.007

300). Wang, T., Gunasekaran, S. (2006). State of water in chitosan–PVA hydrogel. *Journal of applied polymer science*, *101*(5), 3227-3232. https://doi.org/10.1002/app.23526

301). Wang, W.D., Niu, J.L., Cui, Z.J. (2005). Biodegradation of pesticides: a review. *Journal of heilongjiang august first land reclamation university*, 17(2):18.

302). Wang, X., Mu, Z., Shangguan, F., Liu, R., Pu, Y., Yin, L. (2013b). Simultaneous detection of fenitrothion and chlorpyrifos-methyl with a photonic suspension array. *PloS one*, *8*(6), e66703. https://doi.org/10.1371/journal.pone.0066703

303). Wu, M., Wang, L., Zeng, B., Zhao, F. (2016). Ionic liquid polymer functionalized carbon nanotubes-doped poly (3, 4-ethylenedioxythiophene) for highly-efficient solid-phase microextraction of carbamate pesticides. *Journal of Chromatography A*, *1444*, 42-49. https://doi.org/10.1016/j.chroma.2016.03.074

304). Wu, S., Hu, H., Lin, Y., Zhang, J., Hu, Y. H. (2020). Visible light photocatalytic degradation of tetracycline over TiO_2. *Chemical Engineering Journal*, *382*, 122842. https://doi.org/10.1016/j.cej.2019.122842

305). Wu, S., Li, D., Wang, J., Zhao, Y., Dong, S., Wang, X. (2017). Gold nanoparticles dissolution based colorimetric method for highly sensitive detection of organophosphate pesticides. *Sensors and Actuators B: Chemical*, *238*, 427-433. https://doi.org/10.1016/j.snb.2016.07.067

306). Xu, C., Ding, J., Qiu, J., Ma, Y. (2013). Biodegradation of acetochlor by a newly isolated *Achromobacter* sp. strain D-12. *Journal of Environmental Science and Health, Part B*, *48*(11), 960-966. https://doi.org/10.1080/03601234.2013.816601

307). Xu, D., Xu, Z., Zhu, S., Cao, Y., Wang, Y., Du, X., Gu, Q., Li, F. (2005). Adsorption behaviour of herbicide on typical soils in China and humic acids from soil samples. *J Colloid Interface Sci*, *285*(1), 27–32. https://doi.org/10.1016/j.jcis.2004.11.034

308). Yadav, M., Shukla, A. K., Srivastva, N., Upadhyay, S. N., Dubey, S. K. (2016). Utilization of microbial community potential for removal of chlorpyrifos: a review. *Critical reviews in biotechnology*, *36*(4), 727-742. https://doi.org/10.3109/07388551.2015.1015958

309). Yaduvanshi, S. K., Ojha, A., Pant, S. C., Lomash, V., Srivastava, N. (2010). Monocrotophos induced lipid peroxidation and oxidative DNA damage in rat tissues. *Pesticide biochemistry and physiology*, *97*(3), 214-222. https://doi.org/10.1016/j.pestbp.2010.02.004

310). Yang, C., Wang, M., Li, J. (2012). Influence of rhizosphere microbial ecophysiological parameters from different plant species on butachlor degradation in a riparian soil. *Journal of environmental quality*, *41*(3), 716-723. https://doi.org/10.2134/jeq2011.0223

311). Yang, J. M., Su, W. Y., Yang, M. C. (2004). Evaluation of chitosan/PVA blended hydrogel membranes. *Journal of Membrane Science*, *236*(1-2), 39-51. https://doi.org/10.1016/j.memsci.2004.02.005

312). Yang, X. B., Ying, G. G., Kookana, R. S. (2010). Rapid multiresidue determination for currently used pesticides in agricultural drainage waters and soils using gas chromatography–mass spectrometry. *Journal of Environmental Science and Health Part B*, *45*(2), 152-161. https://doi.org/10.1080/03601230903472165

313). Yang, Y., Wu, N., Wang, C. (2018). Toxicity of the pyrethroid bifenthrin insecticide. *Environmental Chemistry Letters*, *16*(4), 1377-1391. https://doi.org/10.1007/s10311-018-0765-0

314). Yu, B., Zeng, J., Gong, L., Yang, X., Zhang, L., Chen, X. (2008). Photocatalytic degradation investigation of dicofol. *Chinese Science Bulletin*, *53*(1), 27-32. https://doi.org/10.1007/s11434-007-0482-8

315). Yu, Y. L., Chen, Y. X., Luo, Y. M., Pan, X. D., He, Y. F., Wong, M. H. (2003). Rapid degradation of butachlor in wheat rhizosphere soil. *Chemosphere*, *50*(6), 771-774. https://doi.org/10.1016/S0045-6535(02)00218-7

316). Zahran, M. M., Abdel-Aziz, K. B., Abdel-Raof, A., Nahas, E. M. (2005). The effect of subacute doses of organophosphorus pesticide, Nuvacron, on the biochemical and cytogenetic parameters of mice and their embryos. *Res J Agricul Biol Scien*, *1*, 277-283.

317). Zargar, M. Y., Dar, G. H. (1990). Effect of benthiocarb and butachlor on growth and nitrogen fixation by cyanobacteria. *Bulletin of environmental contamination and toxicology*, *45*(2), 232-234. https://doi.org/10.1007/BF01700189

318). Zeng, H., Fisher, B., Giammar, D. E. (2008). Individual and competitive adsorption of arsenate and phosphate to a high-surface-area iron oxide-based sorbent. *Environmental science & technology*, *42*(1), 147-152. https://doi.org/10.1021/es071553d

319). Zeng, X., McCarthy, D. T., Deletic, A., Zhang, X. (2015). Silver/reduced graphene oxide hydrogel as novel bactericidal filter for point-of-use water disinfection. *Advanced Functional Materials*, *25*(27), 4344-4351. https://doi.org/10.1002/adfm.201501454

320). Zhang, J., Zheng, J. W., Liang, B., Wang, C. H., Cai, S., Ni, Y. Y., He, J., Li, S. P. (2011). Biodegradation of chloroacetamide herbicides by *Paracoccus* sp. FLY-8 in

vitro. *Journal of agricultural and food chemistry*, *59*(9), 4614-4621. https://doi.org/10.1021/jf104695g

321). Zhang, L., Li, B., Meng, X., Huang, L., Wang, D. (2015). Degradation of four organophosphorous pesticides catalyzed by chitosan-metal coordination complexes. *Environmental Science and Pollution Research*, *22*(19), 15104-15112. https://doi.org/10.1007/s11356-015-4669-2

322). Zhang, W., Zhang, D., Liang, Y. (2019). Nanotechnology in remediation of water contaminated by poly-and perfluoroalkyl substances: A review. *Environmental Pollution*, *247*, 266-276. https://doi.org/10.1016/j.envpol.2019.01.045

323). Zhang, X., Li, S., Wang, C., Tian, H., Wang, W., Ru, S. (2017). Effects of monocrotophos pesticide on cholinergic and dopaminergic neurotransmitter systems during early development in the sea urchin *Hemicentrotus pulcherrimus*. *Toxicology and Applied Pharmacology*, *328*, 46-53. https://doi.org/10.1016/j.taap.2017.05.003

324). Zhao, X. H., Wang, J. (2012). A brief study on the degradation kinetics of seven organophosphorus pesticides in skimmed milk cultured with *Lactobacillus* spp. at 42 °C. *Food chemistry*, *131*(1), 300-304. https://doi.org/10.1016/j.foodchem.2011.08.046

325). Zheng, J., Li, R., Zhu, J., Zhang, J., He, J., Li, S., Jiang, J. (2012). Degradation of the chloroacetamide herbicide butachlor by *Catellibacterium caeni* sp. nov DCA-1T. *International Biodeterioration & Biodegradation*, *73*, 16-22. https://doi.org/10.1016/j.ibiod.2012.06.003

326). Zhou, L., He, B., Huang, J. (2013). One-step synthesis of robust amine-and vinyl-capped magnetic iron oxide nanoparticles for polymer grafting, dye adsorption, and catalysis. *ACS Applied Materials & Interfaces*, *5*(17), 8678-8685. https://doi.org/10.1021/am402334f

327). Zhu, D., Kwon, S., Pignatello, J. J. (2005). Adsorption of single-ring organic compounds to wood charcoals prepared under different thermochemical conditions. *Environmental science & technology*, *39*(11), 3990-3998. https://doi.org/10.1021/es050129e

328). Zhu, L., Li, W., Zha, J., Wang, M., Yuan, L., Wang, Z. (2014). Butachlor causes disruption of HPG and HPT axes in adult female rare minnow (*Gobiocypris rarus*). *Chemico-biological interactions*, *221*, 119-126. https://doi.org/10.1016/j.cbi.2014.07.016

LIST OF PUBLICATIONS

Publications (accepted and published)

1. **Kaur, R**., & Goyal, D. (2019). Toxicity and degradation of the insecticide monocrotophos. *Environmental Chemistry Letters*, 17, 1299-1324. DOI 10.1007/s10311-019-00884-y (SCI, IF – 9.027).
2. **Kaur, R**., & Goyal, D. (2020). Biodegradation of Butachlor by *Bacillus altitudinis* and Identification of Metabolites. *Current Microbiology*, **77**, 2602–2612. DOI: 10.1007/s00284-020-02031-1 (SCI, IF- 2.188).
3. **Kaur, R**., & Goyal, D. Chitosan/PVA silver nanocomposite for butachlor removal: Fabrication, characterization, adsorption mechanism and isotherms. *Carbohydrate polymer*, 262, Article no 117906. DOI: 10.1016/j.carbpol.2021.117906 (SCI, IF – 9.381)

Manuscripts communicated

1. **Kaur, R**., & Goyal, D. Chitosan/PVA silver nanocomposite for butachlor removal: Photocatalytic degradation, pathway and kinetics. (*Materials Letters;* manuscript number MLBLUE-D-21-02720).

Conferences attended

1. International Conference on Nanoscience and Technology (ICONSAT Pune) 29 Feb – 02 March 2016.

2. Association of microbiologists of India (AMI Hyderabad) 09 - 12 Dec, 2018. Screening of bacterial isolates for degradation of herbicide butachlor

APPENDIX I

A. NUTRIENT BROTH

Ingredients	Quantity (g/L)
Peptic digest of animal tissue	5
Sodium chloride	5
Beef extract	1.5
Yeast extract	1.5

B. NUTRIENT AGAR

Ingredients	Quantity (g/L)
Peptic digest of animal tissue	5
Sodium chloride	5
Beef extract	1.5
Yeast extract	1.5
Agar	15

C. MUELLER HINTON AGAR

Ingredients	Quantity (g/L)
HM infusion B (Equivalent to Beef infusion)	300.00
Acicase (Equivalent to Casein acid hydrolysate)	17.50
Starch	1.500
Agar	17.000
Final pH (at 25°C)	7.3±0.1

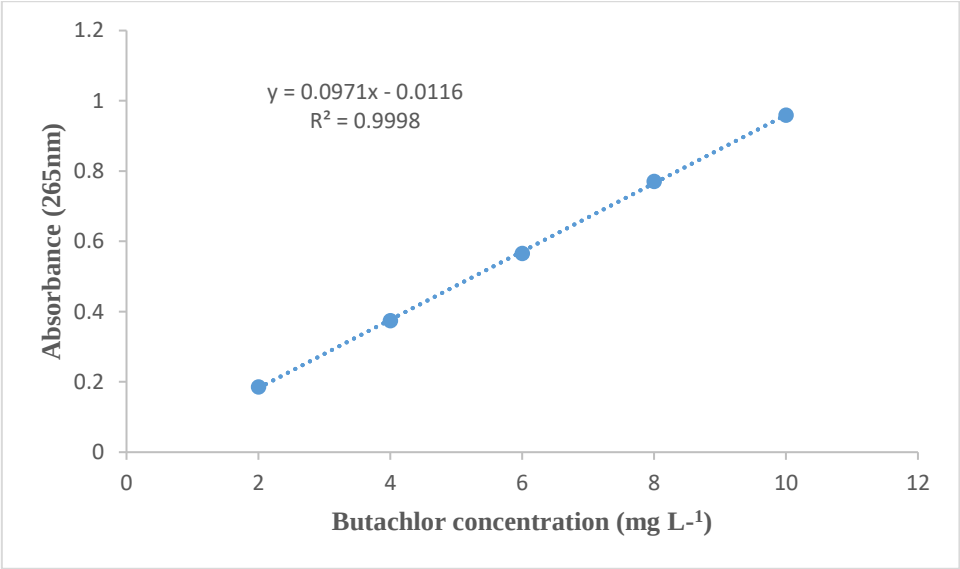
D. BUSHNELL HASS BROTH

Ingredients	Quantity (g/L)
Magnesium sulphate	0.200
Calcium chloride	0.020
Monopotassium phosphate	1.000
Dipotassium phosphate	1.000
Ammonium nitrate	1.000
Ferric chloride	0.050
Final pH (at 25°C)	7.0±0.2

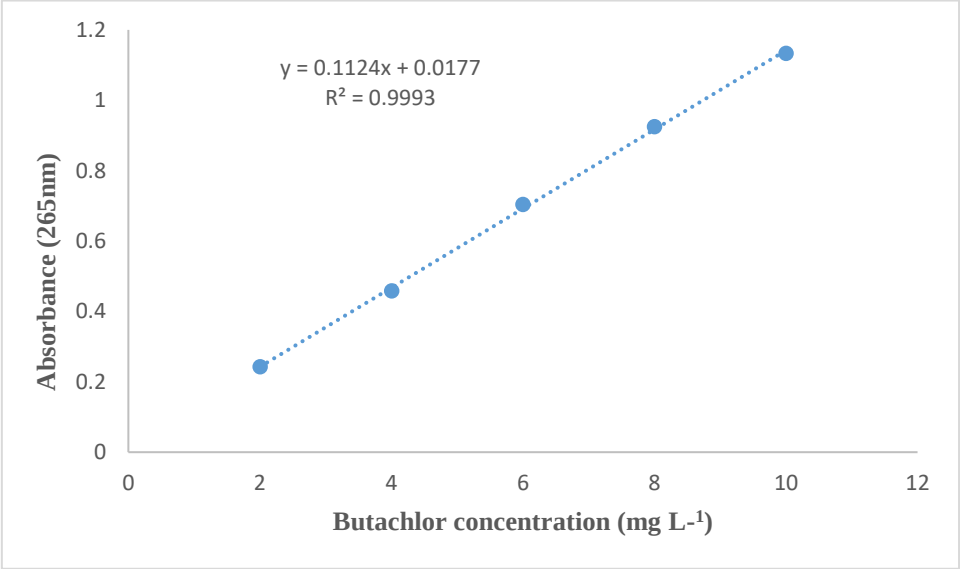
E. AQUA REGIA

Ingredients	parts
Nitric acid	1
Hydrochloric acid	3

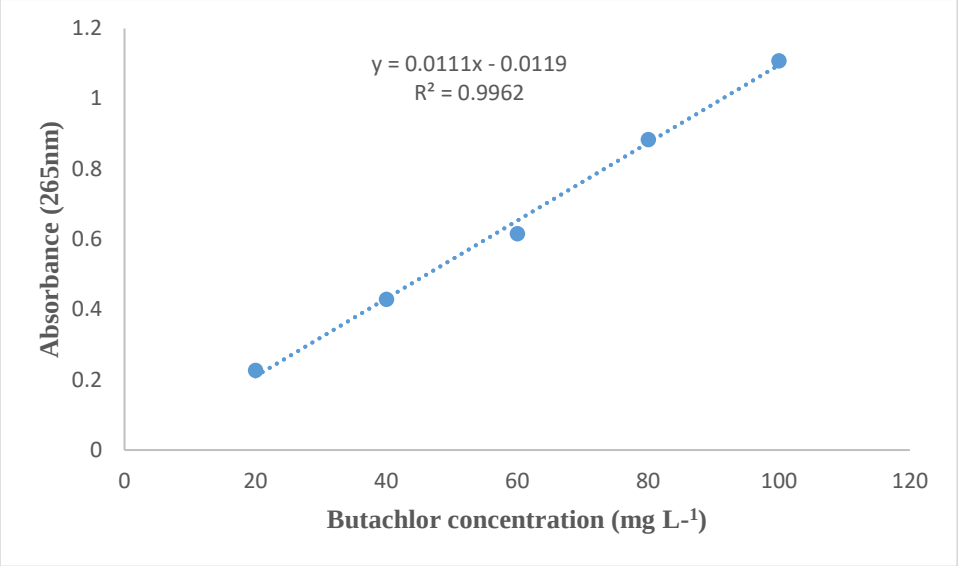
APPENDIX II



A. Standard curve of Butachlor made in Bushnell Haas broth



B. Standard curve of Butachlor made in deionized water



C. Standard curve of Butachlor made in deionized water (Higher concentrations diluted ten fold)

APPENDIX III

Bacillus altitudinis strain A16 16S ribosomal RNA gene, partial sequence

GenBank: MN595198.1

FASTA Graphics

Go to:

```
LOCUS       MN595198                1450 bp    DNA     linear   BCT 01-DEC-
2019
DEFINITION  Bacillus altitudinis strain A16 16S ribosomal RNA gene, partial
            sequence.
ACCESSION   MN595198
VERSION     MN595198.1
KEYWORDS    .
SOURCE      Bacillus altitudinis (Bacillus invictae)
  ORGANISM  Bacillus altitudinis
            Bacteria; Firmicutes; Bacilli; Bacillales; Bacillaceae;
Bacillus.
REFERENCE   1  (bases 1 to 1450)
  AUTHORS   Kaur,R. and Goyal,D.
  TITLE     Degradation of butachlor by Bacillus altitudinis: Kinetics and
            identification of metabolites
  JOURNAL   Unpublished
REFERENCE   2  (bases 1 to 1450)
  AUTHORS   Kaur,R. and Goyal,D.
  TITLE     Direct Submission
  JOURNAL   Submitted (22-OCT-2019) Biotechnology, Thapar Institute of
            Engineering and Technology, Bhadson Road, Patiala, Punjab
147004,
            India
COMMENT     ##Assembly-Data-START##
            Sequencing Technology :: Sanger dideoxy sequencing
            ##Assembly-Data-END##
FEATURES             Location/Qualifiers
     source          1..1450
                     /organism="Bacillus altitudinis"
                     /mol_type="genomic DNA"
                     /strain="A16"
                     /isolation_source="agricultural soil"
                     /db_xref="taxon:293387"
```

```
                     /country="India"
                     /lat_lon="30.3530 N 76.3710 E"
                     /collected_by="Ravneet Kaur"
                     /identified_by="Ravneet Kaur"
                     /PCR_primers="fwd_name: 27F, fwd_seq:
                     agagtttgatcctggctcag, rev_name: 1492R, rev_seq:
                     tacggctaccttgttacgactt"
     rRNA            <1..>1450
                     /product="16S ribosomal RNA"
ORIGIN
        1 gggggctata catgcaagtc gagcggacag aagggagctt gctcccggat gttagcggcg
       61 gacgggtgag taacacgtgg gtaacctgcc tgtaagactg ggataactcc gggaaaccgg
      121 agctaatacc ggatagttcc ttgaaccgca tggttcaagg atgaaagacg gtttcggctg
      181 tcacttacag atggacccgc ggcgcattag ctagttggtg aggtaacggc tcaccaaggc
      241 gacgatgcgt agccgacctg agagggtgat cggccacact gggactgaga cacggcccag
      301 actcctacgg gaggcagcag tagggaatct tccgcaatgg acgaaagtct tgacggagca
      361 acgcccgcgt gagtgatgaa ggtttttcgg atcgtaaagc tctgttgtta gggaagaaca
      421 agtgcaagag taactgcttg caccttgacg gtacctaacc agaaagccac ggctaactac
      481 gtgccagcag ccgcggtaat acgtaggtgg caagcgttgt ccggaattat tgggcgtaaa
      541 gggctcgcag gcggtttctt aagtctgatg tgaaagcccc cggctcaacc ggggagggtc
      601 attggaaact gggaaacttg agtgcagaag aggagagtgg aattccacgt gtagcggtga
      661 aatgcgtaga gatgtggagg aacaccagtg gcgaaggcga ctctctggtc tgtaactgac
      721 gctgaggagc gaaagcgtgg ggagcgaaca ggattagata ccctggtagt ccacgccgta
      781 aacgatgagt gctaagtgtt aggggtttc cgcccccttag tgctgcagct aacgcattaa
      841 gcactccgcc tggggagtac ggtcgcaaga ctgaaactca aaggaattga cgggggcccg
      901 cacaagcggt ggagcatgtg gtttaattcg aagcaacgcg aagaacctta ccaggtcttg
      961 acatcctctg acaaccctag agatagggct ttcccttcgg ggacagagtg acaggtggtg
     1021 catggttgtc gtcagctcgt gtcgtgagat gttgggttaa gtcccgcaac gagcgcaacc
     1081 cttgatctta gttgccagca ttcagttggg cactctaagg tgactgccgg tgacaaaccg
     1141 gaggaaggtg gggatgacgt caaatcatca tgccccttat gacctgggct acacacgtgc
     1201 tacaatggac agaacaaagg gctgcgagac cgcaaggttt agccaatccc acaaatctgt
     1261 tctcagttcg gatcgcagtc tgcaactcga ctgcgtgaag ctggaatcgc tagtaatcgc
     1321 ggatcagcat gccgcggtga atacgttccc gggccttgta cacaccgccc gtcacaccac
     1381 gagagtttgc aacacccgaa gtcggtgagg taacctttat ggagccagcc gccgaaggtg
     1441 gcagaatgtg
//
```

Environmental Chemistry Letters (2019) 17:1299–1324
https://doi.org/10.1007/s10311-019-00884-y

REVIEW

Toxicity and degradation of the insecticide monocrotophos

Ravneet Kaur[1] · **Dinesh Goyal**[1]

Received: 18 January 2019 / Accepted: 11 April 2019 / Published online: 24 April 2019
© Springer Nature Switzerland AG 2019

Abstract
Monocrotophos, commonly named Azodrin or Nuvacron, is an organophosphate insecticide, which in spite of ban is preferred due to its high efficacy against insect pests. With a field application dose of 0.25–1.5 kg ha^{-1}, it has median lethal dose (LD_{50}) of 18–20 mg kg^{-1} for mammals and half-life of 17–96 days. Monocrotophos uncontrolled application in farming has led to the contamination of surface and groundwater, causing neurotoxicity, genotoxicity, hyperglycaemic and stressogenic effects on different organisms. Being readily soluble in water, it is grouped under class I: highly toxic compounds. Microbes such as *Bacillus*, *Pseudomonas*, *Aspergillus*, *Anabaena* and *Nostoc* at 25–37 °C and pH 5.5–8.5 have the ability to utilize monocrotophos as nutrient source and can tolerate up to 500–1200 mg L^{-1} of monocrotophos, causing its complete or partial degradation to dimethyl phosphate, phosphoric acid, valeric or acetic acid. On the other hand, generation of ·OH radicals by photoactivation of the catalyst such as TiO_2 and ZnO leads to complete mineralization of monocrotophos. Biodegradation followed by photocatalytic degradation would be the most efficient and sustainable approach. This review focuses on toxicity, fate of monocrotophos in the environment and its microbial and photocatalytic degradation.

Keywords Monocrotophos · Azodrin · Biodegradation · Organophosphate · Photocatalytic · Microbial

Introduction

Organophosphorus compounds have been extensively used in agriculture worldwide for more than 40 years due to their high effectiveness (Karpouzas and Singh 2006; Abraham and Silambarasan 2015), broad-spectrum action against various pests and biodegradability. They account for approximately 34% of total world insecticide market (Singh and Walker 2006) and are used in agriculture to combat crop pests, in domestic to control mosquitoes and other insects and in veterinary to control mites and flies of cattle. Out of the total applied pesticide, approximately 0.1% reaches its target, rest remains in the environment, resulting in reduction in crop yield, poor agricultural products, worsening soil quality and soil enzyme activity (Riah et al. 2014), water pollution, consequently posing harmful threat to animals and humans (Yadav et al. 2016; Buvaneswari et al. 2017). Although organophosphates are biodegradable, their environmental exposure causes acute and chronic toxicity to mammals and other non-target organisms (Gill et al. 2018). In humans, organophosphate poisoning may cause general weakness, salivation, vomiting, nausea, diarrhoea, tremors and respiratory failure in severe cases, causing death (Kanekar et al. 2004). Annual data estimates of various developing countries indicate that organophosphates are responsible for 3 million poisonings with 200,000 human deaths (Ragnarsdottir 2000; Karpouzas and Singh 2006).

Organophosphorus pesticides were first introduced during the World War II in Germany, in the form of tetraethyl pyrophosphate as a by-product of nerve gas development (Kanekar et al. 2004). They are thiols or esters of phosphinic, phosphonic, phosphoric or phosphoramidic acid. Chemically, organophosphates have aryl or alkyl group (R_1 and R_2), which are bonded to the phosphorus atom either directly (forming phosphinates), or through sulphur or an oxygen atom (forming phosphorothioates or phosphates) (Fig. 1). At least one of the groups is $–NH_2$ in phosphoramidates, which may be mono- or bi-substituted. Phosphorus shares double bond with either sulphur or oxygen. Finally, X group, which is a "leaving group" (as it is released upon

✉ Dinesh Goyal
dgoyal@thapar.edu

[1] Department of Biotechnology, Thapar Institute of Engineering and Technology (Deemed to be University), Patiala, Punjab 147001, India

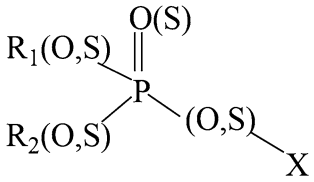


Fig. 1 General structure of organophosphorus compounds. Adapted with permission (Karpouzas and Singh 2006)

hydrolysis of organophosphates), may be a halogen, aromatic, aliphatic or heterocyclic group (Sogorb and Vilanova 2002).

Monocrotophos is a nonspecific systemic organophosphorus pesticide used extensively to protect rice, cotton, maize, groundnut, sugarcane, tobacco, soybeans and vegetables against insect pests (Balamurugan et al. 2010; Abraham and Silambarasan 2015). It was first produced in 1965 by Ciba AG and Shell Development Co. and is registered in about 60 countries including Spain, France, Italy, Austria and Greece. It accounts for a total sale of roughly 3% of all the insecticides (Jia et al. 2006; Barathidasan and Reetha 2013). Statistical data indicate Asia being the top user of monocrotophos, where countries like India (43%), South America (26%), China (15%) and Southeast Asia (9%) account for 90% usage (Kumar et al. 2014). In India, monocrotophos is registered for 14 crops by Central Insecticides Board and Registration Committee (CIBRC) (Bhushan et al. 2013) and the states of Punjab and Andhra Pradesh are the chief consumers of monocrotophos (Kumar et al. 2014). However, European Union and the USA have withdrawn the product for use, in India despite its ban, it is still being used on a large variety of crops and vegetables owing to its high efficiency in controlling pests, low cost and lack of alternative replacements (Kodandaram et al. 2013; Sidhu et al. 2015).

Being readily soluble in water, it easily gains entry to water sources or industrial effluents during manufacturing process, which has led to several incidents of monocrotophos contamination. Waste effluent of monocrotophos manufacturing factory near Pune, India, contained 0–125 mg L^{-1} monocrotophos (Bhadbhade et al. 2002c). In other studies, 4 µg L^{-1} and 0.165 µg L^{-1} of monocrotophos residues were detected in rainwater (Kumari et al. 2007) and tap water in China (Kang et al. 2000). Tariq et al. (2004) reported the presence of up to 8.3 µg L^{-1} monocrotophos in shallow well water samples collected from four cotton-growing districts in Pakistan. Several cases of presence of monocrotophos above the maximum residue limits (MRL) have been reported (Sawaya et al. 1999; Kumari et al. 2004). Monocrotophos residues were found at a mean concentration of 0.063 ± 0.022 mg kg^{-1} in tomatoes (Darko and Akoto 2008). In a study conducted by Arora (2009), 0.4 mg kg^{-1} monocrotophos was reported in okra samples. The residues were also detected at a mean concentration level of 1.63 ng g^{-1} in human breast milk (Sharma et al. 2014). Monocrotophos residues at an average concentration of 0.79 ng mL^{-1} in human blood (Sharma et al. 2015) pose high risk. Owing to the toxicity and its persistent nature, it is necessary to eliminate monocrotophos from the environment. Current review summarizes and presents assessment of various studies and reports on monocrotophos, its fate in the environment, quantification of its toxicity and degradation.

Monocrotophos

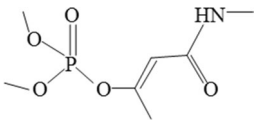
Monocrotophos, a dimethyl oxon compound sold under trade names Azodrin, Apadrin, Pillardrin, Plantdrin, Crisodrin, Nuvacron, Monocron and Bilobran is a commonly used organophosphorus insecticide and acaricide (Mackay et al. 2006; Jose et al. 2015). It is a nonspecific, systemic foliar insecticide used to protect crops from mites, ticks, leaf hoppers, aphids and other insects (Singh and Walker 2006). Monocrotophos refers to a *cis*-isomer with its nomenclature based on its crotonamide structure. The technical grade monocrotophos contains 75–80% of the *cis*-isomer and 9% of the *trans*-isomer along with a range of compounds including *N*-methyl acetoacetamide (2%) and dimethyl phosphate (5%) (Beynon et al. 1973). Trimethyl phosphate and monochloro-monomethyl acetoacetamide are also used for manufacturing monocrotophos (Bhadbhade et al. 2002b).

Monocrotophos (dimethyl(E)-1-methyl-2-(2-methylcarbamoyl)vinyl phosphate) is colourless in its pure form, and its technical grade exists as reddish brown solid/liquid state (Mackay et al. 2006) (Table 1). It is classified as class (I) highly toxic compound by the Environmental Protection Agency (Sidhu et al. 2015), with median lethal dose (LD_{50}) of 18–20 mg kg^{-1} for mammals (Singh and Walker 2006) and 0.9–6.5 mg kg^{-1} for birds (Goldstein et al. 1999). Monocrotophos is readily soluble in water with 100% solubility, but due to its hydrophilic nature, it is weakly sorbed by soil particles (Subhas and Singh 2003; Mackay et al. 2006), posing threat to groundwater contamination due to leaching. It has a half-life of 17–96 days depending upon pH and temperature (Mackay et al. 2006). When stored in polyethylene and glass containers, technical grade monocrotophos is stable and has half-life of 2500 days at 38 °C (JMPR 1972). The formulation of monocrotophos registered in India is 36% SL (Kodandaram et al. 2013) with application rates 0.25–1.5 kg ha^{-1} for cotton (Beynon et al. 1973).

Distribution and fate of monocrotophos in the environment

With regular field application of pesticides, they remain in soil and sediments and even percolate to the groundwater/surface water and enter the food chain directly or indirectly.

Table 1 Characteristics of monocrotophos

S. no.	Properties	Values
1	Common name	Monocrotophos
2	IUPAC name	Dimethyl(E)-1-methyl-2-(2-methylcarbamoyl)vinyl phosphate
3	CAS registry no.	6923-22-4
4	Molecular formula	$C_7H_{14}NO_5P$
5	Structural formula	
6	Molecular weight	223.164 g mol^{-1}
7	Colour	Colourless (pure) Reddish brown solid and liquid (Technical grade)
8	Odour	Mild ester like
9	Melting point (°C)	Pure 54–55 Technical 25–30
10	Boiling point (°C)	125
11	Density at 20 °C (g cm^{-3})	1.22
12	Vapour pressure at 25 °C (Pa)	9.33×10^{-3}
13	Henry's law constant at 25 °C (Pa m^3 mol^{-1})	2.08×10^{-6}
14	Octanol/water partition coefficient (log K_{OW})	− 1.97 to − 0.2
15	Hexane/water partition coefficient	< 0.1
16	Solubility (20 °C)	
	Water	1 kg kg^{-1}
	Acetone	700 g kg^{-1}
	Dichloromethane	800 g kg^{-1}
	Methanol	1 kg kg^{-1}
	Octan-1-ol	250 g kg^{-1}
	Toluene	60 g kg^{-1}
17	Stability	Stable on storage in polyethylene and glass containers. Half-life at 20 °C at different pH: pH 5—96 days pH 7—66 days pH 9—17 days Half-life in soil—30 days
18	Acute oral LD_{50}:	
	Male rats	17–18 mg kg^{-1}
	Female rats	20 mg kg^{-1}

References: JMPR (1972), Beynon et al. (1973), Mackay et al. (2006), Sidhu et al. (2015)

Their fate is governed by different factors, which determines their persistence, mobility and potential for volatilization, leaching, run-off or plant uptake (Gavrilescu 2005; Pam 2015). These factors include properties of pesticide such as soil adsorption, water solubility and half-life and physico-chemical properties of soil such as pH, soil texture, depth, slope and permeability. Interaction of all these factors along with environmental conditions determines the fate and behaviour of a pesticide (Gavrilescu 2005; Yang et al. 2018).

Monocrotophos is a fast-acting and highly toxic cholinesterase-inhibiting organophosphorus insecticide (Bhadbhade et al. 2002c; Sidhu et al. 2015). Being readily water soluble and highly mobile in soil, it quickly contaminates groundwater and penetrates into plant tissues, hence making its removal impossible (Tomlin 1994; Balamurugan et al. 2010; Barathidasan and Reetha 2013). In a study conducted by Imran et al. (2016), less than 0.02 mg L^{-1} monocrotophos residues were found in all 106 samples of different paddy varieties. Among 50 samples analysed, monocrotophos was detected in two samples each of eggplant and tomatoes at mean concentrations of 0.060 ± 0.022 mg kg^{-1} and 0.063 mg kg^{-1}, respectively (Darko and Akoto 2008). Residues of monocrotophos were found in different fruits such as apple, grapes, mango and melon (Hussain et al. 2002;

Asi 2003; Khan 2005), vegetables (Asi 2003; Parveen et al. 2005; Khan 2005) and green tea (Huang et al. 2019). In another study, 0.6748–1.3648 mg kg^{-1} of monocrotophos residues (above maximum residue limit 0.2 mg kg^{-1}) was detected in market samples of grapes (Reddy et al. 2000). In the USA and Europe, organophosphates are one of the causes reported for intoxication of wild birds due to ingestion of grains treated with insecticides. A study conducted on total of 182 dead birds from 2010 to 2013 revealed the presence of 0.6–7557 mg kg^{-1} of monocrotophos in 57 dead birds (Kim et al. 2016).

Uptake of monocrotophos by plants

Pesticide residues in air, water and soil are the major source of pesticide residues in plants (Zhang et al. 2011). Monocrotophos is a foliar insecticide mainly used on cotton crop. Studies on distribution and breakdown of monocrotophos in plants have been reported by Lindquist and Bull (1967) and Beynon and Wright (1972). Individual leaf was treated topically with 40 µg of monocrotophos, whereas 0.5 mg of ^{32}P-labelled monocrotophos was applied to cotton seeds. For stem treatment, 5 mg of ^{32}P-labelled monocrotophos mixed with 95 mg of lanolin was spread around the stem in a 1-inch band. Volatilization caused the loss of 85% of active ingredient in foliar treatment. Degradation of monocrotophos occurred both inside and on surface of treated leaves mainly by hydrolysis. Monocrotophos metabolism in case of seeds was comparatively slower with a half-life of 7 days. 90% of radioactivity in the lanolin was removed 21 days after stem treatment, indicating its stability in lanolin. In general, plants with green waxy stems took greater amount of insecticide than plants having some bark (Bariola et al. 1970). ^{14}C-labelled monocrotophos dissolved in acetone (100–1000 µg mL^{-1}) were further used to study monocrotophos's behaviour in maize, cabbage and apple. Twenty-two days after foliar treatment, 20–27% of the total applied monocrotophos remained unchanged in case of maize, whereas in case of apple leaves half-life of monocrotophos was estimated to be 6–9 days (Beynon and Wright 1972). Approximately 2.8% (i.e. 0.81 ppm) of the total applied 100 ppm of active ingredient (^{14}C) was translocated into the fruits. Under greenhouse conditions, on injecting ^{32}P monocrotophos into the stem of bean plants, it was rapidly translocated to the foliage, where it persisted for several weeks (Menzer and Casida 1965), with estimated half-life to be 14 days. Half-life was further decreased under outdoor conditions and in rains (Beynon and Wright 1972). The breakdown products are mainly hydrophobic compounds such as dimethyl phosphate, which are not cholinesterase inhibitor and have low toxicity.

Metabolism of monocrotophos in different crops was studied using different radiolabels. Monocrotophos degradation studies in beans (Menzer and Casida 1965) and cotton plants (Lindquist and Bull 1967) used ^{32}P-labelled monocrotophos, whereas studies on maize, cabbage and apple trees (Beynon and Wright 1972) used both *O*-[^{14}C] methyl and *N*-[^{14}C]methyl-monocrotophos. By the use of different radiolabels, different metabolites were detected in all plants. Eight days after injecting ^{32}P-monocrotophos to bean plants, Menzer and Casida (1965) detected unchanged monocrotophos, *N*-methylol and the amide, whereas after 32 days only monocrotophos residues were detected. Findings by Lindquist and Bull (1967) suggested dimethyl phosphate, phosphoric acid and *O*-desmethyl monocrotophos as major products along with small amounts of methylol and other polar materials. ^{14}C-labelled monocrotophos was metabolized mainly to hydrophilic compounds such as *O*-desmethyl monocrotophos and dimethyl phosphate along with *N*-methylacetoacetamide, *N*-hydroxymethyl derivative (free and conjugated with sugar), alcohol and amides (Beynon and Wright 1972) (Fig. 2).

Three different metabolic pathways are involved in the mineralization of monocrotophos in different plants:

(1) Breakdown of P–O–CH_3 linkage
(2) Hydrolysis of the P–O-vinyl bond
(3) Hydroxylation of *N*-methyl group, followed by *N*-dealkylation.

Routes (1) and (2) represent major metabolic pathways in all the investigated crops and are essentially detoxification reactions, whereas route (3) is a minor metabolism pathway leading to potent cholineesterase inhibitors (methylol, amide and the conjugates) (Lindquist and Bull 1967; Beynon et al. 1973).

Fate of monocrotophos in mammals

Mode of action of organophosphates involves inhibition of acetylcholine esterase (AChE), an enzyme that catalyzes the hydrolysis of a neurotransmitter acetylcholine (Abraham and Silambarasan 2015). After transmitting nerve impulse to various parts of the body, AChE must hydrolyse acetylcholine into acetyl CoA and choline by binding at its active site (serine 203) and forming an enzyme–substrate complex. This prevents overstimulation of the nervous system. Organophosphorus compounds covalently bind to active site serine 203 amino acid of AChE, thereby modifying its structure and function and inhibiting it. The leaving group breaks off the phosphate by binding to the His 447 at its positive hydrogen and leaving the enzyme phosphorylated (Fukuto 1990; Ragnarsdottir 2000; Singh and Walker 2006). Therefore, nerves are overstimulated and jammed, as regeneration of phosphorylated AChE being very slow may take hours or days, accumulating

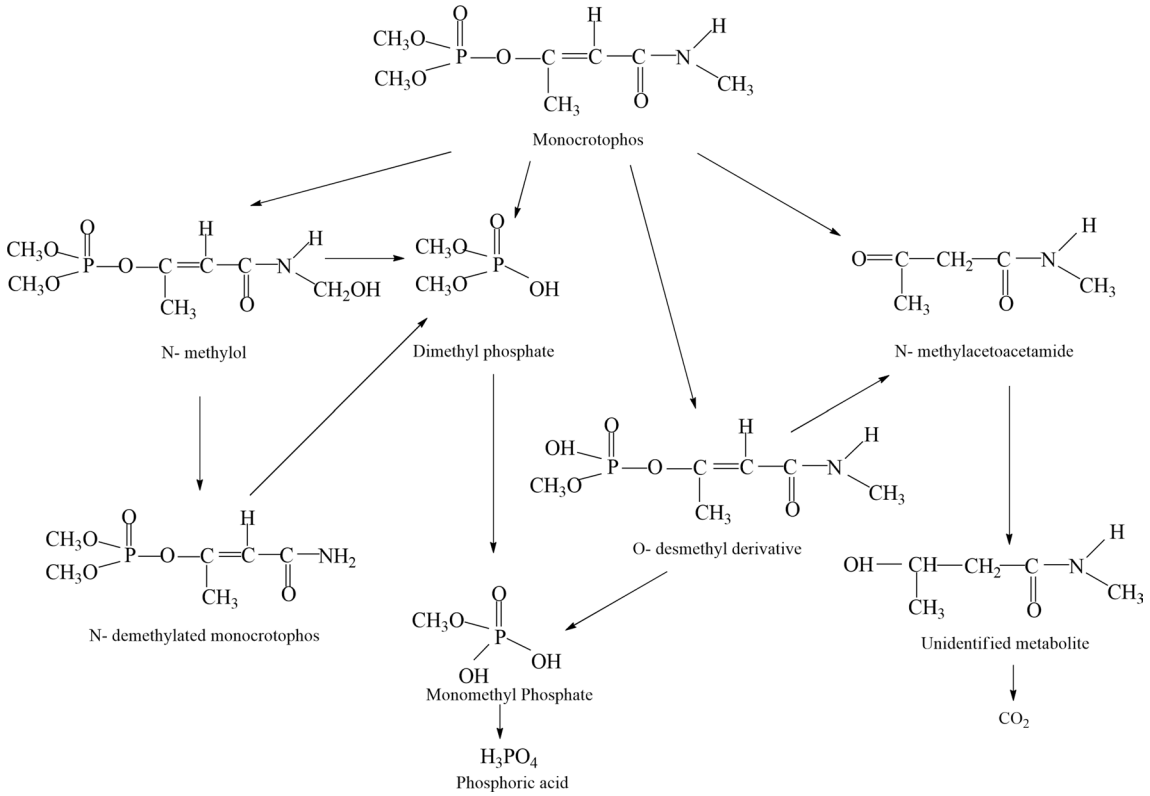


Fig. 2 Proposed pathway for metabolism of monocrotophos in plants and animals, modified after Beynon et al. 1973, Mücke 1994, and Lindquist and Bull 1967. Initial step of breakdown of monocrotophos is the oxidative *N*-demethylation leading to the formation of *N*-demethylated monocrotophos via formation of *N*-methylol. Hydrolysis at *O*-methyl group leads to the formation of *O*-desmethyl derivative. Major metabolic pathway proceeds by cleavage of vinyl phosphate bond leading to the formation of *N*-methylacetoacetamide, following reduction of keto group to unidentified metabolite. Dimethyl phosphate is another major product formed by breakdown of P–O–C linkage, which further forms phosphoric acid via monomethyl phosphate

acetylcholine at synapses which in turn causes confusion, hypersalivation, agitation, convulsion, respiratory failure and ultimately death of insects and mammals (Karpouzas and Singh 2006).

Studies on metabolic fate of monocrotophos have been conducted in different mammals (Menzer and Casida 1965; Bull and Lindquist 1966) by using ^{32}P or ^{14}C radiolabelled monocrotophos. Elimination of intraperitoneally administered ^{32}P-monocrotophos in rats was rapid, accounting for 45–56% of the dose excreted in urine within 6 h after administration (Menzer and Casida 1965; Bull and Lindquist 1966). After 48 h, total 72% was excreted, urine accounting for 65% and faeces 5%. The radioactivity results of the first 6-h urine sample were comprised of 34% monocrotophos, 34% dimethyl phosphate, 10% *O*-desmethyl monocrotophos, 20% methylol derivative and 2% phosphoric acid with trace amounts of *N*-desmethyl (Bull and Lindquist 1966) (Fig. 2). On killing the rats dosed with 2 mg kg^{-1}, residues of different tissues, i.e. bones, blood, lungs, muscle, skin, heart, spleen, kidneys, etc., were investigated. This indicated the presence of a low amount of monocrotophos with butterfat, liver and kidneys showing highest values (i.e. 0.07, 0.05, 0.03 ppm, respectively) (Mücke 1994).

A lactating goat was given a single oral dose of a mixture of ^{32}P and N–[^{14}C] methyl-monocrotophos, 50% of it was excreted in 16 h. After 72 h, elimination of ^{32}P-monocrotophos accounted for 67%, whereas N–[^{14}C] methyl-monocrotophos was higher, i.e. 90%. Rest 1.4% of ^{32}P-monocrotophos and 2.9% of N–[^{14}C] methyl-monocrotophos were excreted with milk (Menzer and Casida 1965). In a similar study where two lactating goats fed with oral dose of 0.5 mg kg^{-1} ^{14}C-monocrotophos for three consecutive days, elimination of monocrotophos in urine, faeces, milk and butterfat accounted for 66%, 13%, 1.8% and 0.5%, respectively. A small amount (0.03–0.16 ppm) was also detected in body tissues. In cows, out of total fed 45 ppm ^{32}P-monocrotophos, 3.6 ppm was eliminated in milk (Mücke 1994).

Zichu et al. (1988) reported penetration of ^{14}C-monocrotophos to human skin and pigs, skin of cheek having the highest penetration rate. 15% of the total 4 µg cm^{-2} ^{14}C-monocrotophos applied topically on the forearms of six male human subjects was excreted with urine in

5 days confirming monocrotophos absorption in humans (Feldmann and Maibach 1974). When same six males were given ^{14}C-monocrotophos dose intravenously, 68% was eliminated with urine in 5 days indicating half-life to be 20 h in humans. The renal elimination was the highest 4–8 h after administration and declined afterwards. In a recent study conducted on five male patients who ingested unknown quantity of monocrotophos, there was a rapid clearance of monocrotophos from plasma with a median renal elimination half-life of 3.3 h (Jose et al. 2015). A large amount of unchanged monocrotophos is excreted in urine probably due to its water-soluble nature.

Quantification of the toxicity of monocrotophos

Acute toxic effects of monocrotophos on different mammals have been studied by different researchers; however, the effects resulting from long-term exposure to low doses are often difficult to quantify and distinguish. Effect of regular intake of foods having pesticide residues is also difficult to detect. Several indices of residue levels are used to predict level of pesticide residues in the human body. Maximum residue limits (MRL) corresponds to maximum concentration of a pesticide residue (mg kg^{-1}), which is recommended by Codex Alimentarius Commission and is legally permitted in food commodities and animal feeds (Darko and Akoto 2008). The acceptable daily intake (ADI), which is the estimated amount of a substance in food (expressed on a body weight basis) that can be ingested daily over a lifetime without appreciable health risk to the consumer, could also be used to predict the dietary intake of pesticide residues. The dietary intake of a pesticide residue in a given food can be estimated by multiplying the residue level in the food with the amount of that food consumed. The estimated average daily intake (EADI) of pesticide residues should be less than its established ADI (WHO 1997).

To evaluate the toxicity of organophosphates to humans, single-spot urine samples have often been used to determine the levels of common organophosphate metabolites used as biomarkers of organophosphorus exposure (Ito et al. 2019). Monocrotophos toxicity can be studied by estimating its residues in urine samples by detecting the purplish blue colour complexes, which results from the reactions of organophosphates and 4-(4-nitrobenzyl) pyridine (NBP) in urine (Namera et al. 2000). However, evaluation of toxicity by animal testing is long and costly; therefore, alternative modelling of quantitative structure–activity relationships (QSARs) is developed to predict acute toxicity of pollutants (Satpathy 2019).

Toxicity of monocrotophos

Monocrotophos dose that kills half of the test organisms, i.e. half maximal inhibitory concentration (IC_{50}), for male and female rats is 17–18 mg kg^{-1} and 20 mg kg^{-1}, respectively. The IC_{50} value for dermal exposure for male rats, female rats and rabbits is 126 mg kg^{-1}, 112 mg kg^{-1} and 354 mg kg^{-1}, respectively (Chakravarthi et al. 2009). In India, monocrotophos has been used as intentional self-harm chemical for committing suicides (Rao et al. 2005a, b; Peter et al. 2010).

Monocrotophos poisoning in humans is characterized by blurred vision, muscular weakness, profuse perspiration, confusion, vomiting, small pupils and even death due to respiratory failure (Yaduvanshi et al. 2010). Most of the monocrotophos's toxicity and mutagenicity studies in humans have been conducted using cultured blood lymphocytes. Tripathi et al. (2017) studied the neurotoxic effects of monocrotophos on cultured neural and glial cells, where monocrotophos exposure triggered the apoptotic cell death. Comet assay conducted using cultured human blood lymphocytes revealed that monocrotophos exposure led to DNA damage due to increase in comet tail length indicating monocrotophos capable of altering the genetic material (Jamil et al. 2004; Das et al. 2006; Chakravarthi et al. 2009). Banu et al. (2001) reported similar results in mice model. Monocrotophos induced oxidative DNA damage along with lipid peroxidation in rat tissues (Yaduvanshi et al. 2010). Zahran et al. (2005) reported induction of structural and numerical chromosomal mutations in both germ and somatic cells of male liver and embryos of pregnant mice on monocrotophos exposure, confirming its mutagenic action. It exerts neurobehavioural effects in rodents by affecting their noncholinergic functions that involve serotonergic and dopaminergic systems associated with increased oxidative stress (Mandhane and Chopde 1995; Sankhwar et al. 2013). Monocrotophos treatment caused an increase in WBC count along with mutagenicity in birds and male rats (Siddiqui et al. 1991, 1993) and induced bone marrow depression along with splenic hyperplasia, which caused significant decrease in haemoglobin count, total RBC and platelet count, erythrocyte sedimentation rate and haematocrit value in mice (Gupta et al. 1982).

Earlier studies revealed exposure of monocrotophos-induced transient hyperglycaemia in rats in acute conditions (Joshi and Rajini 2012; Velmurugan et al. 2013; Nagaraju et al. 2014). It also led to an increase in the weight of key white adipose pads, pancreatic islet diameter and activity of enzymes involved in gluconeogenesis, thereby causing hyperglycaemia, hyperinsulinemia and dyslipidaemia (Nagaraju et al. 2014). Findings of the same group indicated the probability of beta-cell compensation responses under monocrotophos exposure (Nagaraju and Rajini 2016). Velmurugan et al. (2013) studied the cardiotoxicology of

prolonged monocrotophos intake. Wistar rats administered orally with 1/50th of lethal dosage of monocrotophos exhibited mild cardiac oxidative stress leading to cardiotoxicity, which was evidenced by the accumulation of lipid peroxidation, protein carbonyls and glutathione production.

Monocrotophos has histopathological effect on kidney, liver and muscles of both fish and rats, which were studied on the tissues of kidney, gills and intestines of fish *Cirrhinus mrigala* by light microscopy (Velmurugan et al. 2007). Cytotoxic effects of monocrotophos on different aquatic organisms have also been widely studied (Agrahari et al. 2007; Anbumani and Mohankumar 2015; Binukumari et al. 2016; Mundhe et al. 2016; Zhang et al. 2017).

Monocrotophos is a potential endocrine-disrupting chemical with significant oestrogenic properties, which significantly induces both secretion and vitellogenin mRNA expression in male Goldfish (Tian et al. 2009). Oestrogenic effects of monocrotophos are exerted via interfering with the reproductive axis at multiple sites leading to increased 17β-estradiol plasma levels and decreased plasma testosterone concentrations (Tian et al. 2010). This caused severe reproductive abnormalities in fish *Poecilia reticulata* (Tian et al. 2012). It is genotoxic to *Meretrix* ovum and induces retardation of somatic growth of the mussel (Revankar and Shyama 2009).

Monocrotophos has proved to be extremely toxic to birds. Monocrotophos contamination was held responsible for mass deaths of raptors, owls, Swainson's hawks (*Buteo swainsoni*), Sarus cranes (*Grus antigon*) and peafowls reported in different parts of the world (Mendelssohn and Paz 1977; Goldstein et al. 1999; Pain et al. 2004; Narang et al. 2016). Prolonged exposure of monocrotophos is also toxic to termites (Rao et al. 2005a), earthworms (Rao and Kavitha 2004; Govindarajan 2014) and roundworms (Salim and Rajini 2017).

Detection and monitoring of monocrotophos

Several techniques have been developed to monitor the presence of monocrotophos and its degraded residues in the environment. Quantification of monocrotophos in food items including fruits and vegetables is often performed by liquid chromatography (LC) or gas chromatography (GC) coupled with several detectors such as flame ionization detector (FID), electron capture detector and nitrogen phosphorus detector (Chandra et al. 2014; Mao et al. 2019). In recent years, LC and GC are equipped with mass analysers for pesticide residue analysis, such as LC–MS, GC–MS, LC–MS/MS, GC–MS/MS (Mao et al. 2019). QuEChERS (quick, easy, cheap, effective, rugged and safe) methodology has been widely employed for monitoring pesticide residues in fruits and vegetables, edible fungi (Cao et al. 2016), chicken eggs (Li et al. 2016) and edible oils (Mao et al. 2019).

Ismail et al. (2000) have developed a simple reversed-phase column liquid chromatographic method using C_{18} column and UV detection at wavelength 218 nm for the determination of *cis* and *trans* isomers of monocrotophos. A new method of molecularly imprinted solid-phase extraction coupled with high-performance liquid chromatography was reported for the determination of monocrotophos in vegetables, reporting 1.2 ng g^{-1} limit of detection (Wang et al. 2014). Similar method was developed for determining trace monocrotophos in fruits, giving limit of detection 0.015 mg kg^{-1} (Li et al. 2017). In a green tea sample, spiked with 50 µg kg^{-1} monocrotophos, 95.7% of the insecticide was recovered with a modified QuEChERS protocol, coupled to HPLC–MS/MS (Huang et al. 2019). Thin-layer chromatography (TLC) is also used for the detection of monocrotophos in biological samples by the use of diazotized sulphanilamide or sulphanilic acid (Patil and Shingare 1994).

Since these conventional chromatography methods are expensive, time-consuming and require a well-trained technician for instrument handling, nanotechnology-based electrochemical biosensors are another promising technique used these days. They are user-friendly, rapid, stable and very sensitive (Sundarmurugasan et al. 2016; Srivastava et al. 2018). Since monocrotophos can inhibit AChE, the enzyme has been chosen by several researchers for the detection of monocrotophos. AChE catalyzes the hydrolysis of acetylthiocholine to thiocholine, which produces oxidation peak proportional to concentration of insecticide present (Liu and Wei 2014; Sundarmurugasan et al. 2016). Dimcheva et al. (2013) achieved monocrotophos detection with detection limit 1 µM and a linear range of 50–400 nM, using AChE immobilized on gold nanoparticles. Liu and Wei (2014) developed a sensitive and stable AChE biosensor based on platinum–carbon aerogels composite which showed 2.7×10^{-12} M detection limits for monocrotophos and exhibited good reproducibility. Multi-walled carbon nanotubes (MWCNT), surface modified by several functional groups, hydrophobic alkyl groups and ionic groups were employed as AChE carrier for monocrotophos detection in various vegetable samples. Ionic liquid ($-IL_1$)-modified MWCNT was the best carrier for the enzyme with detection limit 3.3×10^{-11} M and recovery 90–104% (Bin et al. 2018). Some of the AChE biosensors are inert silica nanoparticle or magnetic nanoparticle based, which exhibit good stability (Du et al. 2007; Sun et al. 2008; Wu et al. 2011; Bagheri et al. 2019).

Degradation of monocrotophos

Monocrotophos reaches the soil and aquatic environment directly or indirectly, upon its application to the target crops, where it undergoes degradation by various chemical, photochemical and microbiological processes. Degradation is also influenced by various distribution processes such as adsorption/desorption, volatilization, leaching, run-off, plant and aquatic life uptake.

To investigate degradation behaviour of monocrotophos in soil, several experiments were conducted on different types of soils under aerobic and anaerobic conditions. On application of 1.5 kg a.i. ha^{-1} of 5% granular monocrotophos formulation to clay soil (Agnihotri et al. 1981), it rapidly disappeared from 0 to 15 cm soil layer, estimating a half-life of 10.3 days. Small traces were also detected in 15–30 cm layer due to its vertical movement, but 45 days after the treatment, no detectable residues were found. Gundi and Reddy (2006) studied degradation of 10 and 100 µg g^{-1} monocrotophos in two Indian agricultural soils (black vertisol and red alfinsol) at 60% water holding capacity, under aerobic conditions. The degradation in both the soil samples was rapid and accounted for 96–98% of the total application with half-lives 9.2 and 11.4 days, respectively, following first-order kinetics. Metabolism studies of ^{14}C-radiolabelled monocrotophos showed its rapid decomposition into *N*-methylacetoacetamide, *O*-desmethyl monocrotophos, *N*-(hydroxymethyl) monocrotophos, 3-hydroxy-*N*-methylbutyramide, monomethyl, and dimethyl phosphates and $^{14}CO_2$ (Dutton et al. 1974; Lee et al. 1990).

Monocrotophos degradation is greatly affected by the presence and absence of soil microbial biomass. Decrease in degradation rate was observed in soils that were either air-dried (Schuler and Held 1964) or sterilized (Lee et al. 1980), indicating that the absence of or reduction in microbial biomass decreases the rate of monocrotophos degradation in soil. Anaerobic conditions also decreased the rate of degradation with a half-life time of approximately 8 days compared with a 4-day half-life under aerobic conditions in the same soil (Hernandez et al. 1986; Lee et al. 1990).

Biodegradation of monocrotophos

Microbial diversity plays a significant role in degradation of synthetic contaminants present in the environment by utilizing them as carbon and energy source. Monocrotophos is characterized by an amide bond and P–O–C linkage. It has been reported to be utilized as sole source of carbon or phosphorus in soil or aqueous medium (Singh and Walker 2006; Abraham and Silambarasan 2015). Monocrotophos degradation using the different soil microflora has been widely studied in several enrichment cultures (Table 2).

Bacterial degradation of monocrotophos

Several bacterial species showing capability to utilize monocrotophos as nutrient source and degrading it in liquid medium or soil have been isolated and characterized. Monocrotophos metabolization by different bacteria has been reported through catabolic mechanisms, where monocrotophos provides carbon or phosphorus source to the degrading micro-organisms (Singh and Walker 2006). It acts as carbon source for *Pseudomonas* sp., *Arthrobacter* sp., *Arthrobacter atrocyaneus, Bacillus megaterium* (Bhadbhade et al. 2002b) and as phosphorus source for *Clavibacter michiganense* SBL11 and *Pseudomonas aeruginosa* F10B (Subhas and Singh 2003).

In several studies, microbes have been employed for the degradation of monocrotophos (Table 2). Due to the presence of novel catabolic enzymes, bacteria can survive in diverse ecological niches. *Rhodococcus phenolicus* strain MCP1 along with *Rhodococcus ruber* strain MCP-2, isolated from groundnut soils, was able to utilize monocrotophos as a carbon source by hydrolysis leading to the formation of *N*-methylacetoacetamide, indicating the decomposition of parent compound (Srinivasulu et al. 2017). Different *Bacillus* sp. including *Bacillus licheniformis*, *Bacillus subtilis* (Acharya et al. 2015; Sidhu et al. 2015; Buvaneswari et al. 2017), *Bacillus coagulans*, *Bacillus brevis* (Bhadbhade et al. 2002a), *Bacillus megaterium* MCM B-423 (Bhadbhade et al. 2002b) and *Lactobacillus bulgaricus* (Zhao and Wang 2012) have been widely studied to metabolize monocrotophos present in the soil. Degradation of monocrotophos by various *Pseudomonas* strains, viz. *Pseudomonas stutzeri* (Barathidasan and Reetha 2013; Buvaneswari et al. 2017), *Pseudomonas moraviensis* JAS18 (Abraham et al. 2014), *Pseudomonas synxantha* (Sidhu et al. 2015), *Pseudomonas aeruginosa* (Subhas and Singh 2003; Balamurugan et al. 2010) and *Pseudomonas mendocina* (Bhadbhade et al. 2002a), has been widely reported.

Serratia marcescens JAS16 isolated from prolonged exposure of soil to monocrotophos was able to use it as carbon source and degraded 1000 mg L^{-1} of the insecticide in aqueous medium at a degradation rate constant of 136 per day with a half-life of 3.7 days. Degradation rate constant in soil inoculated with bacteria was 105 per day with a half-life of 4.8 days. The bacteria could tolerate 1200 mg L^{-1} of the insecticide. Phytotoxicity of degraded metabolites to seeds of *Vigna unguiculata*, *Vigna radiata* and *Macrotyloma uniflorum* and its genotoxicity to *Allium cepa* bulbs were found to be low (Abraham and

Table 2 Degradation of monocrotophos by different bacteria, fungi and algae

S. no.	Microorganism/s	Sources	Findings	References
Bacteria				
1.	*Bacillus sonorensis* (KY287930), *Pseudomonas stutzeri* (KY287931) and *Bacillus licheniformis* (KY287928)	Isolated from different MCP-contaminated agricultural soil in Sivagangai District, Tamil Nadu, India	Bacteria individually degraded MCP to non-toxic metabolites, whereas in consortia complete degradation occurred	Buvaneswari et al. (2018)
2.	*Sphingobium* sp. YW16	Paddy soil, China	Bacteria utilized degraded metabolite dimethyl phosphate as carbon source but could not utilize *N*-methylacetoacetamide	Sun et al. (2018)
3.	*Rhodococcus phenolicus* strain MCP1, *Rhodococcus ruber* strain MCP-2	Isolated from the Groundnut (*Arachis hypogaea* L.) soils by enrichment culture technique	*R. phenolicus* strain MCP1 and *R. ruber* strain MCP-2 degraded 30% and 45% MCP after 4 days leaving *N*-methylacetoacetamide as the degraded product. About 21% loss of MCP was observed in uninoculated medium after 4th day	Srinivasulu et al. (2017)
4.	*Bacillus subtilis* (BAGN005), *Pseudomonas stutzeri* (BVGN010), *Bacillus licheniformis* (BKGN007)	Isolated from different MCP-contaminated agricultural soil in Sivagangai District, Tamil Nadu, India	3-Hydroxy-*N*-methyl butyramide, methyl phosphate and dimethyl phosphate observed as intermediate compounds	Buvaneswari et al. (2017)
5.	*Bacillus subtilis* (KPA-1)	Isolated from different vegetable and cotton fields of Gujarat, India	Under aerobic conditions, MCP was degraded to an extent of 94.2%. RT-qPCR indicates the presence of an enzyme organophosphate hydrolase (*opd*A)	Acharya et al. (2015)
6.	*Serratia marcescens* strain JAS16	Isolated from soil sample of a sugarcane field, Vellore District, Tamil Nadu, India	50% degradation of 1000 mg L^{-1} MCP 3.7 days, whereas 4.8 days in soil; bacteria were able to tolerate 1200 mg L^{-1} MCP	Abraham and Silambarasan (2015)
7.	*Starkeya novella* YW6	Isolated from soil samples of a paddy field located in Hunan Province, China	0.2 mM MCP was completely degraded within 36 h into different metabolites: *N*-methylacetoacetamide, dimethyl phosphate, *N*-methyl-4-oxopentanamide, 5-(methylamino)-5-oxo-pentanoic acid, methylamine and glutaric acid	Sun et al. (2016)
8.	*Pseudomonas synxantha*, *Bacillus subtilis* and *Salmonella enterica*	Soil samples from Punjab's Malwa region	*Pseudomonas synxantha* showed maximum MCP degradation, i.e. 67.8% (in 17 days), whereas 70.9% MCP still persisted after 120 days in control	Sidhu et al. (2015)
9.	Bacterial consortium containing *Alcaligenes* sp. JAS1, *Ochrobactrum* sp. JAS2, *Sphingobacterium* sp. JAS3 (chlorpyrifos degrading), *Enterobacter ludwigii* JAS17, *Pseudomonas moraviensis* JAS18 and *Serratia marcescens* JAS16 (monocrotophos degrading), *Klebsiella pneumoniae* JAS8, *Enterobacter cloacae* JAS7, *Halophilic bacteria* JAS4, *Enterobacter asburiae* strain JAS5 (endosulfan degrading)	Isolated from different pesticide (chlorpyrifos, monocrotophos and endosulfan)-contaminated soil	MCP degraded at a rate constant of 261.6 per day and 50% degradation in 1.91 days	Abraham et al. (2014)

Table 2 (continued)

S. no.	Microorganism/s	Sources	Findings	References
10.	*Pseudomonas stutzeri*	Obtained from MTCC, Chandigarh	96% degradation of 500 mg L^{-1} in 6 days at 30 °C with ammonia, phosphates and carbon dioxide as degraded products	Barathidasan and Reetha (2013)
11.	*Lactobacillus bulgaricus, L. plantarum* and *L. paracasei*	Obtained from the Centre of Lactic Acid Bacteria, Northeast Agricultural University, China	*L. bulgaricus* showed maximum degradation of MCP (0.5 mg kg^{-1}) in 24 h at 42 °C with half-life time of 31.5 h, followed by *L. plantarum* (34.8 h)	Zhao and Wang (2012)
12.	*Pseudomonas aeruginosa*	MTCC, Chandigarh	Regain of protein, carotenoid and chlorophyll content due to MCP degradation	Balamurugan et al. (2010)
13.	*Burkholderia sp.* strain KR100	Rice paddy field, Korea	96.4% degradation of 300 µg mL^{-1} MCP	Kim and Ahn (2009)
14.	*Paracoccus* sp. (M1)	Sludge sample from the chemical factory's wastewater treatment system	79.92% MCP (300 mg L^{-1}) degraded rapidly in 6 h at 30 °C, pH 7.5; 500 mg L^{-1} MCP was toxic for bacterial growth	Jia et al. (2006)
15.	*Pseudomonas aeruginosa* F10B, *Clavibacter michiganense* subsp. *insidiosum* SBL 11	Soil samples from cotton fields of Ludhiana, Punjab, India	98.9% and 86.9% degradation of technical MCP, whereas 79% and 80% degradation of pure MCP by *P. aeruginosa* F10B and *C. michiganense* subsp. *Insidiosum* SBL 11, respectively, within 24 h at 37 °C, followed by increase in generation time of bacteria. Optimal concentration of MCP was 500 ppm	Subhas and Singh (2003)
16.	*Pseudomonas mendocina, P. stutzeri, Bacillus licheniformis, Bacillus coagulans, Bacillus brevis* and three different *Arthrobacter* sp.	MCP-treated black cotton field soil from Satara, Maharashtra, India,	*Pseudomonas mendocina* showed maximum degradation (73%) of MCP (500 mg L^{-1}) at pH 7, 150 rpm at 28 ± 2 °C in 8 days	Bhadbhade et al. (2002a)
17.	*Arthrobacter atrocyaneus* MCM B-425, *Bacillus megaterium* MCM B-423	MCP-contaminated vegetable farm soil in Manjri and cotton field soil in Jalna, Maharashtra, India	93% and 83% MCP (1000 mg L^{-1}) degradation within 8 days, at 30 °C by *A. atrocyaneus* MCM B-425 and *B. megaterium* MCM B-423, respectively. Phosphates, ammonia and carbon dioxide were the degraded products with methylamine and acetic or valeric acid as intermediate products	Bhadbhade et al. (2002b)
18.	*Arthrobacter atrocyaneus*, *Bacillus megaterium*, and *Pseudomonas mendocina*	MCP-contaminated soil	Maximum MCP degradation (65–77%) at pH 8, temperature 35 °C by *B. megaterium* and *P. mendocina* and at temperature 30 °C by *A. atrocyaneus*	Bhadbhade et al. (2002c)
19.	*Azospirillum lipoferum* and 4 *Bacillus* sp.	Black soil from a groundnut field	After 14 days, 40% MCP lost in uninoculated culture, whereas 62.86% MCP degraded by *A.lipoferum* and 79.16% by *Bacillus* sp.	Rangaswamy and Venkateswarlu (1992)
20.	*Bacillus* sp.	Field soil near Forest Research Institute from Dehradun	*Bacillus* sp. was able to degrade MCP (0.5%)	Samal and Kotiyal (2013)

Table 2 (continued)

S. no.	Microorganism/s	Sources	Findings	References
Fungi				
21.	*Aspergillus sojae strain* JPDA1	MCP-contaminated paddy field soil, Vellore District, Tamil Nadu, India	500 mg L^{-1} MCP degraded in 72 h in minimal media. In soil amended with nutrients, 500 mg L^{-1} MCP degraded in 144 h compared to soil devoid of nutrients in 168 h	Abraham et al. (2016)
22.	*A. niger*, *A. flavus, A. fumigatus, P. lanosum* and *T. viride*	MCP-contaminated soil of Vallam and Rajagiri, Thanjavur District	*A. niger* and *T. viride* showed maximum MCP (12 ppm) degradation	Thirugnanam and Senthilkumar (2016)
23.	*Aspergillus niger* JQ660373	–	After 15 days, residual MCP concentration found was 64.94 ± 0.42 µg mL^{-1} with rate constant of 0.002 per day (first-order kinetics) and half-life of 12.64 days	Jain and Garg (2015)
24.	*Aspergillus fumigatus*	–	*A. fumigatus* could tolerate only 1% MCP; No growth at higher concentration (2% and 3%). Presence of 1% Tween 80 increased growth rate	Pandey et al. (2014)
25.	*Aspergillus niger* JQ660373, *Penicillium aculeatum* JQ660374, *Aspergillus flavus, Macrophomina* sp. and *Fusarium pallidoroseum*	Agricultural soil containing chickpea, pearl millet and mung beans near Banasthali campus, Rajasthan, India	78% MCP (0.5% stock) degradation in 168 h with significant increase in phosphatase activity. Order of MCP degradation: *A. niger* JQ660373 > *P. aculeatum* JQ660374 > *A. flavus* > *F. pallidoroseum* > *Macrophomina* sp.	Jain et al. (2015)
26.	*Aspergillus flavus, Macrophomina* sp. and *Fusarium pallidoroseum*	Agricultural soil near Banasthali campus, Rajasthan, India	Degradation constant and half-life for MCP degradation (150 mg L^{-1}) by *A. flavus, Macrophomina* sp. and *F. pallidoroseum*: 0.007, 0.005 and 0.002 per day and 4.21, 6.32 and 12.64 days Overall order: *A. flavus* > *Macrophomina sp.* > *F. pallidoroseum*	Jain et al. (2014)
27.	*Aspergillus* sp.	Snake gourd crop *Trichosanthes cucumerina* L.) field	Complete degradation of 0.5% MCP in 8 days into non-toxic, volatile fatty acids—palmitic acid, behenic acid, stearic acid, etc.	Anitha and Das (2011)
28.	*Trichoderma viridae*	MTCC Chandigarh	Moderate rate of MCP degradation. Decrease in protein, carotenoid and chlorophyll content. No significant effect on root length	Balamurugan et al. (2010)
29.	Seven isolates: *Cunninghamella echinulata* (M1), *Fusarium oxysporum* (M5), *Emericella nivea* (M9), *Aspergillus niger* (E11), *Aspergillus oryzae* (E12), *Emericella nivea* (E16) and *Aspergillus oryzae* ARIFCC 1054 (M4)	MCP-contaminated soil	*Aspergillus oryzae* ARIFCC 1054 (M4) exhibited the highest tolerance of MCP (900 mg L^{-1}) and possessed phosphatase activity; 70% degradation of MCP in 50 h, undetectable (< 1 mg L^{-1}) at 168 h	Bhalerao and Puranik (2009)

Table 2 (continued)

S. no.	Microorganism/s	Sources	Findings	References
Algae				
30.	*Chlorogloea fritschii* ARM 342, *Nostoc* sp. BDU-2, *Nostoc muscorum* ARM 221, *Anabaena azollae* AX61A, *Aulosira fertilissima* ARM 68, *Anabaena* sp. ARM 340, *Tolypothrix tenuis* ARM 76, *Calothrix brevissima* ARM 451, *Haplosiphon* sp. ARM 98 and *Mastigocladus* sp. ARM 351	National Facility for Blue Green Algal Collections, IARI, New Delhi, and R. W. Fischer, Virginia Commonwealth University, Virginia, USA	*Aulosira fertilissima* ARM 68 and *Nostoc muscorum* ARM 221 could tolerate MCP up to100 ppm and used it as phosphorus source. MCP-induced acid phosphatase activity	Subramanian et al. (1994)
31.	Soil microflora and different algal species: *Anabaena variabilis, Lyngbya gracilis, Nostoc punctiforme* and *Phormidium foveolarum*	Rice field	Algae could grow even at 1 and 2 kg ha^{-1} of MCP. Under flooded conditions no toxicity observed. MCP decreased to trace amounts in 20 days	Megharaj et al. (1988)
32.	Two green algae: *Scenedesmus bijugatus* and *Chlorella vulgaris* Three BGA: *Phormidium tenue*, *Nostoc linckia* (Roth) B and F and *Synechococcus elongatus* Nageli	Soil	60.4% MCP recovered in uninoculated samples, whereas in inoculated samples it decreased to 16.7% to insignificant levels in 30 days	Megharaj et al. (1987)
33.	*Chlorella vulgaris, Gloeocystis gigas, Chlorococcum humicola, N. punctiforme, Scenedesmus bijugatus, Phormidium* sp., *Nostoc linckia* and *Synechococcus elongatus*	Cotton field	MCP (0.5–2 kg ha^{-1}) triggered germination of resting algal species. 5 kg ha^{-1} increased algal population by sixfold	Megharaj et al. (1986a)
34.	Green alga—*Scenedesmus bijugatus* Three blue-green algae—*Nostoc linckia*, *Synechococcus elongatus* and *Phormidium tenue*	Black soil of a cotton field	5–10 µg mL^{-1} MCP enhanced cell number and chlorophyll *a* content of all algae. *S. elongatus* could grow at 100 µg mL^{-1} MCP; toxic above 20, 50 and 100 µg mL^{-1} to *S. bijugatus, Phormidium tenue* and *Nostoc linckia,* respectively	Megharaj et al. (1986b)

MCP monocrotophos

Silambarasan 2015). Another bacterial isolate, YW6, characterized as *Starkeya novella* could utilize monocrotophos for its growth as the sole carbon and nitrogen source. Within 36 h, it degraded 0.2 mM monocrotophos with no lag period. The initial rate of monocrotophos degradation was slowed down by the addition of carbon source, whereas the presence of a more favourable nitrogen source enhanced the degradation of monocrotophos (Sun et al. 2016). In another research, *Paracoccus* sp. M1 was able to mineralize 300 mg L^{-1} of monocrotophos along with other organophosphorus insecticides and amide herbicides under different culture conditions. The key enzyme responsible for the initial breakdown of monocrotophos was a constitutively expressed cytosolic protein (Jia et al. 2006).

Subhas and Singh (2003) studied two bacterial isolates *Pseudomonas aeruginosa* F10B and *Clavibacter michiganense* subsp. *insidiosum* SBL 11 capable of degrading 98.9% and 86.9% technical monocrotophos, respectively, under laboratory conditions and 79% and 80% of pure monocrotophos within 24 h at 37 °C, where 500 ppm was the optimal monocrotophos concentration required for their normal growth by the production of enzyme phosphotriesterase (PTE). Purified PTE isolated from *Clavibacter michiganense* subsp. *insidiosum* SBL11 was found to be a monomeric enzyme (molecular mass—43.5 kDa; pI—7.5), while PTE from *Pseudomonas aeruginosa* F10B was a heterodimeric enzyme (molecular mass—43 and 41 kDa; pI—7.9 and 7.35). The enzyme isolated from strain F10B was more thermostable (half-life 7.3 h) than that from SBL11 (half-life 6.4 h at 50 °C), while both the enzymes showed the same temperature optimum of 37 °C (Das and Singh 2006). Similar research was conducted by a research group, where they isolated 17 bacterial isolates (16 different *Bacillus* sp. and *Arthrobacter atrocyaneus*) (Bhadbhade et al. 2002b). Among them, *Bacillus megaterium* and *Arthrobacter atrocyaneus* were selected for further studies on monocrotophos degradation and its metabolic pathway. Within 8 days, the isolates degraded monocrotophos to an extent of 93% and 83%, respectively, from synthetic media spiked with 1000 mg L^{-1} monocrotophos. Enzymes are the key factors responsible for bioremediation of pesticides including monocrotophos (Table 3).

Phosphatases (mono and dimethyl) and esterases are the enzymes involved in the biodegradation of monocrotophos into ammonia, carbon dioxide, and phosphates through formation of intermediate compounds as valeric acid or acetic acid, methylamine and other metabolites (Bhadbhade et al. 2002b). The first step of monocrotophos degradation involves hydrolysis, producing *N*-methyl acetoacetamide along with dimethyl phosphate (Beynon et al. 1973). In the next step, degradation of *N*-methyl acetoacetamide produces valeric acid in *Arthrobacter atrocyaneus* and acetic acid in *Bacillus megaterium* (Bhadbhade et al. 2002b) (Fig. 3). Acetic acid is the key intermediate of the metabolic pathways in different microbes.

Fungal degradation of monocrotophos

Fungi are important part of the environment due to their significant role in biogeochemical cycles and their capacity to degrade xenobiotics including pesticides. Results of different published studies showed that fungi are capable of causing minor changes in the chemical structure of the applied pesticide resulting in the formation of bio-transformed products which are further taken up and degraded by other potential soil microbes (Maqbool et al. 2016). Benefits of better tolerance, oxidizing ability and mycelial niche are offered by fungi, and they do not require prior exposure to any specific pollutant and are cost-effective bioremedial agent (Jain et al. 2014).

Among twenty-five isolated strains, isolate M-4, i.e. *Aspergillus oryzae* ARIFCC 1054, degraded 500 mg L^{-1} of monocrotophos, where monocrotophos concentration reached undetectable levels (< 1 mg L^{-1}) in 168 h (Bhalerao and Puranik 2009) (Table 2). Complete enzymatic mineralization of monocrotophos by *Aspergillus* sp. in 8 days was reported by Anitha and Das (2011). Monocrotophos was broken down into non-toxic volatile fatty acids (stearic acid, palmitic acid and behenic acid) and other unknown metabolites. In another study, *Aspergillus fumigatus* was able to degrade 1% monocrotophos, whereas it was unable to grow at higher concentration (2% and 3%). However, the presence of 1% Tween 80 enhanced monocrotophos degradation and increased fungal growth (Pandey et al. 2014). Also, *Aspergillus niger* and *Trichoderma viride* isolated from monocrotophos-contaminated soil showed monocrotophos (12 mg L^{-1}) degradation (Thirugnanam and Senthilkumar 2016). *Aspergillus sojae* strain JPDA1 isolated from sugarcane fields could degrade 500 mg L^{-1} of monocrotophos in 72 h in minimal media. Two types of trials were carried out in this study, where soil was spiked with 500 mg L^{-1} of monocrotophos. In the first trail, soil was amended with nutrients, whereas in the second trail soil was devoid of nutrients. In the former trail, the strain degraded the insecticide in 144 h, whereas in the latter, it took 168 h for degradation (Abraham et al. 2016).

Jain and Garg (2015) studied biomineralization of monocrotophos by *Aspergillus niger* JQ660373. After an incubation of 15 days, the resulting residual concentration was 64.94 ± 0.42 µg mL^{-1}, following first-order kinetics with the rate constant of 0.002 per day and half-life of 12.64 days. Rate of monocrotophos degradation by fungus was compared with degradation by enzymatic method. Various enzymes, viz. hydrolases and acid phosphatases, isolated and purified from the various fungal isolates like *Penicillium aculeatum*, *Aspergillus flavus*, *Fusarium pallidoroseum*,

Table 3 Enzymatic degradation of monocrotophos

S. no.	Enzyme/s used	Source	Findings	References
1.	Laccase	*Pseudomonas* sp. S2	Alkali—stable extracellular enzymes; degraded 80.56 ± 0.6% MCP, without addition of any mediator	Chauhan and Jha (2017)
2.	Hydrolases	*Aspergillus niger* JQ660373	After 15 days, residual MCP was 16.95 ± 0.55 µg mL^{-1} with rate constant of 0.136 per day (first-order kinetics) and half-life of 5.14 days	Jain and Garg (2015)
3.	Hydrolases	*Aspergillus niger J*Q660373	MCP half-life time with enzymatic method was 0.79 days	Jain and Garg (2014)
4.	Hydrolases (OPH33 and OPH67)	*Penicillium aculeatum* ITCC 7980.10 (M3) and *Fusarium pallidoroseum* ITCC 7785.10 (M4)	M3 OPH67 hydrolase was more efficient in bioremediation of MCP.	Jain et al. (2013a)
5.	Acid phosphatases (P33 and P67)	*Aspergillus niger* ITCC 7782.10	Both the acid phosphatases can be used in MCP bioremediation	Jain et al. (2013b)
6.	Hydrolases	*Aspergillus niger* (M1), *Aspergillus flavus* (M2), *Penicillium aculeatum* (M3), *Fusarium pallidoroseum* (M4), and *Macrophomina* sp. (M5)	90% MCP degraded by 150 µg ml^{-1} of enzyme in 120 h, with rate constants 0.0368, 0.0138, 0.048, 0.016 and 0.0138 per day and half-life of 0.79, 2.11, 0.6, 1.8 and 2.11 days for M1, M2, M3, M4 and M5, respectively. Overall order of degradation: *P. aculeatum* > *A. niger* > *F. pallidoroseum* > *A. flavus* = *Macrophomina* sp.	Jain and Garg (2013)
7.	Phosphotriesterase	*Pseudomonas aeruginosa* F10B and *Clavibacter michiganense* subsp. *insidiosum* SBL11	MCP degrading phosphotriesterase was capable of degrading other organophosphate insecticides like paraoxon. Also degraded tris-*p*-nitrophenyl phosphate	Das and Singh (2006), Subhas and Singh (2003)
8.	Genetically engineered enzyme	Carboxylesterase B1 gene transferred to *E. coli*	13.4% MCP degraded in 2 h at 37 °C	Qiao et al. (2003)

MCP monocrotophos

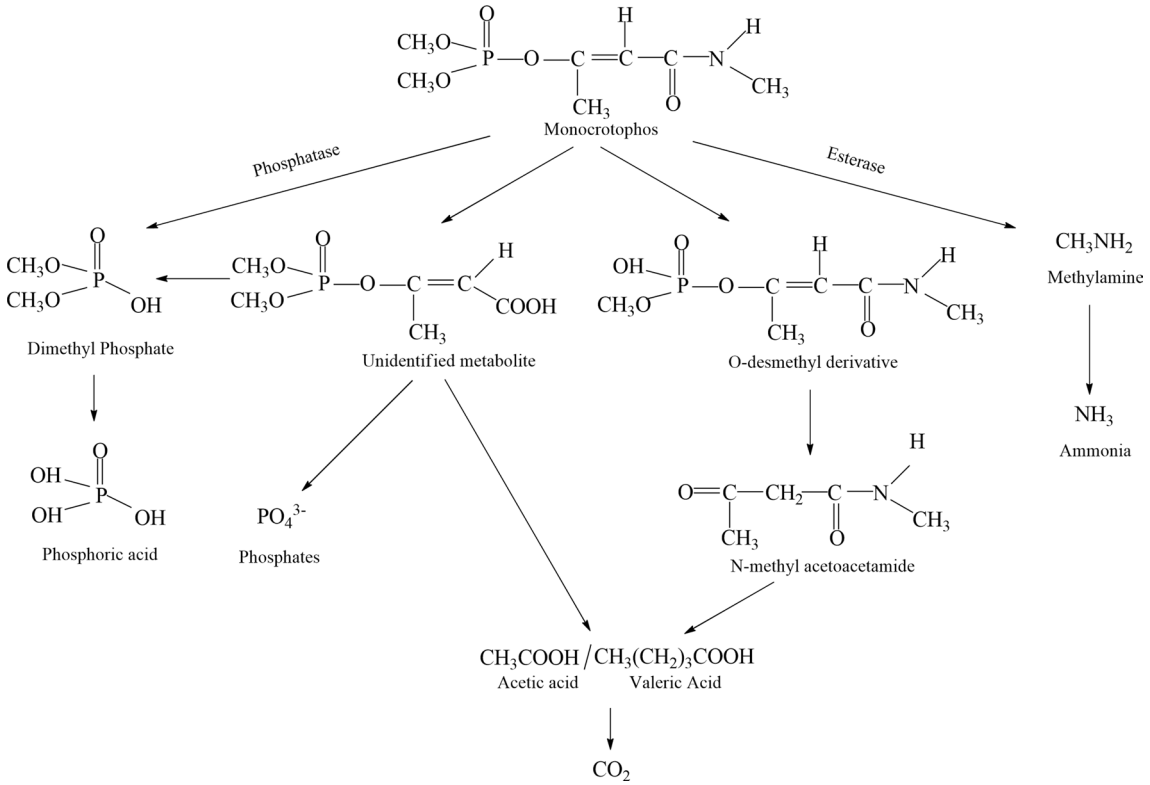


Fig. 3 Proposed pathway of microbial degradation of monocrotophos. Mineralization takes place by hydrolysis of P–O alkyl bond by phosphatase forming dimethyl phosphate, which further produces phosphoric acid. Cleavage of vinyl phosphate bond forms *N*-methyl acetoacetamide via *O*-desmethyl derivative. Esterase or phosphotriesterase cleaves C–N bond of monocrotophos forming methylamine, which is oxidized into ammonia by methylamine dehydrogenase. Acetic acid, valeric acid, phosphates and carbon dioxide are produced along with an unidentified metabolite

Macrophomina sp., *Penicillium aculeatum* ITCC 7980.10, *Fusarium pallidoroseum* ITCC 7785.10, *Aspergillus niger* ITCC 7782.10 and *Aspergillus niger* JQ660373 (Jain and Garg 2013, 2015; Jain et al. 2013a, b) showed different capacity to degrade monocrotophos.

Algal degradation of monocrotophos

Different algal species have been studied for the biodegradation of monocrotophos (Table 2). Among various algal isolates, *Nostoc muscorum* ARM 221 and *Aulosira fertilissima* ARM 68 used monocrotophos as phosphorus source and could tolerate it up to100 ppm. Monocrotophos induced acid phosphatase activity (Subramanian et al. 1994), and 0.5–2 kg ha^{-1} of the compound triggered germination of different resting algal species (*Chlorococcum humicola, Chlorella vulgaris, Nostoc linckia, Gloeocystis gigas, N. punctiforme, Scenedesmus bijugatus, Phormidium* sp. and *Synechococcus elongatus*). On using 5 kg ha^{-1} of monocrotophos, it increased algal population by sixfold (Megharaj et al. 1986a). Lower concentration of monocrotophos (5–10 µg mL^{-1}) enhanced cell number along with chlorophyll *a* content of all algae. Blue-green algae *S. elongatus* could grow at 100 µg mL^{-1}, whereas other algal isolates *S. bijugatus, Phormidium tenue*, and *Nostoc linckia* could not tolerate even 20 µg mL^{-1} monocrotophos (Megharaj et al. 1986b). After 30 days of incubation with different algal isolates (*Scenedesmus bijugatus, Chlorella vulgaris, Phormidium tenue*, *Nostoc linckia* (Roth) B and F and *Synechococcus elongatus* Nageli), monocrotophos level decreased to 16.7%, confirming their efficiency to degrade the insecticide (Megharaj et al. 1987). Other algal isolates, viz. *Anabaena variabilis, Lyngbya gracilis, Nostoc punctiforme* and *Phormidium foveolarum*, utilized 1 and 2 kg ha^{-1} of monocrotophos, and no toxicity was observed (Megharaj et al. 1988).

Factors affecting biodegradation of monocrotophos

The degradation ability of microbes is influenced by several factors. The operating parameters like pesticide concentration, temperature, pH, moisture content, and available nutrients have been extensively studied for effective biodegradation of monocrotophos. The available literature shows that degradation efficiency of microbes decreases with higher initial concentration of pesticide. Samal and Kotiyal (2013) assessed the growth of *Bacillus* sp. in Bushnell Haas media

spiked with different monocrotophos concentration (0.5%, 1%, 1.5%). Bacteria showed the best growth in media spiked with 0.5% monocrotophos. *Paracoccus* sp. (M1) could easily degrade 300 mg L^{-1} of monocrotophos, whereas 500 mg L^{-1} monocrotophos was toxic for its growth (Jia et al. 2006). *Bacillus megaterium, Arthrobacter atrocyaneus* and *Pseudomonas mendocina* were able to tolerate 2500 mg L^{-1} monocrotophos and use it as carbon source (Bhadbhade et al. 2002c).

Most of the research conducted shows the optimum temperature for monocrotophos degradation by bacteria ranges from 30 to 37 °C (Abraham et al. 2014; Abraham and Silambarasan 2015; Acharya et al. 2015). Optimum degradation temperature for fungus ranges from 25 to 30 °C (Balamurugan et al. 2010; Jain et al. 2014; Abraham et al. 2016), whereas for algae it is 27–30 °C (Megharaj et al. 1986a, 1987; Subramanian et al. 1994). Different microbes degrade monocrotophos in the pH ranging from 5.5 to 8.5; however, the conclusions are divergent. *Bacillus megaterium, Arthrobacter atrocyaneus* and *Pseudomonas mendocina* showed maximum degradation of monocrotophos (100–500 mg L^{-1}) at varying temperature 30–35 °C, pH 7.0–8.0 and inoculum density 10^8 cells/mL under aerated conditions (Bhadbhade et al. 2002c).

The decomposition of pesticides by micro-organisms is greatly affected by the availability of both macro- and micro-nutrients (C, N, O, H, P, etc.) in the soil (Yadav et al. 2016). KaviKarunya and Reetha (2012) reported maximum growth of *Pseudomonas fluorescens, Bacillus subtilis* and *Klebsiella* sp. at pH 6 and 35 °C. Bacteria showed maximum growth in the presence of dextrose as carbon source and malt extract as nitrogen source, whereas lesser growth in the case of mannose (carbon source) and beef extract (nitrogen source). *Starkeya novella* effectively decomposed 0.2 mM monocrotophos in 36 h with no lag phase. Supplementing media with more carbon source slowed down the initial rate of monocrotophos degradation, whereas monocrotophos transformation was enhanced by addition of more favourable nitrogen source, which was ammonium chloride (Sun et al. 2016). Monocrotophos degradation in soil was enhanced by light (UV/sunlight), moisture content (more in flooded soil) and the type of water (more in tap water than the distilled water) (Dureja 1989). Proper aeration and shaking conditions are better for monocrotophos removal than the static conditions (Bhadbhade et al. 2002c).

Photocatalytic degradation of monocrotophos

In recent years, photobased processes involving utilization of light radiation (sunlight or external UV light) have been extensively studied for the mineralization of harmful pesticides, including monocrotophos. Pesticide absorbs the light energy (photons), gets activated and transforms into other chemical form through its homolytic cleavage. The excited molecule further undergoes processes like homolysis, heterolysis, photoionization or itself decomposes with light energy (Reddy and Kim 2015). This process termed as photolysis has several advantages like low cost, easy handling, high efficiency and no waste disposal problem (Bhatkhande et al. 2002; Reddy and Kim 2015).

Dureja (1989) studied the photolysis of monocrotophos in soil, water and plant foliage in the presence of sunlight as well as ultraviolet light. His study proved that sunlight degraded monocrotophos to a greater extent. Gas liquid chromatography analysis recovered 98% monocrotophos from the sample exposed to dark conditions, whereas only 72.8% monocrotophos was recovered back in 8 h from sunlight-exposed samples, indicating photodecomposition. Experiments conducted on different types of soil proved that alluvial soil showed the lowest monocrotophos recovery, indicating maximum photolysis capacity. Also, monocrotophos degradation increased in flooded soil. Rate of monocrotophos degradation in tap water was twice as in distilled water.

Photocatalysis entails the combination of radiation and catalyst. Owing to its lower cost, structural stability, non-toxicity, long life span, high photocatalytic activity and its tolerance to both acidic and alkaline solutions, titanium dioxide (TiO_2) has been widely employed as photocatalyst (Shifu and Gengyu 2005; Anandan et al. 2009). Among the three forms of Titania (i.e. brookite, anatase and rutile), anatase due to its stability has been employed most commonly in ambient conditions. Titania photocatalysts are commercially available under different trade names such as Degussa P25, PC 500 and Millennium (Reddy and Kim 2015). Titanium-mediated photocatalytic degradation of monocrotophos along with the effect of O_2 and H_2O_2 on the photodegradation was demonstrated by Hua et al. (1995). The presence of anions Cl^-, ClO_4^-, NO_3^- and PO_4^{3-} and Cu^{2+} above 10^{-5} M showed detrimental effect on monocrotophos degradation, whereas SO_4^{2-} and Cu^{2+} below 10^{-5} M promoted the rate of degradation. Addition of O_2 and H_2O_2 during the process also enhanced the degradation rate. 0.65×10^{-4} mol dm^{-3} monocrotophos along with other organophosphates was completely photocatalytically degraded to the final degradation product PO_4^{3-} using TiO_2 thin films (Mengyue et al. 1995) or TiO_2 supported on fibreglass cloth (Shifu et al. 1996) (Table 4).

Ku and Jung (1998) showed that monocrotophos degradation by UV/TiO_2 photocatalysis was more effective for acidic solutions than alkaline ones. Also, the presence of dissolved oxygen enhanced monocrotophos decomposition to a certain limit, after which it posed no further effect. Shankar et al. (2004) studied monocrotophos degradation using bare TiO_2 and Hβ-supported TiO_2. The latter showed higher activity due to greater monocrotophos adsorption on

Table 4 Photocatalytic degradation of monocrotophos

S. no.	Photocatalyst used	Source of light	Intermediates or end products detected	Comments	References
1	TiO_2	16 W UV light source	–	Photocatalytic efficiency was maximum at pH 5	Amalraj and Pius (2015)
2	Aeroxide P-25 TiO_2 and LR grade TiO_2	UV and sunlight	–	Addition of H_2O_2 had positive effect on photocatalytic activity	Sraw et al. (2014)
3	Pure TiO_2 and Mg^{2+} doped TiO_2	High-pressure 400 W mercury lamp	Phosphate ion	Doped catalyst had greater photocatalytic efficiency than pure TiO_2 and Degussa P-25	Avasarala et al. (2011)
4	TiO_2	UV lamp	–	Catalyst concentration had positive impact up to 4 g L^{-1} and no change occurred beyond it	Sivagami et al. (2011)
5	TiO_2 and IO_3^--doped TiO_2	UV light	–	The high activity of IO_3^--doped TiO_2 was strongly dependent on nanoparticles' structural, morphological and composition properties	Anandan et al. (2009)
6	ZnO, La-doped ZnO, TiO_2	Low-pressure mercury lamps	Carbon dioxide, water, phosphates and nitrates	0.8 wt% La-doped ZnO has higher photocatalytic activity than pure ZnO and TiO_2	Anandan et al. (2007)
7	Zeolites Hβ, HY and HZSM-5 (supports), ZnO, supported ZnO (ZnO/Hβ(I), ZnO/Hβ(M), ZnO/HY(I), ZnO/HZSM-5(I)) and TiO_2/Hβ	Low-pressure mercury lamps	–	There was a mutual synergistic influence between supports and catalyst on MCP	Anandan et al. (2006)
8	$TiO_2.SiO_2$ beads	Sunlight	Phosphate ion	Complete degradation in 420 min	Shifu and Gengyu (2005)
9	TiO_2 and TiO_2/Hβ	Low-pressure mercury lamps	–	Hβ-supported TiO_2 had greater MCP decomposition activity	Shankar et al. (2004)
10	Degussa P-25 TiO_2	365 nm black blue fluorescent 15 W UV lamp	Carbonate ions, phosphorus- and nitrogen-containing organic intermediates	Acidic solutions had higher decompositions rates; decomposition increased with increase in light intensity	Ku and Jung (1998)
11	TiO_2 supported on fibreglass	UV 372 W mercury lamp	Phosphate ion	No significant loss of photocatalytic activity of TiO_2 after 120 h of UV illumination	Shifu et al. (1996)
12	Thin films of TiO_2	UV 372 W mercury lamp	Phosphate ion	Addition of H_2O_2 (6×10^{-3} mol dm^{-3}) or Fe^{3+} (10^{-4} mol dm^{-3}) increased photodegradation	Mengyue et al. (1995)
13	Degussa P-25 TiO_2	20 W black light fluorescent tube	Phosphate ion	51% degradation in 1 h; anions had detrimental effect, whereas low concentration of Cu^{2+} (below 10^{-5} M) enhanced the photocatalytic rate slightly	Hua et al. (1995)

MCP monocrotophos

the support and capacity to delocalize the conduction band electrons of excited Titania. Shifu and Gengyu (2005) studied the feasibility of monocrotophos decomposition in sunlight using floating $TiO_2{\cdot}SiO_2$ photocatalyst beads that were prepared by the dip coating method by using hollow glass microbeads as carrier along with titanium tetraisopropoxide [$Ti(iso\text{-}OC_3H_7)_4$] and ethyl silicate as raw materials. As per their results, the best heat treatment condition for $TiO_2{\cdot}SiO_2$ beads was at 650 °C for 5 h and 0.20 (molecular fraction) is the optimum amount of SiO_2. Anandan et al. (2006) studied monocrotophos degradation with different supports (Hβ, HY and HZSM-5), ZnO, supported ZnO and TiO_2/Hβ. Hβ, HY and HZSM-5 were the H-forms of zeolites produced from sodium forms β, Y and ZSM-5. The supported catalysts, ZnO/Hβ(I), showed higher percentage of adsorption than others.

The breakdown of monocrotophos in an aqueous suspension using synthesized La-doped ZnO nanoparticles was studied by the same group (Anandan et al. 2007). 0.8 wt% La-doped ZnO showed high relative photonic efficiencies as well as high monocrotophos degradation photocatalytic activity, which was due to small particle size, separation of charge carriers (e^-/h^+), rough and high porous surface of La-doped ZnO. Anandan et al. (2009) showed that iodine-doped (IO_3^-) TiO_2 has greater photocatalytic activity in monocrotophos decomposition in comparison with Degussa-P25. It could also be used for the degradation of other contaminants in water.

Avasarala et al. (2011) studied the monocrotophos degradation with Mg-doped TiO_2 and pure TiO_2. Maximum degradation of 50 mM monocrotophos was shown by 0.5gm of 1.0 wt% of Mg^{2+} dopant, at pH 3, which was due to decreased particle size and increased surface area of Mg^{2+}–TiO_2. Due to amphoteric nature of TiO_2, rate of degradation of monocrotophos is the highest at acidic pH (Sivagami et al. 2011; Amalraj and Pius 2015). Sraw et al. (2014) compared the photocatalytic activity of aeroxide TiO_2 and LR grade TiO_2 both under sunlight and UV light. At constant temperature, P25 showed maximum degradation, i.e. 86.9% and 83.55% under UV and sunlight, whereas LR grade TiO_2 showed 66.21% and 72.5% degradation under similar conditions at pH 5. The combination of ultraviolet radiation and ultrasound irradiation along with heterogenous or homogenous catalyst and oxidizing reagent (i.e. Fenton reagent, H_2O_2, ozone) has also been used to decompose monocrotophos (Ku and Wang 1999; Madhavan et al. 2010; Üstün et al. 2015; Sivagami et al. 2016). Photolytic degradation rate of monocrotophos using TiO_2 was lower than that of sonolysis due to the interference of phosphate ions formed as an intermediate, but is greater than sonophotocatalytic degradation rate (Madhavan et al. 2010). ZnS, CdS, Si, SnO_2, Fe_2O_3 are some of the other potential photocatalysts used (Bhadbhade et al. 2002a, b, c; Avasarala et al. 2011) for remediation.

Mechanism of photocatalytic degradation

The principle behind photocatalysis of any compound is the photo-excitation of a semiconductor catalyst due to the absorption of electromagnetic radiation in the presence of either UV or visible spectrum. When a semiconductor catalyst is illuminated with photons, electrons present in the valence band of the semiconductor are excited to the conduction band upon absorption of light energy, leaving a positive hole in the valence band. This empty hole on the valence band (± charge) and electron on the conduction band (− charge) are capable of inducing reduction or oxidation of monocrotophos or other adsorbate either directly or by reacting with electron donors like water to form hydroxyl radicals (·OH), which in turn react with the pollutant (Reddy and Kim 2015; Goel and Seepana 2016). The photocatalytic degradation reaction of monocrotophos along with other organophosphates occurs on the surface of catalyst TiO_2, primarily in trapped holes. Oxygen (O_2) and water (H_2O) are necessary components of photocatalytic degradation, whereas ·OH radicals and peroxide ion (O_2^{2-}) are proposed as the primary reactive species (Mengyue et al. 1995). On this basis, a lot of research has been done on monocrotophos degradation using TiO_2 nanoparticles as photocatalyst. When a photocatalyst TiO_2 is illuminated by photons, electrons are ejected from the valence band to the conduction band leaving positive holes in the valence band.

$$TiO_2 + h\nu \rightarrow TiO_2\left(e_{cb}^- + h_{vb}^+\right) \quad (1)$$

$$TiO_2\left(h_{vb}^+\right) + H_2O \rightarrow TiO_2 + {\cdot}OH + H^+ \quad (2)$$

$$TiO_2\left(h_{vb}^+\right) + OH^- \rightarrow TiO_2 + {\cdot}OH \quad (3)$$

$$TiO_2\left(e_{cb}^-\right) + O_2 \rightarrow TiO_2 + {\cdot}O_2^- \quad (4)$$

$${\cdot}O_2^- + H^+ \rightarrow HO_2{\cdot} \quad (5)$$

$${\cdot}O_2^- + HO_2{\cdot} \rightarrow {\cdot}OH + O_2 + H_2O_2 \quad (6)$$

$$2HO_2{\cdot} \rightarrow O_2 + H_2O_2 \quad (7)$$

$$TiO_2\left(e_{cb}^-\right) + H_2O_2 \rightarrow TiO_2 + OH^- + {\cdot}OH \quad (8)$$

$$\begin{aligned}{\cdot}OH + \text{monocrotophos} &\rightarrow \text{intermediate metabolites} \\ &\rightarrow CO_2 + H_2O + PO_4^{3-}\end{aligned} \quad (9)$$

Oxygen adsorbed on TiO_2 surface prevents the recombination of electron–hole pairs by trapping electrons, generating superoxide radical (O_2^-), which in turn produces hydrogen peroxide (H_2O_2), hydroperoxyl ($HO_2{\cdot}$) and ·OH radicals (Avasarala et al. 2011; Reddy and Kim 2015). ·OH

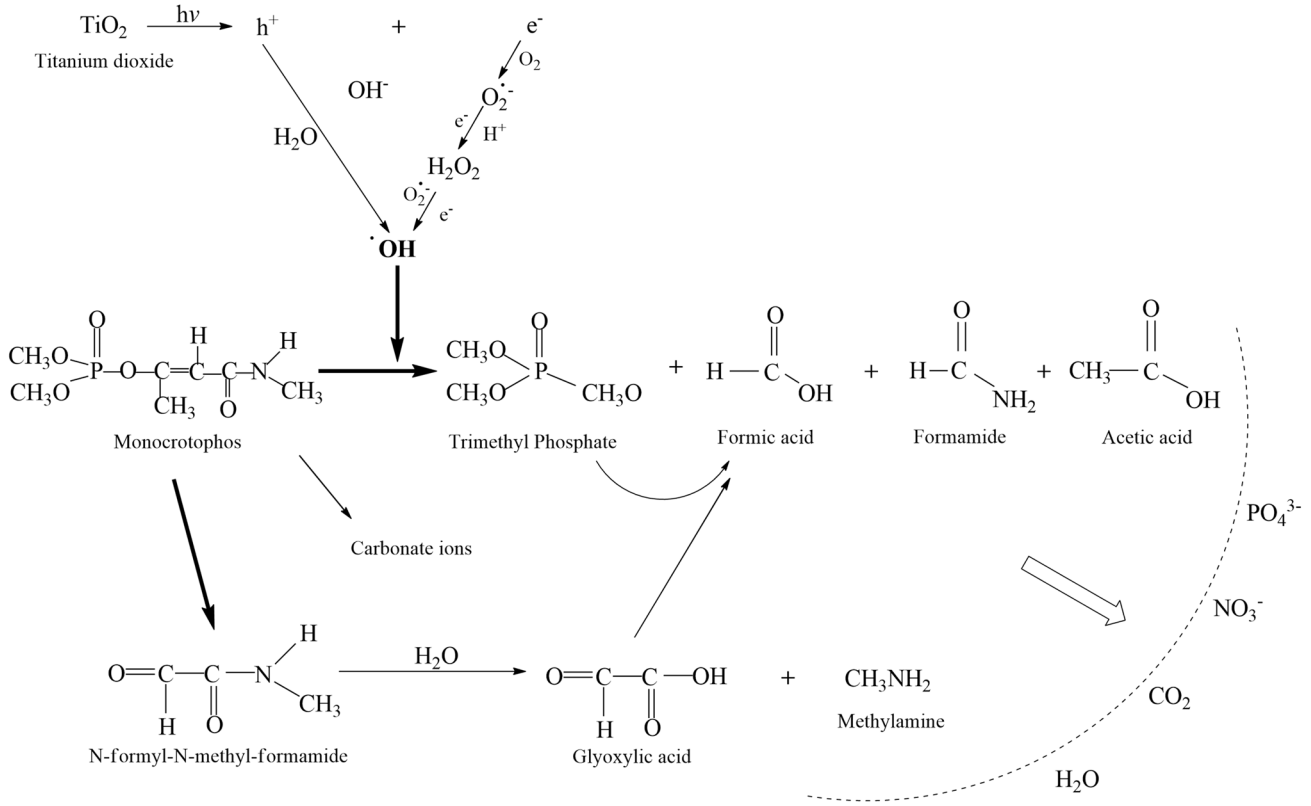


Fig. 4 Proposed photocatalytic pathway for the degradation of monocrotophos. Monocrotophos is completely mineralized into phosphates, nitrates, carbon dioxide and water by reacting with hydroxyl radical produced on photonic activation of TiO_2 via formation of *N*-formyl-*N*-methyl-formamide or trimethyl phosphate along with formic acid, formamide and acetic acid. *N*-formyl-*N*-methyl-formamide undergoes hydrolysis to form glyoxylic acid and methylamine, which further produces formic acid. Carbonate ions are also produced at the beginning of the reaction

radicals are formed from the holes reacting with either H_2O or OH^- adsorbed on TiO_2 surface. In Eqs. (1)–(9), ·OH and O_2^{2-} are the most important oxidants and H_2O_2, O_2 and HO_2· are suitable for trapping electrons (Mengyue et al. 1995).

Monocrotophos undergoes breakdown to simpler compounds when it reacts with ·OH produced on photonic activation of TiO_2 (Fig. 4). The oxidizing power of the ·OH radicals is strong enough to break ester group of monocrotophos that has strong acidity (Mengyue et al. 1995; Shifu and Gengyu 2005). The breakdown probably occurs in two possible ways: by the formation of either phosphate compound such as trimethyl phosphate or nitrogenous compound such as *N*-formyl-*N*-methyl-formamide (Sraw et al. 2018). Apart from trimethyl phosphate, other intermediate metabolites formed during the process are formic acid, formamide, acetic acid and other small organic molecules. Trimethyl phosphate is directly photochemically degraded to phosphate ions (PO_4^{3-}) and formic acid. Formation of carbonate ions also occurs very early during the decomposition of monocrotophos (Ku and Jung 1998). The intermediate compounds are further broken down into nitrates, phosphates, CO_2 and H_2O by means of hydrolysis and redox reactions (Ku and Jung 1998; Shifu and Gengyu 2005; Sraw et al. 2018).

Other methods for removal of monocrotophos

The degradation or removal of monocrotophos along with other pesticides has been achieved through various advanced oxidation processes such as ozonation (Ku et al. 1998; Ku and Wang 1999; Hongsibsong and Sapbamrer 2018), photolysis (Ku et al. 2000), photocatalysis (Sraw et al. 2014; Aziz et al. 2017), electrolysis (Yatmaz and Uzman 2009), Electro-Fenton process (Guivarch et al. 2003) and chemical oxidation (Wei et al. 2017a, b). Advanced oxidation processes using gamma irradiation (Ismail et al. 2014) and hydroxyl and sulphate radical anions (Yang et al. 2017; Xiao et al. 2018) have gained much attention these days. Due to the large surface area, silica (Bapat et al. 2016) and silver (Saifuddin et al. 2011) nanoparticles are used for decontamination of drinking water. However, due to their small size, these nanoparticles can easily enter the food chain and can induce several

other toxicological responses (Ranjan et al. 2018). Photocatalysis offers several advantages including chemical stability, low cost, complete mineralization, mild temperature, and pressure conditions and no waste disposal issues (Bhadbhade et al. 2002a, b, c; Avasarala et al. 2011). Photocatalysts such as ZnO and CdS lack long-term stability in aqueous media. Metal sulphide semiconductors are unstable as they undergo photocathodic corrosion (Bhadbhade et al. 2002a, b, c). Catalyst separation from the solution is one of the major problems faced in photocatalytic degradation (Goel and Seepana 2016; Sivagami et al. 2016). Though TiO_2 is favoured over other catalysts, due to its high band gap (3.2 eV) it is only active under UV light, restricting the use of visible light or sunlight. Another issue that limits its photocatalytic activity is low photoquantum efficiency, which is the result of high rate of electron–hole recombination at the surface of TiO_2 particles (Avasarala et al. 2011). These issues are overcome by surface immobilization of photocatalyst or doping, which, however, lowers the efficiency (Avasarala et al. 2011; Sivagami et al. 2016).

Another most popular and efficient process that plays important part in removal of pesticides is adsorption (Wei et al. 2017a; Moon et al. 2019). pH- and temperature-dependent adsorption of monocrotophos from aqueous solution has been achieved by the use of agricultural waste jute fibre. It showed the adsorption capacity of 124 mg L^{-1} (Sadasivam et al. 2010). Biopolymer (chitosan/gum ghatti/polylactic acid)-modified montmorillonite (MMT)-CuO composites were used for adsorption of monocrotophos, where MMT-CuO-polylactic acid showed maximum removal (83.99%) (Sahithya et al. 2016).

Perspectives

Degradation of monocrotophos using microbes has been widely studied, and there is a need to further screen anaerobic microbes and extremophiles, which may prove to be more effective in monocrotophos degradation. Genetic manipulation can help in the development of efficient enzymatic methods for pesticide degradation. Genes like *mpd* and *opd* are highly capable of degrading organophosphates (Karpouzas and Singh 2006). However, many efforts are required to study specific genes responsible for the degradation of specific pesticides.

Most of the reported monocrotophos remediation studies lack information on kinetics of monocrotophos biodegradation. This knowledge would enhance our understanding and contribute towards various processes for in situ application of microbial communities for the biodegradation of monocrotophos. One of the major challenges is scaling up of the laboratory results to the fields, whether the behaviour of microbes studied differs in the soil or still remains same. In addition, studies on interactions between microbes are also to be carried out, as synergistic interactions may enhance remediation process. Microbial consortium needs to be grown on large scale in bioreactors and requires process development and their large-scale field application. Nanotechnology is an emerging field, which can also be employed in removal of contaminants along with the use of certain polymers. Although physical and chemical methods are fast, they are expensive and inefficient in comparison with microbial degradation, which is cheap and eco-friendly (Bapat et al. 2016).

Conclusion

In the present scenario, the farmers are more concerned for the agricultural yield than the environmental safety. Field application of monocrotophos is banned, but still it is used at the rate of 0.25–1.5 kg ha^{-1} by the Indian farmers and in other parts of the world. Accumulation of monocrotophos in living tissues poses harmful threat to humans and adverse effects on non-target living systems present in the environment. It causes histopathological, acute, genotoxic, cardiotoxicity, hyperglycaemic and stressogenic effects to different living organisms. There is an urgent need to completely ban on its manufacturing, sale as well as usage and monitor its residues in soil and water.

Bacterial systems such as *Bacillus* sp., *Arthrobacter atrocyaneus*, *Azospirillum lipoferum*, *Paracoccus* sp. and *Pseudomonas* sp. can catabolize monocrotophos due to their ability to grow rapidly in diverse range of pH, temperature and other harsh conditions as compared to fungi and algae. Various enzymes such as hydrolases and acid phosphatases have been characterized and evaluated for their catalytic activity in monocrotophos degradation. Photocatalytic degradation has gained a lot of attention due to rapid mineralization of hazardous compounds, that occurs as a result of production of ·OH radicals by photonic activation of TiO_2 or ZnO catalysts. To combat adverse effects of monocrotophos and its intermediates, its biodegradation would be the most promising, relatively efficient and cost-effective way followed by photocatalytic degradation.

Acknowledgements The authors are thankful to the Director, Thapar Institute of Engineering and Technology (Deemed to be University), Patiala, for infrastructural and financial support.

References

Abraham J, Silambarasan S (2015) Bacterial degradation of monocrotophos and phyto-and cyto-toxicological evaluation of

metabolites. Toxicol Environ Chem 97(9):1202–1216. https://doi.org/10.1080/02772248.2015.1092541
Abraham J, Silambarasan S, Logeswari P (2014) Simultaneous degradation of organophosphorus and organochlorine pesticides by bacterial consortium. J Taiwan Inst Chem Eng 45(5):2590–2596. https://doi.org/10.1016/j.jtice.2014.06.014
Abraham J, Mukherjee P, Bose D, Dutta A (2016) Utilization of monocrotophos by *Aspergillus sojae* strain JPDA1 isolated from sugarcane fields of Vellore district in India. Res J Pharm Technol 9(12):2155–2160. https://doi.org/10.5958/0974-360X.2016.00437.6
Acharya KP, Shilpkar P, Shah MC, Chellapandi P (2015) Biodegradation of insecticide monocrotophos by *Bacillus subtilis* KPA-1, isolated from agriculture soils. Appl Biochem Biotechnol 175(4):1789–1804. https://doi.org/10.1007/s12010-014-1401-5
Agnihotri NP, Pandey SY, Jain HK, Srivastava KP (1981) Persistence, leaching and movement of chlorfenvinphos, chlorpyriphos, disulfoton, fensulfothion, monocrotophos and tetrachlorvinphos in soil. Indian J Agric Chem (India) 14:27–31
Agrahari S, Pandey KC, Gopal K (2007) Biochemical alteration induced by monocrotophos in the blood plasma of fish, *Channa punctatus* (Bloch). Pest Biochem Physiol 88(3):268–272. https://doi.org/10.1016/j.pestbp.2007.01.001
Amalraj A, Pius A (2015) Photocatalytic degradation of monocrotophos and chlorpyrifos in aqueous solution using TiO_2 under UV radiation. J Water Process Eng 7:94–101. https://doi.org/10.1016/j.jwpe.2015.06.002
Anandan S, Vinu A, Venkatachalam N, Arabindoo B, Murugesan V (2006) Photocatalytic activity of ZnO impregnated Hβ and mechanical mix of ZnO/Hβ in the degradation of monocrotophos in aqueous solution. J Mol Catal A Chem 256(1–2):312–320. https://doi.org/10.1016/j.molcata.2006.05.012
Anandan S, Vinu A, Lovely KLPS, Gokulakrishnan N, Srinivasu P, Mori T, Murugesan V, Sivamurugan V, Ariga K (2007) Photocatalytic activity of La-doped ZnO for the degradation of monocrotophos in aqueous suspension. J Mol Catal A Chem 266(1–2):149–157. https://doi.org/10.1016/j.molcata.2006.11.008
Anandan S, Kathiravan K, Murugesan V, Ikuma Y (2009) Anionic (IO_3^-) non-metal doped TiO_2 nanoparticles for the photocatalytic degradation of hazardous pollutant in water. Catal Commun 10(6):1014–1019. https://doi.org/10.1016/j.catcom.2008.12.054
Anbumani S, Mohankumar MN (2015) Cytogenotoxicity assessment of monocrotophos and butachlor at single and combined chronic exposures in the fish *Catla catla* (Hamilton). Environ Sci Pollut Res 22(7):4964–4976. https://doi.org/10.1007/s11356-014-3782-y
Anitha S, Das SSM (2011) Mycoremediation of monocrotophos. Int J Pharma Bio Sci 2(1):B337–B342
Arora S (2009) Analysis of insecticides in okra and brinjal from IPM and non-IPM fields. Environ Monit Assess 151(1–4):311–315. https://doi.org/10.1007/s10661-008-0272-z
Asi MR (2003) Solid-phase extraction and chromatographic determination of pesticides in food and water samples. Dissertation, Institutue of Chemistry University of the Punjab Lahore, Pakistan
Avasarala BK, Tirukkovalluri SR, Bojja S (2011) Photocatalytic degradation of monocrotophos pesticide—an endocrine disruptor by magnesium doped titania. J Hazard Mater 186(2–3):1234–1240. https://doi.org/10.1016/j.jhazmat.2010.11.132
Aziz F, Ouazzani N, Mandi L, Muhammad M, Uheida A (2017) Composite nanofibers of polyacrylonitrile/natural clay for decontamination of water containing Pb(II), Cu(II), Zn(II) and pesticides. Sep Sci Technol 52(1):58–70. https://doi.org/10.1080/01496395.2016.1231692
Bagheri N, Khataee A, Hassanzadeh J, Habibi B (2019) Sensitive biosensing of organophosphate pesticides using enzyme mimics of magnetic ZIF-8. Spectrochim Acta A Mol Biomol Spectrosc 209:118–125. https://doi.org/10.1016/j.saa.2018.10.039
Balamurugan K, Ramakrishnan M, Senthilkumar R, Ignacimuthu S (2010) Research article Biodegradation of methyl parathion and monochrotophos by *Pseudomonas aeruginosa* and *Trichoderma viridae*. Asian Sci Technol 6:123–126
Banu BS, Devi KD, Mahboob M, Jamil K (2001) In vivo genotoxic effect of zinc sulfate in mouse peripheral blood leukocytes using comet assay. Drug Chem Toxicol 24(1):63–73. https://doi.org/10.1081/DCT-100103086
Bapat G, Labade C, Chaudhari A, Zinjarde S (2016) Silica nanoparticle based techniques for extraction, detection, and degradation of pesticides. Adv Colloid Interface Sci 237:1–14. https://doi.org/10.1016/j.cis.2016.06.001
Barathidasan K, Reetha D (2013) Microbial degradation of monocrotophos by *Pseudomonas stutzeri*. Indian Streams Res J 3(5):1–7
Bariola LA, Lingren PD, Lindquist DA, Ridgway RL (1970) Uptake of systemic insecticides after application to the stems of the cotton plant. J Econ Entomol 63(6):1898–1901
Beynon KI, Wright AN (1972) The breakdown of [^{14}C] monocrotophos insecticide on maize, cabbage and apple. Pest Manag Sci 3(3):277–292. https://doi.org/10.1002/ps.2780030306
Beynon KI, Hutson DH, Wright AN (1973) The metabolism and degradation of vinyl phosphate insecticides. Residue Rev 47:55–142. https://doi.org/10.1007/978-1-4615-8488-9_2
Bhadbhade BJ, Dhakephalkar PK, Sarnaik SS, Kanekar PP (2002a) Plasmid-associated biodegradation of an organophosphorus pesticide, Monocrotophos, by *Pseudomonas mendocina*. Biotechnol Lett 24(8):647–650. https://doi.org/10.1023/A:1015099409563
Bhadbhade BJ, Sarnaik SS, Kanekar PP (2002b) Biomineralization of an organophosphorus pesticide, Monocrotophos, by soil bacteria. J Appl Microbiol 93(2):224–234. https://doi.org/10.1046/j.1365-2672.2002.01680.x
Bhadbhade BJ, Sarnaik SS, Kanekar PP (2002c) Bioremediation of an industrial effluent containing monocrotophos. Curr Microbiol 45(5):346–349. https://doi.org/10.1007/s00284-002-3681-1
Bhalerao TS, Puranik PR (2009) Microbial degradation of monocrotophos by *Aspergillus oryzae*. Int Biodeterior Biodegrad 63(4):503–508. https://doi.org/10.1016/j.ibiod.2008.11.011
Bhatkhande DS, Pangarkar VG, Beenackers AA (2002) Photocatalytic degradation for environmental applications—a review. J Chem Technol Biotechnol 77(1):102–116. https://doi.org/10.1002/jctb.532
Bhushan C, Bhardwaj A, Misra SS (2013) State of pesticide regulations in India. Centre for Science and Environment, New Delhi, pp 1–72
Bin Z, Yanhong C, Jiaojiao X, Jing Y (2018) Acetylcholinesterase biosensor based on functionalized surface of carbon nanotubes for monocrotophos detection. Anal Biochem 560:12–18. https://doi.org/10.1016/j.ab.2018.08.024
Binukumari S, Devi KA, Vasanthi J (2016) Applications in environmental risk assessment of biochemical analysis on the Indian fresh water fish, *Labeo rohita* exposed to monocrotophos pesticide. Environ Toxicol Pharmacol 47:200–205. https://doi.org/10.1016/j.etap.2016.08.014
Bull DL, Lindquist DA (1966) Metabolism of 3-hydroxy-*N*-methyl-*cis*-crotonamide dimethyl phosphate (azodrin) by insects and rats. J Agric Food Chem 14(2):105–109
Buvaneswari G, Thenmozhi R, Nagasathya A, Thajuddin N (2017) Screening of efficient monocrotophos degrading bacterial isolates from paddy field soil of Sivagangai District, Tamil Nadu, India. J Environ Sci Technol 10:13–24. https://doi.org/10.3923/jest.2017.13.24
Buvaneswari G, Thenmozhi R, Nagasathya A, Thajuddin N, Kumar P (2018) GC–MS and molecular analyses of monocrotophos

biodegradation by selected bacterial isolates. Afr J Microbiol Res 12(3):52–61. https://doi.org/10.5897/AJMR2017.8696

Cao X, Liu S, Yang X, Liu Z, Liu L (2016) A modified quechers sample preparation method for simultaneous determination of 62 pesticide residues in edible fungi using gas chromatography–triple quadrupole mass spectrometry. Food Anal Methods 9(1):263–274. https://doi.org/10.1007/s12161-015-0200-0

Chakravarthi BK, Naravaneni R, Philip GH, Redddy CS (2009) Investigation of monocrotophos toxic effects on human lymphocytes at cytogenetic level. Afr J Biotechnol 8(10):2042–2046

Chandra S, Mahindrakar AN, Shinde LP (2014) Gas chromatography–mass spectrometry determination of pesticide residue in fruits. Int J Chemtech Res 6(1):124–130

Chauhan PS, Jha B (2017) Pilot scale production of extracellular thermo-alkali stable laccase from *Pseudomonas* sp. S2 using agro waste and its application in organophosphorous pesticides degradation. J Chem Technol Biotechnol 93:1022–1030. https://doi.org/10.1002/jctb.5454

Darko G, Akoto O (2008) Dietary intake of organophosphorus pesticide residues through vegetables from Kumasi, Ghana. Food Chem Toxicol 46(12):3703–3706. https://doi.org/10.1016/j.fct.2008.09.049

Das S, Singh DK (2006) Purification and characterization of phosphotriesterases from *Pseudomonas aeruginosa* F10B and *Clavibacter michiganense* subsp. *Insidiosum* SBL11. Can J Microbiol 52(2):157–168. https://doi.org/10.1139/w05-113

Das GP, Shaik AP, Jamil K (2006) Estimation of apoptosis and necrosis caused by pesticides in vitro on human lymphocytes using DNA diffusion assay. Drug Chem Toxicol 29(2):147–156. https://doi.org/10.1080/01480540600561387

Dimcheva N, Horozova E, Ivanov Y, Godjevargova T (2013) Self-assembly of acetylcholinesterase on gold nanoparticles electrodeposited on graphite. Cent Eur J Chem 11(11):1740–1748. https://doi.org/10.2478/s11532-013-0307-3

Du D, Chen S, Cai J, Zhang A (2007) Immobilization of acetylcholinesterase on gold nanoparticles embedded in sol–gel film for amperometric detection of organophosphorous insecticide. Biosens Bioelectron 23(1):130–134. https://doi.org/10.1016/j.bios.2007.03.008

Dureja P (1989) Photodecomposition of monocrotophos in soil, on plant foliage, and in water. Bull Environ Contam Toxicol 43(2):239–245. https://doi.org/10.1007/BF01701754

Dutton AJ, Roberts TR, Stoydin G (1974) The degradation of Azodrin in soil. Shell-report WKGR. 0053.74

Feldmann RJ, Maibach HI (1974) Percutaneous penetration of some pesticides and herbicides in man. Toxicol Appl Pharmacol 28:126–132

Fukuto TR (1990) Mechanism of action of organophosphorus and carbamate insecticides. Environ Health Perspect 87:245–254

Gavrilescu M (2005) Fate of pesticides in the environment and its bioremediation. Eng Life Sci 5(6):497–526. https://doi.org/10.1002/elsc.200520098

Gill JPK, Sethi N, Mohan A, Datta S, Girdhar M (2018) Glyphosate toxicity for animals. Environ Chem Lett 16(2):401–426. https://doi.org/10.1007/s10311-017-0689-0

Goel M, Seepana M (2016) Photochemical removal of pesticides: a review. Mater Sci Forum 855:127–138. https://doi.org/10.4028/www.scientific.net/MSF.855.127

Goldstein MI, Lacher TE, Woodbridge B, Bechard MJ, Canavelli SB, Zaccagnini ME, Cobb GP, Scollon EJ, Tribolet R, Hopper MJ (1999) Monocrotophos-induced mass mortality of Swainson's Hawks in Argentina, 1995–1996. Ecotoxicology 8(3):201–214. https://doi.org/10.1023/A:1026496331396

Govindarajan B (2014) Toxic effect of insecticide (monocrotophos) on protein content of *Eudrilus Eugeniae* under experimental conditions. Int J Pharm Ther 5(1):01–02

Guivarch E, Oturan N, Oturan MA (2003) Removal of organophosphorus pesticides from water by electrogenerated Fenton's reagent. Environ Chem Lett 1(3):165–168. https://doi.org/10.1007/s10311-003-0029-4

Gundi VA, Reddy BR (2006) Degradation of monocrotophos in soils. Chemosphere 62(3):396–403. https://doi.org/10.1016/j.chemosphere.2005.04.076

Gupta M, Bagchi G, Bandyopadhyay S, Sasmal D, Chatterjee T, Dey SN (1982) Hematological changes produced in mice by Nuvacron or Furadan. Toxicology 25(2–3):255–260. https://doi.org/10.1016/0300-483X(82)90034-8

Hernandez H, Stearns SM, Fukuto JM (1986) Anaerobic soil metabolism of SD 9129. Shell-Report RIR-22-018-86

Hongsibsong S, Sapbamrer R (2018) Removal of organophosphorus pesticide residues in leaf and non-leaf vegetables by using ozone water. Chiang Mai J Sci 45(4):1759–1769

Hua Z, Manping Z, Zongfeng X, Low GK (1995) Titanium dioxide mediated photocatalytic degradation of monocrotophos. Water Res 29(12):2681–2688. https://doi.org/10.1016/0043-1354(95)00141-7

Huang Y, Shi T, Luo X, Xiong H, Min F, Chen Y, Nie S, Xie M (2019) Determination of multi-pesticide residues in green tea with a modified QuEChERS protocol coupled to HPLC-MS/MS. Food Chem 275:255–264. https://doi.org/10.1016/j.foodchem.2018.09.094

Hussain S, Masud T, Ahad K (2002) Determination of pesticides residues in selected varieties of mango. Pak J Nutr 1(1):41–42

Imran A, Hussain T, Nadeem A, Saeed S, Ejaz R, Murtaza MA, Aslam N, Ibrahim M, Shafi M, Raza SMM (2016) Chromatographic determination of residual contents of pesticides in rice samples from different geographical regions of Punjab. FUUAST J Biol 6(2):155–160

Ismail N, Vairamani M, Rao RN (2000) Determination of *cis* and *trans* isomers of monocrotophos in technical products by reversed-phase column liquid chromatography. J Chromatogr A 903(1–2):255–260. https://doi.org/10.1016/S0021-9673(00)00876-1

Ismail M, Sayed M, Khan HM, Cooper WJ (2014) Analysis of pesticides in water samples and removal of monocrotophos by gamma irradiation. J Anal Bioanal Tech 5(1):181. https://doi.org/10.4172/2155-9872.1000181

Ito Y, Ueyama J, Nakayama SF, Isobe T, Oya N, Sato H, Ebara T, Yoshimasu K, Tsuno K, Tatsuta N, Nakai K, Kamijima M (2019) Within-individual and interlaboratory variability analyses of urinary metabolites measurements of organophosphorus insecticides. J Expo Sci Environ Epidemiol. https://doi.org/10.1038/s41370-019-0124-7

Jain R, Garg V (2013) Enzymatic degradation of monocrotophos by extracellular fungal OP hydrolases. Appl Biochem Biotechnol 171(6):1473–1486. https://doi.org/10.1007/s12010-013-0438-1

Jain R, Garg V (2014) Comparative analysis of chemical, fungal and enzymatic degradation of MCP. SAJ Biotechnol 1(1):101. https://doi.org/10.18875/2375-6713.1.101

Jain R, Garg V (2015) Degradation of monocrotophos in soil, microbial versus enzymatic method. J Environ Occup Sci 4(1):44–52. https://doi.org/10.5455/jeos.20141214124733

Jain R, Garg V, Dangwal K, Lily MK (2013a) Comparative purification and characterization of two distinct extracellular monocrotophos hydrolases secreted by *Penicillium aculeatum* and *Fusarium pallidoroseum* isolated from agricultural fields. Biosci Biotechnol Biochem 77(5):961–965. https://doi.org/10.1271/bbb.120907

Jain R, Garg V, Dangwal K, Lily MK (2013b) Purification and characterization of acid phosphatase from monocrotophos (MCP) hydrolyzing *Aspergillus niger* ITCC 7782.10 isolated from local agricultural field. Turk J Biochem/Turk Biyokimya Dergisi. https://doi.org/10.5505/tjb.2013.19870

Jain R, Garg V, Yadav D (2014) In vitro comparative analysis of monocrotophos degrading potential of *Aspergillus flavus, Fusarium pallidoroseum* and *Macrophomina* sp. Biodegradation 25(3):437–446. https://doi.org/10.1007/s10532-013-9672-z

Jain R, Garg V, Saxena J (2015) Effect of an organophosphate pesticide, monocrotophos, on phosphate-solubilizing efficiency of soil fungal isolates. Appl Biochem Biotechnol 175(2):813–824. https://doi.org/10.1007/s12010-014-1309-0

Jamil K, Shaik AP, Mahboob M, Krishna D (2004) Effect of organophosphorus and organochlorine pesticides (monochrotophos, chlorpyriphos, dimethoate, and endosulfan) on human lymphocytes in vitro. Drug Chem Toxicol 27(2):133–144. https://doi.org/10.1081/DCT-120030725

Jia KZ, Cui ZL, He J, Guo P, Li SP (2006) Isolation and characterization of a denitrifying monocrotophos-degrading *Paracoccus* sp. M-1. FEMS Microbiol Lett 263(2):155–162. https://doi.org/10.1111/j.1574-6968.2006.00389.x

Joint FAO/WHO meeting on Pesticide Residues (JMPR 1972). 244. Monocrotophos (WHO pesticide residues series 2). http://www.inchem.org/documents/jmpr/jmpmono/v072pr22.htm. Accessed 21 Sept 2018

Jose A, Selvakumar R, Peter JV, Karthik G, Fleming DH, Fleming JJ (2015) Estimation of monocrotophos renal elimination half-life in humans. Clin Toxicol 53(7):629–632. https://doi.org/10.3109/15563650.2015.1054500

Joshi AKR, Rajini PS (2012) Hyperglycemic and stressogenic effects of monocrotophos in rats: evidence for the involvement of acetylcholinesterase inhibition. Exp Toxicol Pathol 64(1–2):115–120. https://doi.org/10.1016/j.etp.2010.07.003

Kanekar PP, Bhadbhade BJ, Deshpande NM, Sarnaik SS (2004) Biodegradation of organophosphorus pesticides. Proc Indian Natl Sci Acad B 70(1):57–70

Kang Y, Zhang G, Sheng G, Fu J (2000) Analysis of organophosphorous pesticides from source water using solid-phase extraction technique. China Environ Sci 20(1):1–4

Karpouzas DG, Singh BK (2006) Microbial degradation of organophosphorus xenobiotics: metabolic pathways and molecular basis. Adv Microb Physiol 51:119–225. https://doi.org/10.1016/S0065-2911(06)51003-3

KaviKarunya S, Reetha D (2012) Biological degradation of chlorpyrifos and monocrotophos by bacterial isolates. Int J Pharm Biol Arch 3(3):685–691

Khan AB (2005) Studies on the residues of commonly used insecticides on fruits and vegetables grown in NWFP-Pakistan. Dissertation, NWFP Agriculture University, Peshawar

Kim JR, Ahn YJ (2009) Identification and characterization of chlorpyrifos-methyl and 3,5,6-trichloro-2-pyridinol degrading *Burkholderia* sp. strain KR100. Biodegradation 20(4):487–497. https://doi.org/10.1007/s10532-008-9238-7

Kim S, Park MY, Kim HJ, Shin JY, Ko KY, Kim DG, Kim M, Kang HG, So B, Park SW (2016) Analysis of insecticides in dead wild birds in Korea from 2010 to 2013. Bull Environ Contam Toxicol 96(1):25–30. https://doi.org/10.1007/s00128-015-1688-0

Kodandaram MH, Saha S, Rai AB, Naik PS (2013) Compendium on pesticide use in vegetables. IIVR Ext Bull 50:133

Ku Y, Jung IL (1998) Decomposition of monocrotophos in aqueous solution by UV irradiation in the presence of titanium dioxide. Chemosphere 37(13):2589–2597. https://doi.org/10.1016/S0045-6535(98)00158-1

Ku Y, Wang W (1999) The decomposition kinetics of monocrotophos in aqueous solutions by the hydrogen peroxide-ozone process. Water Environ Res 71(1):18–22. https://doi.org/10.2175/106143099X121652

Ku Y, Wang W, Shen YS (1998) Ozonation of monocrotophos in aqueous solution. Ind Eng Chem Res 37(2):367–373. https://doi.org/10.1021/ie970219v

Ku Y, Wang W, Shen YS (2000) Reaction behaviors of decomposition of monocrotophos in aqueous solution by UV and UV/O_3 processes. J Hazard Mater 72(1):25–37. https://doi.org/10.1016/S0304-3894(99)00150-8

Kumar V, Upadhyay N, Kumar V, Kaur S, Singh J, Singh S, Datta S (2014) Environmental exposure and health risks of the insecticide monocrotophos—a review. J Biodivers Environ Sci 5(1):111–120

Kumari B, Madan VK, Singh J, Singh S, Kathpal TS (2004) Monitoring of pesticidal contamination of farmgate vegetables from Hisar. Environ Monit Assess 90(1–3):65–71. https://doi.org/10.1023/B:EMAS.0000003566.63111.f6

Kumari B, Madan VK, Kathpal TS (2007) Pesticide residues in rain water from Hisar, India. Environ Monit Assess 133(1–3):467–471. https://doi.org/10.1007/s10661-006-9601-2

Lee PW, Vanderlinden HF, Stackhouse SC (1980) Comparative aerobic metabolism of SD 9129 in sterilized and unsterilized Hanford sandy loam soil. ShellReport RIR-22-014-80

Lee PW, Fukuto JM, Hernandez H, Stearns SM (1990) Fate of monocrotophos in the environment. J Agric Food Chem 38(2):567–573

Li Y, Chen Z, Zhang R, Luo P, Zhou Y, Wen S, Ma M (2016) Simultaneous determination of 42 pesticides and herbicides in chicken eggs by UHPLC–MS/MS and GC–MS using a QuEChERS-based procedure. Chromatographia 79(17–18):1165–1175. https://doi.org/10.1007/s10337-016-3132-y

Li D, Zhang X, Kong F, Qiao X, Xu Z (2017) Molecularly imprinted solid-phase extraction coupled with high-performance liquid chromatography for the determination of trace trichlorfon and monocrotophos residues in fruits. Food Anal Methods 10(5):1284–1292. https://doi.org/10.1007/s12161-016-0687-z

Lindquist DA, Bull DL (1967) Fate of 3-hydroxy-*N*-methyl-*cis*-crotonamide dimethyl phosphate in cotton plants. J Agric Food Chem 15(2):267–272

Liu Y, Wei M (2014) Development of acetylcholinesterase biosensor based on platinum–carbon aerogels composite for determination of organophosphorus pesticides. Food Control 36(1):49–54. https://doi.org/10.1016/j.foodcont.2013.08.005

Mackay D, Shiu WY, Ma KC, Lee SC (2006) Handbook of physical-chemical properties and environmental fate for organic chemicals. CRC Press, Boca Raton

Madhavan J, Kumar PSS, Anandan S, Grieser F, Ashokkumar M (2010) Sonophotocatalytic degradation of monocrotophos using TiO_2 and Fe^{3+}. J Hazard Mater 177(1–3):944–949. https://doi.org/10.1016/j.jhazmat.2010.01.009

Mandhane SN, Chopde CT (1995) Neurobehavioural effects of acute monocrotophos administration in rats and mice. Indian J Pharmacol 27(4):245–249

Mao X, Yan A, Wan Y, Luo D, Yang H (2019) Dispersive solid-phase extraction using microporous sorbent UiO-66 coupled to gas chromatography-tandem mass spectrometry: a QuEChERS-type method for the determination of organophosphorus pesticide residues in edible vegetable oils without matrix interference. J Agric Food Chem 67(6):1760–1770. https://doi.org/10.1021/acs.jafc.8b04980

Maqbool Z, Hussain S, Imran M, Mahmood F, Shahzad T, Ahmed Z, Azeem F, Muzammil S (2016) Perspectives of using fungi as bioresource for bioremediation of pesticides in the environment: a critical review. Environ Sci Pollut Res 23(17):16904–16925. https://doi.org/10.1007/s11356-016-7003-8

Megharaj M, Venkateswarlu K, Rao AS (1986a) Effect of monocrotophos and quinalphos on soil algae. Environ Pollut A 40(2):121–126. https://doi.org/10.1016/0143-1471(86)90079-6

Megharaj M, Venkateswarlu K, Rao AS (1986b) Growth response of four species of soil algae to monocrotophos and quinalphos. Environ Pollut A 42(1):15–22. https://doi.org/10.1016/0143-1471(86)90041-3

Megharaj M, Venkateswarlu K, Rao AS (1987) Metabolism of monocrotophos and quinalphos by algae isolated from soil. Bull Environ Contam Toxicol 39(2):251–256. https://doi.org/10.1007/BF01689414

Megharaj M, Venkateswarlu K, Rao AS (1988) Microbial degradation and algal toxicity of monocrotophos and quinalphos in flooded soil. Chemosphere 17(5):1033–1039. https://doi.org/10.1016/0045-6535(88)90073-2

Mendelssohn H, Paz U (1977) Mass mortality of birds of prey caused by Azodrin, an organophosphorus insecticide. Biol Conserv 11(3):163–170. https://doi.org/10.1016/0006-3207(77)90001-5

Mengyue Z, Shifu C, Yaowu T (1995) Photocatalytic degradation of organophosphorus pesticides using thin films of TiO_2. J Chem Technol Biotechnol 64(4):339–344. https://doi.org/10.1002/jctb.280640405

Menzer RE, Casida JE (1965) Nature of toxic metabolites formed in mammals, insects, and plants from 3-(dimethoxyphosphiny1oxy)-*N*,*N*-dimethylckrotonamide and its *N*-methyl analog. J Agric Food Chem 13(2):102–112

Moon Y, Jafry AT, Kang SB, Seo JY, Baek KY, Kim EJ, Pan JG, Choi JY, Kim HJ, Lee KH, Jeong K (2019) Organophosphorus hydrolase-poly-β-cyclodextrin as a stable self-decontaminating bio-catalytic material for sorption and degradation of organophosphate pesticide. J Hazard Mater 365:261–269. https://doi.org/10.1016/j.jhazmat.2018.10.094

Mücke W (1994) Metabolism of monocrotophos in animals. In: Reviews of environmental contamination and toxicology. Springer, New York, pp 59–65

Mundhe AY, Bhilwade H, Pandit SV (2016) Genotoxicity and oxidative stress as biomarkers in fresh water mussel, *Lamellidens marginalis* (Lam.) exposed to monocrotophos. Indian J Exp Biol 54:822–828

Nagaraju R, Rajini PS (2016) Adaptive response of rat pancreatic β-cells to insulin resistance induced by monocrotophos: biochemical evidence. Pest Biochem Physiol 134:39–48. https://doi.org/10.1016/j.pestbp.2016.04.009

Nagaraju R, Joshi AKR, Rajini PS (2014) Organophosphorus insecticide, monocrotophos, possesses the propensity to induce insulin resistance in rats on chronic exposure. J Diabetes 7(1):47–59. https://doi.org/10.1111/1753-0407.12158

Namera A, Utsumi Y, Yashiki M, Ohtani M, Imamura T, Kojima T (2000) Direct colorimetric method for determination of organophosphates in human urine. Clin Chim Acta 291(1):9–18. https://doi.org/10.1016/S0009-8981(99)00189-8

Narang G, Mahajan NK, Jadhav VJ, Mittal D, Mishra AC (2016) Monocrotophos toxicity in peafowl in Haryana. Haryana Vet 55(1):73–75

Pain DJ, Gargi R, Cunningham AA, Jones A, Prakash V (2004) Mortality of globally threatened Sarus Cranes *Grus antigon* from monocrotophos poisoning in India. Sci Total Environ 326(1–3):55–61. https://doi.org/10.1016/j.scitotenv.2003.12.004

Pam AA (2015) Sorption kinetics study of monocrotophos (MCP) pesticide in unsterilized soil. Am Chem Sci J 7(3):183–192. https://doi.org/10.9734/ACSj/2015/17495

Pandey B, Baghel PS, Shrivastava S (2014) To study the bioremediation of monocrotophos and to analyze the kinetics effect of tween 80 on fungal growth. Indo Am J Pharm Res 4(2):925–930

Parveen Z, Khuhro MI, Rafiq N (2005) Monitoring of pesticide residues in vegetables (2000–2003) in Karachi, Pakistan. Bull Environ Contam Toxicol 74(1):170–176. https://doi.org/10.1007/s00128-004-0564-0

Patil VB, Shingare MS (1994) Thin-layer chromatographic detection of monocrotophos in biological materials. Talanta 41(12):2127–2130. https://doi.org/10.1016/0039-9140(94)00194-4

Peter JV, Jerobin J, Nair A, Bennett A, Samuel P, Chrispal A, Abraham OC, Mathews KP, Fleming JJ, Oommen A (2010) Clinical profile and outcome of patients hospitalized with dimethyl and diethyl organophosphate poisoning. Clin Toxicol 48(9):916–923. https://doi.org/10.3109/15563650.2010.528425

Qiao CL, Huang J, Li X, Shen BC, Zhang JL (2003) Bioremediation of organophosphate pollutants by a genetically-engineered enzyme. Bull Environ Contam Toxicol 70(3):455–461. https://doi.org/10.1007/s00128-003-0008-2

Ragnarsdottir KV (2000) Environmental fate and toxicology of organophosphate pesticides. J Geol Soc 157(4):859–876. https://doi.org/10.1144/jgs.157.4.859

Rangaswamy V, Venkateswarlu K (1992) Degradation of selected insecticides by bacteria isolated from soil. Bull Environ Contam Toxicol 49(6):797–804. https://doi.org/10.1007/BF00203150

Ranjan S, Dasgupta N, Singh S, Gandhi M (2018) Toxicity and regulations of food nanomaterials. Environ Chem Lett. https://doi.org/10.1007/s10311-018-00851-z

Rao JV, Kavitha P (2004) Toxicity of azodrin on the morphology and acetylcholinesterase activity of the earthworm *Eisenia foetida*. Environ Res 96(3):323–327. https://doi.org/10.1016/j.envres.2004.02.014

Rao JV, Parvathi K, Kavitha P, Jakka NM, Pallela R (2005a) Effect of chlorpyrifos and monocrotophos on locomotor behaviour and acetylcholinesterase activity of subterranean termites, *Odontotermes obesus*. Pest Manag Sci 61(4):417–421. https://doi.org/10.1002/ps.986

Rao S, Venkateswarlu V, Surender T, Eddleston M, Buckley NA (2005b) Pesticide poisoning in south India: opportunities for prevention and improved medical management. Trop Med Int Health 10(6):581–588. https://doi.org/10.1111/j.1365-3156.2005.01412.x

Reddy PVL, Kim KH (2015) A review of photochemical approaches for the treatment of a wide range of pesticides. J Hazard Mater 285:325–335. https://doi.org/10.1016/j.jhazmat.2014.11.036

Reddy JD, Rao NB, Sultan AM (2000) Insecticide residues in market samples of grape berries. Pestology 24(9):17–22

Revankar PR, Shyama SK (2009) Genotoxic effects of monocrotophos, an organophosphorous pesticide, on an estuarine bivalve, *Meretrix ovum*. Food Chem Toxicol 47(7):1618–1623. https://doi.org/10.1016/j.fct.2009.04.010

Riah W, Laval K, Laroche-Ajzenberg E, Mougin C, Latour X, Trinsoutrot-Gattin I (2014) Effects of pesticides on soil enzymes: a review. Environ Chem Lett 12(2):257–273. https://doi.org/10.1007/s10311-014-0458-2

Sadasivam S, Krishna SK, Ponnusamy K, Nagarajan GS, Kang TW, Venkatesalu SC (2010) Equilibrium and thermodynamic studies on the adsorption of an organophosphorous pesticide onto "waste" jute fiber carbon. J Chem Eng Data 55(12):5658–5662. https://doi.org/10.1021/je1005906

Sahithya K, Das D, Das N (2016) Adsorptive removal of monocrotophos from aqueous solution using biopolymer modified montmorillonite–CuO composites: equilibrium, kinetic and thermodynamic studies. Process Saf Environ 99:43–54. https://doi.org/10.1016/j.psep.2015.10.009

Saifuddin N, Nian CY, Zhan LW, Ning KX (2011) Chitosan-silver nanoparticles composite as point-of-use drinking water filtration system for household to remove pesticides in water. Asian J Biochem 6(2):142–159. https://doi.org/10.3923/ajb.2011.142.159

Salim C, Rajini PS (2017) Glucose-rich diet aggravates monocrotophos-induced dopaminergic neuronal dysfunction in *Caenorhabditis elegans*. J Appl Toxicol 37(6):772–780. https://doi.org/10.1002/jat.3426

Samal B, Kotiyal PB (2013) Bioremediation of Monocrotophos and Malathion by *Bacillus* sp. In: Environmental sustainability: concepts, principles, evidences and innovations. pp 88–93. ISBN:978-93-83083-75-6

Sankhwar ML, Yadav RS, Shukla RK, Singh D, Ansari RW, Pant AB, Parmar D, Khanna VK (2013) Monocrotophos induced oxidative stress and alterations in brain dopamine and serotonin receptors in young rats. Toxicol Ind Health 32(3):422–436. https://doi.org/10.1177/0748233713500834

Satpathy R (2019) Quantitative structure–activity relationship methods for the prediction of the toxicity of pollutants. Environ Chem Lett 17(1):123–128. https://doi.org/10.1007/s10311-018-0780-1

Sawaya WN, Al-Awadhi FA, Saeed T, Al-Omair A, Ahmad N, Husain A, Khalafawi S, Al-Zenki S, Al-Amiri H, Al-Otaibi J, Al-Saqer J (1999) Dietary intake of pesticides: state of Kuwait total diet study. Food Addit Contam 16(11):473–480. https://doi.org/10.1080/026520399283768

Schuler JF, Held HJ (1964) Soil stability of C1414. Ciba-Geigy-Report of 5 November 1964

Shankar MV, Cheralathan KK, Arabindoo B, Palanichamy M, Murugesan V (2004) Enhanced photocatalytic activity for the destruction of monocrotophos pesticide by TiO_2/Hβ. J Mol Catal A Chem 223(1–2):195–200. https://doi.org/10.1016/j.molcata.2004.03.059

Sharma A, Gill JPS, Bedi JS, Pooni PA (2014) Monitoring of pesticide residues in human breast milk from Punjab, India and its correlation with health associated parameters. Bull Environ Contam Toxicol 93(4):465–471. https://doi.org/10.1007/s00128-014-1326-2

Sharma A, Gill JPS, Bedi JS (2015) Monitoring of pesticide residues in human blood from Punjab, India. Bull Environ Contam Toxicol 94(5):640–646. https://doi.org/10.1007/s00128-015-1522-8

Shifu C, Gengyu C (2005) Photocatalytic degradation of organophosphorus pesticides using floating photocatalyst TiO_2·SiO_2/beads by sunlight. Sol Energy 79(1):1–9. https://doi.org/10.1016/j.solener.2004.10.006

Shifu C, Mengyue Z, Yaowu T (1996) Photocatalytic degradation of organophosphorus pesticides using TiO_2 supported on fiberglass. Microchem J 54:54–58

Siddiqui MKJ, Rahman MF, Mustafa M, Bhalerao UT (1991) A comparative study of blood changes and brain acetylcholinesterase inhibition by monocrotophos and its analogues in rats. Ecotoxicol Environ Saf 21(3):283–289. https://doi.org/10.1016/0147-6513(91)90067-Y

Siddiqui MKJ, Rahman MF, Mustafa M (1993) Target enzyme inhibition by novel thion analogues of monocrotophos: an acute in vivo study in the rat. Bull Environ Contam Toxicol 51(3):409–415. https://doi.org/10.1007/BF00201760

Sidhu PK, Dhanjal NIK, Cameotra SS, Sud D (2015) Persistence and biodegradation of monocrotophos using soil microbes. Desalin Water Treat 54(8):2293–2298. https://doi.org/10.1080/19443994.2014.899516

Singh BK, Walker A (2006) Microbial degradation of organophosphorus compounds. FEMS Microbiol Rev 30(3):428–471. https://doi.org/10.1111/j.1574-6976.2006.00018.x

Sivagami K, Krishna RR, Swaminathan T (2011) Studies on photocatalytic degradation of monocrotophos in an annular slurry reactor using factorial design of experiments. J Water Sustain 1(1):75–84

Sivagami K, Ravi Krishna R, Swaminathan T (2016) Optimization studies on degradation of monocrotophos in an immobilized bead photo reactor using design of experiment. Desalin Water Treat 57(59):28822–28830. https://doi.org/10.1080/19443994.2016.1195288

Sogorb MA, Vilanova E (2002) Enzymes involved in the detoxification of organophosphorus, carbamate and pyrethroid insecticides through hydrolysis. Toxicol Lett 128(1):215–228. https://doi.org/10.1016/S0378-4274(01)00543-4

Sraw A, Wanchoo RK, Toor AP (2014) Optimization and kinetic studies for degradation of insecticide monocrotophos using LR grade and P25 TiO_2 under UV/sunlight conditions. Environ Prog Sustain Energy 33(4):1201–1208. https://doi.org/10.1002/ep.11909

Sraw A, Kaur T, Pandey Y, Sobti A, Wanchoo RK, Toor AP (2018) Fixed bed recirculation type photocatalytic reactor with TiO_2 immobilized clay beads for the degradation of pesticide polluted water. J Environ Chem Eng 6(6):7035–7043. https://doi.org/10.1016/j.jece.2018.10.062

Srinivasulu M, Nilanjan PC, Chakravarthi BVSK, Jayabaskaran C, Jaffer MG, Naga RM, Manjunatha B, Darwin RO, Juan OT, Rangaswamy V (2017) Biodegradation of monocrotophos by bacteria isolated from soil. Afr J Biotechnol 16(9):408–417. https://doi.org/10.5897/AJB2015.14885

Srivastava AK, Dev A, Karmakar S (2018) Nanosensors and nanobiosensors in food and agriculture. Environ Chem Lett 16(1):161–182. https://doi.org/10.1007/s10311-017-0674-7

Subhas Singh DK (2003) Utilization of monocrotophos as phosphorus source by *Pseudomonas aeruginosa* F10B and *Clavibacter michiganense* subsp. *insidiosum* SBL 11. Can J Microbiol 49(2):101–109. https://doi.org/10.1139/w03-013

Subramanian G, Sekar S, Sampoornam S (1994) Biodegradation and utilization of organophosphorus pesticides by cyanobacteria. Int Biodeterior Biodegrad 33(2):129–143. https://doi.org/10.1016/0964-8305(94)90032-9

Sun X, Xia K, Liu B (2008) Design of fluorescent self-assembled multilayers and interfacial sensing for organophosphorus pesticides. Talanta 76(4):747–751. https://doi.org/10.1016/j.talanta.2008.04.020

Sun L, Zhu S, Yang Z, Chen Q, Liu H, Zhang J, Hu G, Li S, Hong Q (2016) Degradation of monocrotophos by *Starkeya novella* YW6 isolated from paddy soil. Environ Sci Pollut Res 23(4):3727–3735. https://doi.org/10.1007/s11356-015-5606-0

Sun L, Liu H, Gao X, Chen W, Huang K, Zhang S (2018) Isolation of monocrotophos-degrading strain *Sphingobium* sp. YW16 and cloning of its Tn*opdA*. Environ Sci Pollut Res 25:4942–4950. https://doi.org/10.1007/s11356-017-0718-3

Sundarmurugasan R, Gumpu MB, Ramachandra BL, Nesakumar N, Sethuraman S, Krishnan UM, Rayappan JB (2016) Simultaneous detection of monocrotophos and dichlorvos in orange samples using acetylcholinesterase–zinc oxide modified platinum electrode with linear regression calibration. Sens Actuators B Chem 230:306–313. https://doi.org/10.1016/j.snb.2016.02.066

Tariq MI, Afzal S, Hussain I (2004) Pesticides in shallow groundwater of bahawalnagar, Muzafargarh, DG Khan and Rajan Pur districts of Punjab, Pakistan. Environ Int 30(4):471–479. https://doi.org/10.1016/j.envint.2003.09.008

Thirugnanam J, Senthilkumar R (2016) Degradation of pesticide by using geofungi from Thanjavur District. Ijsrm. Human 4(3):225–230

Tian H, Ru S, Wang Z, Cai W, Wang W (2009) Estrogenic effects of monocrotophos evaluated by vitellogenin mRNA and protein induction in male goldfish (*Carassius auratus*). Comp Biochem Physiol C Toxicol Pharmacol 150(2):231–236. https://doi.org/10.1016/j.cbpc.2009.04.014

Tian H, Ru S, Bing X, Wang W (2010) Effects of monocrotophos on the reproductive axis in the male goldfish (*Carassius auratus*): potential mechanisms underlying vitellogenin induction. Aquat Toxicol 98(1):67–73. https://doi.org/10.1016/j.aquatox.2010.01.011

Tian H, Li Y, Wang W, Wu P, Ru S (2012) Exposure to monocrotophos pesticide during sexual development causes the feminization/demasculinization of the reproductive traits and a reduction in the reproductive success of male guppies (*Poecilia reticulata*). Toxicol Appl Pharmacol 263(2):163–170. https://doi.org/10.1016/j.taap.2012.06.006

Tomlin C (1994) The pesticide manual. British Crop Protection Council, Farnham, p 1250

Tripathi VK, Kumar V, Pandey A, Vatsa P, Dhasmana A, Singh RP, Appikonda SHC, Hwang I, Lohani M (2017) Monocrotophos induces the expression of xenobiotic metabolizing cytochrome P450s (CYP2C8 and CYP3A4) and neurotoxicity in human brain cells. Mol Neurobiol 54(5):3633–3651. https://doi.org/10.1007/s12035-016-9938-7

Üstün GE, Solmaz SKA, Azak HS (2015) Experimental design of fenton process for the oxidation and mineralization of monocrotophos. Clean (Weinh) 43(9):1344–1349. https://doi.org/10.1002/clen.201400139

Velmurugan B, Selvanayagam M, Cengiz EI, Unlu E (2007) The effects of monocrotophos to different tissues of freshwater fish *Cirrhinus mrigala*. Bull Environ Contam Toxicol 78(6):450–454. https://doi.org/10.1007/s00128-007-9190-y

Velmurugan G, Babu DV, Ramasamy S (2013) Prolonged monocrotophos intake induces cardiac oxidative stress and myocardial damage in rats. Toxicology 307:103–108. https://doi.org/10.1016/j.tox.2012.11.022

Wang X, Tang Q, Wang Q, Qiao X, Xu Z (2014) Study of a molecularly imprinted solid-phase extraction coupled with high-performance liquid chromatography for simultaneous determination of trace trichlorfon and monocrotophos residues in vegetables. J Sci Food Agric 94(7):1409–1415. https://doi.org/10.1002/jsfa.6429

Wei Z, Luo S, Xiao R, Khalfin R, Semiat R (2017a) Characterization and quantification of chromate adsorption by layered porous iron oxyhydroxide: an experimental and theoretical study. J Hazard Mater 338:472–481. https://doi.org/10.1016/j.jhazmat.2017.06.001

Wei Z, Villamena FA, Weavers LK (2017b) Kinetics and mechanism of ultrasonic activation of persulfate: an in situ EPR spin trapping study. Environ Sci Technol 51(6):3410–3417. https://doi.org/10.1021/acs.est.6b05392

WHO (1997) Guidelines for predicting dietary intake of pesticide residues (revised) global environment monitoring system—food contamination monitoring and assessment programme (GEMS/Food) in collaboration with Codex Committee on pesticide residues Programme of Food Safety and Food Aid, pp 1–44

Wu S, Zhang L, Qi L, Tao S, Lan X, Liu Z, Meng C (2011) Ultra-sensitive biosensor based on mesocellular silica foam for organophosphorous pesticide detection. Biosens Bioelectron 26(6):2864–2869. https://doi.org/10.1016/j.bios.2010.11.029

Xiao R, Luo Z, Wei Z, Luo S, Spinney R, Yang W, Dionysiou DD (2018) Activation of peroxymonosulfate/persulfate by nanomaterials for sulfate radical-based advanced oxidation technologies. Curr Opin Chem Eng 19:51–58. https://doi.org/10.1016/j.coche.2017.12.005

Yadav M, Shukla AK, Srivastva N, Upadhyay SN, Dubey SK (2016) Utilization of microbial community potential for removal of chlorpyrifos: a review. Crit Rev Biotechnol 36(4):727–742. https://doi.org/10.3109/07388551.2015.1015958

Yaduvanshi SK, Ojha A, Pant SC, Lomash V, Srivastava N (2010) Monocrotophos induced lipid peroxidation and oxidative DNA damage in rat tissues. Pest Biochem Physiol 97(3):214–222. https://doi.org/10.1016/j.pestbp.2010.02.004

Yang Z, Su R, Luo S, Spinney R, Cai M, Xiao R, Wei Z (2017) Comparison of the reactivity of ibuprofen with sulfate and hydroxyl radicals: an experimental and theoretical study. Sci Total Environ 590:751–760. https://doi.org/10.1016/j.scitotenv.2017.03.039

Yang Y, Wu N, Wang C (2018) Toxicity of the pyrethroid bifenthrin insecticide. Environ Chem Lett 16(4):1377–1391. https://doi.org/10.1007/s10311-018-0765-0

Yatmaz HC, Uzman Y (2009) Degradation of pesticide monochrotophos from aqueous solutions by electrochemical methods. Int J Electrochem Sci 4(5):614–626

Zahran MM, Abdel-Aziz KB, Abdel-Raof A, Nahas EM (2005) The effect of subacute doses of organophosphorus pesticide, Nuvacron, on the biochemical and cytogenetic parameters of mice and their embryos. Res J Agric Biol Sci 1(3):277–283

Zhang ZY, Shan WL, Song WC, Gong Y, Liu XJ (2011) Phytotoxicity and uptake of chlorpyrifos in cabbage. Environ Chem Lett 9(4):547–552. https://doi.org/10.1007/s10311-011-0320-8

Zhang X, Li S, Wang C, Tian H, Wang W, Ru S (2017) Effects of monocrotophos pesticide on cholinergic and dopaminergic neurotransmitter systems during early development in the sea urchin *Hemicentrotus pulcherrimus*. Toxicol Appl Pharmacol 328:46–53. https://doi.org/10.1016/j.taap.2017.05.003

Zhao XH, Wang J (2012) A brief study on the degradation kinetics of seven organophosphorus pesticides in skimmed milk cultured with *Lactobacillus* spp. at 42 °C. Food Chem 131(1):300–304. https://doi.org/10.1016/j.foodchem.2011.08.046

Zichu G, Huifen L, Qiuping G, Guangzu S (1988) Percutaneous permeability of ^{14}C-monocrotophos. Zhoughua Laodong Weisheng Zhiyebing Zazhi 6:336–338

Publisher's Note Springer Nature remains neutral with regard to jurisdictional claims in published maps and institutional affiliations.

Current Microbiology
https://doi.org/10.1007/s00284-020-02031-1

Biodegradation of Butachlor by *Bacillus altitudinis* and Identification of Metabolites

Ravneet Kaur[1] · **Dinesh Goyal**[1]

Received: 7 January 2020 / Accepted: 14 May 2020
© Springer Science+Business Media, LLC, part of Springer Nature 2020

Abstract
Butachlor is a chloroacetamide pre-emergence herbicide, with a half-life of 1.6 to 29 days. It is a suspected carcinogen, genotoxin, neurotoxin and persists in the environment having toxic effect on living systems. Butachlor degrading bacterial strain A16 was isolated from coal tar contaminated soil, which showed 99.38% similarity with *Bacillus altitudinis* 41KF2b^T as revealed by 16S rRNA analysis. *B. altitudinis* strain A16 utilised butachlor as a sole source of carbon and degraded 90% of 50 mg L^{-1} butachlor in 5 days at a rate constant and half-life ($t_{1/2}$) of 0.02 h^{-1} and 34.65 h, respectively, following the first-order reaction kinetics. Five metabolites (*N*-(butoxymethyl)-*N*-(2-chloroethyl)-2,6-diethylaniline, (*N*-(butoxymethyl)-2-chloro-*N*-(2-ethylphenyl) acetamide, *N*-(butoxymethyl)-2,6-diethyl-*N*-propylaniline, 2-chloro-*N*-(2,6-diethylphenyl) acetamide and 2,6-diethylaniline) were produced during the breakdown of butachlor by *B. altitudinis* A16 as identified by GC–MS analysis, which are further mineralized to carbon dioxide and water. A metabolic pathway is proposed and compared with other bacteria. The findings have immense beneficial application since such microbes can be used on large scale for faster soil bioremediation and minimizing negative impact of pesticide butachlor on health and environment.

Introduction

Butachlor (*N*-(butoxymethyl)-2-chloro-*N*-(2,6-diethylphenyl)acetamide), commonly known as machete, is a chloroacetamide compound extensively used as a pre-emergence or early post-emergence herbicide for controlling unwanted annual grass, certain broadleaved weeds and underwater macrophytes found in freshwater and fish water bodies [1, 2]. It is a selective and systemic herbicide which acts by inhibiting the enzymes responsible for geranylgeranyl pyrophosphate cyclization and elongation of the long-chain fatty acids [2]. It has become a very popular herbicide across Asia with a utilization rate of about 4.5×10^7 kg per year [3, 4] at a recommended field dosage of 3000 mL ha^{-1} [5]. India accounts for approximately 6.75×10^6 kg of annual usage of butachlor [6].

Butachlor has a half-life of 1.6 days to 29 days in soil [7]. Persistence of butachlor in the environment due to its indiscriminate application has led to several health and environmental complications [8]. It is suspected to be carcinogenic in nature, known to induce malignant transformation in vitro by stimulating cell proliferation, mitochondrial dysfunction, chromosomal breakage, oxidative DNA damage [9] and disrupting endocrine system [10]. Several reports suggest butachlor to be a neurotoxin [11] and growth retardant in earthworms [12]. Due to these adverse effects, its removal from soil and water becomes necessary. Although various chemical and physical processes such as photooxidation, chemical hydrolysis and adsorption are available for treating pesticides, low cost and environment friendly bioremediation technologies are a better approach [3, 13].

Several reports describe the isolation and identification of mainly Gram-negative bacteria such as *Stenotrophomonas acidaminiphila* JS-1 [8], *Novosphingobium chloroacetimidivorans* sp.[14], *Ammoniphilus* sp. JF [4], *Serratia ureitylica* strain AS1 and *Enterobacter cloacae* [15, 16] capable of catabolizing butachlor. Despite wide usage of butachlor in Indian agriculture, reports on its biodegradation are limited. In this study, we report degradation of butachlor by a gram-positive bacterial isolate from coal tar contaminated soil and identification of metabolites.

✉ Dinesh Goyal
dgoyal@thapar.edu

[1] Department of Biotechnology, Thapar Institute of Engineering & Technology (Deemed to be University), Patiala, Punjab 147001, India

Published online: 20 May 2020

Materials and Methods

Media and Chemicals

Certified standard analytical grade herbicide butachlor with 97.7% purity was procured from Sigma-Aldrich and its stock solution was prepared in acetone (HPLC grade), filtered and stored in dark bottles. Minimal salt media Bushnell Hass (BH) containing (g L^{-1}): $CaCl_2$, 0.02; $FeCl_3$, 0.050; $MgSO_4$, 0.2; KH_2PO_4, 1.0; K_2HPO_4, 1.0; NH_4NO_3, 1.0 and pH 7.0 ± 0.2 was procured from Himedia and used to study butachlor degradation by bacterial isolates. Nutrient broth used for growth of bacterial cultures was purchased from Himedia. Solid agar medium used in the study was prepared by mixing 1.8% (w/v) agar (purchased from Himedia) to the liquid broth. All other reagents such as dichloromethane were of high purity and analytical grade.

Isolation of Butachlor Degrading Bacteria

Soil sample for bacterial isolation was collected from coal tar contaminated soil of Patiala (Punjab), located at 30.3530° N, 76.3710° E, 310 m above the sea level [17]. 5 g of the collected soil sample (dry) was added to a conical flask (250 mL) containing 100 mL Bushnell Haas (BH) broth spiked with 50 mg L^{-1} butachlor as a sole carbon source and incubated for 5 days (120 h) in an incubator shaker at 120 rpm, 37 °C. 5 mL of the enrichment culture was subcultured into fresh BH, containing 50 mg L^{-1} butachlor, every 5 days. The residual concentration of butachlor in broth from the fifth transfer was measured by UV scan in the range of 200–800 nm (λ_{max} for butachlor was 265 nm) [18, 23]. Enrichment culture (strain A16) showing significant removal of butachlor was tenfold serially diluted and uniformly spread onto BH agar plates spiked with 50 mg L^{-1} butachlor, followed by incubation at 37 °C for 5 days [19].

Identification of Strain A16 by 16S rRNA Analysis

Genomic DNA from bacterial strain A16 was isolated using DNA Extraction Solution (Cat No. 2120600021730), followed by amplification of its 16S rRNA gene by polymerase chain reaction (PCR) using dNTPs, enzyme Taq DNA Polymerase and primers (27F (5′-AGAGTTTGATCCTGGCTCAG-3′) & 1492R (5′-TACGGCTACCTTGTTACGACTT-3′). Total volume of reaction mixture used for PCR was 50 µL and the thermal cycler was run for 35 cycles. Bacterial isolate A16 was sequenced (16S rRNA gene sequencing) at Genei Laboratories Pvt Ltd; 16S rRNA gene sequence obtained was 1450 bp long. In order to identify the strain A16, sequences closely related to its 16S rRNA gene were downloaded from the NCBI website (16S ribosomal RNA sequences (Bacteria and Archaea) database) using an algorithm Basic Local Alignment Search Tool (BLAST). Identification of 16S rRNA sequence of A16 was confirmed using available DNA data in EzTaxon-e database (https://eztaxon-e.ezbiocloud.net/) introduced by Kim et al. [20]. Closely related sequences obtained were subjected to pairwise alignment (CLUSTALW) and phylogenetic tree was constructed by MEGA X software, using neighbour-joining method with Kimura two-parameter distance model for calculating evolutionary distances [21]. Bootstrap analysis with 1000 replications was performed to assess the statistical support for the phylogenetic tree.

Biodegradation of Butachlor by Strain A16

Bacterial cells (A16) grown in Bushnell Hass broth containing 50 mg L^{-1} butachlor were separated in the late log phase by centrifuging at 8000 rpm and 4 °C. Cell pellet was washed thrice with BH broth; inoculum size was adjusted to 0.02 (OD_{600nm}) with BH broth spiked with 50 mg L^{-1} of butachlor and was then incubated for a time period of 5 days (120 h) at 37 °C, 120 rpm in an incubator shaker. After time intervals of 24 h, aliquots of culture were collected and cell density (OD_{600nm}) was determined. To determine residual concentrations of butachlor, supernatant obtained after centrifuging (12,000 rpm for 8 min) culture aliquot was subjected to UV scan in the range of 200–800 nm on Elisa reader with additional cuvette port (Thermo Fischer Scientific) [18, 22, 23]. Calibration curve (OD_{265nm}) from known concentrations of butachlor in BH was prepared to calculate its residual concentration. A control devoid of the bacteria was run under the same conditions. Percent degradation (χ) was calculated according to the equation

$$\chi = \frac{C_0 - C_1}{C_0} \times 100, \tag{1}$$

where C_1 is the concentration of butachlor after 120 h and C_0 is the concentration of butachlor at zero-time interval. The kinetics of butachlor degradation by strain A16 was studied by testing four different kinetic models: (a) first order, (b) pseudo-first order, (c) second order, and (d) pseudo-second order [24]. These models were expressed by the following equation:

$$\text{First order}: \ln C = \ln C_0 - kt, \tag{2}$$

$$\text{Pseudo} - \text{first order}: \ln[C_0 - C] = \ln C - kt, \tag{3}$$

$$\text{Second order}: \frac{1}{C} = \frac{1}{C_0} + kt, \tag{4}$$

$$\text{Pseudo} - \text{second order}: \frac{t}{C} = \frac{t}{C_0} + \frac{1}{kC_0^2}, \quad (5)$$

where C_0 is the initial butachlor concentration at time zero; C is butachlor concentration at time t, and k is the kinetic rate constant.

Chemical Analysis and Identification of Intermediates

Butachlor and its degraded metabolites in the liquid medium were analysed after a time interval of 48 h and 120 h. 2 mL of the sample aliquot was sonicated and centrifuged at 12,000 rpm for 8 min; the supernatant was subjected to solvent extraction using double volume of dichloromethane in a separating funnel. The extract was dried over anhydrous sodium sulphate and evaporated. The herbicide residue obtained was dissolved in acetonitrile, filtered (pore size—0.22 µm) and stored until gas chromatography-mass spectrometry (GC–MS) analysis was done. The analysis was carried out in electron ionization mode (ionization energy—70 eV) on Perkin-Elmer clarus 500 GC device, equipped with Elite-5MS capillary column (25 m length × 0.20 mm inner diameter × 0.33 µm film thickness), using helium as a carrier gas at a constant flow rate of 1 mL min^{-1}. The column temperature was programmed at 100 °C for 2 min and then increased to 280 °C at 10 °C min^{-1} (20 min hold), with injection temperature set at 250 °C. The samples were injected in split mode (1:20) and detected in the mass range from m/z 30 to 650. Based on the GC–MS analysis degradation pathway was proposed.

Results and Discussion

Bacterial Degradation of Butachlor

Bacterial isolate from coal tar contaminated soil was rod shaped, aerobic, spore forming, and Gram-positive capable of utilizing sucrose, glucose, and fructose as carbon source [25]. Colonies after 24 h of growth on nutrient agar were white coloured, round, and convex with an average diameter of 1.5–3 mm. The 1450 bp 16S rRNA gene sequence of *B. altitudinis* A16 was assigned an accession number MN595198 after submission to the Genbank database and phylogenetic analysis showed 99.38% similarity with *Bacillus altitudinis* 41KF2b^T (Fig. 1). *Bacillus altitudinis* A16 did not grow in BH media supplemented with only acetone; however, it utilized butachlor as a sole source of carbon (Fig. 2a) for its growth which was associated with

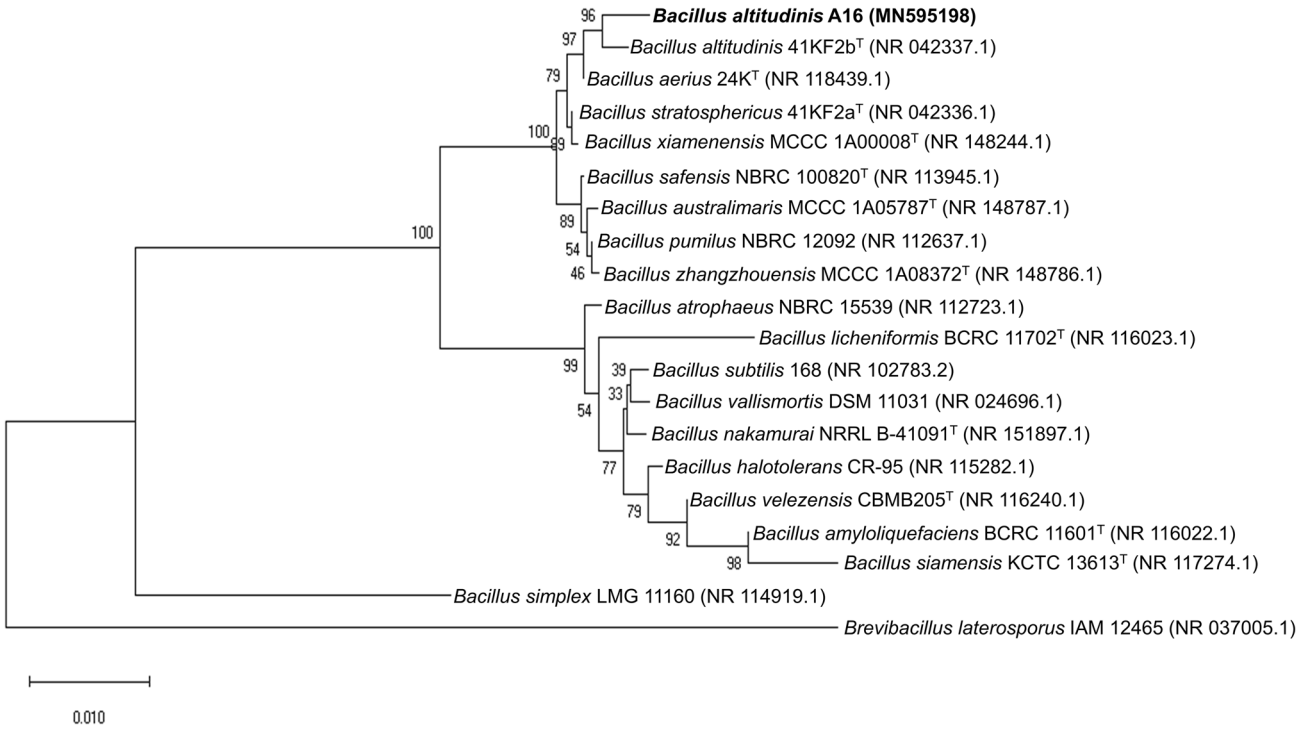


Fig. 1 Neighbour- joining tree depicting the phylogenetic relationship between *Bacillus altitudinis* A16 with other related bacterial species based on 16S rRNA gene sequences. Bootstrap values were expressed as percentage of 1000 replications. *Brevibacillus laterosporus* IAM 12465 was used as an outgroup. Scale bar represents an evolutionary distance of 0.01 substitutions per nucleotide position

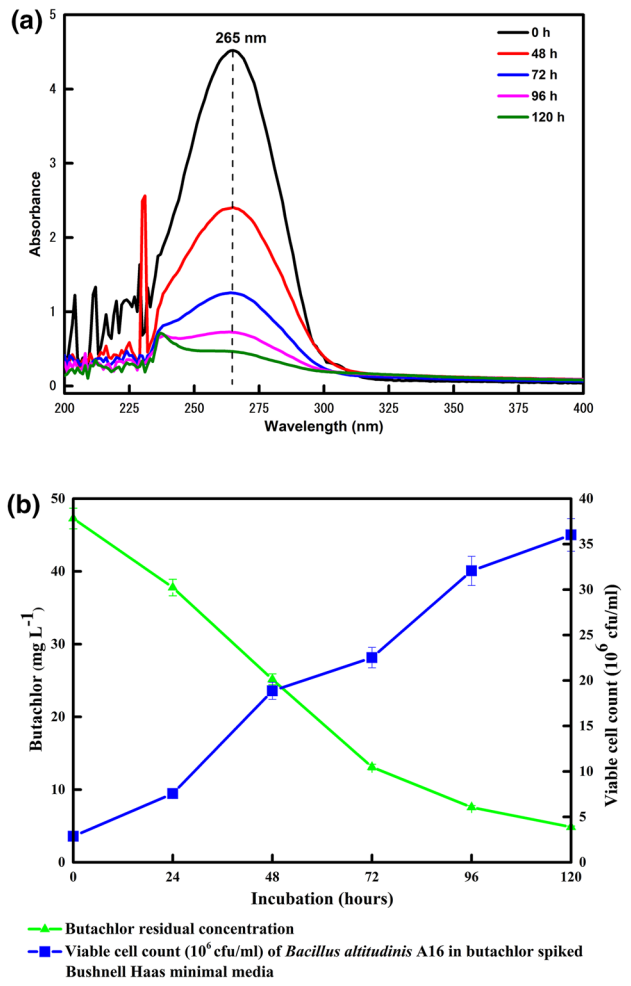


Fig. 2 **a** Change in absorption spectra of time course degradation of butachlor by *Bacillus altitudinis* A16, **b** Growth of *Bacillus altitudinis* A16 in the presence of 50 mg L^{-1} of butachlor in Bushnell Haas broth at different time intervals

increase in cell density (OD_{600nm}) from 0.02 to 0.33, and corresponding increase in viable cell count from 2.87×10^6 to 36.01×10^6 cfu mL^{-1} in 120 h (Fig. 2b). There was almost 50% reduction in the concentration of butachlor after 48 h and after 120 h more than 90% butachlor was catabolized, with control showing no significant change in residual concentration. Degradation of butachlor occurred in the wide range of temperature (25–40 °C) and pH (5–9) (data not shown). Maximum degradation was observed at 37 °C and pH 7 with inoculum density of 0.02 (OD_{600nm}); however, with an increase in cell density to 0.2–0.4 (OD_{600nm}) it showed rapid removal of butachlor from media.

Biodegradation of different chloroacetamide herbicides by several bacteria has been reported, where most of the reports are based on degradation by gram-negative bacteria (Table 1). Xu et al. [19] isolated *Achromobacter* sp., which could effectively degrade approximately 95% of 10 mg L^{-1} acetochlor within 5 days. *Paracoccus* sp. strain FLY-8 showed 65.2% degradation of butachlor (100 mg L^{-1}) in minimal salt medium within incubation period of 5 days [26]. *Catellibacterium caeni* sp. nov DCA-1^T could also degrade 81.2% of butachlor (50 mg L^{-1}) in 84 h [27]. *Ammoniphilus* sp. JF could completely mineralize butachlor (100 mg L^{-1}) within 24 h of incubation [4]. Different species of *Bacillus* have been used for the degradation of pollutants from crude oil, endocrine disrupting phthalate esters and Bisphenol A [28–30]. Gao et al. [3] isolated *Bacillus* sp. hys-1 which degraded 90% of 100 mg L^{-1} butachlor in 7 days at 30 °C and pH 6.5 with cell density of 0.21 to 0.92 (OD_{600} nm). However, strain A16 degraded 90% of butachlor in 5 days at minimum cell density ($OD_{600nm} = 0.02$) at 37 °C and pH 7.

Butachlor degradation rate kinetics was studied using different kinetic models (Table 2). The best fit reaction kinetics was obtained in a first-order model for degradation of butachlor by the bacterium in BH broth, based on highest regression coefficient (R^2) which was 0.979 (Fig. 3). The degradation was characterized by a rate constant (k) of 0.02 h^{-1} and half-life ($t_{1/2}$) of 34.65 h, within which the initial concentration of butachlor was mineralized to 50% by strain A16. R^2 values for other three kinetic models were far from unity (Table 2) and were not suitable to explain butachlor degradation. Dwivedi et al. [8] reported first-order kinetic model for the complete biodegradation of 3.2 mmol L^{-1} butachlor in soil, with a half-life and a rate constant of 4 days and 0.17 day^{-1}, respectively. In other similar studies conducted in soil, kinetics of butachlor degradation was also best fitted to its first-order kinetics model [31, 32].

Identification of Metabolites and Degradation Pathway

The intermediate compounds produced during butachlor degradation by bacterial isolate A16 were identified by GC–MS analysis at 0 h, 48 h and 120 h. The detected metabolites were determined by matching with the electron ionization mass spectra provided by National Institute of Standards and Technology (NIST) library. The characteristic fragment ion peaks were also matched with earlier reports. Single peak with RT = 17.22 min found in control sample was identified as butachlor by NIST library. Sample collected after 48 h of degradation process gave a peak (*A*) with RT (17.26 min), but lower intensity/area than control suggesting partial degradation of butachlor (Fig. 4a). Butachlor has a molecular weight of 311.17 and showed characteristic fragment ion peaks at m/z 281.16, 251.99, 207.17, 176.22, 160.14, 77.02, 57.13 (Fig. 5a). Five major metabolites corresponding to B (RT 16.91 min), C (RT 16.61 min), D (RT

Table 1 Degradation of butachlor by bacteria

Bacterial strain	Gram character	Inoculum size	Degradation of butachlor	Metabolites produced	Reference
Stenotrophomonas acidaminiphila sp. JS-1	Gram − ive	0.1 ml	3.2 mmol l^{-1} in 20 days	–	[8]
Paracoccus sp. FLY-8	Gram − ive	1% v/v	65.2% of 100 mg L^{-1} in 5 days	Alachlor, 2-chloro-*N*-(2,6-dimethylphenyl) acetamide, 2,6-diethylaniline	[25]
Catellibacterium caeni sp. nov DCA-1^T	Gram − ive	2%	81.2% of 50 mg L^{-1} in 84 h	*N*-hydroxymethyl-2-chloro-*N*-(2,6-diethyl-phenyl)-acctamide, 2-chloro-*N*-(2,6-diethyl-phenyl)-acetamide, (2,6-diethyl-phenyl)-ethoxymethyl-carbamic acid, *N*-(2,6-diethyl-phenyl)-*N*-hydroxymeth-ylacetamide and *N*-(2,6-diethyl-phenyl)-*N*-hydroxymethyl-formamide	[26]
Rhodococcus sp. strain B1	Gram + ive	1.4×10^6 cfu mL^{-1}	100 mg L^{-1} within 5 days	2-chloro-*N*-(2,6-dimethylphenyl) acetamide and butoxymethanol	[22]
Mycobacterium sp. J7A and *Sphingobium* sp. J7B	Gram + ive, Gram -ive	$OD_{600\ nm} = 0.004$	100 mg L^{-1} in 24 h	2-chloro-*N*-(2,6-diethylphenyl) acetamide and 2,6-diethylaniline	[23]
Novosphingobium chloroacetimidivorans sp. BUT-14^T	Gram − ive	5% (v/v)	90.5 ± 14.1% of 100 mg L^{-1} in 5 days	–	[14]
Bacillus sp. hys-1	Gram + ive	$OD_{600nm} = 1.0$	More than 90% of 100 mg L^{-1} in 7 days	2-chloro-*N*-(2,6-diethylphenyl)-*N*-methylacetamide, 2-chloro-*N*-(2,6-diethylphenyl)-acetamide, and 2,6-diethy-laniline	[3]
Sphingomonas chloroacetimidivorans sp. $Y1^T$	Gram − ive	5% (v/v)	68.5 ± 8.7% of 100 mg L^{-1} in 7 days	–	[33]
Roseomonas chloroacetimidivorans sp. BUT-13^T	Gram − ive	5% (v/v)	48.6 ± 6.5% of of 100 mg L^{-1} in 4 days	–	[34]
Ammoniphilus sp. JF	Gram variable	$OD_{600\ nm} = 0.002$	100 mg L^{-1} within 24 h	1,2-benzenedicarboxylic acid, bis(2-methylpropyl) ester and 2,4-bis(1,1-dimethylethyl)-phenol	[4]
Bacillus altitudinis A16	Gram + ive	$OD_{600\ nm} = 0.002$	More than 90% of 50 mg L^{-1} in 5 days	*N*-(butoxymethyl)-*N*-(2-chloroethyl)-2,6-diethylaniline, (*N*-butoxymethyl)-2-chloro-*N*-(2-ethylphenyl) acetamide, *N*-(butoxymethyl)-2,6-diethyl-*N*-propy-laniline, 2-chloro-*N*-(2,6-diethylphenyl) acetamide and 2,6-diethylaniline	Current study

Table 2 Kinetic models of butachlor degradation by *Bacillus altitudinis* A16

Kinetic models	Equation	Rate constant (k)	R^2 values
First order	$\ln C = \ln C_0 - kt$	2×10^{-2} h^{-1}	0.979
Pseudo-first order	$\ln[C_0 - C] = \ln C - kt$	2.16×10^{-2} h^{-1}	0.755
Second order	$1/C = 1/C_0 + kt$	0.1×10^{-2} mg L^{-1} h^{-1}	0.851
Pseudo-second order	$t/C = t/C_0 + 1/kC_0^2$	19.46×10^{-2} mg L^{-1} h^{-1}	0.781

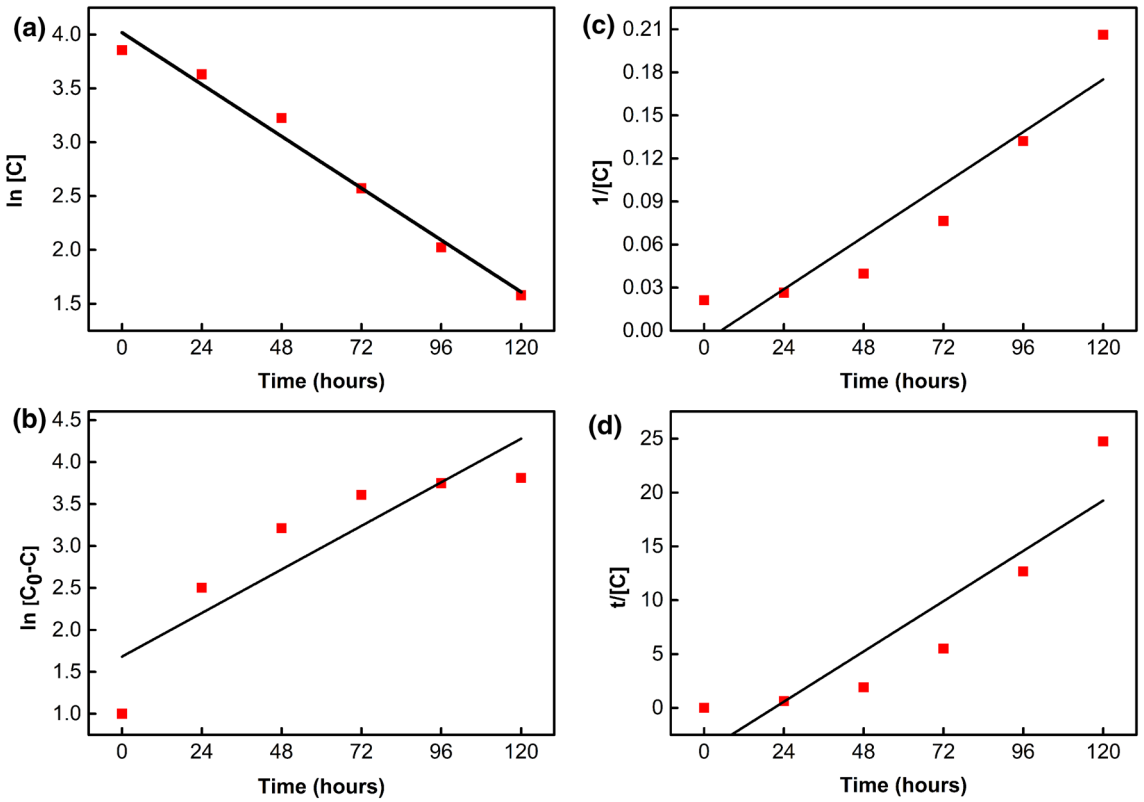


Fig. 3 Kinetic model fitting for rate of degradation of butachlor by strain A16—**a** first order, **b** pseudo-first order, **c** second order, **d** pseudo-second order

15.86 min), E (RT 15.17 min), and F (14.51 min) were detected in sample collected after 120 h (Fig. 4b).

Peak B with RT 16.91 min was supposed to be *N*-(butoxymethyl)-*N*-(2-chloroethyl)-2,6-diethylaniline, which showed a positive ion chemical ionization at 297.23 and fragment ion peaks at m/z at 283, 252.06, 207,182.45, 147.03, 119.17, 105.20, 77.10, 51.16 (Fig. 5(b)). Peak C (RT 16.61 min) was observed to be *N*-(butoxymethyl)-2-chloro-*N*-(2-ethylphenyl) acetamide with molecular weight 283.13 and ion fragments at m/z 281.23, 252.13, 207,10, 182.10, 105.13, 91.15, 77.02 (Fig. 5(c)). Peak D (RT 15.86 min) was identified as *N*-(butoxymethyl)-2,6-diethyl-*N*-propylaniline and has a molecular weight of 277.44. It showed a positive ion chemical ionization at 277.19 and fragment ions at m/z at 251.99, 235.19, 218.85, 207.24, 163.04, 137.39, 105.20, 78.16, 76.95, 57.13 (Fig. 5d). Peak E (RT 15.17) displayed fragment ions at m/z 201.43, 195.20, 188.54, 161.06, 147.03,131.15, 118.11, 104.99,95.34, 93.42,77.10 and was identified as 2-chloro-*N*-(2,6-diethylphenyl) acetamide. Molecular weight of the identified compound is 225.09. (Fig. 5e). The molecular weight of compound having RT 14.51 min (peak F) is 149.12. Based on the molecular weight and its fragment ion peaks (147.31, 133.21, 119.24, 96.19,

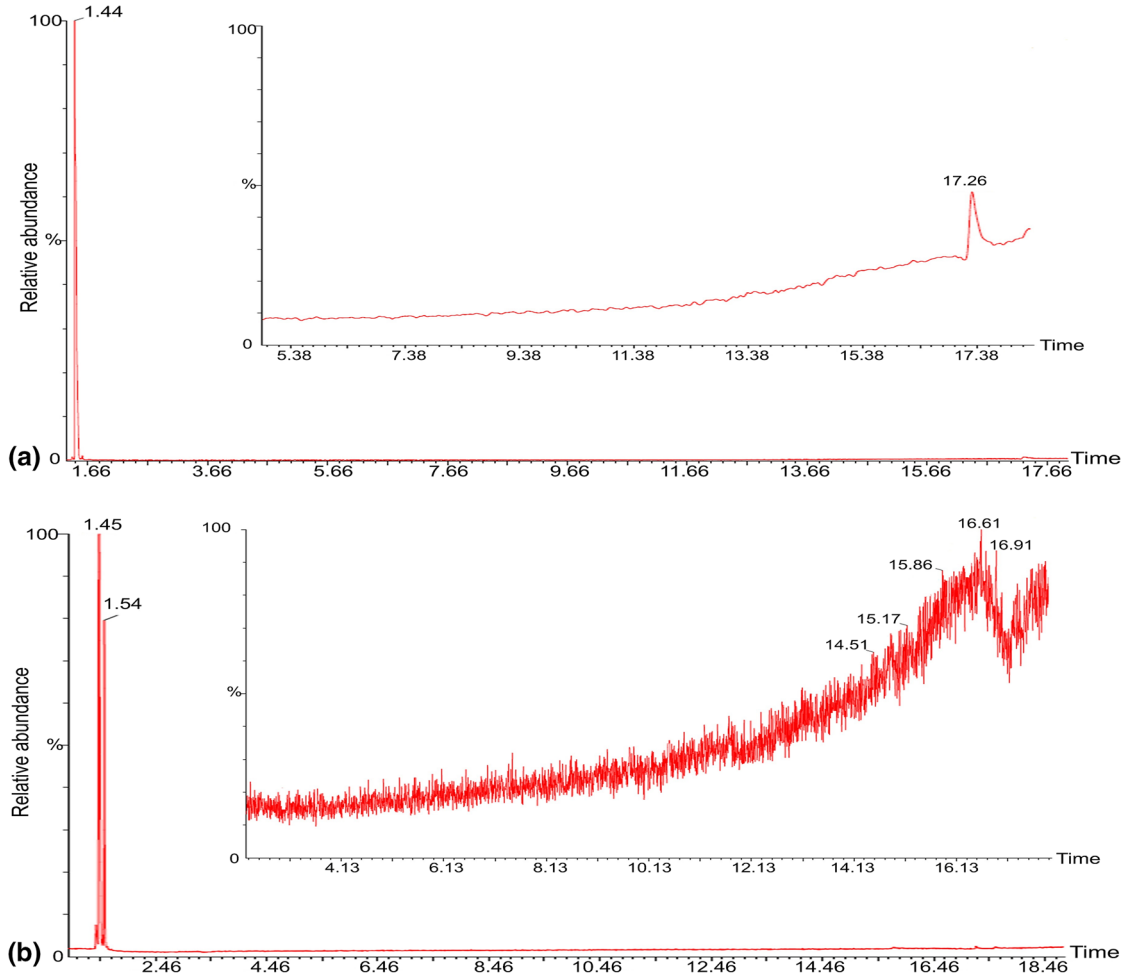


Fig. 4 GC–MS analysis of residual butachlor in culture broth at **a** 48 h, **b** 120 h. Peaks with RT 17.26 min, 16.91 min, 16.61 min, 15.86 min, 15.17 min and 14.51 min showing breakdown into different metabolites

73.19, 69.14), the compound was identified as 2,6-diethylaniline (Fig. 5f).

In our study, GC–MS analysis gave 5 metabolites, among which *N*-(butoxymethyl)-*N*-(2-chloroethyl)-2,6-diethylaniline and *N*-(butoxymethyl)-2-chloro-*N*-(2-ethylphenyl) acetamide were not previously reported. Butachlor could possibly be degraded into *N*-(butoxymethyl)-*N*-(2-chloroethyl)-2,6-diethylaniline by deacylation at nitrogen group of butachlor which further underwent dechlorination to form *N*-(butoxymethyl)-2,6-diethyl-*N*-propylaniline. Dealkylation of *N*-(butoxymethyl)-2,6-diethyl-*N*-propylaniline led to the formation of *N*-(butoxymethyl)-2-ethylaniline, which was comparable with the pathway reported by Singh and Nandabalan [4]. The major compounds found were 2-chloro-*N*-(2,6-diethylphenyl) acetamide and 2,6-diethylaniline, which were previously reported in several butachlor degradation studies [3, 22, 26]. Formation of 2-chloro-*N*-(2,6-diethylphenyl) acetamide was the result of debutoxylation and dealkylation reactions. Liu et al. [22] proposed hydrolysis of butachlor through N-dealkylation resulting in the formation of butoxymethanol and 2-chloro-*N*-(2,6-dimethylphenyl)-acetamide where hydrolase Ch1H was the enzyme involved the degradation process. Zhang et al. [26] detected oxygenases (aniline dioxygenase and catechol 1, 2-dioxygenase) during butachlor degradation by *Paracoccus* sp., which were induced by butachlor and 2,6-diethylaniline. Detection of metabolite 2,6-diethylaniline in our study indicates 2,6-diethylaniline was subsequently metabolized into CO_2 and H_2O via oxidation of aniline and catechol through ortho/meta-cleavage pathway. In another

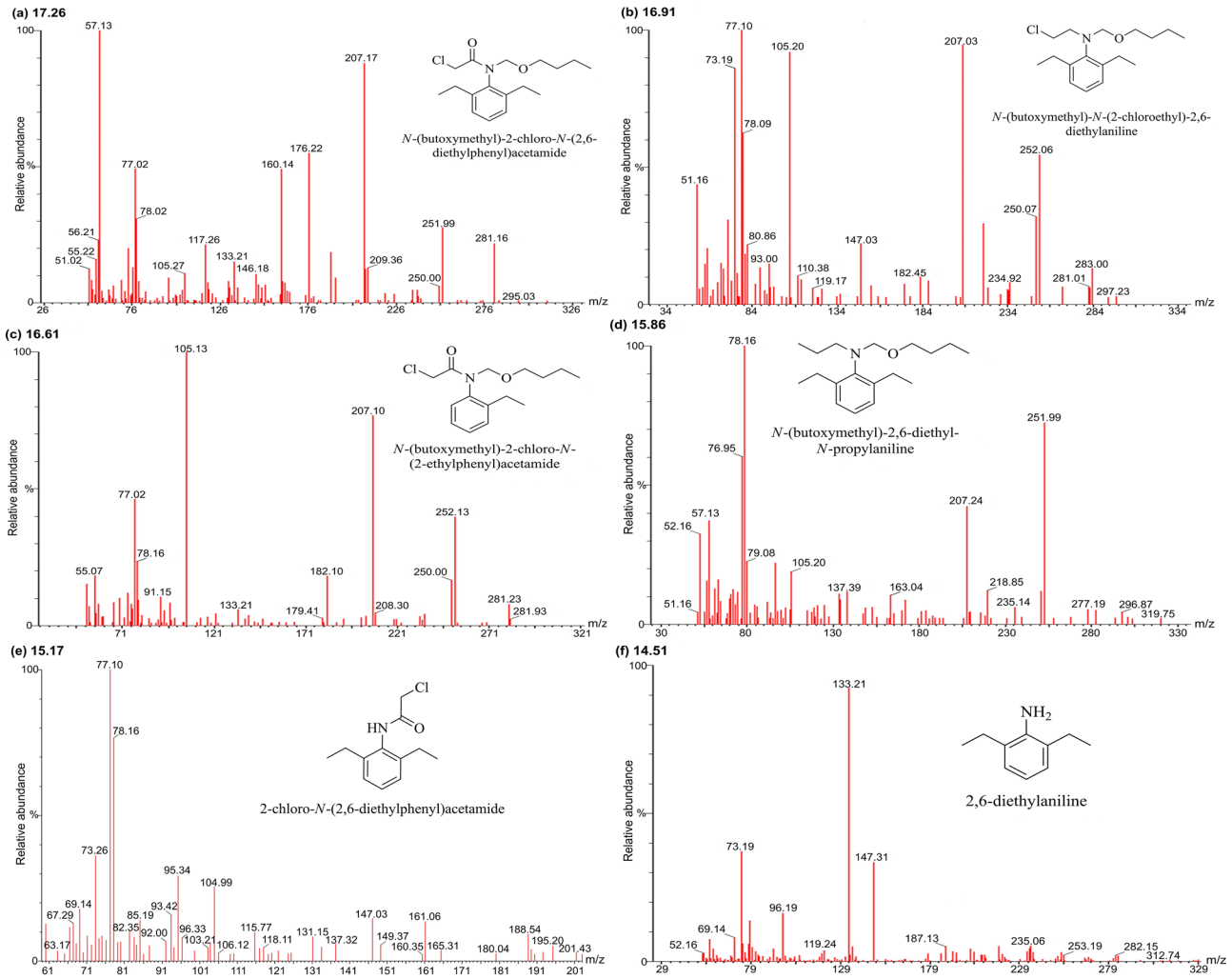


Fig. 5 Mass spectra analysis for peaks **a** RT 17.26 (butachlor), **b** RT 16.91 (*N*-butoxymethyl)-*N*-(2-chloroethyl)-2,6-diethylaniline), **c** RT 16.61 (*N*-(butoxymethyl)-2-chloro-*N*-(2-ethylphenyl) acetamide), **d** RT 15.86 (*N*-(butoxymethyl)-2,6-diethyl-*N*-propylaniline), **e** RT 15.17 (2-chloro-*N*-(2,6-diethylphenyl) acetamide) and **f** RT 14.51 (2,6-diethylaniline)

study conducted by Zheng et al. [27] a Gram-negative bacteria *Catellibacterium caeni* sp. nov DCA-1^{T} degraded butachlor into five different metabolites. Hydrolases and oxygenases (aniline dioxygenase, catechol 1,2-dioxygenase, catechol 2,3-dioxygenase) in crude cell extracts of *Bacillus* sp. Hys-1 [3], *Rhodococcus* [22], and *Paracoccus* [26] are involved in degradation of butachlor and no enzyme activity was detected in cell extracts when glucose was used as substrate. In our study we report growth of *Bacillus altitudinis* A16 from coal tar contaminated soil in the presence of butachlor as sole carbon source and its utilization through degradation by cell extract with the formation of similar metabolites following three possible initial steps (Fig. 6) based on previous reports and our findings.

Conclusion

Bacillus altitudinis strain A16, isolated from soil demonstrated excellent butachlor removal capacity by degrading 90% of 50 mg L^{-1} butachlor at minimum cell density, at 37 °C and pH 7. The half-life of butachlor was observed to be 34.65 h. Five different metabolites were identified in culture filtrates by GC–MS among which *N*-(butoxymethyl)-*N*-(2-chloroethyl)-2,6-diethylaniline and *N*-(butoxymethyl)-2-chloro-*N*-(2-ethylphenyl) acetamide are reported for the first time and based on past literature and present findings, three possible metabolic pathways for complete mineralization of butachlor by *Bacillus altitudinis* strain A16 is proposed. *Bacillus altitudinis* can be used for bioremediation of pesticide butachlor in soils where its bioavailability is low by mass culturing and soil inoculation.

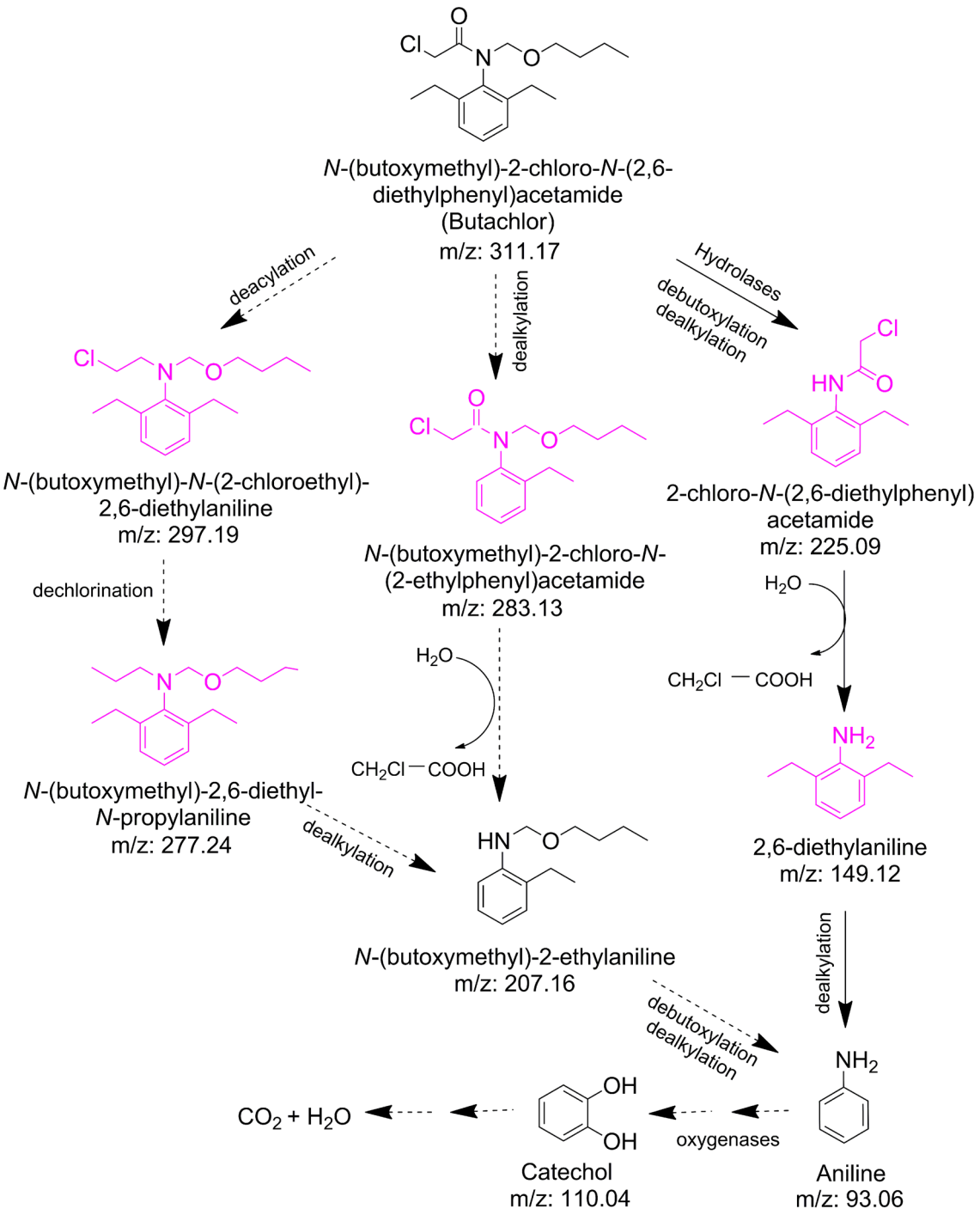


Fig. 6 Proposed possible metabolic pathways of butachlor degradation by *Bacillus altitudinis* A16

Acknowledgement The authors would like to thank the Director, Thapar Institute of Engineering & Technology (Deemed to be University), Patiala, for infrastructural support and to DST-SERB (Science and Engineering Research Board, Department of Science and Technology, Government of India) for financial support vide Grant EMR/2016/002524.

Author Contributions RK conducted the experiments. RK and DG contributed equally towards the manuscript editing and its submission.

Compliance with Ethical Standards

Conflict of interest The authors declare that there is no conflict of interest.

References

1. Wang S, Li H, Lin C (2013) Physiological, biochemical and growth responses of Italian ryegrass to butachlor exposure. Pestic Biochem Phys 106(1–2):21–27. https://doi.org/10.1016/j.pestbp.2013.03.007
2. Abigail MEA, Samuel SM, Ramalingam C (2015) Addressing the environmental impacts of butachlor and the available remediation strategies: a systematic review. Int J Environ Sci Technol 12(12):4025–4036. https://doi.org/10.1007/s13762-015-0866-2
3. Gao Y, Jin L, Shi H, Chu Z (2015) Characterization of a novel butachlor biodegradation pathway and cloning of the debutoxylase (Dbo) gene responsible for debutoxylation of butachlor in *Bacillus* sp. hys-1. J Agric Food Chem 63(38):8381–8390. https://doi.org/10.1021/acs.jafc.5b03326
4. Singh J, Nandabalan YK (2018) Prospecting *Ammoniphilus* sp. JF isolated from agricultural fields for butachlor degradation. 3 Biotech 8(3):164. https://doi.org/10.1007/s13205-018-1165-7
5. Alla MN, Badawi AM, Hassan NM, El-Bastawisy ZM, Badran EG (2008) Effect of metribuzin, butachlor and chlorimuron-ethyl on amino acid and protein formation in wheat and maize seedlings. Pestic Biochem Phys 90(1):8–18. https://doi.org/10.1016/j.pestbp.2007.07.003
6. Verma JP, Jaiswal DK, Sagar R (2014) Pesticide relevance and their microbial degradation: a-state-of-art. Rev Environ Sci Biotechnol 13(4):429–466. https://doi.org/10.1007/s11157-014-9341-7
7. National Center for Biotechnology Information (2019) PubChem Database. Butachlor, CID=31677, https://pubchem.ncbi.nlm.nih.gov/compound/Butachlor. Accessed 22 Oct 2019
8. Dwivedi S, Singh BR, Al-Khedhairy AA, Alarifi S, Musarrat J (2010) Isolation and characterization of butachlor-catabolizing bacterial strain *Stenotrophomonas acidaminiphila* JS-1 from soil and assessment of its biodegradation potential. Lett Appl Microbiol 51(1):54–60. https://doi.org/10.1111/j.1472-765X.2010.02854.x
9. Dwivedi S, Saquib Q, Al-Khedhairy AA, Musarrat J (2012) Butachlor induced dissipation of mitochondrial membrane potential, oxidative DNA damage and necrosis in human peripheral blood mononuclear cells. Toxicology 302(1):77–87. https://doi.org/10.1016/j.tox.2012.07.014
10. Chang J, Liu S, Zhou S, Wang M, Zhu G (2013) Effects of butachlor on reproduction and hormone levels in adult zebrafish (*Danio rerio*). Exp Toxicol Pathol 65(1–2):205–209. https://doi.org/10.1016/j.etp.2011.08.007
11. Liu WY, Wang CY, Wang TS, Fellers GM, Lai BC, Kam YC (2011) Impacts of the herbicide butachlor on the larvae of a paddy field breeding frog (*Fejervarya limnocharis*) in subtropical Taiwan. Ecotoxicology 20(2):377–384. https://doi.org/10.1007/s10646-010-0589-6
12. Muthukaruppan G, Janardhanan S, Vijayalakshmi G (2005) Sublethal toxicity of the herbicide butachlor on the earthworm *Perionyx sansibaricus* and its histological changes (5 pp). J Soils Sediments 5(2):82–86. https://doi.org/10.1065/jss2004.09.111
13. Kaur R, Goyal D (2019) Toxicity and degradation of the insecticide monocrotophos. Environ Chem Lett 17(3):1299–1324. https://doi.org/10.1007/s10311-019-00884-y
14. Chen Q, Zhang J, Wang CH et al (2014) *Novosphingobium chloroacetimidivorans* sp. nov., a chloroacetamide herbicide–degrading bacterium isolated from activated sludge. Int J Syst Evol Microbiol 64(8):2573–2578. https://doi.org/10.1099/ijs.0.062950-0
15. Mohanty SS, Jena HM (2019) Evaluation of butachlor biodegradation efficacy of *Serratia ureilytica* strain AS1: a statistical optimization approach. Int J Environ Sci Technol 16(10):5807–5816. https://doi.org/10.1007/s13762-018-1958-6
16. Mohanty SS, Jena HM (2018) Process optimization of butachlor bioremediation by Enterobacter cloacae using Plackett Burman design and response surface methodology. Process Saf Environ 119:198–206. https://doi.org/10.1016/j.psep.2018.08.009
17. Khanna P, Goyal D, Khanna S (2012) Characterization of pyrene utilizing *Bacillus* spp. from crude oil contaminated soil. Braz J Microbiol 43(2):606–617. https://doi.org/10.1590/S1517-83822012000200024
18. Haq AU, Saeed M, Usman M, Muneer M, Adeel S, Abbas S, Iqbal A (2019) Removal of butachlor from aqueous solution using cantaloupe seed shell powder: kinetic, equilibrium and thermodynamic studies. Int J Environ Sci Technol 16(10):6029–6042. https://doi.org/10.1007/s13762-018-1992-4
19. Xu C, Ding J, Qiu J, Ma Y (2013) Biodegradation of acetochlor by a newly isolated *Achromobacter* sp. strain D-12. J Environ Sci Health B 48(11):960–966. https://doi.org/10.1080/03601234.2013.816601
20. Kim OS, Cho YJ, Lee K et al (2012) Introducing EzTaxon-e: a prokaryotic 16S rRNA gene sequence database with phylotypes that represent uncultured species. Int J Syst Evol Microbiol 62(3):716–721. https://doi.org/10.1099/ijs.0.038075-0
21. Kumar S, Stecher G, Li M, Knyaz C, Tamura K (2018) MEGA X: molecular evolutionary genetics analysis across computing platforms. Mol Biol Evol 35(6):1547–1549. https://doi.org/10.1093/molbev/msy096
22. Liu HM, Cao L, Lu P et al (2012) Biodegradation of butachlor by *Rhodococcus* sp. strain B1 and purification of its hydrolase (ChlH) responsible for N-dealkylation of chloroacetamide herbicides. J Agric Food Chem 60(50):2238–12244. https://doi.org/10.1021/jf303936j
23. Kim NH, Kim DU, Kim I, Ka JO (2013) Syntrophic biodegradation of butachlor by *Mycobacterium* sp. J7A and *Sphingobium* sp. J7B isolated from rice paddy soil. FEMS Microbiol Lett 344(2):114–120. https://doi.org/10.1111/1574-6968.12163
24. Agnihotri S, Sillu D, Sharma G, Arya RK (2018) Photocatalytic and antibacterial potential of silver nanoparticles derived from pineapple waste: process optimization and modeling kinetics for dye removal. Appl Nanosci 8(8):2077–2092. https://doi.org/10.1007/s13204-018-0883-9
25. Shivaji S, Chaturvedi P, Suresh K (2006) *Bacillus aerius* sp. nov., *Bacillus aerophilus* sp. nov., *Bacillus stratosphericus* sp. nov. and *Bacillus altitudinis* sp. nov., isolated from cryogenic tubes used for collecting air samples from high altitudes. Int J Syst Evol Microbiol 56(7):1465–1473. https://doi.org/10.1099/ijs.0.64029-0
26. Zhang J, Zheng JW, Liang B et al (2011) Biodegradation of chloroacetamide herbicides by *Paracoccus* sp. FLY-8 in vitro. J Agric Food Chem 59(9):4614–4621. https://doi.org/10.1021/jf104695g

27. Zheng J, Li R, Zhu J, Zhang J, He J, Li S, Jiang J (2012) Degradation of the chloroacetamide herbicide butachlor by *Catellibacterium caeni* sp. nov. DCA-1^{T}. Int Biodeter Biodegr 73:16–22. https://doi.org/10.1016/j.ibiod.2012.06.003
28. García-Alcántara JA, Maqueda-Gálvez AP, Téllez-Jurado A, Hernández-Martínez R, Lizardi-Jiménez MA (2016) Maya crude-oil degradation by a *Bacillus licheniformis* consortium isolated from a Mexican thermal source using a bubble column bioreactor. Water Air Soil Pollut 227(11):413. https://doi.org/10.1007/s11270-016-3121-7
29. Surhio MA, Talpur FN, Nizamani SM et al (2017) Effective bioremediation of endocrine-disrupting phthalate esters, mediated by *Bacillus* strains. Water Air Soil Pollut 228(10):386. https://doi.org/10.1007/s11270-017-3567-2
30. Suyamud B, Inthorn D, Panyapinyopol B, Thiravetyan P (2018) Biodegradation of bisphenol A by a newly isolated *Bacillus megaterium* strain ISO-2 from a polycarbonate industrial wastewater. Water Air Soil Pollut 229(11):348. https://doi.org/10.1007/s11270-018-3983-y
31. Yu YL, Chen YX, Luo YM, Pan XD, He YF, Wong MH (2003) Rapid degradation of butachlor in wheat rhizosphere soil. Chemosphere 50(6):771–774. https://doi.org/10.1016/S0045-6535(02)00218-7
32. Yang C, Wang M, Li J (2012) Influence of rhizosphere microbial ecophysiological parameters from different plant species on butachlor degradation in a riparian soil. J Environ Qual 41(3):716–723. https://doi.org/10.2134/jeq2011.0223
33. Chen K, Chen Q, Wang GX et al (2015) *Sphingomonas chloroacetimidivorans* sp. nov., a chloroacetamide herbicide-degrading bacterium isolated from activated sludge. Antonie Van Leeuwenhoek 108(3):703–710. https://doi.org/10.1007/s10482-015-0526-z
34. Chu CW, Chen Q, Wang CH et al (2016) *Roseomonas chloroacetimidivorans* sp. nov., a chloroacetamide herbicide-degrading bacterium isolated from activated sludge. Antonie Van Leeuwenhoek 109(5):611–618. https://doi.org/10.1007/s10482-016-0664-y

Publisher's Note Springer Nature remains neutral with regard to jurisdictional claims in published maps and institutional affiliations.

Carbohydrate Polymers 262 (2021) 117906

Contents lists available at ScienceDirect

Carbohydrate Polymers

journal homepage: www.elsevier.com/locate/carbpol

Chitosan/PVA silver nanocomposite for butachlor removal: Fabrication, characterization, adsorption mechanism and isotherms

Ravneet Kaur [a], Dinesh Goyal [a,*], Shekhar Agnihotri [a,b]

[a] Department of Biotechnology, Thapar Institute of Engineering & Technology (Deemed to be University), Patiala, 147001, Punjab, India
[b] Department of Agriculture and Environmental Sciences, National Institute of Food Technology Entrepreneurship and Management, Kundli, Sonepat, 131028, Haryana, India

ARTICLE INFO

Keywords:
Chitosan
PVA
Hydrogel
Adsorption
Silver nanocomposite

ABSTRACT

Silver nanoparticle (AgNP) incorporated chitosan-Polyvinyl alcohol (Ch/PVA) hydrogel nanocomposite was fabricated by repeated freeze-thaw treatment using glutaraldehyde as crosslinker for removal of herbicide butachlor from aqueous solution. Ch/PVA hydrogel provided a matrix for *in-situ* immobilization of AgNPs and were characterized by various physicochemical techniques. AgNPs of size 5−20 nm possessed crystalline structure, led to increase in thermal stability and surface area after incorporation into Ch/PVA hydrogel. Ch/PVA hydrogel nanocomposite showed maximum adsorption of butachlor (86.55 %) at 30 °C and pH 3.0, while Ch/PVA-Ag showed a slight increase in adsorption of butachlor following pseudo-second order kinetics. Langmuir and Freundlich models with different error functions (R^2, R^2_{adj}, RSME, χ^2 and RSS), confirmed monolayer adsorption of butachlor.

1. Introduction

Chloroacetamide herbicide butachlor (*N*-(butoxymethyl)-2-chloro-*N*-(2,6-diethylphenyl) acetamide) is extensively used as a selective, systemic herbicide for controlling unwanted weeds and annual grass in wheat-rice cultivation (Fig. 1). It is a pre-emergence or early post-emergence herbicide, which inhibits the enzymes involved in geranylgeranyl pyrophosphate cyclization and elongation of the long-chain fatty acids (Abigail et al., 2015; Kaur & Goyal, 2020). Low cost and broad-spectrum activity make butachlor one of the most commonly used herbicides in Asia with an annual utilization rate of about 4.5×10^7 kg (Singh & Nandabalan, 2018).

Indiscriminate application of butachlor has led to its persistence in the environment by erosion, leaching and runoff water from the areas of its application, which adversely affects aquatic life as well as the human health (Haq et al., 2019; Watanabe et al., 2007). It has been detected in soil, surface and underground water with residual concentrations ranging from 29.5 - 74 μg kg^{-1} in soil (Yang et al., 2010) and 0.1–1.4 μg L^{-1} in surface water (Mamun et al., 2009), respectively. Being lipophilic in nature, it is resistant to degradation in the environment and tend to bioaccumulate in aquatic organisms, causing several toxic effects (Li et al., 2016). Toxicological studies on different aquatic organisms have shown butachlor to be a suspected carcinogen (Ou et al., 2000; Tu et al., 2013) and resulted in morphological abnormalities, inhibited embryo hatching and caused significant mortality in zebrafish *Danio rerio* (Tu et al., 2013). It has a potential to cause cytotoxicity and oxidative toxicity in fish by depressing glutathione detoxification system in kidney and also affects reproduction and sex steroid endocrine systems in zebrafish (Chang et al., 2013; Farombi et al., 2008; Zhu et al., 2014). Several reports suggest butachlor to be genotoxic to frogs (Liu et al., 2011), a growth retardant in earthworm (Muthukaruppan et al., 2005) and potential tumor promoter with carcinogenic activity in mouse liver cells (Ou et al., 2000). Dwivedi et al. (2012) reported genotoxicity and clastogenicity of butachlor in exposed human peripheral blood mononuclear cells which was indicated by cell cycle alterations and necrosis due to chromosomal and mitochondrial membrane damage. Butachlor is not expected to undergo hydrolysis in the environment due to the lack of hydrolyzable functional groups nor to directly photolyze due to the lack of absorption in the environmental UV spectrum (>290 nm) (NCBI, 2021). Therefore, it is very important to remove butachlor from the environment.

Over the years, various techniques such as biodegradation, ion-exchange, advanced oxidation processes, solid phase extraction, adsorption and photocatalytic methods have been studied for removal of

* Corresponding author.
E-mail address: dgoyal@thapar.edu (D. Goyal).

https://doi.org/10.1016/j.carbpol.2021.117906
Received 20 November 2020; Received in revised form 15 February 2021; Accepted 1 March 2021
Available online 5 March 2021
0144-8617/© 2021 Published by Elsevier Ltd.

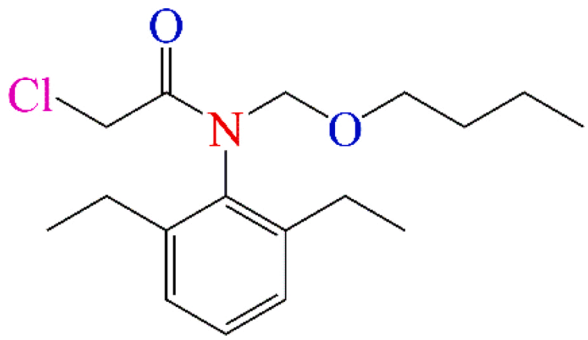


Fig. 1. Chemical structure of butachlor ($C_{17}H_{26}ClNO_2$).

different pesticides (Dwivedi et al., 2014). However, sorption and photocatalytic methods using bio sorbents and their nano-composites have gained much attention due to their biocompatible nature, high efficiency, cost effective and easy availability (Dwivedi et al., 2014; Haq et al., 2019). Many biosorbents and their nano-composites such as mangosteen peel (Ahmad & Alrozi, 2010), rambutan peel (Ahmad & Alrozi, 2011), pistachio shell (Dolas et al., 2011), chitosan-gold nanoparticles (Dwivedi et al., 2014), chitosan zinc oxide nanoparticle composite (Dehaghi et al., 2014) and cantaloupe seed shell powder (Haq et al., 2019) have been reported for contaminant removal. Activated charcoal (AC) is another widely used adsorbent for removal of pesticides, dyes or other harmful chemicals from aqueous systems. However, its usage is sometimes restricted on economic consideration, as higher is the quality, greater is the cost of AC. It is non-selective and regeneration of saturated carbon by chemical or thermal techniques is expensive and results in loss of its adsorption capacity (Saifuddin et al., 2011). Among all these, chitosan in the hydrogel or beads form has gathered a significant attention due to low cost and easy separation after adsorption.

Hydrogel is a gel-like, water-insoluble, cross-linked polymeric network which has a potential to retain water and shows swelling properties due to the presence of functional groups such as hydroxyl, amino, amide, sulphonic and carboxyl in the polymers constituting hydrogel network (Agnihotri et al., 2012). Chitosan (β-1,4-linked polysaccharide) is a cationic polymer produced in bulk from chitin (crustaceans shells) as a by-product (Agnihotri et al., 2012; Gholamali et al., 2020). Because of its extraordinary properties, such as gel forming capability, low toxicity, biodegradability, biocompatibility, eco-friendliness and adsorption capacity, chitosan is used as a sorbent for removal of contaminants (Agnihotri et al., 2012; Habiba et al., 2019). Its sorption efficiency is attributed to the amino and hydroxyl groups present on the glucosamine unit (Dwivedi et al., 2014). The limitation associated with chitosan hydrogel is its poor mechanical strength on swelling and sensitivity to pH, which can be minimized by chemical crosslinking it with another polymer possessing greater mechanical strength by addition of cross-connecting agents (Agnihotri et al., 2012; Habiba et al., 2019). Considering the type of crosslinker applied, the crosslinking process may proceed via covalent or ionic bonds. Chitosan crosslinked with ionic crosslinkers such as sodium tripolyphosphate (TPP) is less stable in acidic solutions and dissolves at pH 3. Whereas, using covalent crosslinkers such as glutaraldehyde and epichlorohydrin (EPI), stable covalent bonds (even at pH 1) are formed between the polymers and the crosslinkers, which is an irreversible reaction (Jóźwiak et al., 2017). As per material safety data sheet (MSDS) ratings, glutaraldehyde is rated 2 (moderately Health hazard), whereas, EPI is rated as 3 (serious Health hazard), suggesting glutaraldehyde less harmful and better crosslinker than EPI (Gonenc & Us, 2019). Polyvinyl alcohol (PVA) is a water soluble, vinyl type polymer, extensively studied due to its hydrophilicity, excellent chemical stability, gel and film forming ability, biocompatibility, greater mechanical strength and non-toxic nature (Agnihotri et al., 2012; Krstić et al., 2014; Gholamali et al., 2020). To enhance the adsorption properties and complete elimination of the contaminants, nanoparticles are incorporated within the crosslinked and swollen networks to form nanocomposite hydrogels (Habiba et al., 2019; Gholamali et al., 2020). These chitosan-based hydrogels are low cost, non- toxic and easy to handle adsorbents, which give us an additional benefit of easy adsorbent separation.

In this study, we have synthesized chitosan-PVA (Ch/PVA) nanocomposite hydrogel with immobilized silver nanoparticles (Ch/PVA-Ag) for removal of butachlor from water. Also, a comparative sorption study has been conducted between blank Ch/PVA hydrogel and Ch/PVA-Ag nanocomposite to determine the change in sorption capacity of Ch/PVA hydrogel by incorporating AgNPs within it.

2. Materials and methods

2.1. Materials

Chitosan, in powder form (>90 % deacetylation degree; low MW ~1,20,000 Da) was procured from Marine Hydrocolloids, Cochin, Kerala and was used without any treatment. PVA (MW 1,60,000), sodium hydroxide and sodium borohydride were purchased from Himedia. Silver nitrate and butachlor (analytical grade, 97.7 % purity) were obtained from Sigma Aldrich. Other analytical grade chemicals, such as glacial acetic acid and glutaraldehyde solution (25 wt%) were obtained from SD Fine Ltd. Deionized water was used in the entire study.

2.2. Methods

2.2.1. Fabrication of chitosan/PVA hydrogel

Chitosan solution was prepared by dissolving chitosan (2/ 2.5/ 3 % w/v) in glacial acetic acid (2 % v/v) at room temperature under continuous stirring, while aqueous solution of PVA (3/ 4/ 5 % w/v) was made by dissolving PVA in deionized water at 60 °C for 5 h. The viscous chitosan solution was filtered to remove impurities and mixed with the PVA solution. This polymer blend was stirred at 60 °C for 2 h and then left overnight for continuous stirring to obtain a homogenous polymeric mixture. Cross-linking agent glutaraldehyde (10/20/30/40/50 mM) was added to the resulting blend drop-wise and mixed well for 5 min to achieve polymeric network formation. The resultant solution was casted in the test tubes and placed in oven at 60 °C for about 6 h to obtain hydrogel discs. The hydrogels were removed from the test tubes by precipitating with aqueous NaOH (12 % w/v) at room temperature and soaked in deionized water for 24 h after repetitive rinsing with water. Finally, to obtain porous semi-interpenetrating polymer networks, the hydrogel formed was subjected to repeated freeze-thaw cycles at −20 °C for 6 h and room temperature for 2 h, respectively. In this way, Ch/PVA hydrogel was prepared.

2.2.2. Preparation of Ch/PVA-Ag nanocomposite hydrogels

Ch/PVA hydrogel was cut into circular discs (10 mm diameter) and introduced into silver ion precursor i.e. silver nitrate ($AgNO_3$) solution (5 mM) for 24 h to load silver ions within the hydrogel. The silver ion-loaded Ch/PVA discs were rinsed thrice with deionized water for removal of the unbound silver ions and subjected to reduction by sodium borohydride solution (10 mM). After successful reduction, Ag immobilized disc were again rinsed with deionized water and kept for further characterization after lyophilization.

2.2.3. Swelling studies of the chitosan/PVA hydrogel discs

Ch/PVA and Ch/PVA-Ag hydrogel discs (10 mm) were vacuum dried for about 72 h to measure their dry weight (DW). In order to determine the swelling ratio of the hydrogels, vacuum dried hydrogels were immersed in deionised water at room temperature for 2.5 h and their wet weight (WW) was recorded after removal of the surface water using a filter paper. Swelling ratio (S%) was determined in terms of absorbed water content using the following Eq. (1)

$$S\% = \frac{WW - DW}{DW} \times 100 \quad (1)$$

2.2.4. Characterization and analysis of fabricated hydrogels

The morphology of dried hydrogels and presence of silver in Ch/PVA-Ag hydrogel was studied using JEOL JSM-6510LV Scanning electron microscope (SEM) coupled with Energy dispersive spectroscopy (EDS) and FE-SEM (Carl Zeiss Supra 55). The average size and shape of the AgNPs inside the fabricated hydrogel was measured using Tecnai T20 transmission electron microscope (TEM) at an acceleration voltage of 200 kV. Incorporation of AgNPs in the Ch/PVA-Ag nanocomposite was determined with inductively coupled plasma-atomic emission spectrometer (ICP-AES; ARCOS ICP spectrophotometer, Germany) as mentioned by Agnihotri et al. (2012). The average hydrodynamic size of AgNPs within the hydrogel was determined by Malvern (ZEN3600) particle size analyzer. The Fourier transform infrared (FTIR) spectra of Ch/PVA and Ch/PVA-Ag hydrogels with and without AgNPs, before and after adsorption were recorded in the wave range of 4000- 400 cm^{-1}, with a resolution of 2 cm^{-1} with FTIR-Spectrophotometer (Perkin Elmer Spectrum Version 10.4.00) using KBr pellet. To determine various crystalline phases of nanosilver particles within the hydrogel, the X-ray diffraction (XRD) pattern was studied using Pan Analytical (X'Pert-pro) diffractometer with Cu-Kα (1.54 A°) at 45 kV and scan range (2θ) 5° to 90°, with a step size of 0.02. Chemical states of the functional groups were studied by X-ray photoelectron spectroscopy (XPS). The complex peaks obtained using XPS (Physical Electronics, PHI 5000 VersaProbe III) were deconvoluted into component Gaussian peaks using origin software. Thermal stability of the hydrogels was studied using thermogravimetric analysis (TGA) on Mettler Toledo Instrument under N_2 atmosphere, over a temperature range of 25−1000 °C and heating rate of 10 °C min^{-1}. To determine surface area and pore size distribution of the hydrogels, BET (Brunauer Emmett Teller) analysis was done using Quanta Chrome Novae-2200 instrument based on N_2 adsorption-desorption method after degassing at 150 °C for 6 h.

2.2.5. Adsorption of butachlor

Adsorption studies for removal of butachlor by Ch/PVA and Ch/PVA-Ag hydrogels from water were performed in batch mode. The experiments were performed in the month of April with average temperature of 30 °C. 50 mL of butachlor with its varying initial concentrations (10–100 mg L^{-1}) was stirred at 200 rpm on a magnetic stirrer, with a known amount of sorbent (Ch/PVA & Ch/PVA-Ag) in 100 mL Erlenmeyer flask. The pH of the solution was adjusted with 0.1 M HCl/ 0.1 M NaOH. At regular time intervals, sample aliquots were withdrawn, centrifuged at 5000 rpm for 2 min and analyzed for absorbance change at λ_{max} (265 nm) on Thermo Fischer Scientific Elisa reader with additional cuvette port. Calibration curve at λ =265 nm was used to calculate residual concentration of butachlor. Different parameters affecting butachlor removal were studied, including pH (3–11), butachlor initial concentration (10−100 mg L^{-1}), sorbent dosage (50–1000 mg), temperature (303–338 K) and contact time. Different adsorption isotherm models (Langmuir linear, Langmuir non-linear, Freundlich linear and Freundlich non-linear) along with multiple error functions were analyzed. The percentage removal and amount of butachlor adsorption per unit mass of Ch/PVA and Ch/PVA-Ag were evaluated as:

$$\text{Removal } \% = \left(\frac{C_0 - C_e}{C_0}\right) \times 100 \quad (2)$$

$$q_e = \left(\frac{C_0 - C_e}{m}\right) \times V \quad (3)$$

where, C_0 and C_e are the initial and final butachlor concentrations (mg L^{-1}), q_e is the amount of butachlor adsorbed (mg g^{-1}), m is the mass of Ch/PVA or Ch/PVA-Ag (g) and V is the total volume of the solution (L).

Further, to explore mechanism of butachlor removal by the hydrogels, two kinetic models (pseudo- first order and pseudo- second order) were studied.

3. Results and discussion

Swelling ratio is considered as an important parameter for adsorption process, since expansion allows large number of adsorbent molecules to penetrate within the adsorbate (Huo et al., 2021), therefore precursor hydrogels were synthesized by varying amount of chitosan (2/2.5/3 %), PVA (3/4/5 %) and glutaraldehyde (10/20/30/40/50 mM) and were analysed for their water uptake capacity and stability (Table S1). The water uptake by the prepared hydrogels was studied for 24 h, where water uptake/ swelling ratio increased with time, until it reached equilibrium after 2.5 h for all the hydrogels, suggesting hydrogels' high affinity for water. The water uptake behaviour is greatly influenced by the chemical composition of the synthesized hydrogels (Khozemy et al., 2018; Nasef et al., 2019). With increase in chitosan content, increase in swelling ratio was observed which may be attributed to the presence of more hydrophilic moities. Hydrogels synthesized with 3 % chitosan led to immediate polymerization of hydrogel on addition of the glutaraldehyde, leading to uneven distribution of crosslinker and formation of clumps. Increase in swelling ratio was observed with increase in crosslinker concentration from 30 to 50 mM. Hydrogels crosslinked with 10 mM and 20 mM glutaraldehyde were not stable and could easily disintegrate on swelling, whereas, hydrogels with 30−50 mM crosslinker were highly stable. Wang & Gunasekaran (2006) investigated the effect of amount of crosslinker on the swelling ratio of the hydrogel and concluded that increase in swelling ratio with higher crosslinker amount was the result of higher degree of localization of water molecules inside the polymeric hydrogel network. Hydrogel formed with chitosan, PVA and glutaraldehyde composition (2.5 % / 3 % /50 mM) showed maximum water uptake upto 306.02 % ± 10.99, followed by 290.40 % ± 0.11 with (2.5 % / 4 % /30 mM) chemical composition. Considering the toxic effects of glutaraldehyde, the lowest concentration of 30 mM was chosen for precursor hydrogel formation. Also, several studies have reported removal of unreacted glutaraldehyde on washing with distilled water or sodium borohydride (Gard & Kropf, 1993; Hoffmann et al., 2009). In our study, the crosslinked hydrogels were washed several times with deionized water to ensure removal of unreacted glutaraldehyde. Therefore, 2.5 % / 3 % /50 mM was taken as the optimized amount of chitosan, PVA and glutaraldehyde for synthesis of precursor hydrogel, which was further used for immobilization of AgNPs.

On addition of the entirely swollen Ch/PVA hydrogel discs to $AgNO_3$ solution (precursor), some of the Ag^+ ions get trapped in the free spaces between the crosslinked polymeric hydrogel networks and others are absorbed by a number of hydrophilic hydroxides and amines present in the hydrogel *via* electrostatic interactions (Gholamali et al., 2020). The reduced Ag^+ ions were uniformly distributed within the hydrogel, forming a hydrogel nanocomposite Ch/PVA-Ag. Compared to Ch/PVA hydrogel discs with 30 mM glutaraldehyde, the swelling ratio of silver incorporated Ch/PVA-Ag hydrogel decreased from 290.40 % ± 0.11 (Ch/PVA) to 111.51 % ± 6.58 (for Ch/PVA-Ag), probably due to additional cross-linking between AgNPs and the electron-rich O and N atoms of −OH and NH_2 present in the Ch/PVA hydrogel, which restricts the penetration of water within the hydrogel nanocomposite, thereby reducing the swelling behaviour (Fig. S1). Also, the flexibility of silver loaded hydrogel is enhanced with the formation of AgNPs due to the interaction between Ag and hydroxyl groups, resulting in decreased hydrophilicity of the nanocomposite and reduced swelling behaviour (Ma et al., 2009). These results are in consistence with that of Vimala et al. (2011) and Agnihotri et al. (2012). Dhiman and Agnihotri (2020) have recently evidenced that immobilizing AgNPs on to the semi-interpenetrating networks of Ch-PVA nanocomposite yielded a distinct reduction in their swelling capacity. This happened because of the reduced availability of hydrophilic surface function groups, present

onto the polymers to form stable hydrogen bonds with the incoming water molecules due to the immobilization of AgNPs. Such an induced-lowering in the overall hydrophilicity of the Ch/PVA-Ag nanocomposite due to increase in the Ag content severely affected the diffusivity of water inside the nanocomposite thereby, elicited a reduced swelling behavior.

3.1. Structural and morphological properties

To study the cross-sectional morphology and confirm the *in-situ* formation of AgNPs in the Ch/PVA hydrogel, both the hydrogels were examined by SEM and FE-SEM with EDX technique. Fig. 2a and b shows the structural morphology of chitosan and PVA. Fig. 2c (SEM) and Fig. 2e (FE-SEM) shows the morphology of Ch/PVA hydrogel, where a porous structure was seen, with no metal nanoparticles within it. Fig. 2d (SEM) and Fig. 2f (FE-SEM) shows evenly distributed nanoparticles within the hydrogel and confirms that *in situ* loading of AgNPs did not affect the structural morphology and integrity of the hydrogel. EDX analysis (Fig. 2g) also confirmed that Ch/PVA-Ag nanocomposite contained 0.97 % of silver within it, which corroborates well with the elemental mapping of Ch/PVA-Ag, where Ag was homogenously distributed throughout the nanocomposite network, though with a very less proportion (Fig. 2(i)–(k)).

To determine size of the synthesized AgNPs, TEM analysis was done. TEM image (Fig. 2h) indicates the presence of spherical nanoparticles (~5−20 nm in size) with no signs of lumps or aggregates. Average hydrodynamic size of the synthesized nanoparticles measured by dynamic light scattering using zetasizer nano was 61.89 nm. The amount of silver loaded in the Ch/PVA-Ag hydrogel was determined by ICP-AES. Pre-weighed (0.5 g) hydrogel discs were crushed and sonicated to retrieve AgNPs from hydrogel matrix and further nitric acid digestion was carried out for their dissolution following further dilution. The total amount of silver content present in Ch/PVA-Ag hydrogel was calculated as 2.73 $\pm$ 0.36 mg g^{-1} of hydrogel.

FTIR spectra of Ch/PVA and silver incorporated Ch/PVA-Ag hydrogels were evaluated to examine the cross-linking between the polymers and studying the interaction of the functional groups in hydrogel synthesis along with incorporation of AgNPs within it. Significant changes occurred after synthesis of AgNPs within Ch/PVA hydrogel (Fig. 3a). Although there's a possibility of overlapping between O—H and N—H stretching, presence of sharp, broad peaks at 3340 and 3344 cm^{-1} in Ch/PVA and Ch/PVA-Ag hydrogels indicate O—H stretching vibration (Elbarbary & El-sawy, 2017; Nguyen et al., 2011). The C–H stretching in the hydrogels has strong peak at 2950-2850 cm^{-1} (Elbarbary & El-sawy, 2017). The peaks at 1642, 1416 and 1076 cm^{-1} are attributed to absorption of $NHCOCH_3$ groups, presence of C–H bonds and the stretching vibration of C—O—C in glucose unit, respectively (Agnihotri et al., 2012; Nithya et al., 2015; Yang et al., 2004). The appearance of a new bands 1734 cm^{-1} and 1218 cm^{-1} in fingerprint region of Ch/PVA-Ag hydrogel at 1218 cm^{-1} indicates presence of AgNPs. 1734 cm^{-1} corresponds to carbonyl group, indicating $–NH_2$ of chitosan and free −OH moieties of PVA as the ideal sites for anchoring of silver ions and AgNP immobilization (Agnihotri et al., 2012; Elbarbary & El-sawy, 2017). Additionally, band at 1416 cm^{-1} corresponding to C–H bonds was shifted to 1368 cm^{-1} after synthesis of AgNPs which was probably due to co-ordination bond formation between the silver atom and the electron rich groups of chitosan (Vimala et al., 2011).

Fig. 3b shows change in the XRD pattern of Ch/PVA hydrogel after incorporation of AgNPs. Chitosan showed characteristic diffraction peaks at $2\theta = 10.8°$ and 20.12°, corresponding to the respective equatorial (100) and (020) reflections (Zhang et al., 2020). Three peaks at 19.81°, 23.11° and 40.90° were observed in PVA, indicating its semi-crystalline structure (Fig. S2). After crosslinking both the polymers, peaks at 20.02°, 22.8°and 40.8° were seen, with reduced intensity, probably due to reduction in crystallinity. Significant peak at diffraction angle of 20.02 and 40.67° in Ch/PVA-Ag hydrogel indicated the

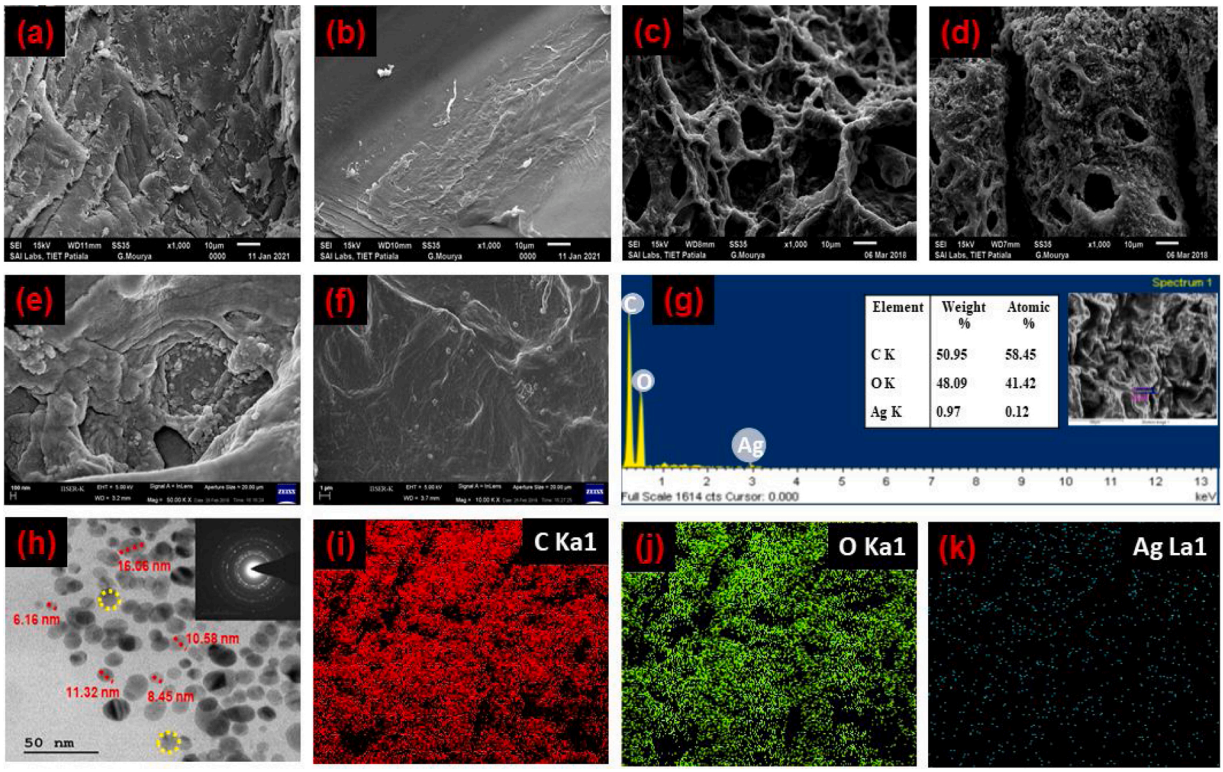


Fig. 2. SEM images of (**a**) chitosan, (**b**) PVA, (**c**) pure Ch/PVA hydrogel, (**d**) AgNP loaded Ch/PVA-Ag hydrogel, FE- SEM images of (**e**) pure Ch/PVA hydrogel and (**f**) AgNP loaded Ch/PVA-Ag hydrogel, (**g**) EDX spectra confirming presence of silver within the hydrogel, **h**) TEM image of synthesized AgNPs within the Ch/PVA-Ag hydrogel and (**i**–**k**) elemental mapping of Ch/PVA-Ag hydrogel.

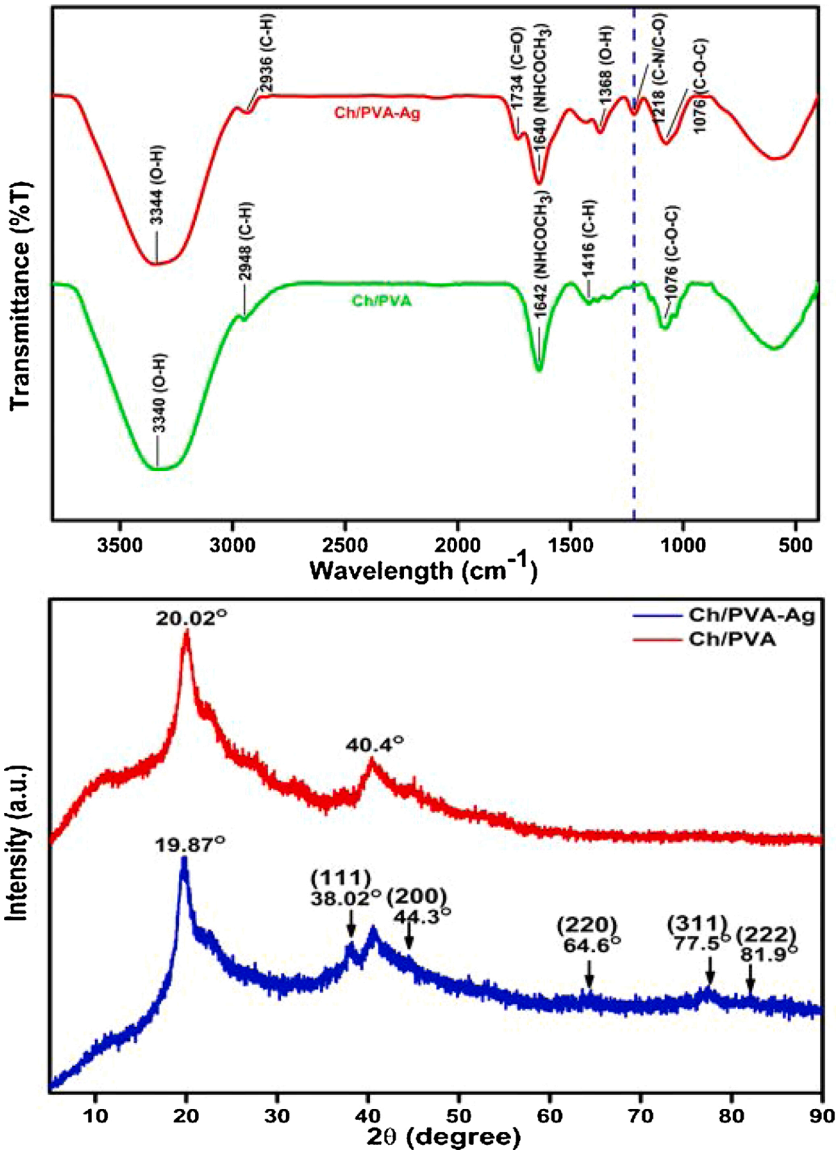


Fig. 3. **a**) FTIR spectra **b**) XRD pattern of Ch/PVA hydrogel with and without AgNP loading confirming synthesis and crystalline structure of AgNPs within it.

polymeric Ch/PVA matrix. The diffractogram of Ch/PVA-Ag hydrogel also showed five peaks at 2θ values of 38.02°, 44.3°, 64.6°, 77.5° and 81.9° corresponding to Bragg's reflections from (1 1 1), (2 0 0), (2 2 0), (3 1 1) and (2 2 2) planes of the face centered cubic (FCC) crystal structure of AgNPs (ICDD card no. 03-065-2871), confirming crystalline structure of AgNPs.

XPS analysis was carried out as survey and narrow region spectra to confirm the formation of AgNPs in Ch/PVA-Ag nanocomposite. The survey spectrum was fitted by multiple Gaussians and confirmed the presence of carbon, oxygen and silver in the nanocomposite (Fig. 4a). The high- resolution spectra of Ag 3d and O 1s were calibrated to the binding energy of C 1s at 284.8 eV and deconvoluted using gaussian function and Levenberg-Marquardt iteration algorithm. The C 1s peak was deconvoluted into two peaks with binding energy (BE) 284.8 eV and 286.2 eV corresponding to C—C/C–H and C-O/C−OH, respectively (Nešović et al., 2018) (Fig. 4c). In Fig. 4d O 1s spectra shows two peaks at the BE 530.5 eV and 531.5 eV corresponding to C—O and C−OH, respectively. Fig. 4b corresponds to Ag 3d core levels deconvoluted to get characteristic peaks for Ag $3d_{5/2}$ and Ag $3d_{3/2}$ with a spin energy separation of 6.0 eV (Table S2). The peaks at the BE of 369.1 eV and 375.1 eV confirms the presence of metallic silver in the nanocomposite, whereas two peaks with the lower BE 367.5 eV and 373.5 eV indicates the presence of Ag ions (Arjunan et al., 2016). Presence of silver ions could be the result of interaction/reaction of AgNPs either with chitosan or the oxygen present in the solution or air (An et al., 2011).

3.2. Thermal behaviour and BET surface area analysis

TGA and derivative weight loss (DTG) analyses were done to evaluate the thermal decomposition of Ch-PVA nanocomposite before and after immobilization of nano-silver (Fig. 5, Table 1). A known mass of the hydrogel discs was heated in alumina crucible in non-oxidized conditions (nitrogen atmosphere) from ambient temperature to 1000 °C. The first thermal event occurred at a temperature range 80−150 °C and is accompanied by a significant weight loss (10 %) in the sample. This loss accounts for the majority of residual water present in the sample, either physically adsorbed or weakly/strongly H-bonded, which get evaporated within this range. Furthermore, an initial thermal decomposition of the polymeric structures appeared at 204–375 °C and 229–410 °C for Ch/PVA and Ch/PVA-Ag, respectively. Interestingly, while Ch-PVA showed its characteristic exothermic peak at 308 °C, which is ascribed to the decomposition of chitosan, the corresponding

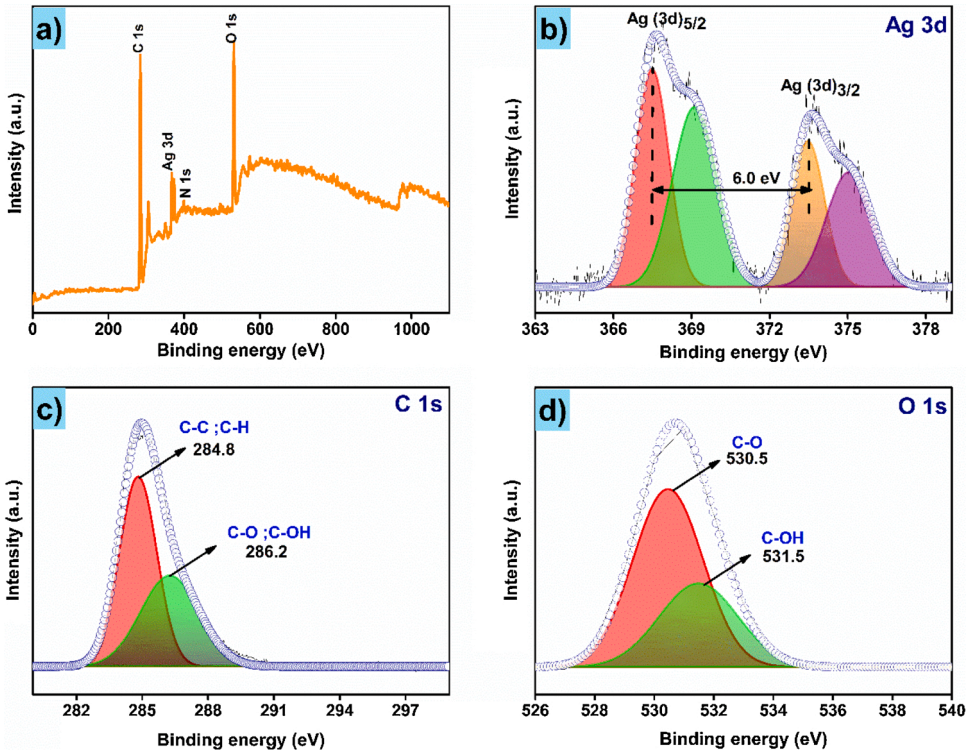


Fig. 4. XPS analysis **a**) survey XPS spectra of Ch/PVA-Ag nanocomposite, **b**) Ag (3d), **c**) C (1 s) and **d**) O (1s).

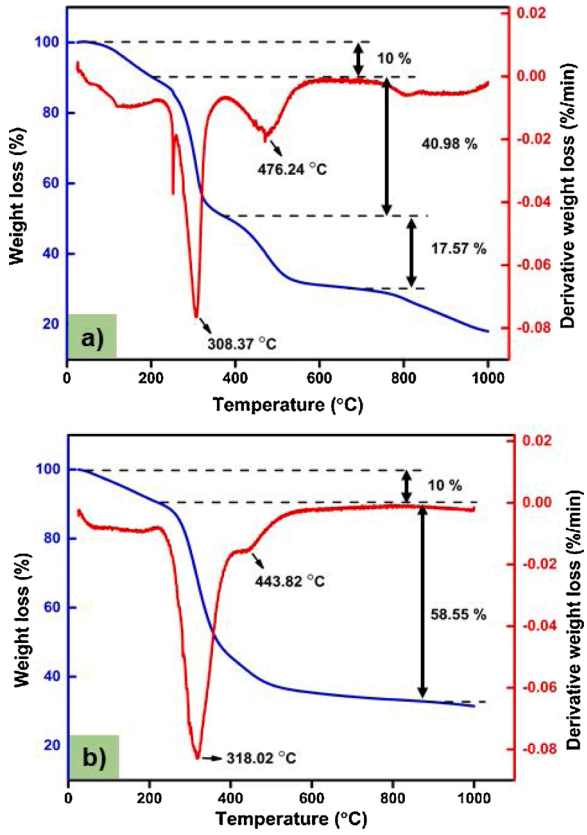


Fig. 5. TGA and DTG curves for **a**) Ch/PVA and **b**) Ch/PVA-Ag hydrogel.

peak was shifted to 318 °C for Ch/PVA-Ag nanocomposite. It clearly indicates that the addition of silver nanoparticles increased the thermal stability of the resulting nanocomposite, as also evidenced in previous

Table 1
Thermal analysis of Ch/PVA and Ch/PVA-Ag hydrogel.

Hydrogel	T_{10} (°C)[a]	T_{50} (°C)[b]	Charred mass (%) at 1000 °C
Ch/PVA	204.67	384	18.036
Ch/PVA-Ag	229.33	369	31.45

[a] Temperature at which 10 % weight loss was recorded by TGA.
[b] Temperature at which 50 % weight loss was recorded by TGA.

analyses. The next thermal decomposition of polymeric networks occurred in between 375–550 °C (Ch/PVA) and 410–500 °C (Ch/PVA-Ag) due to the complete depolymerisation of polymer chains and their subsequent degradation through deamination and dehydration reactions (Zawadzki & Kaczmarek, 2010). At 1000 °C, ~18 % char residue was seen in case of Ch/PVA, whereas, for Ch/PVA-Ag ~31 % char residue was recorded. In a study conducted by Mallakpour and Rashidi-moghadam (2020), thermal analysis of glutaraldehyde cross-linked Ch/PVA yielded a charred mass of 42 % at 800 °C, which further increased on incorporation of nanoparticles. Zawadzki & Kaczmarek (2010) reported that the thermal decomposition of chitosan occurs mainly via free radical mechanism, where the formed intermediates can spontaneously recombine resulting in the generation of crosslinked structures, which could be even more stable than their linear chains and may exist as charred residues.

The Nitrogen adsorption-desorption isotherms were obtained using N_2 adsorption-desorption analyzer (Fig. 6a-b). The surface area and pore volume of blank Ch/PVA hydrogel and silver loaded Ch/PVA hydrogel were calculated by employing multi-point BET analysis and Barrett–Joyner–Halenda (BJH) method, respectively. Fig. 6a shows hysteresis loops and a type III isotherm for both the hydrogels, stating the formation of micropores as shown by Arjunan et al. (2016). For Ch/PVA, the surface area and pore diameter were found to be 6.579 $m^2\ g^{-1}$ and 1.98 nm, with pore volume of 0.011 cc g^{-1}. Under similar conditions, surface area, pore diameter and pore volume for Ch/PVA-Ag hydrogel were determined as 8.316 $m^2\ g^{-1}$, 2.33 nm and 0.016 cc g^{-1}, respectively. This

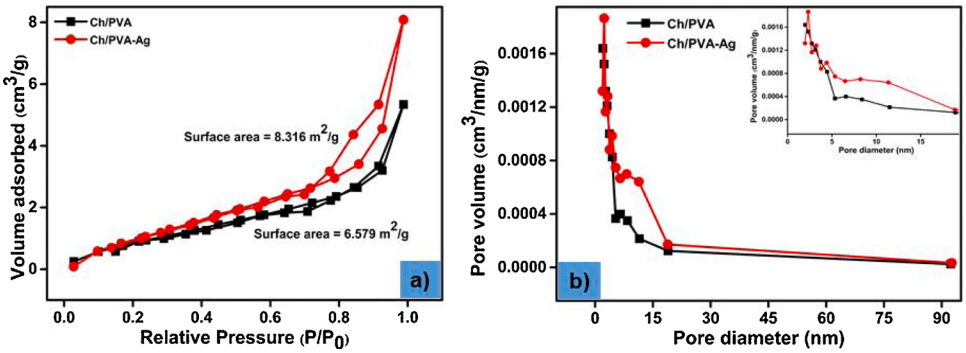


Fig. 6. BET analysis **a**) Nitrogen adsorption-desorption plots **b**) pore size distribution (BJH curve).

increased surface area of the Ch/PVA-Ag hydrogel could be due to the presence of AgNPs. Loading of metal nanoparticles in the polymeric matrix increases the crosslinking density, resulting in the appearance of nano porosity and the increased surface area in the polymer gel (Dwivedi et al., 2014). The BET analysis was carried out with the dried hydrogel, which swells during the experimentation while adsorption. Therefore, the actual surface area of the hydrogel in the swollen state is expected to be much higher.

3.3. Removal of butachlor

Removal of butachlor from aqueous solution using fabricated Ch/PVA-Ag nanocomposite was studied by conducting adsorption experiments, where distilled water spiked with butachlor (10–100 mg L^{-1}) was used as a test pollutant. Comparative adsorption potential of both blank Ch/PVA and silver immobilized Ch/PVA-Ag hydrogel was carried out until adsorption- desorption equilibrium was achieved.

The main mechanism for adsorption of butachlor is believed to be through electrostatic interactions (mainly hydrogen bonding) and π-π interaction (Li et al., 2020). Since, Ch/PVA polymeric blend has several functional moieties such as —NH_2, –OH and —C═O, these groups can form hydrogen bond with butachlor. Butachlor can also bind to the functional groups on chitosan via electrostatic interactions or dipole-dipole interactions. Another mechanism could be attributed to the π-π interaction between aromatic ring of butachlor and chitosan. Under acidic conditions, -NHCO- groups in Ch/PVA hydrogel become protonated, providing more hydrogen bonding sites to increase the capacity of butachlor adsorption (Muda et al., 2020). As the pH of the solution increases, lesser number protons were available to protonate the imine groups, decreasing the hydrogen-bonding sites and thus reducing the adsorption capacity of the hydrogel. This proposed mechanism was also supported by FTIR analysis of the Ch/PVA and Ch/PVA-Ag hydrogels before and after adsorption of butachlor (Fig. 7).

After adsorption of butachlor, addition/ removal or change in position and intensities of some of the peaks was observed in both the hydrogel systems, indicating successful sorption of butachlor. Peaks at 2948 cm^{-1} and 2936 cm^{-1} corresponding to C–H bond in both the hydrogels were lost after butachlor adsorption. The bands at 1232 cm^{-1} and 1230 cm^{-1} in Ch/PVA and Ch/PVA-Ag hydrogels formed after adsorption of butachlor were ascribed to occurrence of C—N/C-O bonds (Jin & Bai, 2002). A peak at 1144 cm^{-1} (C—N/ C—O stretching) was shifted to 1232 cm^{-1} after adsorption by Ch/PVA hydrogel and a new peak corresponding to C═O stretching at 1738 cm^{-1} was formed (Elbarbary & El-sawy, 2017; Jin & Bai, 2002) (Fig. 7a). As shown in Fig. 7b, two peaks at 1430 cm^{-1} and 1076 cm^{-1} assigned to C–H bending and the stretching vibration of C—O—C were lost after butachlor adsorption in Ch/PVA-Ag nanocomposite (Nguyen et al., 2011; Nithya et al., 2015). The electron rich O and N atoms present in the synthesized hydrogel networks help in efficient adsorption of butachlor by the hydrogels. Based on earlier reports (Agnihotri et al., 2012) an

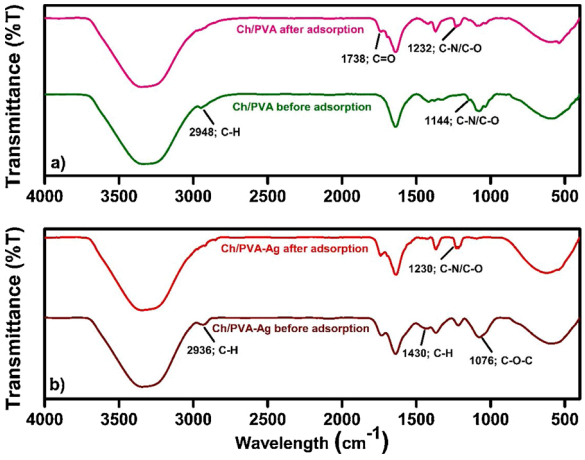


Fig. 7. FTIR analysis of (**a**) Ch/PVA hydrogel and (**b**) Ch/PVA-Ag hydrogel, before and after adsorption of butachlor.

in-situ approach was employed for the synthesis of AgNPs concurrent to their immobilization on to Ch/PVA polymer without using any surface functionalization treatments. It was established while a majority of silver ions were anchored directly on to the surface of Ch/PVA through ion-exchange mechanism, the remaining silver ions were occupied within the semi-interpenetrating network of the Chitosan–PVA polymeric composite. The amine and hydroxyl functional groups, present within the Ch/PVA provided the necessary nucleation sites for stable anchoring of silver ions, which were transformed into nanoparticulate form (AgNPs) through reduction reaction. Fabrication of Ch/PVA-Ag nanocomposite could also be due to additional crosslinking, that occurred between the newly formed AgNPs and the hydrogel, other than that appeared through glutaraldehyde (Dhiman and Agnihotri, 2020). So, Ch/PVA-Ag hydrogel showed approximately 10 % higher butachlor adsorption than Ch/PVA probably due to these additional cross-links between AgNPs and the hydrogel (Agnihotri et al., 2012). A schematic representation of possible interaction of butachlor with both the hydrogels is presented in Fig. 8.

3.3.1. Effect of pH

Effect of pH, butachlor initial concentration, hydrogel dosage, temperature and contact time on sorption efficiency of hydrogels with and without AgNPs was studied. pH is one of the vital parameters, which plays an important role in adsorption process as it monitors the electrostatic interactions between adsorbate and adsorbent (Sharma et al., 2017). To examine the adsorption capacity of Ch/PVA and Ch/PVA-Ag hydrogels for butachlor, a set of experiments was performed at different pH (3–11), with 50 mL distilled water spiked with 10 mg L^{-1} butachlor and 100 mg hydrogels discs for 270 min (4.5 h) at room temperature. As

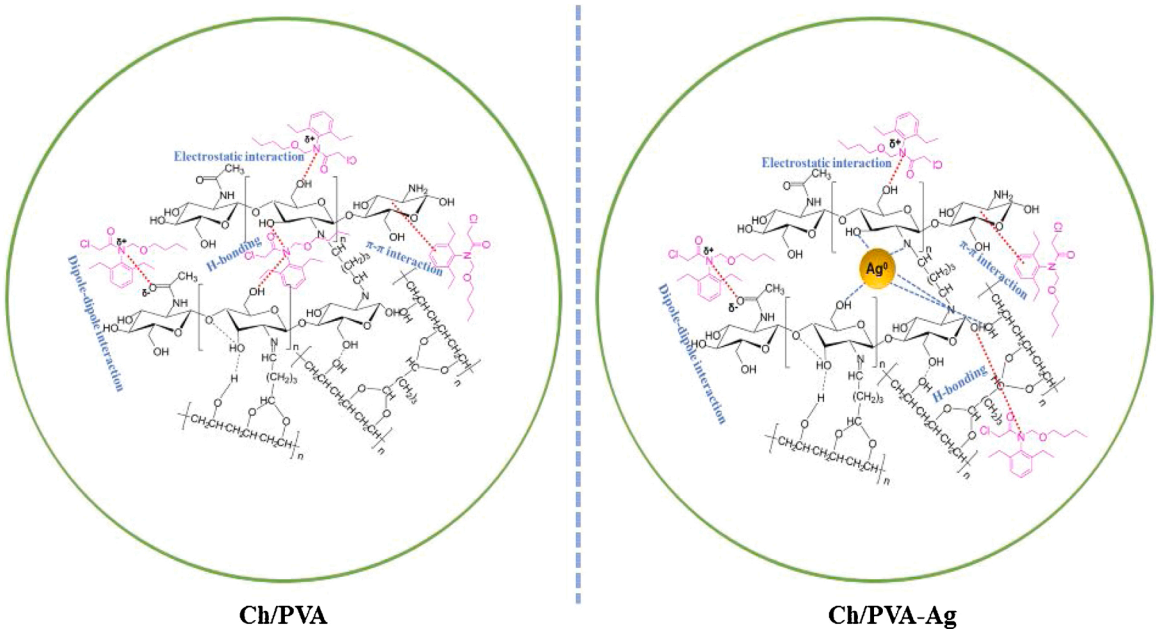


Fig. 8. Possible interaction between butachlor and the hydrogels.

shown in Fig. 9(b), the maximum removal of butachlor by hydrogels was observed at pH 3, where after % removal was declined from 86.55%–81.17 % for Ch/PVA and 96.87%–90.52 % for Ch/PVA-Ag. The predicted pKa value for butachlor is 1.20 ± 0.50 (Machette, 2017), therefore, at a pH lower than pKa value, butachlor is positively charged, while at a higher pH, it is negatively charged (Hanh et al., 2019). The point of zero charge (pH_{PZC}) of Ch/PVA and Ch/PVA-Ag obtained by the protocol given by Brouers and Al-Musawi (2015) was 11.02 and 9.77, respectively, indicating positively charged surface at pH < pH_{PZC} and negatively charged surface at pH > pH_{PZC} (Fig. 9a). Therefore, at acidic pH, the electrostatic interaction between butachlor and hydrogels lead to better adsorption efficiency than basic pH. Since, adsorption was also observed at higher pH, suggesting strong involvement of physical forces such as Vander waals forces and hydrogen bonding in the adsorption process (Sun et al., 2008).

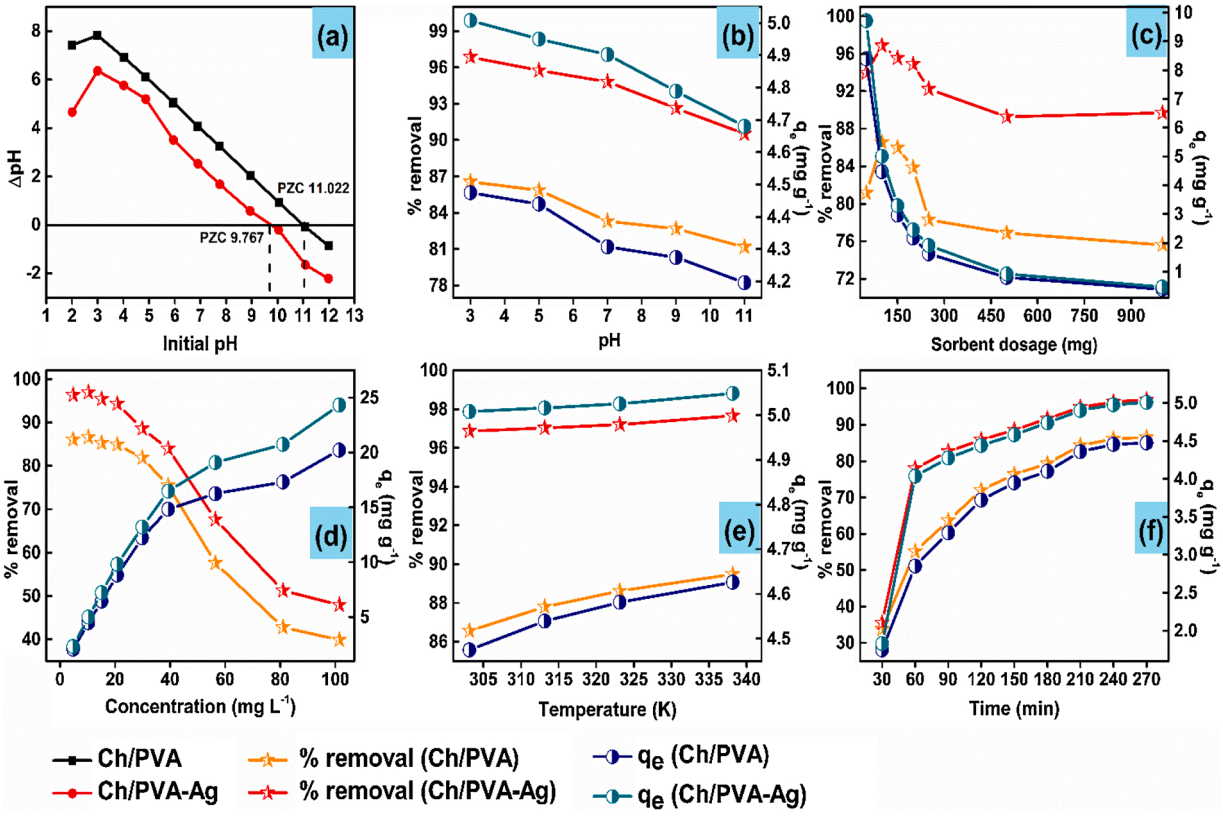


Fig. 9. **a**) PZC plot for the hydrogels; Adsorption plots for effect of (**b**) pH, (**c**) sorbent dosage, (**d**) butachlor concentration (**e**) temperature and (**f**) time.

3.3.2. Effect of sorbent dosage

Fig. 9(c) depicts the effect of sorbent dosage on percentage removal of butachlor from its solution. The effect of Ch/PVA and Ch/PVA-Ag hydrogels dosage was studied in the range of 50−1000 mg in 50 mL butachlor solution of concentration 10 mg L^{-1}, keeping other parameters constant. With an increase in mass of hydrogel discs from 50−100 mg, the percentage adsorption was found to increase from 81.14%–86.55 % for Ch/PVA and 93.97%–96.87% for Ch/PVA-Ag hydrogel discs. Afterwards, a decrease in percentage adsorption values was observed in both hydrogel discs, which was 85.98 % to 75.61 % for Ch/PVA and 95.54–89.26 % for Ch/PVA-Ag. The initial increase in butachlor uptake with increase in hydrogel dosage was due to more active sites and optimal surface area supplying more functional groups for bonding with butachlor, boosting adsorption process. Later, decrease in adsorption might be due to increase in steric hindrance due to overcrowding of more active sites within constant volume leading to decrease in butachlor adsorption (Sharma et al., 2018). On contrary, a decrease in sorption capacity (8.39 - 0.39 mg g^{-1} for Ch/PVA and 9.72 - 0.46 mg g^{-1} for Ch/PVA-Ag) was observed with increase in sorbent dosage. Similar effect was studied by Haq et al. (2019), where relatively greater number of the active sites remain unsaturated with high sorbent dosage leading to decreased sorption capacity at a fixed butachlor concentration. Therefore, an optimum dosage of 100 mg (i.e. 2 g L^{-1}) was selected for subsequent set of experiments.

3.3.3. Effect of initial concentration of butachlor

The effect of butachlor initial concentration on the sorption capacity of the hydrogel and percentage removal was investigated by varying its concentration from 5 to 100 mg L^{-1}, keeping other factors constant. Percentage removal of butachlor was maximum at concentration 10 mg L^{-1} for both the hydrogels (Fig. 9(d)). With increase in butachlor concentration from 10 to 100 mg L^{-1}, percentage removal of butachlor declined from 86.55 to 39.85 % for Ch/PVA and 96.86 to 47.95 % for Ch/PVA-Ag. At butachlor concentration 5 and 10 mg L^{-1}, adsorption was higher because the number of butachlor molecules in comparison to active sites on the Ch/PVA & Ch/PVA-Ag was small, leading to a good interaction between butachlor and active sites of hydrogels, therefore, increasing the removal of butachlor. As the concentration increases, the competition between butachlor molecules for interaction with the active sites on the hydrogel also intensifies, leading to decrease in butachlor uptake due to lower availability of vacant sites (Dwivedi et al., 2014; Haq et al., 2019). On the other hand, a gradual increase in sorption capacity (q_e) for both the hydrogels was observed with increase in butachlor concentration.

3.3.4. Effect of temperature

Butachlor is decomposed at temperature greater than or equal to 165 °C and gets disintegrated on heating, emitting toxic fumes of nitrous oxides and hydrogen chloride (Abigail et al., 2015). So, butachlor removal was studied by varying the magnetic stirrer temperature from 303.15 to 338.15 K (30–65 °C), under optimized conditions of pH of solution (pH-3), adsorbent dosage (100 mg) and butachlor concentration (10 mg L^{-1}) (Fig. 9(e)). Increase in temperature from 303.15 to 338.15 K does not exert a much stronger influence on the adsorption process. For blank Ch/PVA hydrogel, increase in percentage removal from 86.55 to 89.47 % was observed, with sorption capacity (q_e) going down from 4.47 to 4.62 mg g^{-1}. In contrast, a very small increase in percentage removal of butachlor by Ch/PVA-Ag (96.86–97.64 %) was observed, with negligible change in q_e values i.e., 5.01–5.05 mg g^{-1}. So, based on the results, experiments were conducted at room temperature.

3.3.5. Effect of contact time

Time of agitation i.e., contact time between Ch/PVA / Ch/PVA-Ag hydrogels and butachlor molecules helps in establishing adsorption-desorption relation between the two and determining maximum adsorption. With 100 mg hydrogel in 50 mL of 10 mg L^{-1} butachlor (pH 3; 30 °C), the time effect was studied in the range of 30−270 min, where increase in the percentage removal of butachlor was observed with the passage of time (Fig. 9(f)). At the beginning of the adsorption process, more vacant active sites were available for butachlor uptake, but with the passage of time, repulsive forces between solute molecules on the hydrogel and liquid phase make it difficult to occupy remaining vacant sites. Therefore, the time of agitation was optimized at 270 min.

3.3.6. Adsorption isotherms

Adsorption process is strongly influenced by change in initial adsorbate concentration. In order to understand the interaction between solute molecules and the sorbent, adsorption isotherms play an important role. Therefore, the experimental data obtained was fitted to Langmuir (linear and non-linear) and Freundlich (linear and non-linear) isotherm models (Fig. 10).

3.3.6.1. Langmuir isotherm. Langmuir isotherm is based on an assumption of monolayer adsorption on the homogenous surface with finite number of active sites (Dwivedi et al., 2014; Haq et al., 2019). The linearized form of Langmuir isotherm model can be expressed as:

$$\frac{C_e}{q_e} = \frac{1}{q_m K_L} + \frac{C_e}{q_m} \tag{4}$$

where, C_e (mg g^{-1}) is the equilibrium concentration, q_e (mg g^{-1}) is the amount of butachlor adsorbed per unit mass of Ch/PVA / Ch/PVA-Ag, K_L (mg g^{-1}) and q_m (L mg^{-1}) are the Langmuir constants related to energy of adsorption and maximum adsorption capacity. As depicted by Fig. 10, the intercept and slope of the linear regression plot between C_e/q_e versus C_e gives the values of K_L and q_m, which are shown in Table 2.

The isotherm is further studied by another dimensionless constant known as equilibrium parameter or separation factor (R_L), which is defined by the equation below:

$$R_L = \frac{1}{1 + K_L C_0} \tag{5}$$

where, C_0 is the initial butachlor concentration (5, 10, 15, 20, 30, 40, 60, 80 and 100 mg L^{-1}). Value of R_L determines the nature of isotherm to be irreversible ($R_L = 0$), linear ($R_L = 1$), favourable ($0 < R_L < 1$) or unfavourable ($R_L > 1$). The calculated R_L values for whole range of initial butachlor concentrations for Ch/PVA (0.50 – 0.048) and Ch/PVA-Ag (0.32 – 0.03) signifies favourable adsorption.

The nonlinear form of langmuir isotherm is represented by the following equation:

$$q_e = q_m \frac{K_L C_e}{1 + K_L C_e} \tag{6}$$

3.3.6.2. Freundlich isotherm. Freundlich isotherm model represents multilayer adsorption mechanism occurring on heterogeneous surfaces, assuming all the active sites on the sorbent are not equal and the stronger binding sites are occupied first. Also, with the increase in degree of site occupation, the binding strength decreases (Dwivedi et al., 2014).

The linearized form of Freundlich model is given as below:

$$\log q_e = \log K_F + \frac{1}{n} \log C_e \tag{7}$$

Also, Freundlich model in nonlinear form can be expressed as:

$$q_e = K_F C_e^{\frac{1}{n}} \tag{8}$$

where, K_F and n are Freundlich constants signifying adsorption capacity and adsorption intensity or surface heterogeneity. The value of n indicates nature of adsorption. Adsorption is poor, relatively difficult or excellent when $n < 1$, $1 < n < 2$ and $2 < n < 10$, respectively.

Considering the R^2 (correlation coefficient) values and the

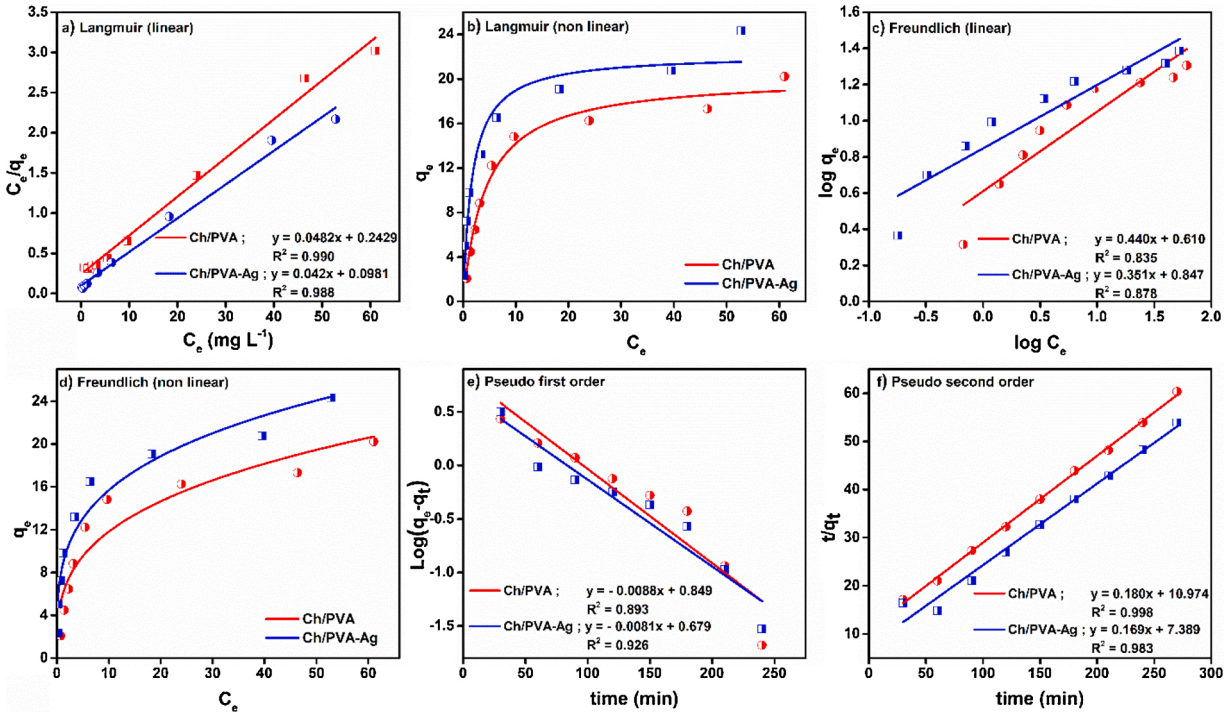


Fig. 10. Adsorption isotherms (**a**) Langmuir (linear), (**b**) Langmuir (non-linear), (**c**) Freundlich (linear) (**d**) Freundlich (non-linear) and Kinetic plots (**e**) Pseudo-first order and (**f**) Pseudo-second order.

Table 2
Adsorption isotherm parameters for butachlor adsorption by Ch/PVA and Ch/PVA-Ag hydrogel.

Isotherm model	Isotherm constants Ch/PVA							Isotherm constants Ch/PVA-Ag						
	q_{exp}(mg g^{-1}) = 20.219							q_{exp}(mg g^{-1}) = 24.33						
Langmuir	q_m (mg g^{-1})	K_L (Lmg^{-1})	R^2	Adj R^2	RMSE	X^2	RSS	q_m (mg g^{-1})	K_L (Lmg^{-1})	R^2	Adj R^2	RMSE	X^2	RSS
–														
Linear	20.75	0.198	0.991	0.989	0.109	0.012	0.083	23.81	0.428	0.989	0.988	0.09	0.008	0.056
Nonlinear	20.25	0.235	0.979	0.976	0.961	0.923	6.46	22.23	0.582	0.964	0.959	1.532	2.347	16.43
Freundlich	n	K_f (Lmg^{-1})	R^2	Adj R^2	RMSE	X^2	RSS	n	K_f (Lmg^{-1})	R^2	Adj R^2	RMSE	X^2	RSS
–														
Linear	2.27	4.07	0.856	0.835	0.132	0.017	0.123	2.85	7.03	0.894	0.878	0.117	0.014	0.095
Nonlinear	3.23	5.79	0.893	0.877	2.197	4.829	33.80	3.76	8.51	0.946	0.938	1.887	3.559	24.915

consistency between q_{exp} and q_m values for both the hydrogels (Table 2), Langmuir isotherm model fitted well with the butachlor adsorption experimental data. Using R^2 alone for data validation is not satisfactory, because experimental data may result in high R^2 values. Therefore, in order to validate isotherm models (linear and nonlinear), five different error functions (Adjusted R-squared – R^2_{adj}, reduced Chi-square - χ^2, root-mean square error – RMSE and residual sum of squares - RSS), including R^2 were employed. Higher value of R^2 and R^2_{adj} (close to 1), and smaller value of RSME, χ^2 and RSS indicates higher fit by the model. Table 2 shows the isotherm parameters along with error function values obtained using a curve fitting tool origin. It can be clearly seen from the experimental data that the high R^2 and R^2_{adj} values and smaller RSME, χ^2 and RSS values of langmuir isotherm for both Ch/PVA and Ch/PVA-Ag hydrogel indicates good correlation between langmuir model and the experimental data, referring to monolayer adsorption of butachlor on the surface of Ch/PVA and Ch/PVA-Ag hydrogel. Also, the surface of the adsorbent exhibits a homologous morphology and energetic equivalence with single binding sites i.e. no more adsorption takes place at the site once it gets occupied by an adsorbate. This is due to reduction in intermolecular forces with distance, which is one of the assumptions of Langmuir model. The calculated R_L values for butachlor adsorption by Ch/PVA and Ch/PVA-Ag were ranging from (0.50 – 0.048) and (0.32 – 0.03), respectively, signifying favourable adsorption. Freundlich model is based on multilayer adsorption on heterogenous surface, accompanied by non- uniform distribution of adsorption heat. The value of n indicates the excellent adsorption as the surface of both adsorbents is favourable for the adsorption of butachlor. Comparison between linear and nonlinear error functions shows the adsorption favours linear model. Hence, removal of butachlor by Ch/PVA / Ch/PVA-Ag was investigated using Langmuir linear model, where Ch/PVA and Ch/PVA-Ag gave maximum monolayer adsorption capacity (q_m) of 20.75 mg g^{-1} and 23.81 mg g^{-1}, respectively (Dwivedi et al., 2014; Vilela et al., 2019).

3.3.7. Butachlor adsorption kinetics

Kinetic studies play a significant role in determining rate of adsorption process. In the present study, pseudo-first order and pseudo-

second order kinetic model were studied to evaluate adsorption rate.

3.3.7.1. Pseudo-first order model. This model describes the relationship between the sorption rate on sorbent surface and contact time (Haq et al., 2019). Linear plot between log (q_e - q_t) versus time (min) is plotted, where slope and intercept are used to determine k_1 and q_e. It can be represented as:

$$\log (q_e - q_t) = \log q_e - \frac{k_1}{2.303}(t) \quad (9)$$

where, q_e and q_t denote sorption capacity at equilibrium and at time t; k_1 (min^{-1}) is the rate constant for pseudo-first order kinetic model.

3.3.7.2. Pseudo-second order model. The model explains that the rate limiting step may be chemical adsorption involving strong interaction between adsorbate and adsorbent. Intercept and slope values obtained from linear plot of t/q_t versus time (min) gives the value of k_2 and q_e. This can be expressed by the following equation:

$$\frac{t}{q_t} = \frac{1}{k_2 q_e^2} + \frac{t}{q_e} \quad (10)$$

where, k_2 (g mg^{-1} min^{-1}) is the rate constant for pseudo-second order kinetic model.

Linear plots of both the kinetic models are presented in Fig. 10(e) and (f) along with various kinetic parameters listed in Table 3, where higher R^2 (correlation coefficient) value of 0.998 for Ch/PVA and 0.983 for Ch/PVA-Ag hydrogels favours applicability of pseudo-second order reaction. The calculated q_e values of 5.548 mg g^{-1} and 5.917 mg g^{-1} for Ch/PVA and Ch/PVA-Ag obtained from pseudo-second order model have quite comparable value to that of q_e obtained from experimental data (4.474 mg g^{-1} and 5.008 mg g^{-1} for Ch/PVA and Ch/PVA-Ag, respectively), suggesting the inclination of butachlor adsorption towards the chemisorption.

3.3.8. Reusability studies

An ideal adsorbent should not only possess high adsorption efficiency but should rather withstand at acidic and basic conditions (Muda et al., 2020). The reusability of the synthesized chitosan-based hydrogels was studied for 5 consecutive runs with the adsorption-desorption cycles of butachlor (Fig. 11). For each cycle, 100 mg of the adsorbent hydrogel discs were put in 50 ml of distilled water spiked with 10 mg L^{-1} butachlor and stirred at 200 rpm for 5 h. The sample was then filtered and washed with distilled water to remove unbound butachlor, followed by stirring in 50 ml 0.1 M KOH under same conditions (Chang et al., 2020; Huo et al., 2021). The discs were again rinsed in water, dried at 60 °C and used for next cycles. Decrease in percentage removal of butachlor from 86.55 % to 71.06 % (Ch/PVA) and 96.87 % to 79.32 % (Ch/PVA-Ag) was observed from cycle one to fifth. This decrease in adsorption can probably be due to occupancy of some of the adsorption sites that were difficult to desorb as compared to others. The results indicate good reusability of the hydrogels.

4. Conclusion

Chitosan/PVA hydrogel with immobilized AgNPs was fabricated. Physiochemical characterization proved successful loading of AgNPs within the hydrogel, forming Ch/PVA-Ag nanocomposite, where the hydrogel provides an immobilizing matrix for AgNPs. The hydrogels exhibited excellent butachlor adsorption capacity of 86.55 % and 96.87 %, respectively, where Ch/PVA-Ag hydrogel showed approximately 10 % higher adsorption, which can be attributed to large surface area and extra cross-links between AgNPs and electron rich O and N atoms of the hydrogels. Adsorption of butachlor by both the hydrogels fitted best with Langmuir linear model suggesting monolayer adsorption, where Ch/PVA and Ch/PVA-Ag gave maximum adsorption capacity of 20.75 mg g^{-1} and 23.81 mg g^{-1}, respectively. Due to AgNP incorporation a slight increase in adsorption was observed, meaning that incorporation of AgNPs plays some role and can be further explored for photocatalytic studies. The Ch/PVA-Ag nanocomposite can be effectively used for the remediation/clean-up of groundwater and agricultural run-off water which is contaminated with harmful pesticides and agro-chemicals.

Table 3
Kinetic parameters for butachlor adsorption on Ch/PVA and Ch/PVA-Ag hydrogels.

Kinetic model	Kinetic Parameter	Value	
		Ch/PVA	Ch/PVA-Ag
Pseudo-first order	q_e (mg g^{-1}); (exp)	4.474	5.008
	q_e (mg g^{-1}); (cal)	7.062	4.775
	k_1 (min^{-1})	0.020	0.019
	R^2	0.893	0.926
Pseudo-second order	q_e (mg g^{-1})	5.548	5.917
	k_2 (g mg^{-1} min^{-1})	0.003	0.004
	R^2	0.998	0.983

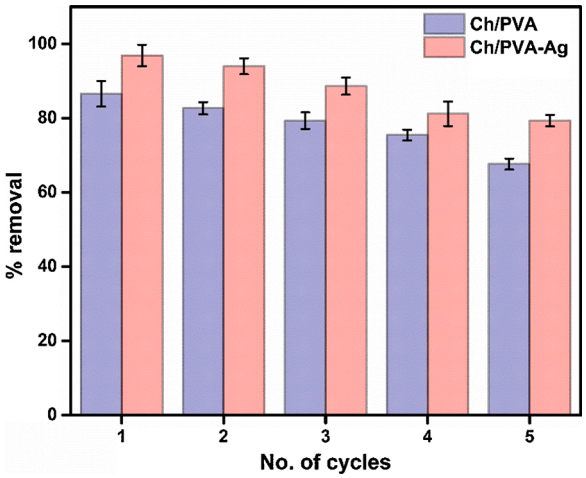


Fig. 11. Reusability studies of Ch/PVA hydrogel with and without AgNPs.

CRediT authorship contribution statement

Ravneet Kaur: Methodology, Validation, Formal analysis, Investigation, Writing - original draft, Visualization. **Dinesh Goyal:** Methodology, Resources, Writing - review & editing, Visualization, Supervision. **Shekhar Agnihotri:** Conceptualization.

Acknowledgements

The authors would like to thank the Director, Thapar Institute of Engineering & Technology (Deemed to be University), Patiala for infrastructural support and to DST-SERB (Science and Engineering Research Board, Department of Science and Technology, Government of India) for financial support vide grant EMR/2016/002524.

Appendix A. Supplementary data

Supplementary data associated with this article can be found, in the online version, at https://doi.org/10.1016/j.carbpol.2021.117906.

References

Abigail, M. E. A., Samuel, S. M., & Ramalingam, C. (2015). Addressing the environmental impacts of butachlor and the available remediation strategies: a systematic review. *International Journal of Environmental Science and Technology, 12*(12), 4025–4036. https://doi.org/10.1007/s13762-015-0866-2

Agnihotri, S., Mukherji, S., & Mukherji, S. (2012). Antimicrobial chitosan–PVA hydrogel as a nanoreactor and immobilizing matrix for silver nanoparticles. *Applied Nanoscience, 2*(3), 179–188. https://doi.org/10.1007/s13204-012-0080-1

Ahmad, M. A., & Alrozi, R. (2010). Optimization of preparation conditions for mangosteen peel-based activated carbons for the removal of Remazol Brilliant Blue R using response surface methodology. *Chemical Engineering Journal, 165*(3), 883–890. https://doi.org/10.1016/j.cej.2010.10.049

Ahmad, M. A., & Alrozi, R. (2011). Optimization of rambutan peel based activated carbon preparation conditions for Remazol Brilliant Blue R removal. *Chemical Engineering Journal, 168*(1), 280–285. https://doi.org/10.1016/j.cej.2011.01.005

An, J., Luo, Q., Yuan, X., Wang, D., & Li, X. (2011). Preparation and characterization of silver-chitosan nanocomposite particles with antimicrobial activity. *Journal of Applied Polymer Science, 120*(6), 3180–3189. https://doi.org/10.1002/app.33532

Arjunan, N., Kumari, H. L. J., Singaravelu, C. M., Kandasamy, R., & Kandasamy, J. (2016). Physicochemical investigations of biogenic chitosan-silver nanocomposite as antimicrobial and anticancer agent. *International Journal of Biological Macromolecules, 92*, 77–87. https://doi.org/10.1016/j.ijbiomac.2016.07.003

Brouers, F., & Al-Musawi, T. J. (2015). On the optimal use of isotherm models for the characterization of biosorption of lead onto algae. *Journal of Molecular Liquids, 212*, 46–51. https://doi.org/10.1016/j.molliq.2015.08.054

Chang, J., Liu, S., Zhou, S., Wang, M., & Zhu, G. (2013). Effects of butachlor on reproduction and hormone levels in adult zebrafish (*Danio rerio*). *Experimental and Toxicologic Pathology, 65*(1-2), 205–209. https://doi.org/10.1016/j.etp.2011.08.007

Chang, Z., Chen, Y., Tang, S., Yang, J., Chen, Y., Chen, S., … Yang, Z. (2020). Construction of chitosan/polyacrylate/graphene oxide composite physical hydrogel by semi-dissolution/acidification/sol-gel transition method and its simultaneous cationic and anionic dye adsorption properties. *Carbohydrate Polymers, 229*, Article 115431. https://doi.org/10.1016/j.carbpol.2019.115431

Dehaghi, S. M., Rahmanifar, B., Moradi, A. M., & Azar, P. A. (2014). Removal of permethrin pesticide from water by chitosan–zinc oxide nanoparticles composite as an adsorbent. *Journal of Saudi Chemical Society, 18*(4), 348–355. https://doi.org/10.1016/j.jscs.2014.01.004

Dhiman, N. K., & Agnihotri, S. (2020). Hierarchically aligned nano silver/chitosan–PVA hydrogel for point-of-use water disinfection: Contact-active mechanism revealed. *Environmental Science: Nano, 7*(8), 2337–2350. https://doi.org/10.1039/D0EN00405G

Dolas, H., Sahin, O., Saka, C., & Demir, H. (2011). A new method on producing high surface area activated carbon: The effect of salt on the surface area and the pore size distribution of activated carbon prepared from pistachio shell. *Chemical Engineering Journal, 166*(1), 191–197. https://doi.org/10.1016/j.cej.2010.10.061

Dwivedi, C., Gupta, A., Chaudhary, A., & Nandi, C. K. (2014). Gold nanoparticle chitosan composite hydrogel beads show efficient removal of methyl parathion from waste water. *RSC Advances, 4*(75), 39830–39838. https://doi.org/10.1039/C4RA03870C

Dwivedi, S., Saquib, Q., Al-Khedhairy, A. A., & Musarrat, J. (2012). Butachlor induced dissipation of mitochondrial membrane potential, oxidative DNA damage and necrosis in human peripheral blood mononuclear cells. *Toxicology, 302*(1), 77–87. https://doi.org/10.1016/j.tox.2012.07.014

Elbarbary, A. M., & El-Sawy, N. M. (2017). Radiation synthesis and characterization of polyvinyl alcohol/chitosan/silver nanocomposite membranes: Antimicrobial and blood compatibility studies. *Polymer Bulletin, 74*(1), 195–212. https://doi.org/10.1007/s00289-016-1708-1

Farombi, E. O., Ajimoko, Y. R., & Adelowo, O. A. (2008). Effect of butachlor on antioxidant enzyme status and lipid peroxidation in fresh water African catfish, (*Clarias gariepinus*). *International Journal of Environmental Research and Public Health, 5*(5), 423–427. https://doi.org/10.3390/ijerph5050423

Gard, D. L., & Kropf, D. L. (1993). Confocal immunofluorescence microscopy of microtubules in oocytes, eggs, and embryos of algae and amphibians. *Methods in Cell Biology, 37*, 147–169. https://doi.org/10.1016/S0091-679X(08)60249-6

Gholamali, I., Asnaashariisfahani, M., & Alipour, E. (2020). Silver nanoparticles incorporated in pH-sensitive nanocomposite hydrogels based on carboxymethyl chitosan-poly (vinyl alcohol) for use in a drug delivery system. *Regenerative Engineering and Translational Medicine, 6*(2), 138–153. https://doi.org/10.1007/s40883-019-00120-7

Gonenc, I., & Us, F. (2019). Effect of glutaraldehyde crosslinking on degree of substitution, thermal, structural, and physicochemical properties of corn starch. *Starch-Stärke, 71*(3-4), Article 1800046. https://doi.org/10.1002/star.201800046

Habiba, U., Joo, T., Arefin, S., Das, R., Ang, B., & Afifi, A. (2019). Synthesis and Characterization of Chitosan/TiO2 Nanocomposite for the adsorption of congo red. *Desalination and Water Treatment, 164*, 361–367. https://doi.org/10.5004/dwt.2019.24391

Hanh, N. T., Tri, N. L. M., Van Thuan, D., Tung, M. H. T., Pham, T. D., Minh, T. D., … Nguyen, M. V. (2019). Monocrotophos pesticide effectively removed by novel visible light driven Cu doped ZnO photocatalyst. *Journal of Photochemistry and Photobiology A: Chemistry, 382*, Article 111923. https://doi.org/10.1016/j.jphotochem.2019.111923

Haq, A. U., Saeed, M., Usman, M., Muneer, M., Adeel, S., Abbas, S., & Iqbal, A. (2019). Removal of butachlor from aqueous solution using cantaloupe seed shell powder: Kinetic, equilibrium and thermodynamic studies. *International Journal of Environmental Science and Technology, 16*(10), 6029–6042. https://doi.org/10.1007/s13762-018-1992-4

Hoffmann, B., Seitz, D., Mencke, A., Kokott, A., & Ziegler, G. (2009). Glutaraldehyde and oxidised dextran as crosslinker reagents for chitosan-based scaffolds for cartilage tissue engineering. *Journal of Materials Science Materials in Medicine, 20*(7), 1495–1503. https://doi.org/10.1007/s10856-009-3707-3

Huo, M. X., Jin, Y. L., Sun, Z. F., Ren, F., Pei, L., & Ren, P. G. (2021). Facile synthesis of chitosan-based acid-resistant composite films for efficient selective adsorption properties towards anionic dyes. *Carbohydrate Polymers, 254*, Article 117473. https://doi.org/10.1016/j.carbpol.2020.117473

Jin, L., & Bai, R. (2002). Mechanisms of lead adsorption on chitosan/PVA hydrogel beads. *Langmuir, 18*(25), 9765–9770. https://doi.org/10.1021/la0259171

Jóźwiak, T., Filipkowska, U., Szymczyk, P., Rodziewicz, J., & Mielcarek, A. (2017). Effect of ionic and covalent crosslinking agents on properties of chitosan beads and sorption effectiveness of Reactive Black 5 dye. *Reactive and Functional Polymers, 114*, 58–74. https://doi.org/10.1016/j.reactfunctpolym.2017.03.007

Kaur, R., & Goyal, D. (2020). Biodegradation of butachlor by *Bacillus altitudinis* and identification of metabolites. *Current Microbiology, 77*, 2602–2612. https://doi.org/10.1007/s00284-020-02031-1

Khozemy, E. E., Nasef, S. M., & Mahmoud, G. A. (2018). Synthesis and characterization of antimicrobial nanocomposite hydrogel based on wheat flour and poly (vinyl alcohol) using γ-irradiation. *Advances in Polymer Technology, 37*(8), 3252–3261. https://doi.org/10.1002/adv.22094

Krstić, J., Spasojević, J., Radosavljević, A., Šiljegović, M., & Kačarević-Popović, Z. (2014). Optical and structural properties of radiolytically in situ synthesized silver nanoparticles stabilized by chitosan/poly (vinyl alcohol) blends. *Radiation Physics and Chemistry, 96*, 158–166. https://doi.org/10.1016/j.radphyschem.2013.09.013

Li, S., Li, M., Wang, Q., Gui, W., & Zhu, G. (2016). Exposure to butachlor causes thyroid endocrine disruption and promotion of metamorphosis in *Xenopus laevis*. *Chemosphere, 152*, 158–165. https://doi.org/10.1016/j.chemosphere.2016.02.098

Li, Z., Liu, Y., Zou, S., Lu, C., Bai, H., Mu, H., & Duan, J. (2020). Removal and adsorption mechanism of tetracycline and cefotaxime contaminants in water by $NiFe_2O_4$-COF-chitosan-terephthalaldehyde nanocomposites film. *Chemical Engineering Journal, 382*, Article 123008. https://doi.org/10.1016/j.cej.2019.123008

Liu, W. Y., Wang, C. Y., Wang, T. S., Fellers, G. M., Lai, B. C., & Kam, Y. C. (2011). Impacts of the herbicide butachlor on the larvae of a paddy field breeding frog (*Fejervarya limnocharis*) in subtropical Taiwan. *Ecotoxicology, 20*(2), 377–384. https://doi.org/10.1007/s10646-010-0589-6

Ma, Y. Q., Yi, J. Z., & Zhang, L. M. (2009). A facile approach to incorporate silver nanoparticles into dextran-based hydrogels for antibacterial and catalytical application. *Journal of Macromolecular Science Part A: Pure and Applied Chemistry, 46*(6), 643–648. https://doi.org/10.1080/10601320902852031

Machette. https://www.chemicalbook.com/ChemicalProductProperty_EN_CB2693046.htm. (Accessed 21 January 2021).

Mallakpour, S., & Rashidimoghadam, S. (2020). Preparation, characterization, and in vitro bioactivity study of glutaraldehyde crosslinked chitosan/poly (vinyl alcohol)/ascorbic acid-MWCNTs bionanocomposites. *International Journal of Biological Macromolecules, 144*, 389–402. https://doi.org/10.1016/j.ijbiomac.2019.12.073

Mamun, M. I. R., Park, J. H., Choi, J. H., Kim, H. K., Choi, W. J., Han, S. S., … Shin, H. C. (2009). Development and validation of a multiresidue method for determination of 82 pesticides in water using GC. *Journal of Separation Science, 32*(4), 559–574. https://doi.org/10.1002/jssc.200800606

Muda, M. S., Kamari, A., Bakar, S. A., Yusoff, S. N. M., Fatimah, I., Phillip, E., & Din, S. M. (2020). Chitosan-graphene oxide nanocomposites as water-solubilising agents for rotenone pesticide. *Journal of Molecular Liquids, 318*, Article 114066. https://doi.org/10.1016/j.molliq.2020.114066

Muthukaruppan, G., Janardhanan, S., & Vijayalakshmi, G. (2005). Sublethal toxicity of the herbicide butachlor on the earthworm *Perionyx sansibaricus* and its histological changes (5 pp). *Journal of Soils and Sediments, 5*(2), 82–86. https://doi.org/10.1065/jss2004.09.111

Nasef, S. M., Khozemy, E. E., Kamoun, E. A., & El-Gendi, H. (2019). Gamma radiation-induced crosslinked composite membranes based on polyvinyl alcohol/chitosan/$AgNO_3$/vitamin E for biomedical applications. *International Journal of Biological Macromolecules, 137*, 878–885. https://doi.org/10.1016/j.ijbiomac.2019.07.033

National Center for Biotechnology Information. (2021). *PubChem compound summary for CID 31677, butachlor*. Retrieved January 17, 2021 from https://pubchem.ncbi.nlm.nih.gov/compound/Butachlor.

Nešović, K., Janković, A., Kojić, V., Vukašinović-Sekulić, M., Perić-Grujić, A., Rhee, K. Y., & Mišković-Stanković, V. (2018). Silver/poly (vinyl alcohol)/chitosan/graphene hydrogels–Synthesis, biological and physicochemical properties and silver release kinetics. *Composites Part B: Engineering, 154*, 175–185. https://doi.org/10.1016/j.compositesb.2018.08.005

Nguyen, T. T. T., Tae, B., & Park, J. S. (2011). Synthesis and characterization of nanofiber webs of chitosan/poly (vinyl alcohol) blends incorporated with silver nanoparticles. *Journal of Materials Science, 46*(20), 6528–6537. https://doi.org/10.1007/s10853-011-5599-0

Nithya, A., JeevaKumari, H. L., Rokesh, K., Ruckmani, K., Jeganathan, K., & Jothivenkatachalam, K. (2015). A versatile effect of chitosan-silver nanocomposite for surface plasmonic photocatalytic and antibacterial activity. *Journal of Photochemistry and Photobiology B: Biology, 153*, 412–422. https://doi.org/10.1016/j.jphotobiol.2015.10.020

Ou, Y. H., Chung, P. C., Chang, Y. C., Ngo, F. Q., Hsu, K. Y., & Chen, F. D. (2000). Butachlor, a suspected carcinogen, alters growth and transformation characteristics of mouse liver cells. *Chemical Research in Toxicology, 13*(12), 1321–1325. https://doi.org/10.1021/tx990076c

Saifuddin, N., Nian, C. Y., Zhan, L. W., & Ning, K. X. (2011). Chitosan-silver nanoparticles composite as point-of-use drinking water filtration system for household to remove pesticides in water. *Asian Journal of Biochemistry, 6*(2), 142–159.

Sharma, G., Kumar, A., Naushad, M., García-Peñas, A., Ala'a, H., Ghfar, A. A., … Stadler, F. J. (2018). Fabrication and characterization of Gum arabic-cl-poly (acrylamide) nanohydrogel for effective adsorption of crystal violet dye. *Carbohydrate Polymers, 202*, 444–453. https://doi.org/10.1016/j.carbpol.2018.09.004

Sharma, G., Naushad, M., Ala'a, H., Kumar, A., Khan, M. R., Kalia, S., … Sharma, A. (2017). Fabrication and characterization of chitosan-crosslinked-poly (alginic acid) nanohydrogel for adsorptive removal of Cr (VI) metal ion from aqueous medium. *International Journal of Biological Macromolecules, 95*, 484–493. https://doi.org/10.1016/j.ijbiomac.2016.11.072

Singh, J., & Nandabalan, Y. K. (2018). Prospecting *Ammoniphilus* sp. JF isolated from agricultural fields for butachlor degradation. *3 Biotech, 8*(3), 164. https://doi.org/10.1007/s13205-018-1165-7

Sun, X. F., Wang, S. G., Liu, X. W., Gong, W. X., Bao, N., & Ma, Y. (2008). The effects of pH and ionic strength on fulvic acid uptake by chitosan hydrogel beads. *Colloids and Surfaces A: Physicochemical and Engineering Aspects, 324*(1-3), 28–34. https://doi.org/10.1016/j.colsurfa.2008.03.023

Tu, W., Niu, L., Liu, W., & Xu, C. (2013). Embryonic exposure to butachlor in zebrafish (*Danio rerio*): Endocrine disruption, developmental toxicity and immunotoxicity. *Ecotoxicology and Environmental Safety, 89*, 189–195. https://doi.org/10.1016/j.ecoenv.2012.11.031

Vilela, P. B., Dalalibera, A., Duminelli, E. C., Becegato, V. A., & Paulino, A. T. (2019). Adsorption and removal of chromium (VI) contained in aqueous solutions using a chitosan-based hydrogel. *Environmental Science and Pollution Research, 26*(28), 28481–28489. https://doi.org/10.1007/s11356-018-3208-3

Vimala, K., Yallapu, M. M., Varaprasad, K., Reddy, N. N., Ravindra, S., Naidu, N. S., & Raju, K. M. (2011). Fabrication of curcumin encapsulated chitosan-PVA silver nanocomposite films for improved antimicrobial activity. *Journal of Biomaterials and Nanobiotechnology, 2*(01), 55. https://doi.org/10.4236/jbnb.2011.21008

Wang, T., & Gunasekaran, S. (2006). State of water in chitosan–PVA hydrogel. *Journal of Applied Polymer Science, 101*(5), 3227–3232. https://doi.org/10.1002/app.23526

Watanabe, H., Nguyen, M. H. T., Souphasay, K., Vu, S. H., Phong, T. K., Tournebize, J., & Ishihara, S. (2007). Effect of water management practice on pesticide behavior in paddy water. *Agricultural Water Management, 88*(1-3), 132–140. https://doi.org/10.1016/j.agwat.2006.10.009

Yang, J. M., Su, W. Y., & Yang, M. C. (2004). Evaluation of chitosan/PVA blended hydrogel membranes. *Journal of Membrane Science, 236*(1-2), 39–51. https://doi.org/10.1016/j.memsci.2004.02.005

Yang, X. B., Ying, G. G., & Kookana, R. S. (2010). Rapid multiresidue determination for currently used pesticides in agricultural drainage waters and soils using gas chromatography–mass spectrometry. *Journal of Environmental Science and Health Part B, 45*(2), 152–161. https://doi.org/10.1080/03601230903472165

Zawadzki, J., & Kaczmarek, H. (2010). Thermal treatment of chitosan in various conditions. *Carbohydrate Polymers, 80*(2), 394–400. https://doi.org/10.1016/j.carbpol.2009.11.037

Zhang, X., Wei, Y., Chen, M., Xiao, N., Zhang, J., & Liu, C. (2020). Development of functional chitosan-based composite films incorporated with hemicelluloses: Effect on physicochemical properties. *Carbohydrate Polymers, 246*, Article 116489. https://doi.org/10.1016/j.carbpol.2020.116489

Zhu, L., Li, W., Zha, J., Wang, M., Yuan, L., & Wang, Z. (2014). Butachlor causes disruption of HPG and HPT axes in adult female rare minnow (*Gobiocypris rarus*). *Chemico-biological Interactions, 221*, 119–126. https://doi.org/10.1016/j.cbi.2014.07.016